COOPERATIVE SPECTRUM SENSING: PERFORMANCE ANALYSIS AND ALGORITHMS

YOUSSIF FAWZI SHARKASI

Submitted in accordance with the requirements

for the degree of Doctor of Philosophy

The University of Leeds

School of Electronic and Electrical Engineering

May 2014

The candidate confirms that the work submitted is his/her own, except where work which has formed part of jointly-authored publications has been included. The contribution of the candidate and other authors to his work has been explicitly indicated below. The candidate confirms that appropriate credit has been given within the thesis where reference has been made to the work of others.

It is to assert that the candidate has contributed solely to the technical part of the joint publications under the guidance of his academic supervisors. Detailed breakdown of the publications is presented in the first chapter of this thesis.

For my parents

Fawzi and Fathia,

my wife Muna and for my beautiful children Ahmed, Sarra and Fawzi.

ACKNOWLEDGMENTS

First and foremost, I would like to express my deepest gratitude to Allah Almighty (subhana wa taala) for endowing me with health, patience, and the knowledge to complete this work.

It gives me great pleasure to express my gratitude to all those people who have supported me and had contributions in making this thesis possible. I cannot express enough thanks to my supervisor Dr McLernon for this continued support and encouragement. I offer him my sincere appreciation for accepting me as a Ph.D student, for his patience, thoughtful guidance and critical comments in preparation of academic papers. I would also like to thank Dr McLernon for teaching me how to be rigorous, accurate and precise in my research. I would like to thank him for his support during the war in Libya and during my illness. Dr McLernon was not only a supervisor during the whole period of my study, but he has been a friend and a father. I will never forget the time that we were together and had discussion about religion and politics. Also I would like to thank my second supervisor Prof Ghogho and express my deepest gratitude for his excellent feedback, insightful discussion, offering valuable advice and discussing new ideas.

In addition, I would like to thank Dr Sami, Dr Assim, Dr Mohamed and Dr Adnan for comments about my Thesis. I would like to thank Dr S. Zaidi for very useful discussions. I am grateful to our research institute the secretary Anne, for assisting me in so many different ways and handling all the paperwork over the years.

I would like to thank all my colleagues in my research group for their good companionship: Edmound, Daniel, Raul, Chinazo, Deki, Nabil, Assem, Sami, Hafed, Omer, Ali, Walid and Mohamed Aref.

My completion of this thesis could not have been accomplished without the support of my caring, loving wife- the great woman Muna, who took for responsibility for everything at home. Her encouragement when the times got rough is much appre-

ciated. When I got ill it was a great comfort and relief to know that she was willing to provide management of our household activities while I completed my work. I would also like to thank my three beautiful children Ahmed, Sarra and Fawzi for making me happy when I got depressed. My children were like a restart button when I got back home from the university.

I would also like to thank the greatest people for me in this world- my parents Fawzi and Fathia. I would like to thank them for supporting me and for everything that they have done for me in this life. I would also like to thank them for supporting me financially during my PhD, as did my brothers Wail and Mustafa for supporting me financially during my PhD. I would like to thank my lovely sister Tojan for her kind words during my study and my parents in law Hassan and Isha for their unlimited support. In addition, I would like to thank my father in Law Hassan for supporting me financially and encouraging me during my illness. Last, but not least, I would like to offer my appreciation to my sister in law Manal and my brother in law Muftah for their encouragement and support during my research.

ABSTRACT

The employment of cognitive (intelligent) radios presents an opportunity to efficiently use the scarce spectrum with the condition that it causes a minimal disturbance to the primary user. So the cognitive or secondary users use spectrum sensing to detect the presence of primary user.

In this thesis, different aspects related to spectrum sensing and cognitive radio performance are theoretically studied for the discussion and in most cases, closed-form expressions are derived. Simulations results are also provided to verify the derivations.

Firstly, robust spectrum sensing techniques are proposed considering some realistic conditions, such as carrier frequency offset (CFO) and phase noise (PN). These techniques are called the block-coherent detector ($\frac{N}{2}$ -BLCD), the second-order matched filter-I (SOMF-I) and the second-order matched filter-II (SOMF-II). The effect of CFO on $\frac{N}{2}$-BLCD and SOMF-I is evaluated theoretically and by simulation for SOMF-II. However, the effect of PN is only evaluated by simulation for all proposed techniques.

Secondly, the detection performance of an energy detector (ED) is analytically investigated over a Nakagami-*m* frequency-selective (NFS) channel.

Thirdly, the energy efficiency aspect of cooperative spectrum sensing is addressed, whereby the energy expenditure is reduced when secondary users report their test statistics to the fusion center (FC). To alleviate the energy consumption overhead, a censored selection combining based power censoring (CSCPC) is proposed. The accomplishment of energy saving is conducted by not sending the test statistic that does not contain robust information or it requires a lot of transmit power. The detection performance of the CSCPC is analytically derived using stochastic geometry tools and verified by simulation. Simulation results show that that the CSCPC

technique can reduce the energy consumption compared with the conventional techniques while a detection performance distortion remains negligible.

Finally, an analytical evaluation for the cognitive radio performance is presented while taking into consideration realistic issues, such as noise uncertainty (NU) and NFS channel. In the evaluation, sensing-throughput tradeoff is used as an examination metric. The results illustrate the NU badly affects the performance, but the performance may improve when the number of multipath increases.

ACRONYMS

NTIA	National Telecommunications and Information Adminstrations
FCC	Federal Communications Commission
OFCOM	Office of Communications
UWB	Ultra wide band
RF	Radio Frequency
DSA	Dynamic spectrum access
ED	Energy detector
MF	Matched filter
FC	Fusion center
SU	Secondary user
PU	Primary user
PPP	Poisson point process
MPPP	Marked poisson point process
PGF	Probability generating function
$\frac{N}{2}-$BLCD	Block-coherent detector
SOMF – I	Second-order matched filter I
SOMF – II	Second-order matched filter II
AD	Autocorrelation detector

CFO	Carrier frequency offset
PN	Phase noise
ATSC	Advanced Television Systems Committee
SU_{TX}	Secondary user transmitter
SU_{RX}	Secondary user receiver
PU_{TX}	Primary user transmitter
PU_{RX}	Primary user receiver
CP	Cyclic prefix
NFF	Nakagami-m flat-fading
NFS	Nakagami-m frequency-selective
NU	Noise uncertainty
PPP	Homogeneous poisson point process
CSC	Censored selection combining
CSCPC	Censored selection combining based power censoring

LIST OF SYMBOLS

$\mathcal{H}_0$	Null hypothesis
$\mathcal{H}_1$	Alternative hypothesis
$s(n)$	Primary signal
$w(n)$	Noise signal
$x(n)$	Received signal by the secondary user
N	Number of received samples
P_p	Primary user transmit power
σ_w^2	Noise power
$\mathcal{CN}(a,b)$	Notation for a complex Gaussian distribution with mean a and variance b
$\mathcal{N}(a,b)$	Notation for a real Gaussian distribution with mean a and variance b
$\triangle f$	Carrier frequency offset
$\varphi(n)$	Phase noise process
P_{FA}	False alarm probability
P_D	Detection probability
T_{ED}	Test statistic when ED is used for sensing
T_{BLCD}	Test statistic when $\frac{N}{2}$-BLCD is used for sensing
$T_{MF,\text{CFO}}$	Test statistic in the presence of CFO when MF is used for sensing
T_{SOMF-I}	Test statistic when SOMF-I detector is used for sensing
$T_{SOMF-II}$	Test statistic when SOMF-II detector is used for sensing
T_{AD}	Test statistic when AD is used for sensing
τ_{ED}	Decision threshold for ED

τ_{BLCD}	Decision threshold for $\frac{N}{2}$-BLCD
τ_{MF}	Decision threshold for MF
τ_{I}	Decision threshold for SOMF-I
τ_{II}	Decision threshold for SOMF-II
τ_{AD}	Decision threshold for AD
χ^2_{2N}	Central chi square random variable with $2N$ degrees of fredom
$\chi^2_{2N}(\beta)$	Non central chi square random variable with $2N$ degrees of fredom and non central parametr β
Φ	Point process
$Q(.)$	Q-function
erf$(.)$	Error function
erfc$(.)$	Complementry error function
$Q_{\chi^2_{2N}}(.)$	Right-tail probability of the chi square random variable
$Q_{\chi^2_{2N}(\beta)}(.)$	Right-tail probability of the non central chi square random variable
$\Gamma(.,.)$	Upper incomplete Gamma function
$Q(.,.)$	Marcum Q-function
$Q^{-1}(.)$	Inverse Q-function
$\Gamma^{-1}(.,.)$	Inverse upper incomplete Gamma function
L	Number of multitaps
γ_{ave}	Average signal to noise ratio at secondary user
δ	Target probability detection
ϵ	Target false alarm probability
h_l	The l th tap (channel gain) between the primary user transmitter and the secondary user transmitter.
$\|h_l\|$	The amplitude of h_l.
h	Impulse response vector of the NFS channel bewteen the $\mathrm{PU_{TX}}$ and the $\mathrm{SU_{TX}}$ with length L

g	Impulse response vector of the NFS channel bewteen $\mathrm{SU_{TX}}$ and $\mathrm{SU_{RX}}$ with length L
f	Impulse response vector of the NFS channel bewteen the $\mathrm{PU_{TX}}$ and the $\mathrm{SU_{RX}}$ with length L
$\mathbb{P}_{\mathrm{out}}$	Outage detection probability
θ	Maximum tolerable value for $\mathbb{P}_{\mathrm{out}}$
δ	Target detection probability
γ_δ	Signal to noise ratio for $P_D = \delta$
$\tau_{ED\theta}$	Threshold value at $\mathbb{P}_{\mathrm{out}} = \theta$
$\tau_{AD\theta}$	Threshold value at $\mathbb{P}_{\mathrm{out}} = \theta$
T_a	It is a random variable which is a function in a random variable a.
$\widehat{f}_{T_a}(t)$	Approximated probability density function of a random variable T_a.
K_{T_a}	Shape parameter of the Gamma distribution.
ϕ_{T_a}	Scale parameter.
$w_i(n)$	i.i.d. circularly symmetric complex Gaussian noise for the ith cognitive radio.
$x_i(n)$	The signal received by ith cognitive radio.
P_p	Primary user transmitted power.
Φ	A homogeneous Poisson point process with intensity λ.
$\mathcal{A}$	A total area in which the secondary users are located
(θ_i, r_i)	θ_i is the angle between the ith cognitive radio and the positive x-axis and r_i is the distance of the ith cognitive radio and the fusion
θ_{pr}	A fixed angle bewteen the primary user and the positive x-axis.
R_{pr}	A fixed distance between the primary user and the fusion center.
r_{pri}	A distance between the primary user and ith cognitive radio.
α	Path loss exponent.
κ	Frequency dependent constant

$q(\theta_i, r_i)$	Is the path loss between the location (θ_i, r_i) and the primary user (θ_{pr}, R_{pr}).
K_a	A shape parameter for a random variable a.
θ_a	A scale parameter for a random variable a.
H_i	A Gamma distribution for the Nakgami-m fading channel between the ith cognitive radio and the primary user.
G_i	A Gamma distribution for the Nakgami-m fading channel between the ith cognitive radio and the fusion center.
T_{EDi}	Test statistic at the ith cognitive radio (when energy detector is used).
T_{max}	A global test statistic at fusion center for selection combining.
p_i	The required transmit power for the ith cognitive radio.
p_t	Transmit power threshold.
p_{ref}	Reference power.
$z(\theta_i, r_i)$	The path loss between the ith cognitive radio and the fusion center.
P_{a1}	Activity probability under $\mathcal{H}_1$.
P_{a0}	Activity probability under $\mathcal{H}_0$.
$f_H(h)$	the probability density function of the random variable H.
$f_G(g)$	the probability density function of the random variable G.
K_G	Shape parameter of the random variable G.
ϕ_G	Scale parameter of the random variabke G.
γ_s	Secondary user's desired SNR threshold (or SINR when the primary is present)
P_p	Primary transmit power
P_s	Secondary transmit power
σ_v^2	Noise variance at secondary receiver
N_d	The data length of the OFDM symbol.
N_c	The cyclic prefix length

$S_m(n)$	The nth complex symbol in the frequency domain of the m- OFDM symbol.
$\mathbf{S_m}$	N_d complex symbols in the frequency domain of the m- OFDM symbol.
$s_m(n)$	the nth symbol of the m- OFDM symbol in time domain.
h_l	The l th tap (channel gain) between the primary user transmitter and the secondary user transmitter.
h	Impulse response vector (each componet is h_l) of the frequency selective channel bewteen the primary user transmitter and the secondary user transmitter L.
g_l	The l th tap (channel gain) between the secondary user transmitter and the secondary user receiver.
g	Impulse response vector (each componet is g_l) of the frequency selective channel bewteen the secondary user transmitter and the secondary user receiver with length L.
$G(k)$	Complex channel gain (in frequency domain) at the kth subcarrie between the secondary user transmitter and the secondary user receiver.
G	Vector of subcarriers gains in frequency domain (each componet is $G(k)$) with length J, between the secondary user transmitter and the secondary user receiver.
f_l	The l th tap (channel gain) between the primary user transmitter and the secondary user receiver.
$F(k)$	Complex channel gain (in frequency domain) at the kth subcarrie between the primary user transmitter and the secondary user receiver.
f	Impulse response vector (each componet is f_l) of the frequency selective channel bewteen the primary user transmitter and the secondary user receiver with length L.

$\mathbf{F}$	Vector of subcarriers gains in frequency domain (each componet is $F(k)$) with length J, between the primary user transmitter and the secondary user receiver.
Ω_{g_l}	Is a controlling spread parameter for the l -th tap of channel $\mathbf{g}$ bewteen the secondary user transmitter and the secondary user receiver.
$\bar{m}_G$	Nakagami parameter for $G(k)$.
$\bar{\Omega}_G$	Is a controlling spread parameter for the k-th tap of channel in frequency domain, $\mathbf{G}$, bewteen the secondary user transmitter and the secondary user receiver.
$\mathcal{G}(\bar{m}_G, \frac{\bar{\Omega}_G}{\bar{m}_G})$	Gamma distribution with a shape parameter $\bar{m}_G$ and scale parameter $\frac{\bar{\Omega}_G}{\bar{m}_G}$.
Ω_{f_l}	Is a controlling spread parameter for the l -th tap of channel $\mathbf{f}$ bewteen the primary user transmitter and the secondary user receiver.
$\bar{m}_F$	Nakagami parameter for $F(k)$.
$\bar{\Omega}_F$	Is a controlling spread parameter for the k-th tap of channel in frequency domain, $\mathbf{F}$, bewteen the primary user transmitter and the secondary user receiver.
T_a	It is a random variable which is a function in a random variable a.
T_{ab}	It is a random variable which is a function in two random variables a and b.
K_{T_a}	Shape parameter of the Gamma distribution random variable T_a.
ϕ_{T_a}	Scale parameter of the Gamma distribution random variable T_a.
$K_{T_{ab}}$	Shape parameter of the Gamma distribution random variable T_{ab}.
$\phi_{T_{ab}}$	Scale parameter of the Gamma distribution random variable T_{ab}.
$SNR_{global0}$	Global signal to noise ratio at secondary receiver side under $\mathcal{H}_0$.
$SNR_{global1}$	Global signal to noise ratio at secondary receiver side under $\mathcal{H}_1$.
$P_p(k)$	Primary transmit power for the kth subcarrier.
$P_s(k)$	Secondary transmit power for the kth subcarrier.

$\sigma_v^2(k)$	Noise variance for the kth subcarrier at the secondary receiver.
f_{xy}	Joint probability density function for a bivariate Nakagami distribution
C_0	Throughput of the secondary link $(\mathrm{SU_{TX}} \rightarrow \mathrm{SU_{RX}})$ under $\mathcal{H}_0$
C_1	Throughput of the secondary link $(\mathrm{SU_{TX}} \rightarrow \mathrm{SU_{RX}})$ under $\mathcal{H}_0$
C	Average secondary throughput
P_{sucss0}	Success probabilitiy under $\mathcal{H}_0$ for the secondary link
P_{sucss1}	Success probabilitiy under $\mathcal{H}_1$ for the secondary link
C_{ED}	Secondary throughput when ED is used for spectrum sensing
C_{AD}	Secondary throughput when AD is used for spectrum sensing
$\Re\{.\}$	Real part of a complex number
N_d	The data length of the OFDM symbol
N_c	The cyclic prefix length
B	Noise uncertainty bound
ρ	Noise uncertainty random variable
Ω_{h_l}	Is a controlling spread parameter for the l -th tap of channel $\mathbf{h}$ bewteen the primary user and the secondary receiver.
$\hat{\sigma}_w^2$	estimated noise power

CONTENTS

LIST OF FIGURES

LIST OF TABLES

1

INTRODUCTION

1.1 BACKGROUND

Today, frequency spectrum is as precious as gold and oil. Service providers must pay millions of dollars to buy the rights to use a certain band of frequency. With the proliferation of wireless communication technologies over the last few decades, new wireless applications have become widespread co-existing in the same geolocation. Because of these technologies, the demand for higher data rates has become essential as the number of wireless subscribers has increased, leading to a saturated frequency spectrum.

The National Telecommunications and Information Administration's (NTIA) frequency allocation chart illustrated in Figure 1.1 shows that most of the frequency spectrum is allocated or licensed to traditional communications systems and services [4]. However, statistics and measurements from the Federal Communications Commission (FCC) state that the licensed spectrum is not used in some time-frequency intervals over certain geographic areas [5]. For example, the utilization of some licensed bands is about 5% or even less [6]. This means 95% of the time or the area is not exploited although there is another operator/service that requires a new band to work on but the spectrum has no space or capacity to accommodate it.

The operation of spectrum allocation, e.g., issuing a license for a specific radio spectrum for exclusive or shared usage, and proclaiming spectrum as unlicensed, is supervised by governmental agencies which are called regulators such as the Office of Communications (Ofcom) in the UK and the FCC in the USA. The traditional

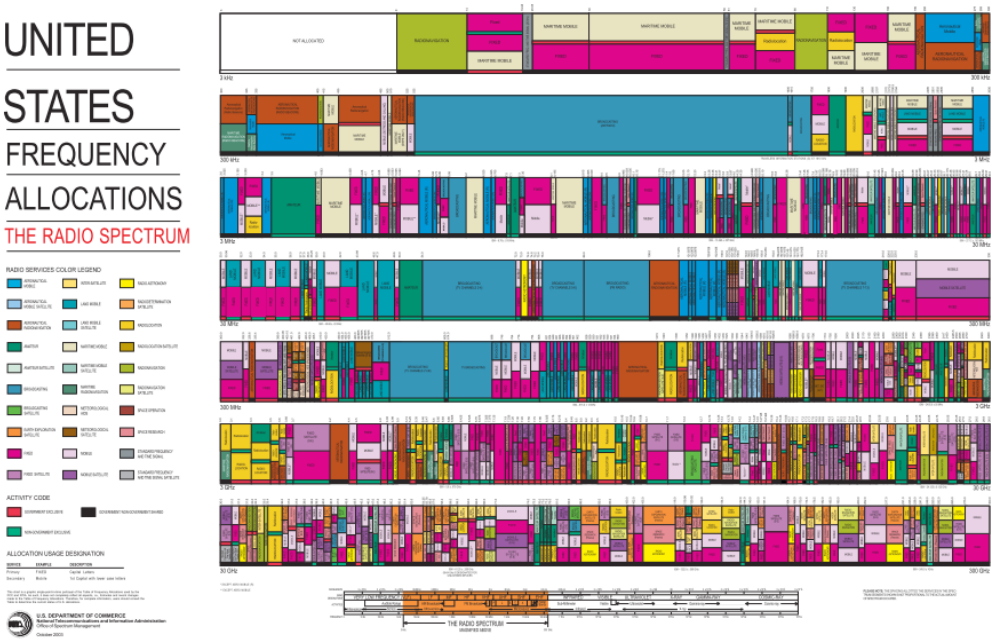

Figure 1.1: U. S. frequency allocations [1].

spectrum allocation policy allocates a static spectrum to a particular system and this spectrum can not be used by other services by new users (even if it is underutilized).

Both *emerging wireless technologies* and the *static spectrum allocation policy* are reasons for the shortage of frequency spectrum. Consequently, there is a request in the communication community that the current spectrum allocation policy should be reformed to be more flexible in order not to waste spectrum without exploitation [7].

A solution for this problem is the recycling of the licensed bands which can be done by cognitive radio (CR) and dynamic spectrum access (DSA). The CR, a term coined by Mitola in 1991 [8], is a promising idea that has been suggested as a solution linking spectrum scarcity and spectrum under-utilization which is an intelligent radio that is aware of its surrounding environment [9]. The DSA implies the utilization of portions of radio spectrum in a flexible manner with respect to technical regulatory and constraints. The DSA aims to change the current spectrum allocation policy to make it more adaptable.

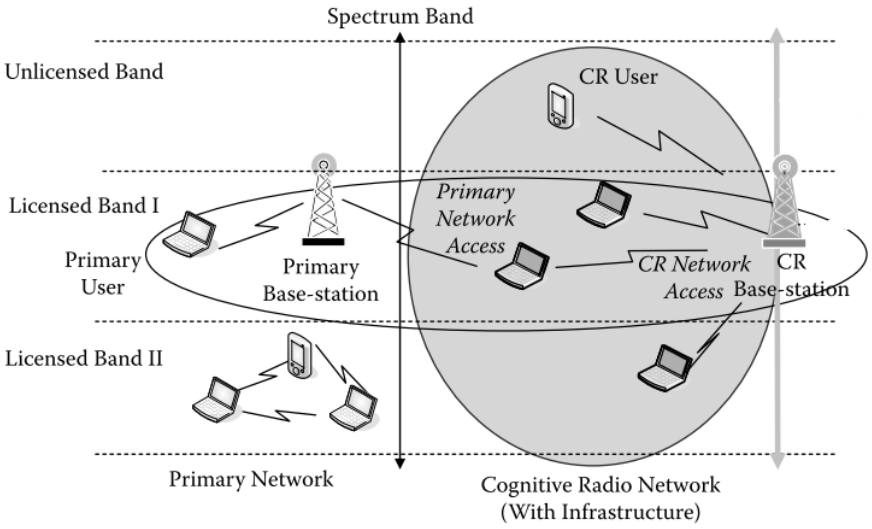

Figure 1.2: A cognitive network [2].

1.2 COGNITIVE RADIO

According to Haykin [6], a CR is "an intelligent wireless communication system that listens to its surrounding environment and uses the methodology to learn from the environment and adapts its internal states by making corresponding changes in certain operating parameters (e.g., transmit-power, carrier frequency and modulation strategy) in real time". From the definition, the CR has two features which are the capability and the reconfigurability which distinguishes the CR from traditional radio. The capability is defined as the ability to sense the surrounding radio environment, analyze the acquired information and accordingly identify the best available spectrum bands for operation. The reconfigurability is defined as the secondary user's ability to adopt its operational parameters such as the transmit-power, carrier frequency, bandwidth and modulation strategy, based to the data collected from the surrounding environment and subsequently the secondary user can operate optimally in the candidate spectrum bands.

The goal of CR technology is to elevate the utilization of the frequency spectrum to be more efficient [10]. In a cognitive radio network there are two opera-

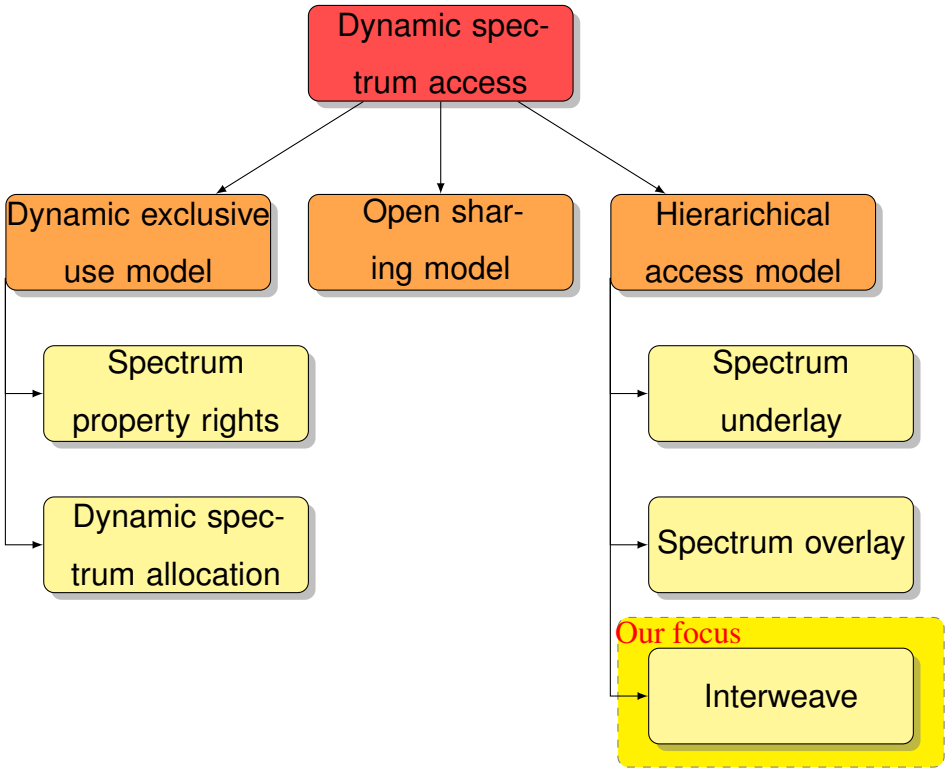

Figure 1.3: Dynamic spectrum access [3].

tors as shown in Figure 1.2. The first operator is a primary user who is defined as the owner (or the licensee) of a particular part of the frequency spectrum and has higher primacy rights to access this part of the spectrum. The second operator is a secondary user/unlicensed device who (having lower rights on the usage of this spectrum) attempts to harness the licensed band/primary band opportunistically in a manner such that the primary receiver is protected from any harmful interference.

1.3 DYNAMIC SPECTRUM ACCESS (DSA)

The driving force behind cognitive radio is DSA in which allows secondary users to access the spectrum if the primary receiver will not be negatively effected. DSA may be widely classified under three models namely; *dynamic exclusive model*, *open sharing model* and *hierarchical access model* [3, 11, 12] as illustrated in Figure 1.3. In the dynamic exclusive model, the basic structure of the current spectrum regulation is maintained. However, the difference is that the primary users can give

secondary users the right to use at a specific band for a certain period of time or a specific location. This model has two approaches:

1. The first approach is the spectrum property rights in which primary users can sell and trade spectrum [13].

2. The second approach is the dynamic spectrum allocation in which, the spectrum at a given region and at a given time is reserved to service exclusive use [14].

This approach could improve spectrum efficiency, but it cannot exploit white space (licensed bands that are not in use for some points in space/time), spectrum holes, or a spectrum opportunity that may occur when the primary user does not access its band.

In open sharing models, all users are allowed to access the spectrum. This model is already in use in the Industrial, Scientific and Medical (ISM) band. Since this model can be used by heterogeneous wireless technologies, the possibility of interference is very high.

In the hierarchical access model, the spectrum can be accessed by secondary users while avoiding interference to the primary users. There are three approaches under this model [15].

1. An underlay approach: in which imposing restrictions on the transmission power of secondary users is adopted, such that no interference is caused to primary users (e.g., ultra wide band (UWB) transmission). This approach, places a restriction on the transmit power of secondary users requiring them to transmit with very low power and in a small area. Furthermore, the secondary user has to estimate or predict the interference limit at the primary receiver which increases system complexity.

2. An overlay approach: in this approach the secondary user uses some information about the primary user such as codebooks and ”assists” the primary user with its transmissions. However, this approach is very complex.

3. Interweave (or opportunistic spectrum access): this approach does not place any severe constraints on the transmission power of secondary users, but expects them not to cause interference to the primary user. This can be done by allowing the secondary users to identify white spaces that can be exploited. As a result, secondary users should have cognitive radio qualifications, i.e., sensing the spectrum to determine the presence or the absence of the primary user.

Due to the above disadvantages for the dynamic exclusive model, open sharing model, underlay approach and overlay approach this thesis focuses on the cognitive radio based interweave approach.

1.4 COGNITIVE RADIO ASPECTS

The most important tool in interweave cognitive radio is *spectrum sensing* and is used to determine the activity of the primary user. If the secondary user finds the primary user absent then the secondary user can access the frequency spectrum such that the primary receiver is protected from interference. Also, the secondary user needs to vacate this frequency spectrum as soon as the primary user starts its transmission.

Many techniques have been suggested to conduct spectrum sensing and among them MF and ED techniques are the most widely used in practice due to their simplicity. Employing them some times depends on the availability of prior information about the primary signal and one may choose one of the above approaches for spectrum sensing in cognitive radio networks. For example, when the secondary user knows some information about the primary user such as a pilot, preamble, or training sequence (used by a primary network for channel estimation or synchronization), the recommended detector is the MF. However, if the secondary user does not have information about the primary user, the ED becomes the optimal detector [16].

In practice, several drawbacks make local sensing difficult. Such drawbacks include severe multipath fading, shadowing, or the secondary user inside buildings

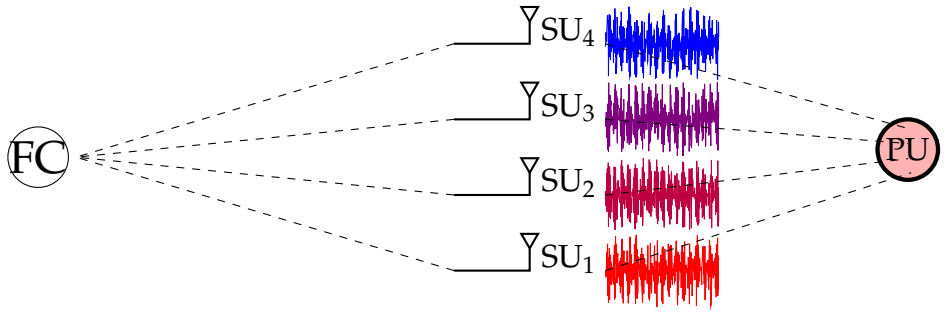

Figure 1.4: Cooperative spectrum sensing.

with penetration loss. As a result, the secondary user may not detect the presence of the primary user, and so accessing the licensed band and causing interference to the primary user. Cooperative spectrum sensing has been proposed in the literature to alleviate these challenges. In cooperative spectrum sensing, there are secondary users distributed over a specific area. Each secondary user (SU) sends its measurement/test statistic regarding the primary user (PU) to a fusion center (FC) to calculate the final decision as illustrated in Figure 1.4.

As mentioned above, that secondary user searches in the licensed or primary band until it finds a vacant channel and then it starts its transmission/communication. This means that the secondary transmitter communicates with the secondary receiver under the condition of not causing a failure to the primary link. Obviously, the secondary transmission depends on the result of spectrum sensing. Thus spectrum sensing and the secondary transmission are intertwined. Therefore, the secondary transmission should also be considered when spectrum sensing is investigated.

To protect the primary receiver from the possibility of any interference, the secondary user is allocated a time slot that is divided into two parts [17]; one for sensing and the other for transmission. Both the sensing and the transmission are conducted periodically over the period of time that the licensed spectrum is used. On one hand, it can be seen that as the time allocated for sensing increases the transmission decreases ensuring the primary receiver is kept secure. On the other hand, as the sensing decreases the transmission time increases and the primary user is exposed to a high potential for interference. From this discussion, it appears that there exists a tradeoff between the spectrum sensing and the secondary transmission. This struc-

ture of the secondary user frame is widely used in cognitive radio papers and is thus adopted in this thesis [18].

1.5 MOTIVATION

As mentioned before, the CR is a promising technology for the conflict between the spectrum scarcity and spectrum under-utilization. To protect the primary user from any potential interference caused by the secondary user, the sensing and transmission should be conducted periodically. To achieve the goal of CR, this thesis studies and investigates in depth two different aspects in CR, which are spectrum sensing and secondary transmission [1].

Although the first aspect (spectrum sensing) has been studied extensively in literature where a lot of practical issues have been tackled depending on the employed detector, many issues have not been covered for local and cooperative spectrum sensing. The first part of the thesis investigates different subjects in spectrum sensing. For example, the thesis exposes some issues that might prevent perfect operation of cognitive radio. Moreover, robust detection techniques are proposed to mitigate some of these issues. Furthermore, spectrum sensing performance will be investigated for unexplored environments. In addition, developing an energy-efficient cooperative spectrum sensing scheme to reduce the energy overhead due to sending the test statistics to the FC.

In the literature, the conventional spectrum sensing algorithms, such as MF, are no longer reliable and effective since these techniques do not take into account realistic scenarios such as CFO and PN [19, 20, 21]. Although, CFO and PN have been extensively studied in a conventional wireless communication system. However, not enough research has been conducted in the area of spectrum sensing in the presence of CFO and PN. These issues motivate us to develop new spectrum sens-

1 This section mentions only the subjects that will be covered throughout the thesis. Each chapter is self contained and so a literature review related to each subject will be presented in a separate chapter.

ing techniques which have the capability to exploit the primary known information and perform perfectly under the CFO and PN conditions.

In addition, previous research on the detection performance of the ED is limited to flat-fading channels [22, 23, 24, 25]. The literature fails to investigate the detection performance of ED over realistic environment such as a Nakagami-*m* frequency-selective (NFS) channel. This gap motivates us to investigate the behavior of the ED over the NFS. This investigation helps the network designers to improve the overall network performance.

Sending the test statistics to the FC consumes a lot of power. In the literature [26, 27, 28, 29, 30, 31, 32], the alleviation of power consumption was based on censoring/not transmitting to the FC test statistics (based on a local threshold) that are not robust. However, all the above mentioned papers have not taken into account the transmit power for secondary users[2], which is a function of the channel, and the distance between the secondary users and the FC. Unlike previous work, this thesis includes a transmit power in the detection problem which might reduce the overhead power for sending test statistics to the FC while the detection performance loss is negligible.

The second part of the thesis focuses on the secondary throughput. After protecting the primary receiver from any potential interference through spectrum sensing, the ultimate goal for the secondary user is to access the licensed band. The CR performance is coupled with spectrum sensing. In the literature [33, 34, 35, 36, 37], the CR performance has been extensively studied in terms of sensing-throughput trade-off by relaxing some realistic scenarios. For example, previous works have assumed that the noise variance at secondary user is known and that the sensing channel is AWGN. The purpose of this relaxation is to provide an analytical study for cognitive radio performance. This thesis provides an analytical evaluation of cognitive radio performance in realistic scenarios such as noise uncertainty (NU) and NFS channel. Studying the cognitive radio performance in the presence of NU and over NFS channels provides an in-depth understanding of system design in industry and academia. The objective and contribution of this thesis are now discussed.

2 The required power to send a test statistic to the FC.

1.6 THESIS OBJECTIVE

1. The first aim of the thesis is to design reliable spectrum sensing techniques for cognitive radio. The objective is to design robust spectrum sensing where RF impairments are present, such as CFO and PN.

2. The second objective of this thesis is the investigation of the performance of the ED over an NFS channel.

3. Furthermore, the thesis develops a reliable energy-efficient cooperative detection technique, taking into account the power needed to transmit the test statistics to the FC. The technique is designed for a realistic scenario that includes small (Nakagami-*m* flat-fading channel (NFF)) and large scale fading (path loss).

4. Finally this thesis provides a theoretical framework for evaluating secondary user throughput over uncertain environments, such as NU and NFS.

1.7 MATHEMATICAL PRELIMINARIES

1.7.1 *Nakagami-*m *distribution*

The Nakagami-*m* probability density function is given by

$$f_X(x) = \frac{2}{\Gamma(m)}\left(\frac{m}{\Omega}\right)^m x^{2m-1}\exp(-mx^2/\Omega), \tag{1.1}$$

where m is the Nakagami fading parameter and $\Omega = \mathbb{E}[X^2]$ is controlling spread. The wide versatility, experimental validity and analytical tractability of the Nakagami distribution has made it a very popular in wireless communications. The reason for adopting this particular model is that the m - distribution includes the Rayleigh and the half-Gaussian as special cases (m = 1, $m = \frac{1}{2}$), and it can be made to approximate other exact or experimentally derived distributions by judicious choice of parameters.

Notice that (1.1) is the p.d.f of channel amplitude. When there is a Nakagami fading channel, the channel power gain (X^2) may follow the Gamma distribution

$$f_{X^2}(t) = \frac{1}{\Gamma(k)\theta^k} \exp\Big(\frac{-t}{\theta}\Big), \tag{1.2}$$

where $k = m$ and $\theta = \frac{\Omega}{m}$ are the shape and scale parameters respectively.

1.7.2 *Stochastic Geometry*

In chapter 4, stochastic geometry is employed to model cooperative spectrum sensing networks. So, here we introduce the basics of stochastic geometry.

Stochastic geometry [38] is a mathematical tool that allows the study of random phenomena in the plane or in higher dimensions. Stochastic geometry is closely related to the theory of point processes $(\mathrm{PP_s})$[39]. The exploitation of stochastic geometry was first used in biology, astronomy and material sciences. Nowadays, it is widely applied in wireless communications **(author?)** [40].

Poisson Point Process (PPP) is the most used, most tractable $\mathrm{PP_s}$ in wireless communication because of its independence [39]. This thesis is interested in two dimensions. So a PP $\Phi = \{(\theta_i, r_i),\ i = 1,2,3,\ \ldots\} \subset \mathbb{R}^2$, where (θ_i, r_i) is the polar location of the ith secondary user, is a PPP if the number of points inside any compact set $\mathcal{E} \subset \mathbb{R}^2$ is a Poisson random variable, and positions are uniformly distributed **(author?)** [40].

Now some useful properties of the PPP are presented.

- For a PPP with intensity λ, the number of secondary users in a certain area $\mathcal{A}$ is a Poisson random variable with parameter $\lambda\mathcal{A}$. When the secondary users face fading channels, the fading marks x_i, are assigned to each secondary user and that forms a Marked PPP[3] (MPPP) with intensity $\lambda f_X(x)$, where $f_X(x)$ is the probability density function for the fading channel gain.

- The thinning of a PPP is defined by selecting some secondary users with probability p and discarding other secondary users with probability $1-p$. This selection or discard results in two independent PPPs of intensity parameters $p\lambda$

3 For more details regarding MPPP please refer to [38].

and $(1-p)\lambda$. For example, using ALOHA as the MAC protocol in a wireless network leads to a thinning of the node set.

- The PPP is called homogenous if the intensity function is a constant λ, otherwise it is called inhomogeneous/nonhomogeneous when its intensity is a function of the position (θ, r), (i.e., $\lambda(\theta, r)$) .

The above properties are very useful in calculating the average of the sum or the product of PPP. If we let $v(\theta, r, x) \ : \ \mathbb{R}^2$ be measurable and Φ is MPPP, then we have the following properties:

1. the probability generating function **(author?)** [38] (PGF) of a MPPP of density $\lambda(\theta, r) f_X(x)$ is given by

$$\begin{aligned} \mathcal{G}(\theta, r) &= \mathbb{E}_{\Phi, x_i}\Big[\prod_{(\theta_i, r_i)\in\Phi} v(\theta_i, r_i, x_i)\Big] \\ &= \exp\Big(-\int_X \int_{\mathbb{R}^2} \lambda(\theta, r)(1 - v(\theta, r, x)) \\ &\quad f_X(x) dx d\theta dr\Big). \end{aligned} \tag{1.3}$$

2. Campbell 's theorem **(author?)** [38] can be used for calculating the mean of the sum

$\sum_{(\theta_i, r_i)\in\Phi} v(\theta_i, r_i, x_i)$

$$\begin{aligned} \mathbb{E}_{\Phi, x_i}\Big[\sum_{(\theta_i, r_i)\in\Phi} v(\theta_i, r_i, x_i)\Big] &= \int_X \int_{\mathbb{R}^2} \lambda(\theta, r) v(\theta, r, x) \\ &\quad \times f_X(x) dx d\theta dr. \end{aligned} \tag{1.4}$$

In general, Campbell's theorem is used to evaluate the average of a sum and the PGF is used for calculating the average of a product of a function over the point process.

1.7.3 *Model of noise uncertainty*

For many spectrum sensing techniques, the receiver noise power is assumed to be known a priori (σ_w^2). However, when there is noise uncertainty (NU) the noise power level may change over time[4] and the noise power will be $\rho\sigma_w^2$, where ρ is

4 More details for noise uncertainty are in chapter 5.

called the NU factor [41]. Here ρ (in dB) is modeled as a uniform distribution in the interval $[-B,\ B]$, where B (in dB) is the NU bound and $B = \sup[10\log_{10}(\rho)]$. The effect of noise uncertainty will be used only for simulations in chapters 2,3,4 and analytically in chapter 5.

1.8 THESIS ORGANIZATION AND CONTRIBUTION

The thesis primarily covers several issues regarding cognitive radio, each of which is presented in a separate chapter. A literature review is provided for every issue. Furthermore, mathematical derivations are provided for the discussion and in most cases, closed-form equations are derived. Simulation results are also provided to verify the derivations.

The contributions of this thesis is the design, investigation and exploration of spectrum sensing and secondary user throughput. A detailed organization is illustrated next.

Chapter 2

This chapter addresses the issue of the spectrum sensing in the presence of RF impairments such as the CFO and the PN. To mitigate the RF impairment issue, three novel detectors have been proposed; a block-coherent detector ($\frac{N}{2}$-BLCD) with a suboptimal number of blocks ($N/2$), a second-order matched filter-I (SOMF-I) and a second-order matched filter-II (SOMF-II). Theoretical derivations are given for the detection performance of $\frac{N}{2}$-BLCD, SOMF-I, and SOMF-II.

The contributions of chapter 2 have been previously presented in the following publications:

1. Y. Sharkasi, D. McLernon, and M. Ghogho, "Robust spectrum sensing in the presence of carrier frequency offset and phase noise for cognitive radio," IEEE WTS, London, UK, 2012.

2. Y. Sharkasi, D. McLernon, and M. Ghogho, "Spectrum sensing in the presence of RF impairments in cognitive radio," International Journal of Interdisciplinary Telecommunications and Networking (IJITN), 2012.

Chapter 3

This chapter investigates the detection performance of the ED over an NFS channel. Theoretical derivations are presented for the average detection probability of the ED over the NFS channel. Also, the analysis of the outage detection probability is given.

The contribution of chapter 3 is based on the following publications:

1. Y. Sharkasi, D. McLernon, and M. Ghogho, "Performance analysis of a cognitive radio energy detector over frequency-selective fading channels," IEEE ISWCS, Paris, France, 2012.

2. Y. Sharkasi, D. McLernon, and M. Ghogho, "Cooperative spectrum sensing over frequency-selective nakagami-*m* fading channels," SSPD, London, UK, 2012.

Chapter 4

This chapter proposes a new algorithm for cooperative spectrum sensing in order to reduce the power needed to transmit the test statistics to the FC. The proposed algorithm is called a censored selection combining detector based on power censoring (CSCPC). Unlike previous work[5], the CSCPC takes into account the needed transmit power to send the test statistics to the FC. Also, the detection performance of a conventional censored cooperative spectrum sensing at the FC is analytically derived and is called censored selection combining (CSC) detector . Both the CSCPC and the CSC approaches are analysed using stochastic geometry.

This chapter's contribution is reflected in the next publications:

1. Y. Sharkasi, M. Ghogho, D. McLernon and S. Zaidi, "Performance analysis of cooperative spectrum sensing for cognitive radio using stochastic geometry," IEEE EUSIPCO, Rabat, Morroco, 2013.

2. Y. Sharkasi, M. Ghogho, D. McLernon and S. Zaidi, "Energy-efficient cooperative spectrum sensing for cognitive radio using stochastic geometry," to be submitted to IEEE Transactions on Wireless Communications.

5 The conventional algorithms for cooperative spectrum sensing based energy effecient are based on censoring test staitsics regrading a local threshold.

Chapter 5

This chapter studies the effect of the NU and the NFS on the tradeoff between the spectrum sensing and secondary transmission. The secondary performance is analytically investigated in terms of sensing threshold under an outage constraint in the presence of NU and over NFS, and success probabilities under the null and alternative hypotheses respectively[6]. This study is based on two different detectors: the ED and the autocorrelation detector (AD)[7]. The theoretical derivation of the sensing threshold under an outage constraint is presented. Then success probabilities under the null and alternative hypotheses are derived.

This contributions of this chapter are published in the following papers:

1. Y. Sharkasi, D. McLernon and M. Ghogho, "Sensing-throughput tradeoff for cognitive radio under Outage constraints over frequency selective fading channels," IEEE ISP, London, UK, 2013.

2. Y. Sharkasi, M. Ghogho, and D. McLernon, "Sensing-throughput tradeoff for OFDM-based cognitive radio under outage constraints," IEEE ISWCS, Paris, France, 2012.

3. Y. Sharkasi, D. McLernon, M. Ghogho and S. Zaidi, "On spectrum sensing, secondary and primary throughput, under outage constraint with noise uncertainty and flat fading," IEEE PIMRC, London, UK, 2013.

4. 3. Y. Sharkasi, D. McLernon and M. Ghogho, "Sensing-throughput tradeoff in the presence of noise uncertainty and over nakagami-m frequency-selective channels," to be submitted to IEEE Transaction on Vehicular Technology.

Chapter 6

This chapter presents the thesis conclusion and talks about future work.

---

6 Here the null hypothesis means that the primary user is not present and only noise is present. The alternative hypothesis means that there is a primary user signal plus noise.

7 For the sake of comparison, another detector is chosen such that it is insensitive to the noise uncertainty problem. This detector is the autocorrelation detector based on an OFDM signal. Thus the spectrum sensing threshold based on an autocorrelation detector is derived.

2

ROBUST SPECTRUM SENSING TECHNIQUES IN THE PRESENCE OF CFO AND PN

2.1 INTRODUCTION

As mentioned in the previous chapter, spectrum sensing is the most important stage in a CR. To protect the primary receiver from any potential interference, spectrum sensing should be robust to an uncertain environment such as synchronization errors, carrier frequency offset (CFO) and phase noise (PN). This chapter deals with designing robust spectrum techniques in the presence of CFO and PN.

In this chapter, the case to be considered is when the secondary user has a-priori knowledge of the primary signal. In this scenario, it is known that the optimal detector is the MF [16]. Information regarding the primary user can be made available for the secondary user via pilots or preambles, which are used for coherent detection. For example, in a digital TV broadcast (ATSC), there is a training-sequence used for channel estimation. In addition, an OFDM system also uses preambles for packet acquisition.

However, when the MF is exploited to detect the availability of the primary user CFO and PN will deteriorate the performance.

This chapter will discuss the behavior of the MF and the energy detector (ED) in the presence of CFO and PN. Also, this chapter investigates the range of the CFO in which the ED surprisingly outperforms the MF for reasons that will be explained later. Moreover, we will propose three different spectrum sensing techniques that are robust to CFO. The first technique is called the block-coherent detector ($\frac{N}{2}$-

BLCD) with a suboptimal number of blocks ($\frac{N}{2}$). The received signal is segmented into several blocks and we then apply the MF for each block. The second technique is called second-order matched filter-I (SOMF-I), the detection performance of which has been studied both theoretically (in the presence of CFO) and confirmed through simulation. The last technique is named the second-order matched filter-II (SOMF-II) and is a modified version of SOMF-I but with a superior performance. The second-order is used in the name for SOMF-I and SOMF-II due to the existence of the term $x(n)x^*(n-1)$ in the test statistic (where $x(n)$ is the received signal). The presence of PN and its effect on the detection performance is then examined via simulation.

To the best of authors' knowledge, spectrum sensing using MF in the presence of CFO and PN has not been dealt with in any previous research. Moreover, new techniques have been proposed to tackle the CFO and PN problems.

2.1.1 *Literature review and motivation*

Most of the work of spectrum sensing in the presence of RF impairments has concentrated on the cyclostationary detector. The research in this area has followed two main directions. The first direction focused on investigating the effect of RF impairments on the detection performance of cyclostationary detectors. For instance, in [42] the authors have shown that the detection performance might deteriorate by increasing the number of samples in the presence of CFO, this presents a challenge to cyclostationary detection in a low signal to noise ratio scenario and because a large number of samples is required to overcome the noise. In [43, 44], an investigation was conducted on the impact of IQ imbalance and PN on the detection performance of the cyclostationary detector. In [45], the authors studied the effect of IQ imbalance on the detection performance of the ED and the cyclostationary detector. The authors have shown that both detectors are not affected by IQ imbalance. In [46, 47] the effect of sampling clock offset has been studied on detection performance for different test statistics-based cyclostationary detectors. The results have shown that the sampling clock offset degrades the detection performance.

The second direction focuses on proposing solutions for the RF impairments issue. For example, in [21] a solution to the sampling clock offset is proposed in pilot based OFDM detection using the spectral correlation function as the test statistic, where the phase offset from one frame to the next is estimated and compensated for in the detection process. In [20], a blind solution to the sampling clock offset problem has been proposed, where the symbol rate of the incoming signal is estimated, and the acquired samples are interpolated at the correct rate. In [48], a new multi-frame test statistic has been proposed to reduce the degradation due to cyclic frequency offsets. Notice that all previous references are based on cyclostationary detectors.

Little research has been done regarding the effect of CFO and PN on the detection performance of spectrum sensing for the MF. The study in [19] deals with spectrum sensing using a MF in the presence of CFO and they studied the performance of the MF in the presence of CFO when the primary user uses a single sine wave pilot. Also, the problem of CFO has been addressed there by processing coherent segments of the received signal block by block. However, they did not determine how many blocks should be used, where every CFO might require an optimal number of blocks. Also**,** a solution was not proposed to overcome the detection performance degradation of the matched filter because of the CFO.

2.2 CHAPTER CONTRIBUTION

The ultimate goal of this chapter is to design robust spectrum sensing techniques in the presence of CFO and PN. This goal has been achieved through the following contributions which are summarized below:

1. Examination of the performance of the MF in the presence of CFO in order to determine over what range of CFO the MF still outperforms the ED. This approach includes both analytical expressions for the receiver operating characteristic (ROC) for the MF (in the presence of CFO) and also computer simulations.

2. A novel block-coherent detector ($\frac{N}{2}$-BLCD) has been proposed, where a block number of $\frac{N}{2}$ shows a better detection performance compared to the ED and the MF in the presence of CFO.

3. Second-order matched filter-I (SOMF-I) and second-order matched filter-II (SOMF-II), are proposed to circumvent the effect of CFO and give a better performance than the ED and the MF in the presence of CFO.

4. The effect of PN has been investigated by simulation on the detection performance of MF, ED, SOMF-II, SOMF-I and $\frac{N}{2}$-BLCD. The simulation results show that the SOMF-II, SOMF-I and $\frac{N}{2}$-BLCD approaches are robust against PN.

2.3 CHAPTER ORGANIZATION

The rest of this Chapter is organized as follows: Section 2.4 introduces the system model. Section 2.5 discusses the performance of both the ED and the MF in the presence of CFO. Section 2.6 analyses the $\frac{N}{2}$-BLCD technique. Section 2.7 presents the two SOMF detectors I and II. In Section 2.8 simulation results are described and finally the chapter is summarized in Section 2.9.

2.4 SYSTEM MODEL

The purpose of spectrum sensing is to inform the secondary user about the existence of the primary user- in other words, to discriminate between two hypotheses, namely: $\mathcal{H}_0$ when the primary user is absent and $\mathcal{H}_1$ when the primary user is present. Thus

$$\begin{aligned} \mathcal{H}_0: \quad x(n) &= \quad w(n) \\ \mathcal{H}_1: \quad x(n) &= \quad As(n)e^{j(2\pi n \triangle f + \varphi(n))} + w(n), \end{aligned} \tag{2.1}$$

where $n = 0, 1, 2, ..., N$; N is the number of samples collected by the secondary user; $x(n)$ is the signal received by the secondary user; $A = |A| e^{j\alpha}$ is the complex

channel gain (which may be assumed constant during the detection interval); $\triangle f$ is the CFO due to the mismatch between the transmitter and the receiver and/or the relative mobility of the receiver; $s(n)$ is the primary signal's known pilot which is deterministic and is known to the secondary user; $w(n)$ is independent identically distributed (*i.i.d.*) circularly symmetric complex Gaussian noise $\mathcal{CN}(0,\sigma_w^2)$; and $\varphi(n)$ is phase noise. The common model for phase noise (PN) is a Wiener random-walk process [49]

$$\varphi(n) = \varphi(n-1) + v(n), \tag{2.2}$$

where $v(n)$ is zero-mean white Gaussian noise with $\left(\mathcal{N}(0,\sigma_n^2)\right)$. Note that $\triangle f$, $|A|$ and α are considered unknown (deterministic) parameters. Finally, the *SNR* at the secondary user is defined as $10\log_{10}\frac{|A|^2P_p}{\sigma_w^2}$, where P_p is the primary user's transmit power.

2.5 CONVENTIONAL DETECTORS

2.5.1 *Energy Detector*

The ED test statistic (T_{ED}) is:

$$T_{ED} = \sum_{n=0}^{N-1} |x(n)|^2 \underset{\mathcal{H}_0}{\overset{\mathcal{H}_1}{\gtrless}} \tau_{ED}, \tag{2.3}$$

where τ_{ED} is a decision threshold used to determine whether the primary user is present or not[1]. It is easily seen that T_{ED} follows a central chi-square distribution with $2N$ degrees of freedom (χ^2_{2N}) under hypothesis $\mathcal{H}_0$. Under hypothesis $\mathcal{H}_1$ it becomes a noncentral chi-square distribution ($\chi^2_{2N}(\beta)$) with $2N$ degrees of freedom with a noncentrality parameter $\beta = \frac{2}{\sigma_w^2}\sum_{n=0}^{N-1}\Big[(A_r s(n))^2 + (A_i s(n))^2\Big]$, where $A = A_r + jA_i$ in (2.1) [16]. The probability density function of T_{ED} after normalizaing by $\frac{\sigma_w^2}{2}$ is given by

1 Decision threshold and sensing threshold are used interchangeably throughout the thesis.

$$f_{T_{ED}}(t) = \begin{cases} \frac{1}{2^N \Gamma(N)} t^{N-1} \exp(-t/2), \; if & \mathcal{H}_0 \\ \frac{1}{2} \left(\frac{t}{\beta}\right)^{\frac{N-1}{2}} \exp(-\frac{\beta+t}{2}) I_{N-1}(\sqrt{2\beta t}), \; if & \mathcal{H}_1 \end{cases}$$

where $I_{N-1}(\sqrt{2\beta t})$ is a modified Bessel function of the first kind [please see [50] equation 8.406.1]. The probabilities of both false alarm (P_{FA}) and detection (P_D) for a given threshold τ_{ED} can easily be shown to be (with or without CFO/PN) **(author?)** [16]:

$$P_{FA} = \text{Prob}\Big\{ T_{ED} > \tau_{ED} \Big| \mathcal{H}_0 \Big\} = Q_{\chi^2_{2N}}\Big(\frac{2\tau_{ED}}{\sigma_w^2}\Big), \tag{2.4}$$

and

$$P_D = \text{Prob}\Big\{ T_{ED} > \tau_{ED} \Big| \mathcal{H}_1 \Big\} = Q_{\chi^2_{2N}(\beta)}\Big(\frac{2\tau_{ED}}{\sigma_w^2}\Big), \tag{2.5}$$

where $Q_{\chi^2_{2N}}(.)$ is the right-tail probability for a χ^2_{2N} random variable and $Q_{\chi^2_{2N}(\beta)}(.)$ is the right tail probability for a $\chi^2_{2N}(\beta)$ random variable [16]. Clearly, (2.4) and (2.5) are not dependent on the CFO and PN. Notice that (2.4) and (2.5) can be written in terms of incomplete Gamma function and Marcum Q-function respectively. Also, the test statistic in (2.3), when N is very large, can be approximated by a Gaussian distribution.

2.5.2 *Matched Filter*

When a MF is employed the test statistic with a decision threshold τ_{MF} is:

$$T_{MF,\text{CFO}} = \Big| \sum_{n=0}^{N-1} x(n) s^*(n) \Big|^2 \underset{\mathcal{H}_0}{\overset{\mathcal{H}_1}{\gtrless}} \tau_{MF}. \tag{2.6}$$

It can be easily shown that ($T_{MF,\text{CFO}}$) follows a central chi-square distribution with 2 degrees of freedom (χ^2_2) under hypothesis $\mathcal{H}_0$. However, under hypothesis $\mathcal{H}_1$ it becomes a noncentral chi-square distribution ($\chi^2_2(\beta')$) with 2 degrees of freedom and a noncentrality parameter **(author?)** [16]

$$\begin{aligned} \beta' = \frac{2|A|^2}{\sum_{n=0}^{N-1} |s(n)|^2 \sigma_w^2} \Big[\Big[\sum_{n=0}^{N-1} |s(n)|^2 \cos(2\pi n \Delta f + \alpha) \Big]^2 \\ + \Big[\sum_{n=0}^{N-1} |s(n)|^2 \sin(2\pi n \Delta f + \alpha) \Big]^2 \Big]. \end{aligned} \tag{2.7}$$

The probabilities of both false alarm and detection can easily be written as

$$P_{FA} = \text{Prob}\left\{ T_{MF,\text{CFO}} > \tau_{MF} \middle| \mathcal{H}_0 \right\} = Q_{\chi_2^2}(\gamma) \tag{2.8}$$

and

$$P_D = \text{Prob}\left\{ T_{MF,\text{CFO}} > \tau_{MF} \middle| \mathcal{H}_1 \right\} = Q_{\chi_2^2(\beta)}(\gamma) \tag{2.9}$$

where $\gamma = \frac{2\tau_{MF}}{\sum_{n=0}^{N-1} |s(n)|^2 \sigma_w^2}$. From (2.8) and (2.9) it is also clear that CFO only affects P_D and not P_{FA}.

2.5.3 *MF performance in the presence of CFO*

Figure 2.1 shows the relationship between $|\triangle f_{Threshold}|$ and N for $P_{FA} = 0.05$. Note that $\pm|\triangle f_{Threshold}|$ represents the two values of CFO such that P_D (of MF) = P_D (of ED) (found by solving the equality between (2.5) and (2.9)) - that is for $|\triangle f| < |\triangle f_{Threshold}|$ the MF outperforms the ED. Note that the region of the graph in Figure 2.1, where the ED exhibits superior performance is greater than the equivalent region where the MF is superior. This is due to the CFO which causes a SNR *degradation* as will be seen next. Section 2.6 will show how to combine the ED and the MF to get another detector called the block-coherent detector ($\frac{N}{2}$-BLCD) that deals with the problem of CFO.

The resulting curve in Figure 2.1 can be interpreted as follows. When $N \geq 1/\overset{*}{\triangle f}$, where $\overset{*}{\triangle f}$ the CFO when $P_D(\text{of MF}) = P_D(\text{of ED})$, the MF detection performance will degrade even if the N has been increased (see Figure 2.4). However, the ED detection performance will improve as N increases. For example, when N=20, the ED outperforms the MF when $\triangle f > 0.05$. Also, when N=100, the ED outperforms the MF when $\triangle f > 0.01$. As a result, the resulting curve is a decreasing function.

2.5.4 *SNR loss of* $T_{MF,\text{CFO}}$

Due to the CFO, the P_D in (2.9) degrades because of the effective loss of SNR within the test statistic expression. This SNR loss (D) of the test statistic in dB can

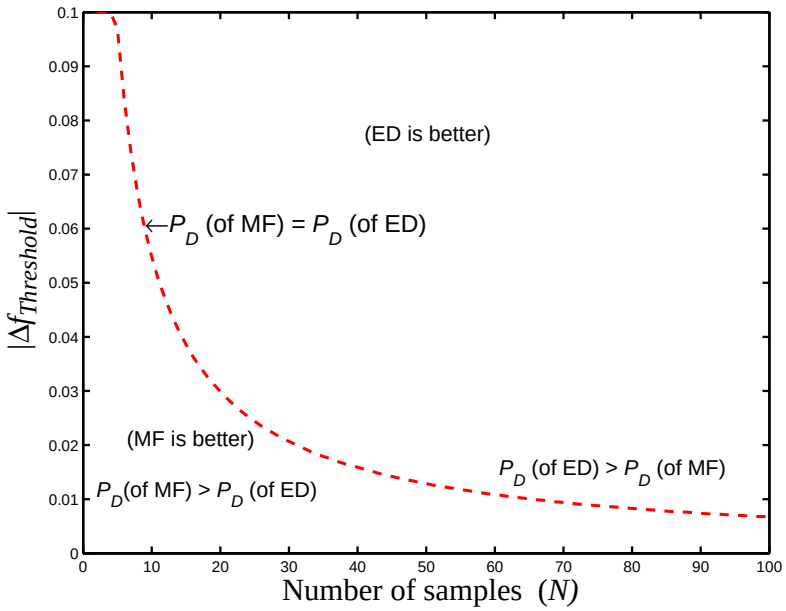

Figure 2.1: $|\triangle f_{Threshold}|$ (found by solving the equality between (2.5) and (2.9)) versus N where $P_{FA} = 0.05$, $SNR = -5$dB and with zero PN.

be defined by the ratio between the useful part of the test statistic in (2.6) (i.e., the part that does not have noise) in the presence of CFO (i.e., $\triangle f \neq 0$) and the useful part in the absence of CFO (i.e., $\triangle f = 0$). Thus

$$\mathrm{D} = \log_{10} \frac{\sin^2(\pi N \triangle f)}{\sin^2(\pi \triangle f)} \quad \text{dB}, \tag{2.10}$$

$s(n) = 1$, $\forall n$ is used in (2.1). By plotting P_D in (2.9) against the received SNR for both (a) CFO present and (b) zero CFO, then it might be supposed that there is a need to increase the received SNR by $|\mathrm{D}|$ dB in (a) to achieve the same P_D performance as in (b). So this SNR increase is defined as $\mathrm{SNR}_{\mathrm{gain}}$ which is the required SNR increase in (a) to maintain the same P_D in (b). This $\mathrm{SNR}_{\mathrm{gain}}$ can be estimated by plotting (a) and (b) via (2.9). Figure 2.2 shows the plot of $(-\mathrm{SNR}_{\mathrm{gain}})$ against $\triangle f$ and also D versus $\triangle f$ (from (2.10)). As expected, both are virtually identical.

We observe in the previous section that the MF performance is affected by the CFO. Therefore, the next sections aim to find solutions to combat the problem of CFO.

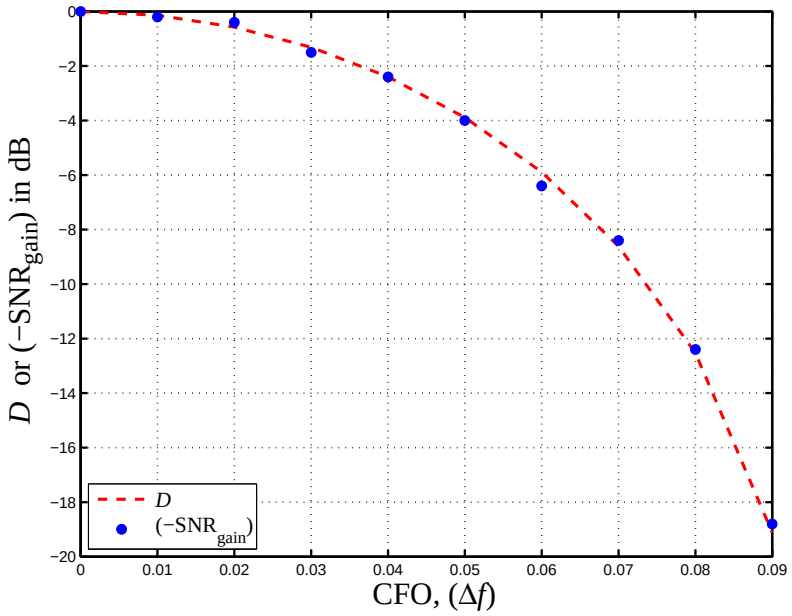

Figure 2.2: Comparison of the effective SNR loss (D, in (2.10)) of the test statistic ($T_{MF,\text{CFO}}$, in (2.6)) and (-SNR_{gain}), defined in subsection (2.5.4), for N=10, $P_{FA} = 0.1$ and with zero PN.

2.6 BLOCK-COHERENT DETECTOR

In order to circumvent the MF's sensitivity to the CFO, a combination of ED and MF is proposed. This new detector is called a block-coherent detector ($\frac{N}{2}$-BLCD), with the $\frac{N}{2}$ term to be explained later. The $\frac{N}{2}$-BLCD test statistic (T_{BLCD}) with a decision threshold τ_{BLCD} is:

$$T_{BLCD} = \sum_{b=0}^{Bl-1} \left| \sum_{m=0}^{K-1} x(m+bK)s^*(m+bK) \right|^2 \underset{\mathcal{H}_0}{\overset{\mathcal{H}_1}{\gtrless}} \tau_{BLCD} \tag{2.11}$$

where Bl is the number of blocks and K is the number of samples per block with $K = N/Bl$. $T_{T_{BLCD}}$ follows a central chi-square distribution with $2Bl$ degrees of freedom (χ^2_{2Bl}) under hypothesis $\mathcal{H}_0$. However, under hypothesis $\mathcal{H}_1$ it becomes a noncentral chi-square distribution ($\chi^2_{2Bl}(\beta)$) with $2Bl$ degrees of freedom and a noncentrality parameter β. Therefore, the P_{FA} and the P_D are given as:

$$P_{FA} = \text{Prob}\left\{ T_{BLCD} > \tau_{BLCD} \middle| \mathcal{H}_0 \right\} = Q_{\chi^2_{2Bl}}(\gamma'), \tag{2.12}$$

and

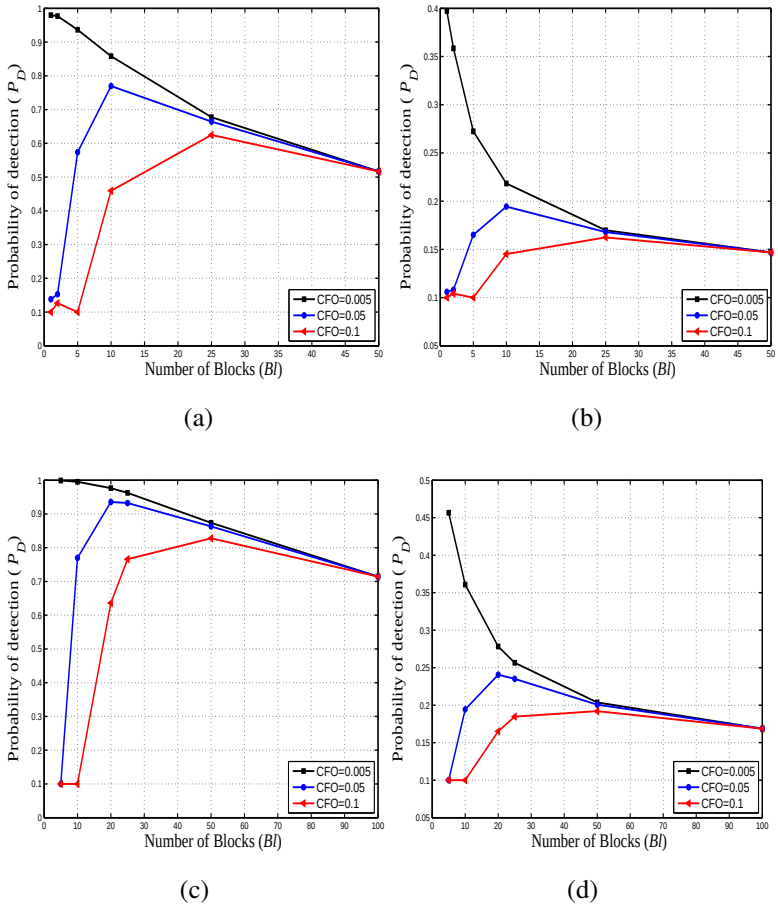

Figure 2.3: P_D versus number of blocks (Bl) (see (2.13), defined in section 2.6). (a) $N = 50$, $P_{FA} = 0.1$ and $SNR = -7$dB. (b) $N = 50$, $P_{FA} = 0.1$ and $SNR = -15$dB. (c) $N = 100$, $P_{FA} = 0.1$ and $SNR = -7$dB. (d) $N = 100$, $P_{FA} = 0.1$ and $SNR = -15$dB.

$$P_D = \text{Prob}\Big\{ T_{BLCD} > \tau_{BLCD} \Big| \mathcal{H}_1 \Big\} = Q_{\chi^2_{2Bl}(\beta)}(\gamma^{'}), \tag{2.13}$$

where $\gamma^{'} = \frac{2\tau_{BLCD}}{\sum_{n=0}^{K-1} |s(n)|^2 \sigma_w^2}$ and a noncentrality parameter

$$\begin{aligned} \beta = C \times \sum_{b=0}^{Bl-1} \Bigg[\Big(\sum_{m=0}^{K-1} s^*(m+bK) \cos(2\pi(m+bK)\Delta f) \Big)^2 \\ + \Big(\sum_{m=0}^{K-1} s^*(m+bK) \sin(2\pi(m+bK)\Delta f) \Big)^2 \Bigg] \end{aligned} \tag{2.14}$$

with $C = \frac{|A|^2}{0.5K\sigma_w^2}$. It is theoretically difficult to find the optimum number of blocks that maximises P_D and so we will use simulation. Without loss of generality, given

that N is an even integer, then it can be observed (as shown in Figure 2.3a) that the optimal number of blocks is $Bl = 1$ for ($N << \frac{1}{\triangle f}$). For other cases ($N >> \frac{1}{\triangle f}$ and $N > \frac{1}{\triangle f}$), however, the optimum number of blocks cannot be found. As a result, a suboptimal number of blocks is proposed, which can be used for any values of N, CFO and SNR. Figure 2.3a shows that a value of $\frac{N}{2}$ is a good candidate. Also, it is clear from Figure 2.3a that $\frac{N}{2}$ is a robust choice for any value of CFO and so it will be called this detector $\frac{N}{2}$-BLCD. Note that the detection performance of the $\frac{N}{2}$-BLCD detector approaches the performance of the ED when B=N. Thus, the $\frac{N}{2}$-BLCD always outperforms the ED. Moreover, From Figures 2.1 and 2.3a we notice that CFO degrades the detection performance of both the MF and the $\frac{N}{2}$-BLCD. This degradation depends on both upon the actual value of CFO ($\triangle f$) and the number of samples taken (N).

Finally, Figures 2.3b, 2.3c and 2.3d represent the detection probability versus the number of blocks for different values of N and SNR. Clearly all figures confirm that although $\frac{N}{2}$ is a suboptimal choice for the number of blocks, it is a reasonable compromise without any a-priori information.

As we have seen that $\frac{N}{2}$-BLCD has improved the performance of the MF when there exists CFO, however, it gives a suboptimal performance. This means that there still remains degrees of freedom to improve the detection performance. Thus, next we seek to develop other detectors that gives better performance compared with $\frac{N}{2}$-BLCD .

2.7 SECOND-ORDER MATCHED FILTER

In this section, two more detectors are proposed that combat the problem of CFO. Here, it is proposed two detectors. The first one is called second-order matched filter-I (SOMF-I). It aims to reduce the effect of N on the performance of a detector in the presence of CFO. The second detector is called second-order matched filter-II (SOMF-II). The goal of this detector to reduce the effects of both CFO and N.

2.7.1 *Second-Order Matched Filter-I*

The SOMF-I test statistic ($T_{\text{SOMF-I}}$) with a decision threshold τ_I is as follows:

$$T_{\text{SOMF-I}} = \text{Real}\Big[\sum_{n=0}^{N-1} s^*(n)s(n-1)x(n)x^*(n-1)\Big] \underset{\mathcal{H}_0}{\overset{\mathcal{H}_1}{\gtrless}} \tau_I. \tag{2.15}$$

It is clear from (2.15), the $x(n)x^*(n-1)$ can mitigate the effect of N. The probabilities of both false alarm (P_{FA}) and detection (P_D) are derived as follows. When the observation interval N is large enough, the test statistic ($T_{\text{SOMF-I}}$) can be approximated as a Gaussian distribution using the central limit theorem [51] where

$$T_{\text{SOMF-I}} \sim N(0, \sigma_0^2), \qquad \text{under } \mathcal{H}_0$$

and

$$T_{\text{SOMF-I}} \sim N(\mu_1, \sigma_1^2), \qquad \text{under } \mathcal{H}_1.$$

To derive the P_{FA} and the P_D, σ_0^2, μ_1, and σ_1^2 have to be calculated:

$$\begin{aligned}\sigma_0^2 &= \mathbb{E}[|T_{\text{SOMF-I}}|^2\big|\mathcal{H}_0] - \mathbb{E}[T_{\text{SOMF-I}}\big|\mathcal{H}_0]^2 \\ &= \mathbb{E}[|T_{\text{SOMF-I}}|^2\big|\mathcal{H}_0].\end{aligned}$$

To derive $\mathbb{E}[|T_{\text{SOMF-I}}|^2\big|\mathcal{H}_0]$, let $w(n) = w_r(n) + jw_i(n)$, then

$$\begin{aligned}T_{\text{SOMF-I}}\big|\mathcal{H}_0 &= \text{Real}\Big[\sum_{n=0}^{N-1} s^*(n)s(n-1)x(n)x^*(n-1)\Big] \\ &= \sum_{n=0}^{N-1} |s(n)||s(n-1)| \\ &\quad \times [w_r(n)w_r(n-1) + w_i(n)w_i(n-1)].\end{aligned}$$

Then

$$\begin{aligned}\sigma_0^2 &= \mathbb{E}[|T_{\text{SOMF-I}}|^2\big|\mathcal{H}_0] \\ &= \sum_{n=0}^{N-1} |s(n)|^2|s(n-1)|^2 \\ &\quad \times [\mathbb{E}[w_r^2(n)]\mathbb{E}[w_r^2(n-1)] + \mathbb{E}[w_i^2(n)]\mathbb{E}[w_i^2(n-1)]] \\ &= 0.5\sigma_w^4 \sum_{n=0}^{N-1} |s(n)|^2|s(n-1)|^2.\end{aligned}$$

If the primary signal is one then $\sigma_0^2 = 0.5N\sigma_w^4$ and μ_1 is calculated as follows:

$$\begin{aligned}\mu_1 &= \mathbb{E}\Big[\text{Real}\Big[\sum_{n=0}^{N-1} s^*(n)s(n-1)x(n)x^*(n-1)\Big]\Big] \\ &= \mathbb{E}\Big[\text{Real}\Big[\sum_{n=0}^{N-1} s^*(n)s(n-1)[As(n)\exp(j2\pi n\triangle f) + w(n)]\Big] \\ &\times [A^*s^*(n-1)\exp(-j2(\pi n-1)\triangle f) + w^*(n-1)]\Big] \\ &= \cos(2\pi\triangle f)|A|^2 \sum_{n=0}^{N-1} |s(n)|^2|s(n-1)|^2.\end{aligned} \tag{2.16}$$

Now σ_1^2 can be computed as follows,

$$\begin{aligned}\sigma_1^2 &= \mathbb{E}[|T_{\text{SOMF-I}}|^2|\mathcal{H}_1] - \mu_1^2 \\ &= 0.5\sigma_w^2|A|^2 \sum_{n=0}^{N-1} |s(n-1)|^4|s(n)|^2 \\ &+ \sigma_w^2|A|^2 \sum_{n=0}^{N-1} |s(n)|^4 \times |s(n-1)|^2 \\ &+ 0.5\sigma_w^2|A|^2 \sum_{n=0}^{N-1} |s(n)|^2 \times |s(n-1)|^4 \\ &+ 0.5\sigma_w^4 \sum_{n=0}^{N-1} |s(n)|^2|s(n-1)|^2.\end{aligned} \tag{2.17}$$

It is evidenced from (2.16) and (2.17), the only parameter that affects on the detection performance is CFO. In fact the N is disjoint from the CFO contrary to the case of MF and $\frac{N}{2}$-BLCD as illustrated in (2.7) and (2.14) respectively. After computing σ_0^2, μ_1, and σ_1^2, the probability of false alarm (P_{FA}) and the probability of detection (P_D) can be written as

$$P_{FA} = \text{Prob}\Big\{T_{\text{SOMF-I}} > \tau_I \big| \mathcal{H}_0\Big\} = Q\Big(\frac{\tau_I}{\sigma_0}\Big) \tag{2.18}$$

and

$$P_D = \text{Prob}\Big\{T_{\text{SOMF-I}} > \tau_I \big| \mathcal{H}_1\Big\} = Q\Big(\frac{\tau_I - \mu_1}{\sigma_1}\Big) \tag{2.19}$$

where $Q(.)$ is the well known Q-function **(author?)** [16].

Figure 2.4 plots P_D against N (for $P_{FA} = 0.1$) for the ED (see (2.5)); the ideal MF (see (2.9)); the $\frac{N}{2}$-BLCD (see (2.13)) and the SOMF-I (see (2.19)). It is clear from Figure 2.4 that SOMF-I has the best detection performance, followed by $\frac{N}{2}$-BLCD.

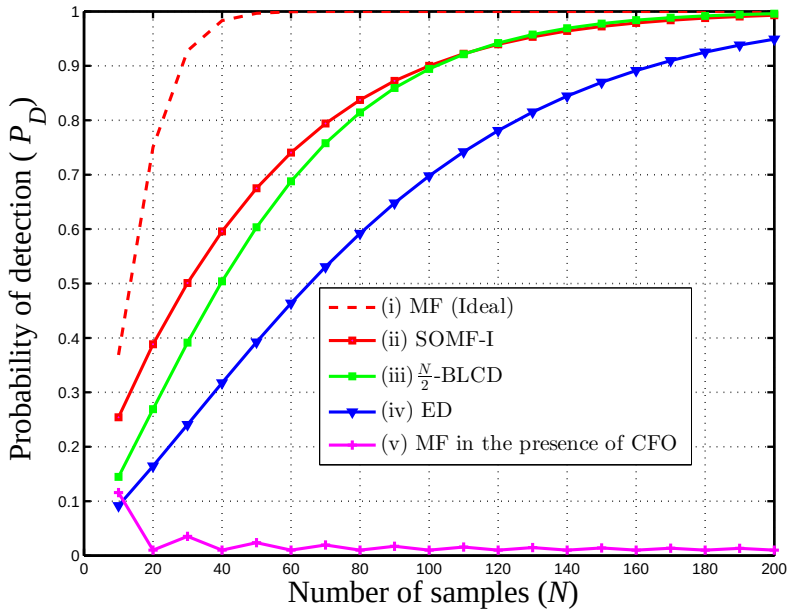

Figure 2.4: P_D versus N: (i) ideal MF (theory - see (2.9) with $\triangle f = 0$), (ii) SOMF-I (theory - see (2.19)) and (iii) $\frac{N}{2}$ -BLCD (theory - see (2.13)), (iv) ED (theory - see (2.5)) and (v) MF in the presence of CFO. In all cases $P_{FA} = 0.1$, $\triangle f = 0.1$ and $SNR = -5$dB.

For all algorithms (except the MF in the presence of CFO) the P_D approaches 1 for large N. Finally, it can be observed that increasing the number of samples (N) does not improve the performance of the MF in the presence of CFO.

In SOMF-I the effect of N has been removed, next we remove the effect of both N and $\triangle f$.

2.7.2 *Second-Order Matched Filter-II*

The SOMF-II detector with a decision threshold τ_{II} has the following test statistic

$$T_{\text{SOMF-II}}(\triangle\hat{f}_0) = \text{Real}\Big[\exp(-j2\pi\triangle\hat{f}_0)\times \sum_{n=0}^{N-1} s(n) \times s^*(n-1)x(n)x^*(n-1)\Big] \underset{\mathcal{H}_0}{\overset{\mathcal{H}_1}{\gtrless}} \tau_{II} \tag{2.20}$$

where $\triangle\hat{f}_0$ is the estimated CFO. By using $\exp(-j2\pi\triangle\hat{f}_0)$ the effect of CFO can be mitigated. The advantage of SOMF-II over the SOMF-I is mitigating the effect

of CFO and N as well. We propose to use $\triangle\hat{f}_0 =$ -0.05, 0 and 0.05 and to choose the maximum value of $T_{SOMF-II}(\triangle\hat{f}_0)$ in (2.20). The idea behind this choice of $\triangle\hat{f}_0$ is as follows. It is well known that the typical values of CFO lie in the range [-0.1,0.1] , so if the value of CFO is small then the appropriate value of $\triangle\hat{f}_0$ is 0. In addition, if the value of the CFO is a large positive or negative value of CFO then the appropriate value of $\triangle\hat{f}_0 =$ is -0.05 or 0.05 respectively.

2.8 SIMULATION RESULTS AND DISCUSSION

In this section some simulations (based on (2.3), (2.11), (2.15) and (2.20)) are compared against theoretical results (based on (2.4), (2.5), (2.8), (2.9), (2.12), (2.13), (2.18), and (2.19)) to illustrate the detection performance of ED, MF, $\frac{N}{2}$-BLCD, SOMF-I and SOMF-II in the presence of CFO and PN. The CFO $(\triangle f)$ is randomly generated from a uniform distribution over $[-0.1, 0.1]$ and is kept constant during all 10^5 Monte Carlo iterations for each SNR value. For the sake of simplicity, the primary user signal is assumed to be $\{s(n)\}_{n=0}^{N-1} = \{1, 1, ..., 1\}$. The phase noise parameter (σ_n^2 in (2.2)) that has been used is for the worst scenario and is $\sigma_n^2 = 0.011$ [49]. The absolute channel gain $|A|$ and phase α are chosen as unknown (deterministic) constants and kept fixed during the Monte Carlo simulations. First we start our simulation results to confirm the theoretical derivations that have been done throughout the chapter.

Result 1: Theoretical results verifications for detection performance (Figures 2.5 and 2.6)**.**

Figures 2.5 and 2.6 clearly show that the theoretical and the simulation results for $\frac{N}{2}$-BLCD and SOMF-I are identical respectively. Next we show the effect of the PN on the proposed detectors.

Result 2: P_D versus P_{FA} in the absence and presence of phase noise (Figures 2.7, 2.8, 2.9, 2.10 and 2.11)**.**

First from Figure 2.7, it is easily seen that the PN slightly affects the MF detection performance. However, Figures 2.8, 2.9, 2.10 and 2.11 show that the three proposed detectors ($\frac{N}{2}$-BLCD, SOMF-I, SOMF-II) and ED are not affected by the PN.

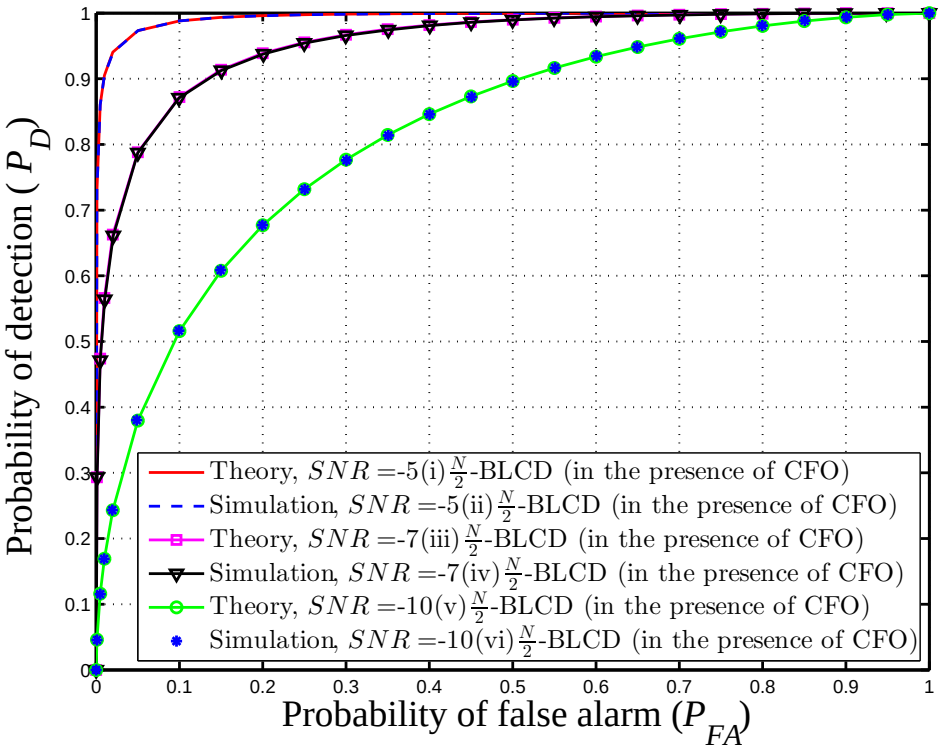

Figure 2.5: The probability of detection versus the probability of false alarm for $\frac{N}{2}$-BLCD for different values of SNR (theory - see (2.12) and (2.13), simulation - see (2.11)). In all cases, $N = 100$, $\Delta f = 0.02$ and with zero PN.

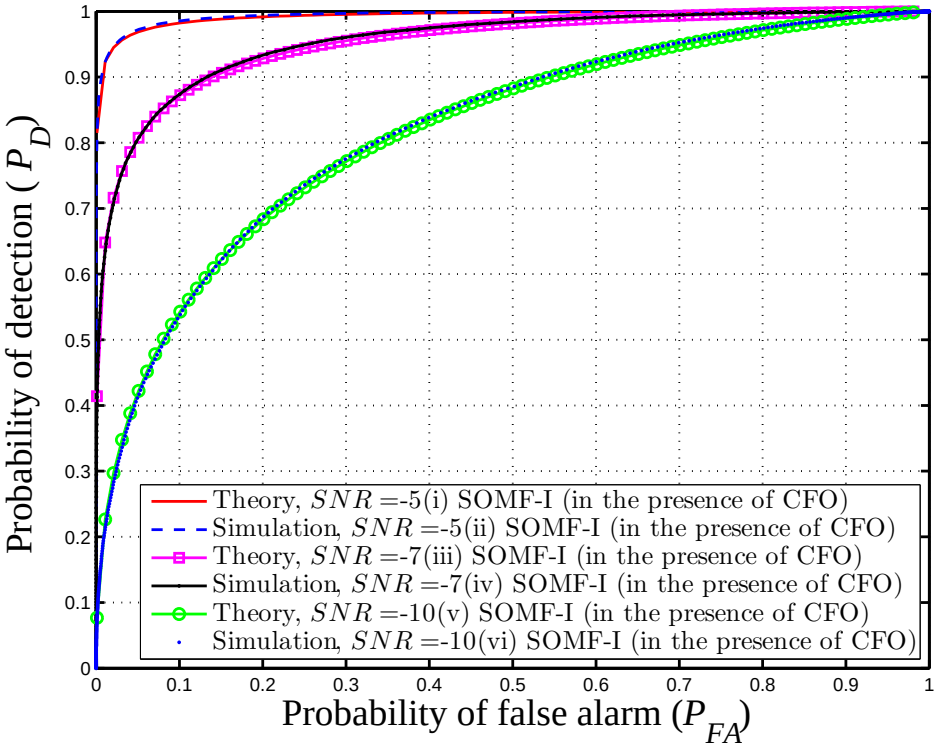

Figure 2.6: The probability of detection versus the probability of false alarm for SOMF-I for different values of SNR (theory - see (2.18) and (2.19), simulation - see (2.15)). In all cases, $N = 100$, $\Delta f = 0.02$ and with zero PN.

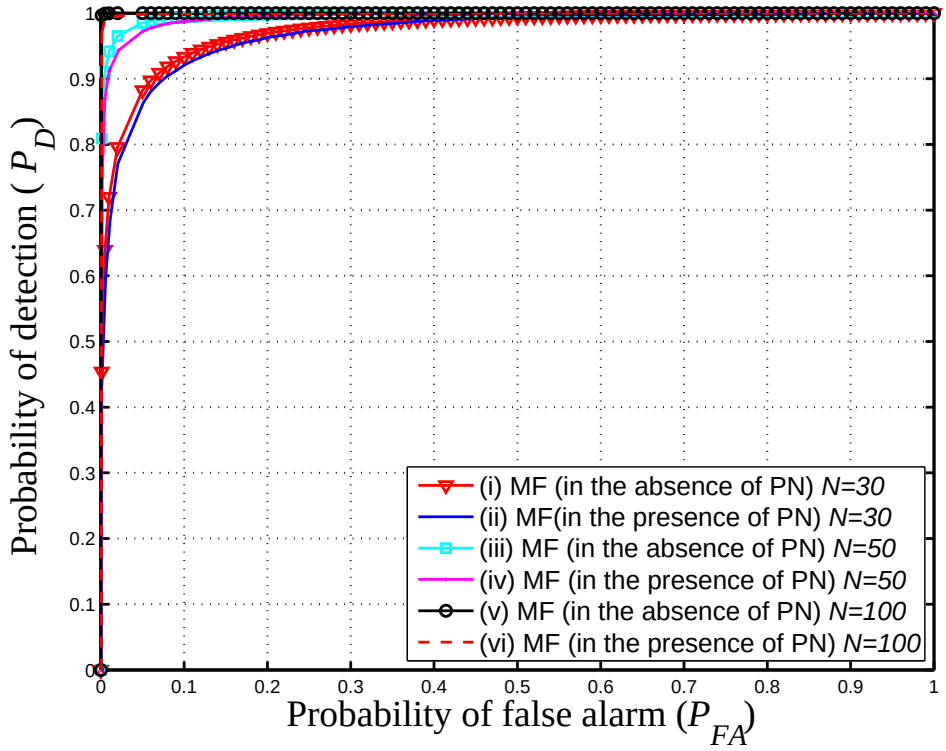

Figure 2.7: The probability of detection versus the probability of false alarm in the absence and the presence of PN for MF for different values of N. In all cases, $\Delta f = 0$ and $SNR = -7$dB.

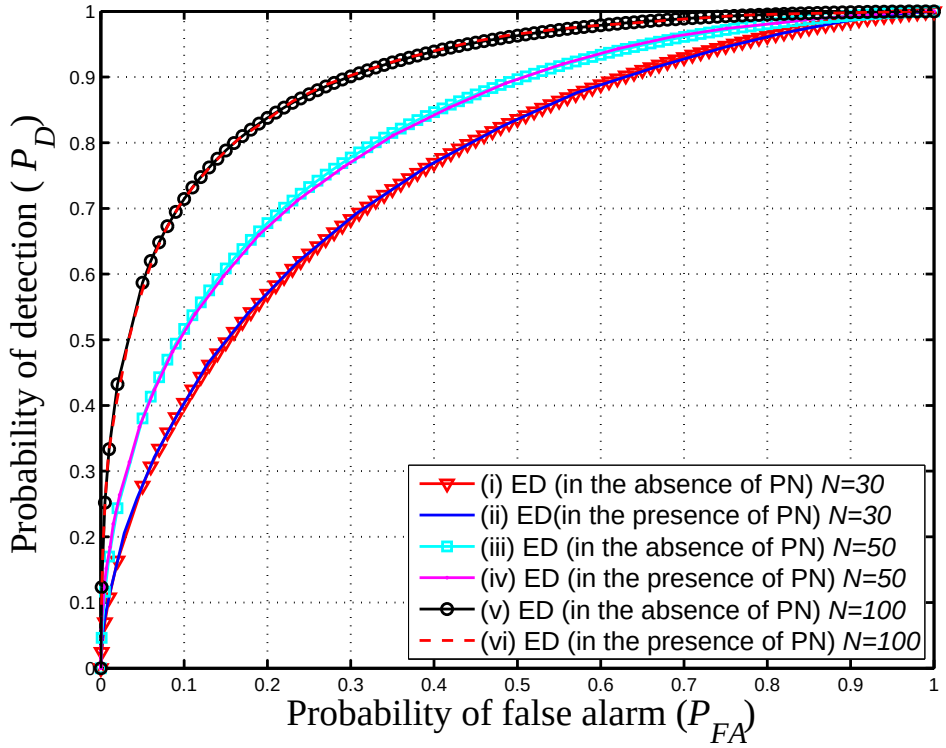

Figure 2.8: The probability of detection versus the probability of false alarm in the absence and the presence of PN for ED for different values of N. In all cases, $\Delta f = 0$, $\sigma_n^2 = 0.011$ and $SNR = -7$dB.

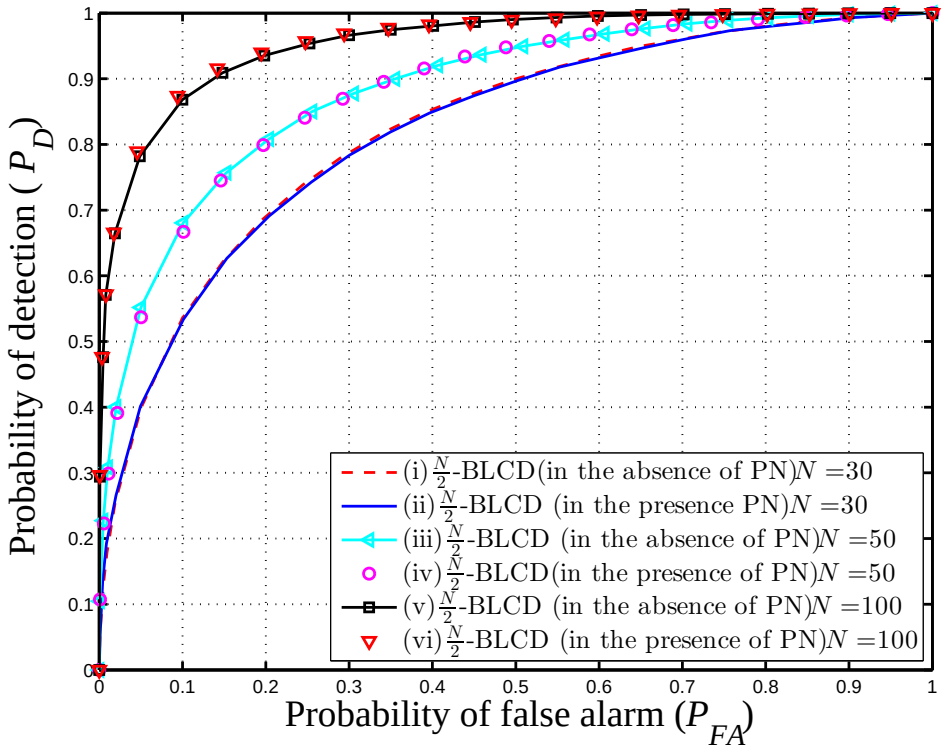

Figure 2.9: The probability of detection versus the probability of false alarm in the absence and the presence of PN for $\frac{N}{2}$-BLCD for different values of N. In all cases, $\Delta f = 0$, $\sigma_n^2 = 0.011$ and $SNR = -7$dB.

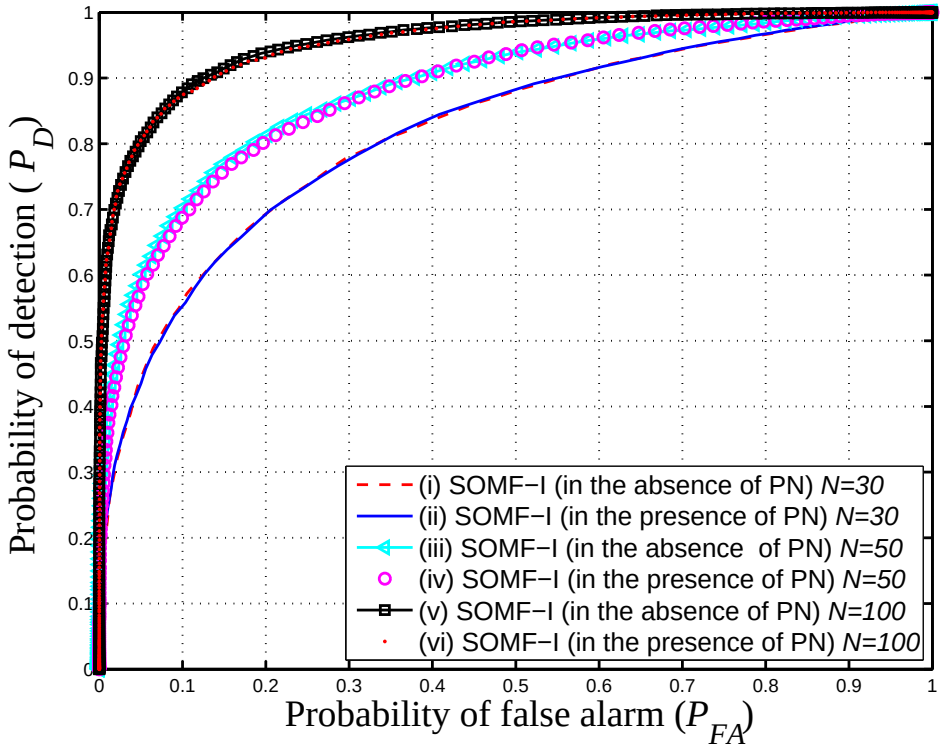

Figure 2.10: The probability of detection versus the probability of false alarm in the absence and the presence of PN for SOMF-I for different values of N. In all cases, $\Delta f = 0$, $\sigma_n^2 = 0.011$ and $SNR = -7$dB.

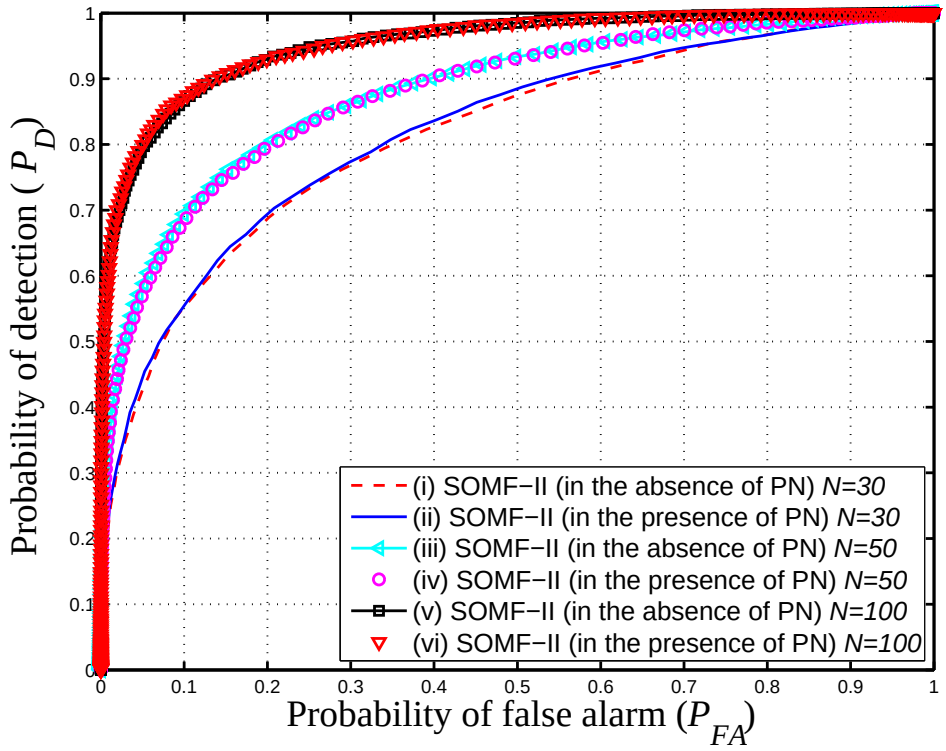

Figure 2.11: The probability of detection versus the probability of false alarm in the absence and the presence of PN for SOMF-II for different values of N. In all cases, $\Delta f = 0$, $\sigma_n^2 = 0.011$ and $SNR = -7$dB.

Result 3: P_D versus P_{FA} comparison between SOMF-II, SOMF-I, $\frac{N}{2}$-BLCD, and ED (Figure **2.12**)**.**

Figure 2.12 shows the detection performance for the proposed techniques $\frac{N}{2}$-BLCD, SOMF-I and SOMF-II. Also, this figure plots P_D against P_{FA} for the ED, the MF in both the ideal case and in the presence of CFO. It is obvious that SOMF-II has the best detection performance compared with the other techniques, except for the ideal MF. We also notice that the gap between SOMF-II and SOMF-I is smaller than that between SOMF-II and $\frac{N}{2}$-BLCD. The next figure Figure (2.13) shows the difference between the proposed techniques for different values of CFO and at low false alarm probability.

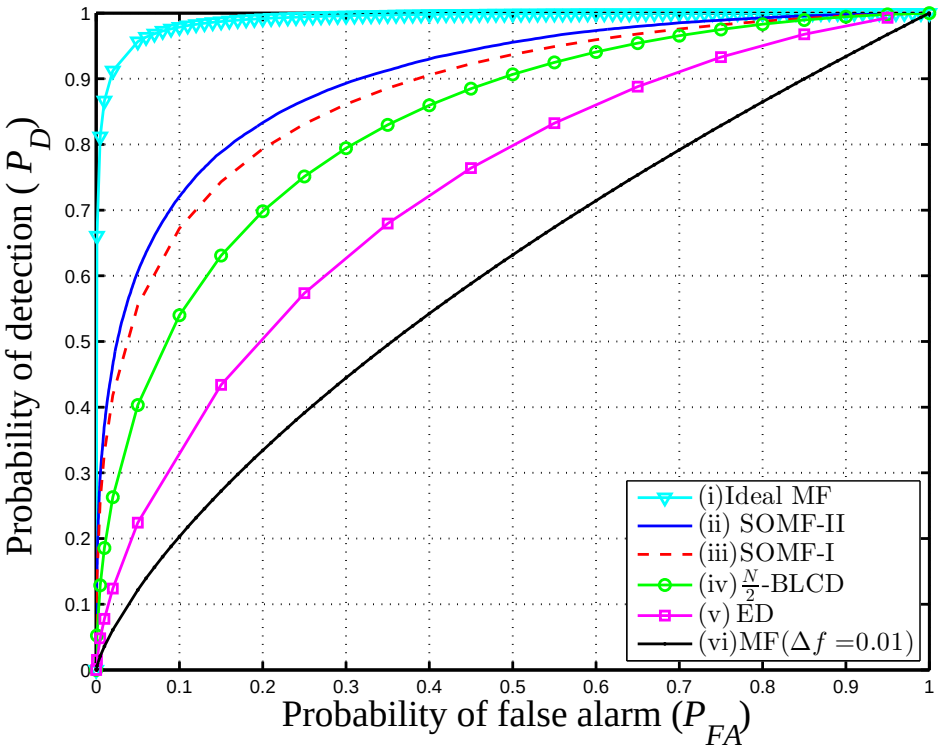

Figure 2.12: The probability of detection versus the probability of false alarm for $\frac{N}{2}$-BLCD, SOMF-I and SOMF-II. In all cases $N = 250$, $SNR = -10$dB and $\Delta f = 0.1$ and with zero PN. Notice that all detectors are analytically plotted except SOMF-II.

Result 4: P_D versus $\triangle f$ (Figure 2.13).

Figure 2.13 illustrates the relationship between P_D and CFO for the ED, MF, $\frac{N}{2}$-BLCD, SOMF-I and the SOMF-II. First, it can be seen that the CFO is more harmful on the MF compared with PN (see - Figure 2.7) and there are small ranges of the CFO where the MF is superior. Moreover, $\frac{N}{2}$-BLCD, SOMF-I and SOMF-II are less sensitive to CFO. Furthermore, it can be seen that at high CFO the detection performance difference between SOMF-I and $\frac{N}{2}$-BLCD is very small. Finally, it can be seen the detection difference between $\frac{N}{2}$-BLCD, SOMF-I and SOMF-II increases as the CFO increases.

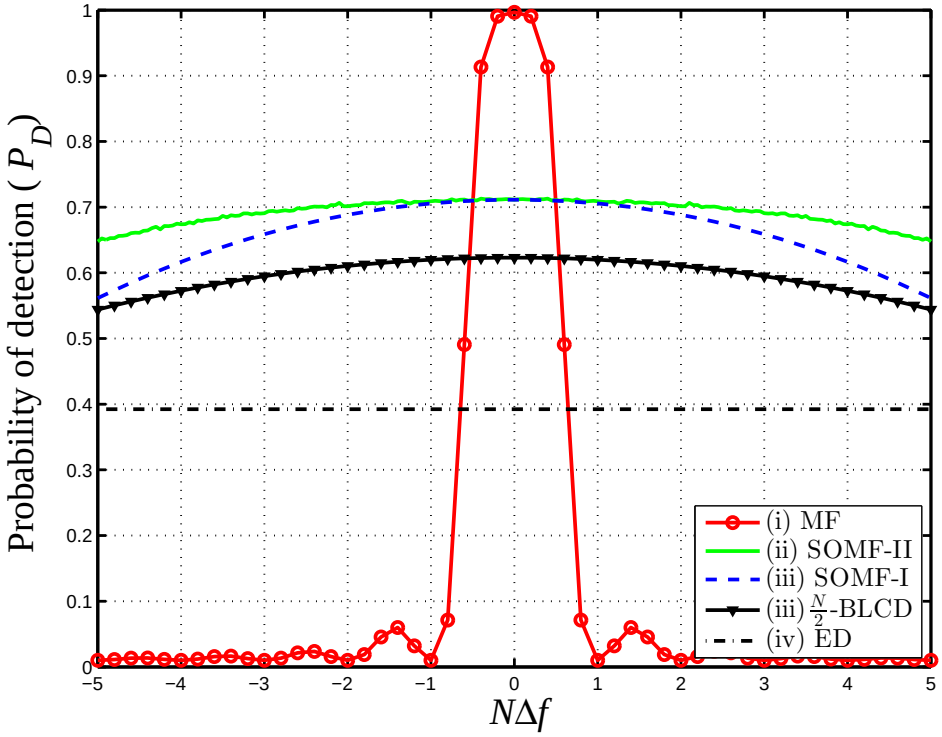

Figure 2.13: P_D versus $\triangle f$: (i) MF (theory - see (2.9)), (ii) SOMF-I (theory - see (2.19)), (iii) ED (theory - see (2.5)), (iv) SOMF-II (simulation - see (2.20)) and (v) $\frac{N}{2}$-BLCD. In all cases $P_{FA} = 0.01$, $SNR = -5$dB, N=50 and with zero PN.

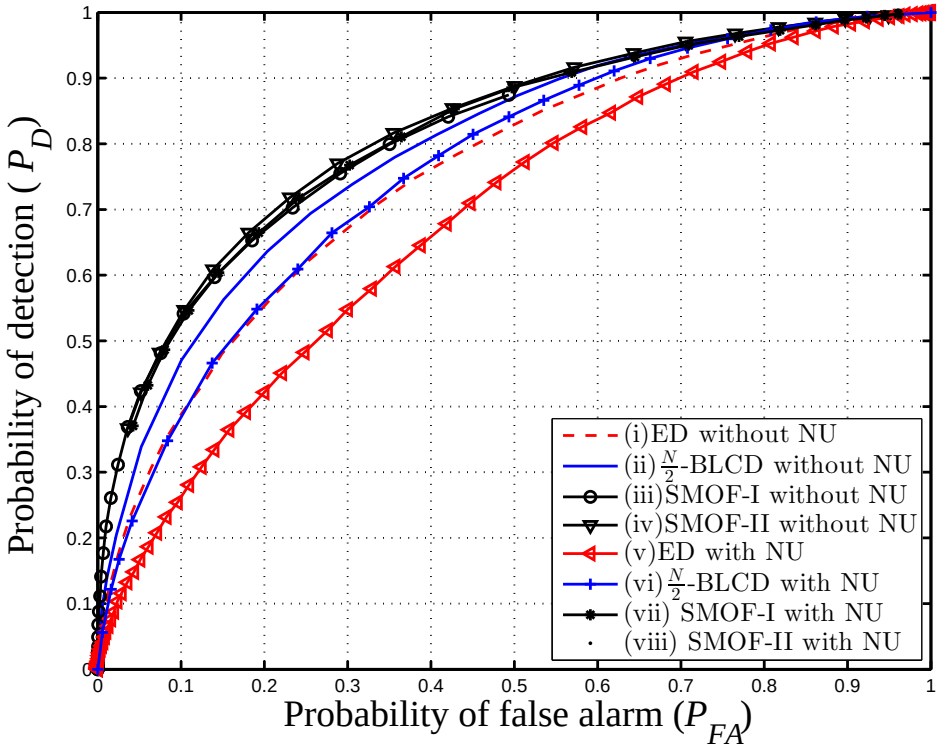

Figure 2.14: The detection probability versus the false alarm probability for the ED, $\frac{N}{2}$-BLCD, SOMF-I and SOMF-II in the presence of NU. In all cases, N=100, SNR=-10dB and B=0.65dB.

Result 5: P_D versus P_{FA} in the presence of NU (Figure 2.14**).**

This figure evaluates (by simulation) the detection performance of the ED, $\frac{N}{2}$-BLCD, SOMF-I and SOMF-II in the presence of NU. The NU has been generated according to the p.d.f. defined in (5.6). Finally, it is shown that the SOMF-I and SOMF-II are insensitive to the NU and the $\frac{N}{2}$-BLCD degrades due to the NU but its performance is still better than that of the ED without NU.

2.9 CHAPTER SUMMARY

Both CFO and PN deteriorate the detection performance of the MF in spectrum sensing. To start with, the performance of the MF was tested in the presence of CFO in order to determine over what range of CFO the MF still outperforms the ED. Three new techniques have been proposed to mitigate the effect of CFO and PN (the simulation results show that the three proposed detectors are insensitive to phase noise). Firstly, the $\frac{N}{2}$-BLCD algorithm was considered. It can be employed for any value of CFO and any number of samples of the received signal, and the detection performance has been theoretically derived. Secondly, the SOMF-I approach is examined. It is robust to the presence of CFO and PN when compared with the MF, and its detection performance has been analytically derived. Thirdly, SOMF-II is a modified version of SOMF-I and it has the best performance when compared with $\frac{N}{2}$-BLCD and SOMF-I. The investigation of SOMF-II has been only conducted by the simulation. Finally, we conclude that the SOMF-II is the best detector in terms of the detection performance and that it comes at great cost, the cost of complexity.

3

PERFORMANCE ANALYSIS OF ENERGY DETECTOR OVER A NAKAGMI FREQUENCY-SELECTIVE (NFS) CHANNEL

3.1 INTRODUCTION

The study in the previous chapter was based on the assumption that the primary user's signal is deterministic and is known to the secondary user. In reality, in most of the cases the primary signal contains information that is random in nature. Thus, it is more realistic to assume that the primary signal appears random for the secondary user instead of deterministic, and that is what is considered in this chapter. In spectrum sensing of cognitive radio networks, the secondary user either does not have a-priori knowledge or has some information (e.g., modulation scheme used) about the primary signal. Indeed, the transmitted primary signal may have different possible waveforms with random data sequences. When the signal has an unknown form, the plausible assumption is to consider the signal as a random process. So, the samples of the transmitted signal constitute an independent and identically random process (i.i.d.) with zero mean and variance $\mathbb{E}[|s(n)|^2] = P_p$. For this scenario, the ED is optimal for detecting the primary user's signal [16].

This chapter aims to study two important parameters in spectrum sensing of cognitive radio networks. Firstly, we analytically investigate the performance of the ED over a Nakagami-*m* frequency-selective channel (NFS). Secondly, we find a closed form expression for the minimum number of samples required to satisfy a target false alarm probability (ϵ) and a target detection probability (δ) over an NFS channel.

To the best of authors' knowledge, the analytical detection performance of the ED over an NFS channel has not previously been examined. In addition, the minimum number of samples that satisfy ϵ and δ over an NFS channel has also not been investigated.

3.1.1 *Literature Review and Motivation*

3.1.1.1 *Detection Performance for an Energy Detector*

The first part of this literature review deals with the detection performance of the ED over different environments. In [52], the authors reviewed the ED for an unknown deterministic signal over a Gaussian channel. The distribution of a test/decision statistic when the primary user is absent is formulated as a central chi-squar distribution and when the primary user is present it is formulated as a non-central chi-square distribution. Subsequently the detection probability and the false alarm probability are also derived.

Motivated by the above research, more papers have appeared on investigating the behavior of the ED over different fading channels scenarios. For example, in [22] the authors derived closed-form expressions for the average detection probability over Rayleigh, Rician, and Nakagami fading channels. The derivation was based on the probability density function approach, in which the Marcum Q-function[1] (representing the detection probability over AWGN channels) is integrated over the probability density function of the signal to noise ratio. The analytical expression of the false alarm probability is the same as [52] because it does not depend on the channel (the test/decision statistic has only the noise component). In [54] the behavior of an ED was investigated under the $\eta - \mu$ fading channel model [2]. In [55], the average detection probability was derived using the moment-generating function method. This direction was pursued to overcome the analytical difficulties that arise

1 Derivations executed based on Marcum Q-function properties in [53].

2 The $\eta - \mu$ distribution is a more general physical fading model, which represents one-sided Gaussian, Rayleigh, Nakagami-m and Hoyt (Nakagami-q) distributions by changing the parameters η and μ.

from the presence of the Marcum Q-function. In [23], the performance of the ED over generalized $\kappa - \mu$ and $\kappa - \mu$ extreme fading channels has been investigated[3]. In [56], an analytical performance for the ED was obtained over wireless channels with composite multipath fading and shadowing effects.

Other work in the literature approximates the distribution of test/decision statistic, under the presence and the absence of the primary user, by a Gaussian distribution [19, 51, 57] for different kind of primary user waveforms such as unknown deterministic and random signals. Accordingly, the false alarm and detection probabilities are found theoretically in terms of the Q-function and this assumption comes from the central limit theorem. The assumption of a Gaussian model is well known in the parameter optimization problems, e.g., optimizing the operating sensing threshold that satisfies δ (i.e., when the throughput is evaluated) and the minimum number of the samples required to achieve a desired receiver operating characteristic (ROC). This model often gives a simple solution for a corresponding sensing threshold of δ compared to the Marcum Q-function, which needs an iterative algorithm to find the sensing threshold.

From the above literature review, it appears that most research concentrates on the flat fading channel case. However, this is not always so in practice. Indeed in many instances, the secondary user's received signal may experience a frequency-selective channel because the primary system technology, in most cases, employs a high data rate transmission. As such, a more appropriate and practical assumption is to consider a frequency-selective channel.

A small numbers of papers deal with spectrum sensing over frequency-selective channels. In [58] the authors proposed an optimal detector for use in multipath fading that requires knowledge of the finite impulse response (FIR) of the channel. This proposed detector was compared with an ED and it was shown that for the same detection performance the ED requires no more than twice the number of samples that was needed for the proposed detector when there exists a large channel length.

3 The $\kappa - \mu$ distribution is a generalized fading model that models multipath fading, in particular for line-of-sight communication systems. Also, it includes as special cases Rician, Nakagami-m, Rayleigh, and one-sided Gaussian distributions.

In [59, 60], the authors studied the multi-antenna spectrum sensing for a modified ED and an equal gain detector when there is a correlation between the channel taps and a spatial correlation between the antennas. The simulation results showed that if the primary signal is correlated, then the channel tap correlation will improve the sensing detection performance. In [61], the authors studied the effect of frequency-selective reporting channels on the cooperative spectrum sensing using a widely linear scheme and a linear one. The average detection probability at the fusion center is obtained only by simulations.

3.1.1.2 *Minimum Number of Samples for an Energy Detector*

The second part of this literature review deals with the number of samples that permits the ED to achieve a desired receiver operating characteristic (ROC). In cognitive radio, the secondary user should determine the minimum number of samples that satisfies a desired ROC (ϵ and δ). In the literature, this parameter (the minimum number of samples that satisfies a desired ROC) has only been derived for AWGN channels [19, 57]. Over fading channels however, there is no a closed-form expression or any simulation result for finding this minimum number of samples.

3.2 CHAPTER CONTRIBUTION

The two main aims of this chapter are investigating the detection performance of the ED over NFS channel and determining the minimum number of samples that satisfies a desired ED performance (ϵ and δ) over an NFS channel. This investigation has been achieved through the following contributions.

1. Analytically evaluating the average detection probability for the ED over an NFS channel. Also, the theoretical results are validated by simulation.

2. Examining theoretically the outage detection probability for the ED over an NFS channel, which is also confirmed by simulation[4].

3. Finding the minimum required number of samples that satisfies ϵ, δ and the outage detection probability is derived mathematically over an NFS channel.

3.3 CHAPTER ORGANIZATION

The rest of this chapter is organized as follows. The system model is introduced in Section 3.4. Spectrum sensing using the ED is presented in Section 3.5. The average probability of detection over NFS is examined in Section 3.6. The outage probability analysis is presented in Section 3.7. Simulation results and discussion are described in Section 3.8. Finally, Section 3.9 summarizes the chapter.

3.4 SYSTEM MODEL

3.4.1 *Primary signal*

Based on the recent paper [62], the performance of the ED can be described mathematically by a Marcum-Q function or a Gaussian distribution using the central limit theorem for large N only when the primary user's signal is unknown deterministic signal, a Gaussian random process (this assumption is valid when the secondary user does not have any information about the primary user's signal) or M-ary Phase Shift Keying (PSK) signal. In this chapter, it is assumed that the secondary user knows the modulation scheme (PSK) that primary user employs.

4 Outage detection probability has an advantage over the average detection probability in finding some spectrum sensing parameters such as the sensing threshold value and the minimum number of samples. Also, an exact closed-form expression can be found compared with the average detection probability. Finally, it is another metric that can confirm the results obtained by the average detection probability.

3.4.2 *Channel Model*

A NFS channel is assumed between the primary user transmitter and the secondary user transmitter and is modeled as an FIR filter with impulse response $\mathrm{h} = [h_0\ h_1\ h_2\ ...\ h_{L-1}]^T$, whose taps are i.i.d. In this work, it is assumed two different models for the power delay profile of h. In the first model, we assume that the channel has an exponential power delay profile. In the second model, it is assumed to have a uniform power delay profile in which all taps have the same power. The latter model is used to more clearly highlight the ED advantages that might be obtained due to the NFS channel (see section 3.7). Also, in both models the power of the channel taps is normalised such that $\sum_{l=0}^{L-1} \mathbb{E}|h_l|^2 = 1$.

Under the exponential model, the probability density function (p.d.f.) of amplitude for each channel tap coefficient, $|h_l|$, is given by

$$f_{|h_l|}(z) = \frac{2}{\Gamma(m)} \left(\frac{m}{\Omega_{h_l}} \right)^m z^{2m-1} \exp\left(\frac{-mz^2}{\Omega_{h_l}}\right), \tag{3.1}$$

where $\Omega_{h_l} = \mathbb{E}[|h_l|^2]$ is a controlling spread parameter for the l-th tap, m is the Nakagami-m fading parameter for the l-th tap and $\Gamma(m) = \int_0^\infty t^{m-1} e^{-t} dt$ is the Gamma function. The Nakagami distribution is selected to model a fading channel since it is reported to accurately fit to most empirical and experimental results [63]. As special cases, for m = 1, the distribution reduces to Rayleigh fading; for $m = \frac{(v+1)^2}{(2v+1)}$ the distribution is approximately Rician with parameter v; and for $m = \infty$ there is no fading [64].

3.4.3 *Received signal*

We have again two hypotheses:

$$\begin{aligned} \mathcal{H}_0 :&\quad x(n) = w(n), \\ \mathcal{H}_1 :&\quad x(n) = \sum_{l=0}^{L-1} h_l s(n-l) + w(n), \end{aligned} \tag{3.2}$$

where $n = 0, 1, 2, ..., N-1$, and N is the number of samples collected by the secondary user; $x(n)$ is the signal received by the secondary user; $s(n)$ is the primary signal which is randomly and independently drawn from a complex constellation with power P_p and $w(n)$ represents independent and identically distributed circularly symmetric complex Gaussian noise with distribution $\mathcal{CN}(0, \sigma_w^2)$, where σ_w^2 is the noise power. Finally the instantaneous signal to noise ratio at the secondary user is $\gamma = \frac{P_p}{\sigma_w^2} \sum_{l=0}^{L-1} |h_l|^2$ and the average signal to noise ratio as $\gamma_{ave} = \frac{P_p}{\sigma_w^2} \sum_{l=0}^{L-1} \mathbb{E}|h_l|^2$.

3.5 ENERGY DETECTOR FOR SPECTRUM SENSING

The test statistic when the secondary user implements an ED is given by:

$$T_{ED} = \frac{1}{N} \sum_{n=0}^{N-1} |x(n)|^2 \underset{\mathcal{H}_0}{\overset{\mathcal{H}_1}{\gtrless}} \tau_{ED}. \tag{3.3}$$

Notice that (unlike (2.3)) the test statistic in (3.3) is divided by N but this does not change the ED performance. The sensing threshold (τ_{ED}) is used to determine whether the primary user is present $(T_{ED} \geq \tau_{ED})$ or not $(T_{ED} < \tau_{ED})$. Although T_{ED} has a chi-square distribution, according to the central limit theorem T_{ED} is asymptotically normally distributed if N is large enough [51]. Specifically, for large N, the test statistics of T_{ED} can be modeled as follows:

$$T_{ED} \sim \begin{cases} \mathcal{N}(\mu_0, \sigma_0^2), \text{ under } \mathcal{H}_0 \\ \mathcal{N}(\mu_1, \sigma_1^2), \text{ under } \mathcal{H}_1. \end{cases}$$

Now to derive P_{FA} and P_D, then μ_0, σ_0^2, μ_1 and σ_1^2 are calculated as follows:

$$\mu_0 = \mathbb{E}[T_{ED}|\mathcal{H}_0] = \frac{1}{N}\mathbb{E}\big[\sum_{n=0}^{N-1} |w(n)|^2\big] = \sigma_w^2 \tag{3.4}$$

and

$$\sigma_0^2 = \mathbb{E}[T_{ED}^2|\mathcal{H}_0] - \mu_0^2 = \frac{\sigma_w^4}{N}. \tag{3.5}$$

The mean (μ_1) and the variance (σ_1^2) under $\mathcal{H}_1$ are calculated, conditioned on the channel, as follows. For simplicity, let us define the following variables,

$$\begin{aligned} a_n &= \sum_{l=0}^{L-1} h_l s(n-l) \\ a_m &= \sum_{l=0}^{L-1} h_l s(m-l) \\ a_{n1} &= a_n w^*(n) + w(n) a_n^* \\ a_{m1} &= a_m w^*(m) + w(m) a_m^*. \end{aligned}$$

Thus

$$\begin{aligned} \mu_1 = \mathbb{E}[T_{ED}|\mathcal{H}_1] &= \frac{1}{N}\mathbb{E}\big[\sum_{n=0}^{N-1} |a_n + w(n)|^2\big] \\ &= \frac{1}{N}\sum_{n=0}^{N-1}\big[\mathbb{E}|a_n|^2 + \mathbb{E}|w(n)|^2 + \mathbb{E}[a_{n1}]\big] \\ &= \sigma_w^2 + P_p \sum_{l=0}^{L-1} |h_l|^2, \end{aligned} \tag{3.6}$$

and

$$\sigma_1^2 = \mathbb{E}[T_{ED}^2|\mathcal{H}_1] - \mu_1^2, \tag{3.7}$$

where

$$\mu_1^2 = \sigma_w^4 + P_p^2 \sum_{l=0}^{L-1} |h_l|^4 + P_p^2 \sum_{\substack{l_1 \& l_2 = 0 \\ l_1 \neq l_2}}^{L-1} |h_{l_1}|^2 |h_{l_2}|^2 + 2P_p\sigma_w^2 \sum_{l=0}^{L-1} |h_l|^2 \tag{3.8}$$

and

$$\begin{aligned} \mathbb{E}[T_{ED}^2|\mathcal{H}_1] &= \frac{1}{N^2}\sum_{m=0}^{N-1}\sum_{n=0}^{N-1} \mathbb{E}\big[|a_n + w(n)|^2 |a_m + w(m)|^2\big] \\ &= \frac{1}{N^2}\sum_{m=0}^{N-1}\sum_{n=0}^{N-1} \mathbb{E}\big[[|a_n|^2 + |w(n)|^2 + a_{n1}] \\ &\quad \times [|a_m|^2 + |w(m)|^2 + a_{m1}]\big] \end{aligned} \tag{3.9}$$

$$\begin{aligned}\mathbb{E}[T_{ED}^2|\mathcal{H}_1] = \frac{1}{N^2}\sum_{m=0}^{N-1}\sum_{n=0}^{N-1}\mathbb{E}\big[&|a_n|^2|a_m|^2 + |w(n)|^2|w(m)|^2 \\ &+ a_{n1}a_{m1} + |a_n|^2|w(m)|^2 + |a_n|^2 a_{m1} + |w(n)|^2|a_m|^2 \\ &+ |w(n)|^2 a_{m1} + a_{n1}|a_m|^2 + a_{n1}|w(m)|^2\big] \\ &= P_p^2\sum_{l=0}^{L-1}|h_l|^4 + (1+\frac{1}{N})P_p^2\sum_{\substack{l_1,l_2=0\\ l_1\neq l_2}}^{L-1}|h_{l_1}|^2|h_{l_2}|^2 + \sigma_w^4 \\ &+ \frac{\sigma_w^4}{N} + \frac{2P_p\sigma_w^2}{N}\sum_{l=0}^{L-1}|h_l|^2 + 2P_p\sigma_w^2\sum_{l=0}^{L-1}|h_l|^2.\end{aligned}$$

By substituting (3.8) and (3.9) into (3.7), then

$$\sigma_1^2 = \frac{\sigma_w^4}{N} + \frac{P_p^2}{N}\sum_{\substack{l_1,l_2=0\\ l_1\neq l_2}}^{L-1}|h_{l_1}|^2|h_{l_2}|^2 + \frac{2P_p\sigma_w^2}{N}\sum_{l=0}^{L-1}|h_l|^2. \tag{3.10}$$

Therefore, the false alarm probability and the detection probability, conditioned on the channel, are given as:

$$P_{FA} = \text{Prob}\Big\{T_{ED} > \tau_{ED}\Big|\mathcal{H}_0\Big\} = Q\Big(\frac{1}{\sqrt{N}}(\frac{\tau_{ED}}{\sigma_w^2} - N)\Big), \tag{3.11}$$

$$P_D = \text{Prob}\Big\{T_{ED} > \tau_{ED}\Big|\mathcal{H}_0\Big\} = Q\left(\frac{\tau_{ED}-\mu_1}{\sigma_1}\right), \tag{3.12}$$

where $Q(.)$ is the Q-function **(author?)** [16]. Here the Gaussian distribution approximation is used instead of the chi-square distribution for the following reasons:

- The simplicity of evaluating the detection performance of the ED over the NFS channel.
- It simplifies the calculation of the minimum number of samples that satisfies ϵ and δ through the outage detection probability as will be seen in section (3.7.2).
- It simplifies the secondary user's throughput analysis, as will be seen in chapter 5.

3.6 AVERAGE DETECTION PROBABILITY DERIVATION

The average P_{FA} (i.e., $\overline{P}_{FA}$) does not depend on the channel (as the received signal has only noise component) and so it is identical to (3.11). A closed-form expression for the average detection probability ($\overline{P}_D$) over an NFS channel can be calculated as follows. To guarantee a cognitive radio works in practice, the analysis might be interested in the worst case of a low signal to noise ratio (SNR) regime. For low SNR (see (3.10)) the variance (σ_1^2) of T_{ED} under $\mathcal{H}_1$, can be approximated as:

$$\sigma_1^2 \approx \frac{\sigma_w^4}{N} + \frac{2P_p\sigma_w^2}{N}\sum_{l=0}^{L-1}|h_l|^2. \tag{3.13}$$

Then from (3.6), (3.12) and (3.13) we have

$$P_D = Q\left(\frac{\tau_{ED} - \sigma_w^2 - P_p\sum_{l=0}^{L-1}|h_l|^2}{\sqrt{\frac{\sigma_w^4}{N} + (\frac{2P_p\sigma_w^2}{N})\sum_{l=0}^{L-1}|h_l|^2}}\right). \tag{3.14}$$

Now, the average probability of detection of the spectrum sensing will be examined when the channel is NFS. The average probability of detection $(\overline{P}_D)$ is evaluated by averaging (3.14) over the p.d.f. $\left(f_{\mathbb{T}_h}(t)\right)$ of $\mathbb{T}_h = \sum_{l=0}^{L-1}|h_l|^2$. Here $\mathbb{T}_h$ is a sum of weighted central chi-square variables. In [65] the p.d.f. of $\mathbb{T}_h$ has been derived, but not found in closed-form and this makes the evaluation complicated. To deal with this the author resorts to approximate the p.d.f of $\mathbb{T}_h$ by Gaussian and Gamma distribution functions. Next we will examine which function (Gaussian/Gamma) is more suitable to approximate the distribution of $\mathbb{T}_h$.

3.6.1 *Distribution of* $\mathbb{T}_h$

In this subsection, the distribution of $\mathbb{T}_h = \sum_{l=0}^{L-1}|h_l|^2$ is examined based on the Gaussian and Gamma p.d.f approximations using the moment matching method for the following reasons:

1. The Gaussian and Gamma distribution functions are Type-V and Type-III Pearson distributions respectively which are widely employed in fitting distributions for positive random variables by matching the first and the second moments [66].

2. The bivariate Gaussian and Gamma distribution functions are simple and tractable and this does not involve any higher order complicated mathematical functions [67].

3.6.1.1 *Gaussian approximation approach*

The random variable $\mathbb{T}_h$ may be approximated by a Gaussian distribution function, $\widehat{f}_{\mathbb{T}_h}(t)$, with a mean $\mu_{\mathbb{T}_h}$ and a variance $\sigma^2_{\mathbb{T}_h}$. The p.d.f of the Gaussian function is given by

$$\widehat{f}_{\mathbb{T}_h}(t) = \frac{1}{\sigma_{\mathbb{T}_h}\sqrt{2\pi}}\exp((t-\mu_{\mathbb{T}_h})^2/\sigma^2_{\mathbb{T}_h}), \;\; t \geqslant 0 \tag{3.15}$$

where $\mu_{\mathbb{T}_h} = \mathbb{E}[\mathbb{T}_h] = \sum_{l=0}^{L-1}\Omega_{h_l}$ and $\sigma^2_{T_h} = \mathbb{E}[\mathbb{T}^2_h] - \mathbb{E}^2[\mathbb{T}_h] = \sum_{l=0}^{L-1}\Omega^2_{h_l}/m$, and $\mathbb{E}[|h_l|^4] = \Omega^2_l[1+1/m]$. Figure 3.1 sketches the simulated p.d.f of $\mathbb{T}_h$ (histogram) and the approximated p.d.f defined in (3.15). It is clear from Figure 3.1 that the Gaussian p.d.f does not capture all the features of the $\mathbb{T}_h$ for all values of L and m.

3.6.1.2 *Gamma approximation approach*

Now $\mathbb{T}_h$ will be approximated by a Gamma distribution function, $\widehat{f}_{\mathbb{T}_h}(t)$, with a shape parameter $K_{\mathbb{T}_h}$ and a scale parameter $\phi_{\mathbb{T}_h}$. The p.d.f of the Gamma function is given by

$$\widehat{f}_{\mathbb{T}_h}(t) = \frac{1}{\Gamma(K_{\mathbb{T}_h})\phi^{K_{\mathbb{T}_h}}_{\mathbb{T}_h}}\exp(-\frac{t}{\phi_{\mathbb{T}_h}})t^{K_{\mathbb{T}_h}-1}, \;\; t \geqslant 0 \tag{3.16}$$

where $K_{\mathbb{T}_h} = \mu^2_{\mathbb{T}_h}/\sigma^2_{\mathbb{T}_h}$, $\phi_{\mathbb{T}_h} = \sigma^2_{\mathbb{T}_h}/\mu_{\mathbb{T}_h}$, $\mu_{\mathbb{T}_h}$ and $\sigma^2_{\mathbb{T}_h}$ are defined in the previous subsection. The analytical p.d.f. of $\mathbb{T}_h$ (see - (3.16)) and the Monte-Carlo simulation of the p.d.f. of $\mathbb{T}_h$ are plotted in Figure 3.2. It is clear that (3.16) is an excellent approximation to the p.d.f. of $\mathbb{T}_h$ for all values of L and m. As a result, the Gamma approximation will be adopted in this chapter. Thus the average probability of detection can be written as:

$$\overline{P}_D = \int_0^\infty Q\left(\frac{\overline{\tau} - N\sigma^2_w - NP_p t}{\sqrt{N\sigma^4_w + 2NP_p\sigma^2_w t}}\right)\widehat{f}_{\mathbb{T}_h}(t)\mathrm{d}t, \tag{3.17}$$

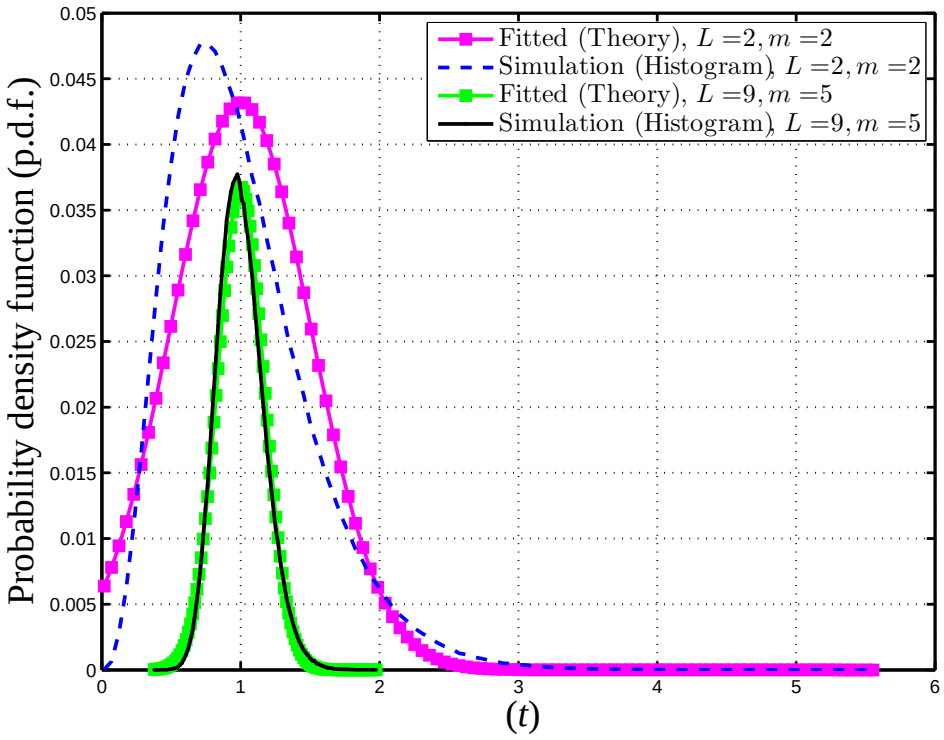

Figure 3.1: Plots of the approximate p.d.f. (3.15) and the simulated p.d.f. of $\mathbb{T}_h$ (10^6 Monte-Carlo runs).

where $\overline{\tau} = N\tau_{ED}$. The evaluation of (3.17) will be executed in the following subsection.

3.6.2 $\overline{P}_D$ *derivation*

Now using the standard identity [50] $Q(v) = \text{erfc}(\frac{v}{\sqrt{2}}) = \frac{1}{2}(1 - \text{erf}(\frac{v}{\sqrt{2}}))$, so (3.17) becomes

$$\overline{P}_D = \frac{1}{2\Gamma(K_{T_h})\phi_{\mathbb{T}_h}^{K_{\mathbb{T}_h}}} \int_0^\infty t^{K_{\mathbb{T}_h}-1} \exp(-t/\phi_{\mathbb{T}_h})(1 - \text{erf}(\frac{t}{\sqrt{2}}))dt. \tag{3.18}$$

Then by expressing the erf(.) function as an infinite series with the aid of [[50], eq. (8.253.1)]

$$\overline{P}_D = \frac{1}{2\Delta} \int_0^\infty t^{K_{\mathbb{T}_h}-1} \exp(-t/\phi_{\mathbb{T}_h}) \big[1 - \frac{2}{\sqrt{\pi}} \sum_{i=1}^{\infty} \frac{(-1)^{i+1}}{(2i-1)(i-1)!} \times \Big(\frac{\overline{\tau} - N\sigma_w^2 - NP_p t}{\sqrt{2}\sqrt{N\sigma_w^4 + 2NP_p\sigma_w^2 t}}\Big)^{2i-1}\big] dt,$$

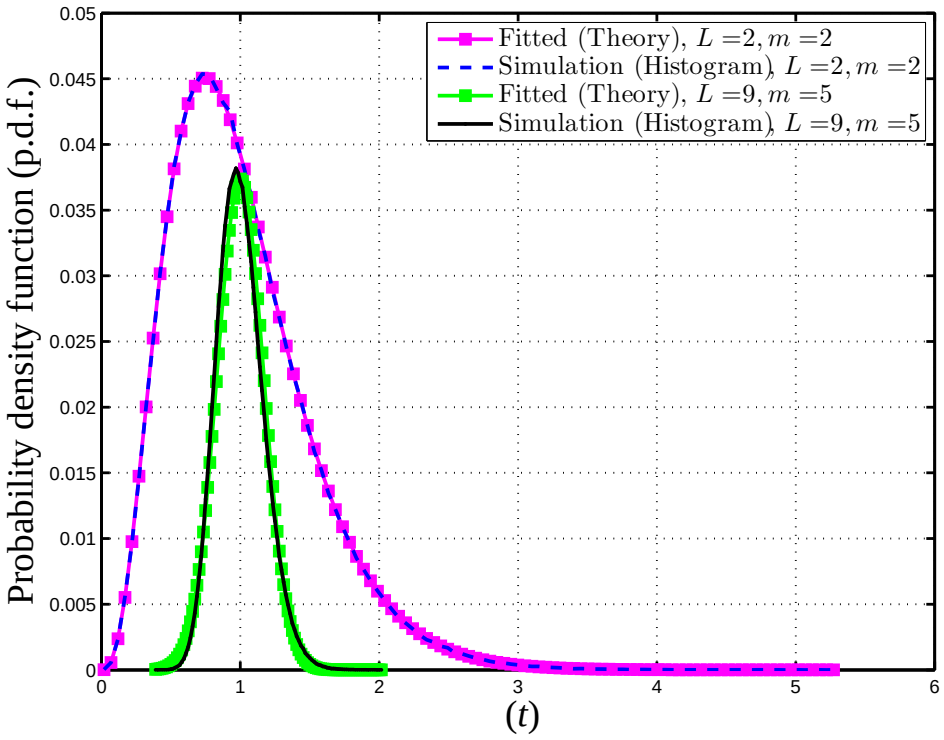

Figure 3.2: Plots of the approximate p.d.f. (3.16) and the simulated p.d.f. of $\mathbb{T}_h$ (10^6 Monte-Carlo runs).

then after some simplifications $\overline{P}_D$ becomes

$$\begin{aligned}\overline{P}_D = &\frac{1}{2\Delta}\int_0^\infty t^{K_{\mathbb{T}_h}-1}\exp(-t/\phi_{\mathbb{T}_h})dt \\ &-\frac{1}{\Delta\sqrt{\pi}}\int_0^\infty t^{K_{\mathbb{T}_h}-1}\exp(-t/\phi_{\mathbb{T}_h}) \\ &\times\sum_{i=1}^{\infty}\frac{(-1)^{i+1}}{(2i-1)(i-1)!}\Big(\frac{\overline{\tau}-N\sigma_w^2-NP_pt}{\sqrt{2}\sqrt{N\sigma_w^4+2NP_p\sigma_w^2t}}\Big)^{2i-1}dt\end{aligned} \tag{3.19}$$

where $\Delta = \Gamma(K_{T_h})\phi_{\mathbb{T}_h}^{K_{\mathbb{T}_h}}$. The first integral integral in (3.19) is expressed in terms of the Gamma function according to [[50], eq. (8.310.1)] and thus (3.19) becomes

$$\begin{aligned}\overline{P}_D = &\frac{1}{2}-\frac{1}{\Delta\sqrt{\pi}}\int_0^\infty t^{K_{\mathbb{T}_h}-1}\exp(-t/\phi_{\mathbb{T}_h})\sum_{i=1}^{\infty}\frac{(-1)^{i+1}}{(2i-1)(i-1)!} \\ &\times\Big(\frac{\overline{\tau}-N\sigma_w^2-NP_pt}{\sqrt{2}\sqrt{N\sigma_w^4+2NP_p\sigma_w^2t}}\Big)^{2i-1}dt.\end{aligned} \tag{3.20}$$

By letting $y = N\sigma_w^4 + 2NP_p\sigma_w^2 t$, then (3.20) (after some simplifications) becomes

$$\begin{aligned}\overline{P}_D =& \frac{1}{2} - \Lambda \sum_{i=1}^{\infty} \frac{(-1)^{i+1}}{(2i-1)2^{i-0.5}(i-1)!} \times \int_{N\sigma_w^4}^{\infty} \frac{(y - N\sigma_w^4)^{K_{\mathbb{T}_h}-1}}{(\sqrt{y})^{2i-1}} \\ & \exp\Big(-\frac{y}{2NP_p\sigma_w^2\phi_{\mathbb{T}_h}}\Big)\Big(-\frac{y}{2P_p\sigma_w^2} + \overline{\tau} - 0.5N\sigma_w^2\Big)^{2i-1} dy,\end{aligned} \tag{3.21}$$

where $\Lambda = \frac{\exp(\frac{\sigma_w^2}{2P_p\phi_{\mathbb{T}_h}})}{\Delta\sqrt{\pi}(2NP_p\sigma_w^2)^{K_{\mathbb{T}_h}}}$. By expanding $(y - N\sigma_w^4)^{K_{\mathbb{T}_h}-1}$ using a binomial series see - [[50], eq. (1.111)] and after some basic mathematical manipulations, then $\overline{P}_D$ is written as

$$\begin{aligned}\overline{P}_D =& \frac{1}{2} - \Lambda \sum_{i=1}^{\infty} \sum_{j=0}^{\lceil K_{\mathbb{T}_h}\rceil - 1} \frac{(-1)^{i+1} \times (-N\sigma_w^4)^{K_{\mathbb{T}_h}-1-j} \times \binom{K_{\mathbb{T}_h}-1}{j}}{(2i-1)2^{i-0.5}(i-1)!} \\ & \int_{N\sigma_w^4}^{\infty} y^{j-i+0.5} \exp\Big(-\frac{y}{2NP_p\sigma_w^2\phi_{\mathbb{T}_h}}\Big) \\ & \times \Big(-\frac{y}{2P_p\sigma_w^2} + \overline{\tau} - 0.5N\sigma_w^2\Big)^{2i-1} dy,\end{aligned} \tag{3.22}$$

where $\lceil . \rceil$ denotes the ceiling function. Again by expanding $(-\frac{y}{2P_p\sigma_w^2} + \overline{\tau} - 0.5N\sigma_w^2)^{2i-1}$ with a binomial series we get

$$\begin{aligned}\overline{P}_D =& \frac{1}{2} - \Lambda \sum_{i=1}^{\infty} \sum_{j=0}^{\lceil K_{\mathbb{T}_h}\rceil - 1} \sum_{z=0}^{2i-1} \frac{(-1)^{i+1} \times \binom{K_{\mathbb{T}_h}-1}{j} \times \binom{2i-1}{z}}{(2i-1)2^{i-0.5}} \\ & \times \frac{(-N\sigma_w^4)^{K_{\mathbb{T}_h}-1-j} \times \Big(\overline{\tau} - 0.5N\sigma_w^2\Big)^z}{(i-1)!(-2P_p\sigma_w^2)^{2i-z+1}} \\ & \times \int_{N\sigma_w^4}^{\infty} y^{i+j-z-0.5} \exp\Big(-\frac{y}{2NP_p\sigma_w^2\phi_{\mathbb{T}_h}}\Big) dy.\end{aligned} \tag{3.23}$$

Finally after some simplifications we get

$$\begin{aligned}\overline{P}_D =& \frac{1}{2} - \Lambda \sum_{i=1}^{\infty} \sum_{j=0}^{\lceil K_{\mathbb{T}_h}\rceil - 1} \sum_{z=0}^{2i-1} \frac{(-1)^{i+1} \times \binom{K_{\mathbb{T}_h}-1}{j} \times \binom{2i-1}{z} \sqrt{N} \times}{(2i-1)2^{i-0.5}(i-1)!} \\ & \frac{(2NP_p\sigma_w^2\phi_{T_h})^{i+j-z+0.5}(-N\sigma_w^4)^{K_{\mathbb{T}_h}-1-j}}{(-2P_p\sigma_w^2)^{2i-z+1}} \\ & \times \Big(\overline{\tau} - 0.5N\sigma_w^2\Big)^z \times \Gamma(j+i-z+0.5, \frac{\sigma_w^2}{2P_p\phi_{\mathbb{T}_h}}),\end{aligned} \tag{3.24}$$

where $\Gamma\big(s,x\big) = \int_x^{\infty} t^{s-1}e^{-t}dt$ is the upper incomplete Gamma function [50]. When the channel of the secondary user is Nakagami-*m* flat-fading (NFF) then the

channel vector $\mathbf{h} = [h_0]$ has only one tap and the false alarm probability is similar to (3.11). The average probability of detection $\overline{P}_D$ is derived in [[22], equation (20)].

When the primary user's signal follows the Gaussian distribution. In this scenario, the mean and the variance of the test statistic defined in (3.3) under $\mathcal{H}_0$ are the same as in (3.4) and (3.5) respectively (because the test statistic under $\mathcal{H}_0$ does not depend on the primary signal). Also, the mean under $\mathcal{H}_1$ is similar to (3.6). However, the variance of the test statistic under $\mathcal{H}_1$ is given as[5]

$$\sigma_1^2 = \frac{1}{N}\Big(P_p \sum_{l=0}^{L-1} |h_l|^2 + \sigma_w^2\Big)^2 \quad ,$$

thus the detection performance is

$$P_D = Q\left(\frac{\tau - \sigma_w^2 - P_p t}{\frac{1}{\sqrt{N}}(\sigma_w^2 + P_p t)}\right).$$

By taking similar steps for PSK signal and using [[68], equation 2.3.6.6 and [50], equation 9.2.11.4], the average detection probability can be written as

$$\begin{aligned}\overline{P}_D = \frac{1}{2} - a_1 \sum_{i=1}^{\infty} \sum_{z=0}^{2i-1} a_2 \Gamma(K_{\mathbb{T}_h}) \sigma_w^{2\sigma_w^2 + K_{\mathbb{T}_h} - 1} \\ \times e^{-\frac{\sigma_w^2}{P_p \phi_{\mathbb{T}_h}}} \Psi(K_{\mathbb{T}_h}, \sigma_w^2 + K_{\mathbb{T}_h}; \frac{\sigma_w^2}{P_p \phi_{\mathbb{T}_h}}),\end{aligned} \tag{3.25}$$

where $a_1 = \frac{P_p^{K_{\mathbb{T}_h}} \exp(\sigma_w^2 / P_p \phi_{\mathbb{T}_h})}{\Delta P_p \sqrt{\pi}}$, $a_2 = C_1 \binom{2i-1}{z} \tau^{2i-1-z} (-1)^z$, $C_1 = \frac{(\sqrt{N})^{2i-1}(-1)^{i+1}}{(\sqrt{2})^{2i-1}(2i-1)(i-1)!}$ and $\Psi(.,.;.)$ is the confluent hypergeometric function defined in [[68], page 793].

3.7 OUTAGE DETECTION PROBABILITY ANALYSIS

This section seeks to ensure the advantage of the ED over an NFS channel. To do so, another metric is proposed which is called the outage detection probability, and for the following reasons.

5 The proof is derived in chapter 5. In chapter 5, the OFDM signal model is used and modeled by a Gaussian distribution.

1. An exact closed-form expression for the behavior of the ED over an NFS channel can be obtained compared with the average probability detection (3.24).

2. The advantage of the ED over an NFS channel (as it will be seen in the simulation results) can be noticed mathematically.

3. The minimum required number of samples that satisfy ϵ and δ can be found analytically over fading channels, which cannot be done when the average probability detection is used.

4. Investigating the sensing-throughput tradeoff needs the determination of the sensing threshold so that the primary receiver is kept safe from any potential interference. By employing the outage detection probability the local sensing threshold can be calculated analytically over a fading channel as will be seen in Chapter 5.

Because of the random channel, P_D is a random variable. Also, in practice there are some realisations of the channel that do not allow the detection probability to be larger than δ (i.e., $P_D \leq \delta$). So to tackle this behavior, the outage detection probability $(\mathbb{P}_{\text{out}})$ should be examined. The outage detection probability, $\mathbb{P}_{\text{out}}$, is defined as

$$\mathbb{P}_{\text{out}} = \text{Prob}(P_D \leq \delta). \tag{3.26}$$

Equation (3.26) can equivalently be written in terms of the instantaneous SNR (γ) for a NFS channel as

$$\mathbb{P}_{\text{out}} = \text{Prob}(\gamma \leq \gamma_\delta), \tag{3.27}$$

where γ_δ is the threshold SNR in which the outage appears, for a target detection probability equal to δ. The γ_δ can be calculated as follows. Equation (3.14) is written in terms of γ for $P_D = \delta$ yielding

$$\begin{aligned} P_D &= Q\left(\frac{\tau_{ED} - \sigma_w^2 - P_p \sum_{l=0}^{L-1} |h_l|^2}{\sqrt{\frac{\sigma_w^4}{N} + (\frac{2P_p\sigma_w^2}{N}) \sum_{l=0}^{L-1} |h_l|^2}}\right) \\ &= Q\left(\frac{(\frac{\tau_{ED}}{\sigma_w^2}) - 1 - (P_p/\sigma_w^2) \sum_{l=0}^{L-1} |h_l|^2}{\sqrt{\frac{1}{N} + (\frac{2P_p}{N\sigma_w^2}) \sum_{l=0}^{L-1} |h_l|^2}}\right) \\ &= Q\left(\frac{(\frac{\tau_{ED}}{\sigma_w^2}) - 1 - \gamma}{\sqrt{\frac{1}{N} + (\frac{2\gamma}{N})}}\right) = \delta \end{aligned}$$

$$\begin{aligned} \Rightarrow \quad & N\gamma^2 + 2N(1 - (\tau_{ED}/\sigma_w^2)) - 2Q^{-1}(\delta)^2\gamma \\ & + N((\tau_{ED}/\sigma_w^2) - N)^2 - Q^{-1}(\delta)^2 = 0. \end{aligned} \tag{3.28}$$

By solving (3.28), two solutions are obtained. The largest solution (γ_δ) is chosen, i.e.,

$$\begin{aligned} \gamma_\delta = & (\tau_{ED}/\sigma_w^2 - 1) + Q^{-1}(\delta)^2/N \\ & + 1/N\sqrt{Q^{-1}(\delta)^2[N((2\tau/\sigma_w^2) - 1) + Q^{-1}(\delta)^2]}\Big\}. \end{aligned} \tag{3.29}$$

Equation (3.27) can now be re-written in terms of the channel coefficients as

$$\mathbb{P}_{\text{out}} = \text{Prob}\Big(\sum_{l=0}^{L-1} |h_l|^2 \leq \frac{\sigma_w^2\gamma_\delta}{P_p}\Big). \tag{3.30}$$

Next an evaluation of (3.30) is conducted for different power delay profiles.

3.7.1 *Power delay profile*

This subsection evaluates the outage detection probability in (3.30) for different power delay profiles of the channel between the primary user and the secondary user.

3.7.1.1 *Exponential power delay profile*

This scenario assumes that the channel between the primary user and the secondary user has an exponential power delay profile. For this scenario, the p.d.f. of $\mathbb{T}_h$ is given by (3.16) and so the outage probability becomes

$$\begin{aligned} \mathbb{P}_{\text{out}} &= \int_0^{\frac{\sigma^2\gamma_\delta}{P_p}} \widehat{f}_{\mathbb{T}_h}(t)dt \\ \mathbb{P}_{\text{out}} &= 1 - \frac{\Gamma\left(K_{\mathbb{T}_h}, \frac{\sigma_w^2\gamma_\delta}{P_p\phi_{\mathbb{T}_h}}\right)}{\Gamma(K_{\mathbb{T}_h})} \end{aligned} \tag{3.31}$$

$K_{\mathbb{T}_h}$ and $\phi_{\mathbb{T}_h}$ defined in section (3.6).

3.7.1.2 *Uniform power delay profile*

Now the outage detection probability is evaluated when the power delay profile is uniform. In this scenario, $\sum_{l=0}^{L-1}|h_l|^2$ follows a Gamma distribution with shape parameter $K_{\mathbb{T}_h} = mL$ and scale parameter $\phi_{\mathbb{T}_h} = \Omega/m$, where $\Omega = \Omega_{h_l}$ for $l = 0 : L-1$. Thus the outage detection probability is given by

$$\mathbb{P}_{\text{out}} = 1 - \frac{\Gamma\left(mL, \frac{\sigma_w^2\gamma_\delta m}{P_p\Omega}\right)}{\Gamma(mL)}. \tag{3.32}$$

Note that from (3.32) the diversity order is mL (because as mL increases (3.32) decreases). Also, notice that the $\mathbb{P}_{\text{out}}$ in (3.32) is an exact closed-form expression unlike the case of the exponential power delay profile. This is because the power of taps/channels is the same so by default the distribution of $\sum_{l=0}^{L-1}|h_l|^2$ is another Gamma distribution with shape parameter mL and scale parameter Ω/m.

The performance improvement of the ED that might be obtained over an NFS channel can be seen mathematically as follows. To see this improvement the $\mathbb{P}_{\text{out}}$ for the flat fading channel has to be found. In this environment $\mathbf{h} = h_0$ and the instantaneous SNR is $\gamma = \frac{P_p|h_0|^2}{\sigma_w^2}$. So $\mathbb{P}_{\text{out}}$ can be written as $\mathbb{P}_{\text{out}} = \text{Prob}\left(|h_0|^2 < \frac{\sigma_w^2\gamma_\delta}{P_p}\right)$, where $|h_0|^2$ is a central chi-square random variable with 2 degrees of freedom. As a result,

$$\mathbb{P}_{\text{out}} = 1 - \frac{\Gamma\left(m, \frac{\sigma_w^2\gamma_\delta m}{P_p\Omega}\right)}{\Gamma(m)}. \tag{3.33}$$

Note that the difference between (3.32) and (3.33) is the number of channel taps (L) and the term (L) in (3.32) clearly gives the ED an improved performance over the NFS channel, where as the term L increases the $\mathbb{P}_{\text{out}}$ decreases.

3.7.2 *Minimum sensing Time*

Here the minimum number of samples required (N_{min}) in (3.3) to achieve ϵ, δ and a target $\mathbb{P}_{\text{out}}$ is analytically derived. In the simulation section we will show, the ED improves over the NFS in terms of N_{min}. In cognitive radio applications, this parameter should be chosen by the secondary user to satisfy a required ED performance. The minimum number of samples can be derived by using (3.11), (3.29) and (3.31) yielding

$$N_{min} = \frac{\left(Q^{-1}(\varepsilon) - Q^{-1}(\delta)\sqrt{\frac{2P_p}{\sigma_w^2}\Gamma^{-1}(\mathbb{P}_{\text{out}}, \delta) + 1} \right)^2}{\left(\frac{P_p}{\sigma_w^2}\Gamma^{-1}(\mathbb{P}_{\text{out}}, \delta) \right)^2} \tag{3.34}$$

where $\Gamma^{-1}(.,.)$ denotes the inverse function of the upper incomplete Gamma function and it is a built function in Matlab. Notice that the N_{min} in (3.34) cannot be derived directly using the average detection probability and it needs an iterative algorithm to find the N_{min}. This shows one advantage of using outage detection probability over the average detection probability.

3.8 RESULTS AND DISCUSSION

In this section simulation results (based on (3.3) and (3.26)) are compared against theoretical results (based on (3.11) (3.24), (3.31) and (3.34)) to illustrate the ED performance in an NFS channel. The primary user signal, $s(n)$, is drawn from a 4-PSK constellation (with $P_p = 1$) during all 10^5 Monte Carlo runs. The amplitudes of the channels taps $\left(\mathbf{h} = [h_0\, h_1\, ...\, h_{L-1}]^T\right)$, have been generated according to a Nakgami distribution with an exponential power delay profile $\mathbb{E}|h_l|^2 = C\exp(-0.2l)$ where

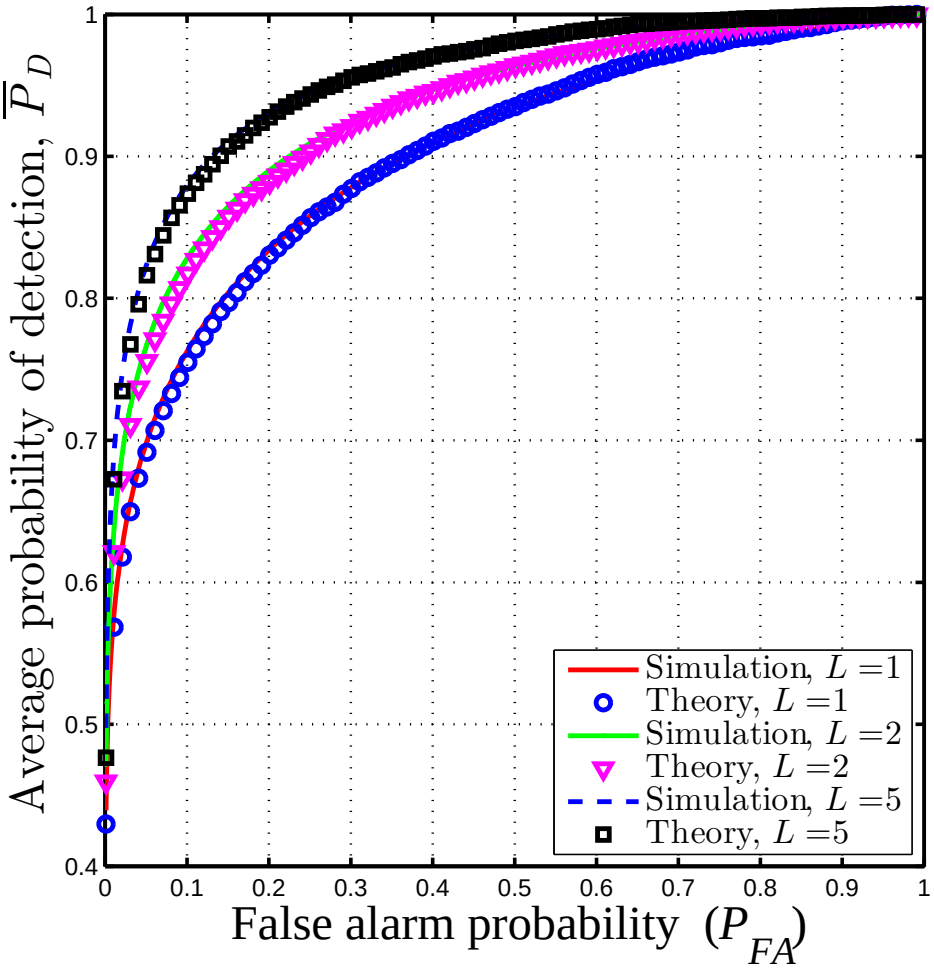

Figure 3.3: $\overline{P}_D$ versus P_{FA} for different channel taps (L). In all cases, m=2 , N=100, and SNR=-5dB.

C is a parameter to guarantee $\sum_{l=0}^{L-1} \mathbb{E}|h_l|^2 = 1$ and the phases of the channel taps have been generated according to a uniform distribution $U[0, 2\pi]$. Finally, 30 terms have been used in (3.24) ($i = 30$) to calculate the average probability of detection, $\overline{P}_D$.

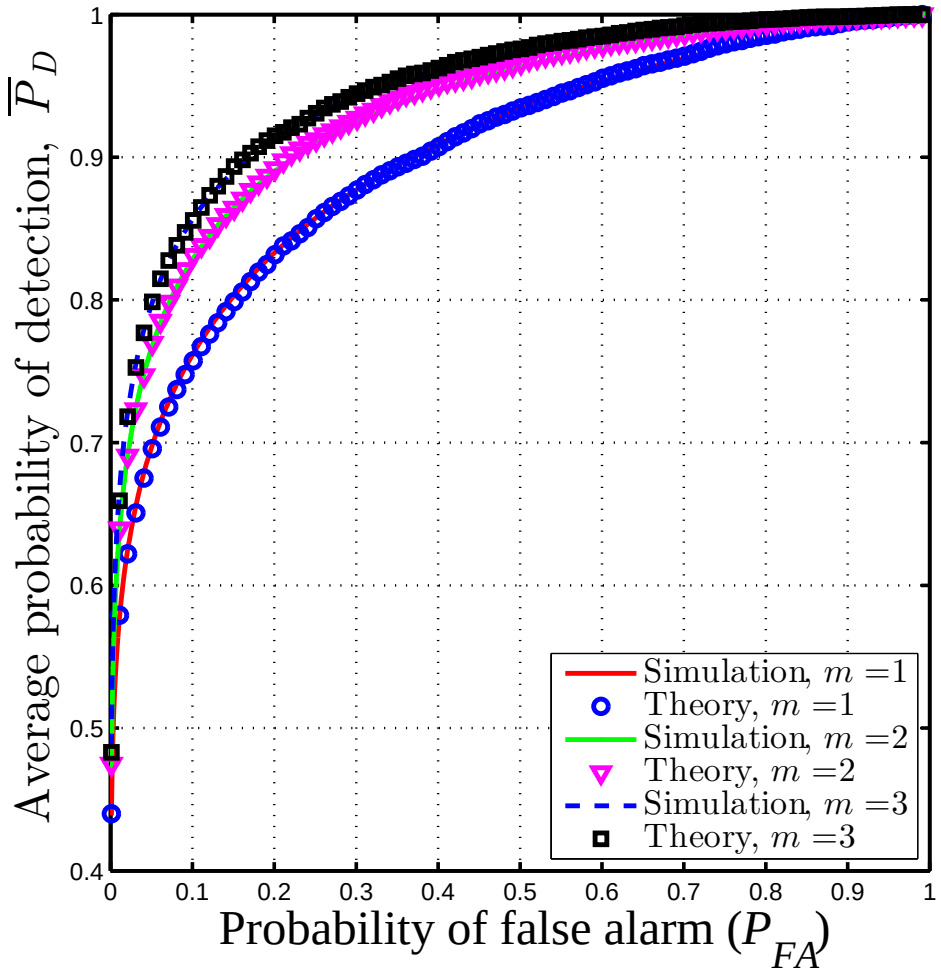

Figure 3.4: $\overline{P}_D$ versus P_{FA} for different values of Nakagami fading parameter (m). In all cases, L=2 , N=200 and SNR=-5dB.

Result 1: Theoretical results verification for detection performance of ED (Figures 3.3 and 3.4).

Figures 3.3 and 3.4 show $\overline{P}_D$ versus the P_{FA} for different values of L and m respectively. It is easily noticed that the theoretical results (see - (3.11) and (3.24)) match the simulation results (see - (3.3)). Also, it can be seen that as L and m increase, the average probability of detection gradually improves. To get the theory for a flat fading channel (see - [22], Equation (16) and Equation (20)).

The improvement of the P_D over the NFS is due to the diversity of the multipath and this appears from the instantaneous signal to noise ratio, for NFS it is $\frac{\sum_{l=0}^{L-1}|h_l|^2}{\sigma_w^2}$.

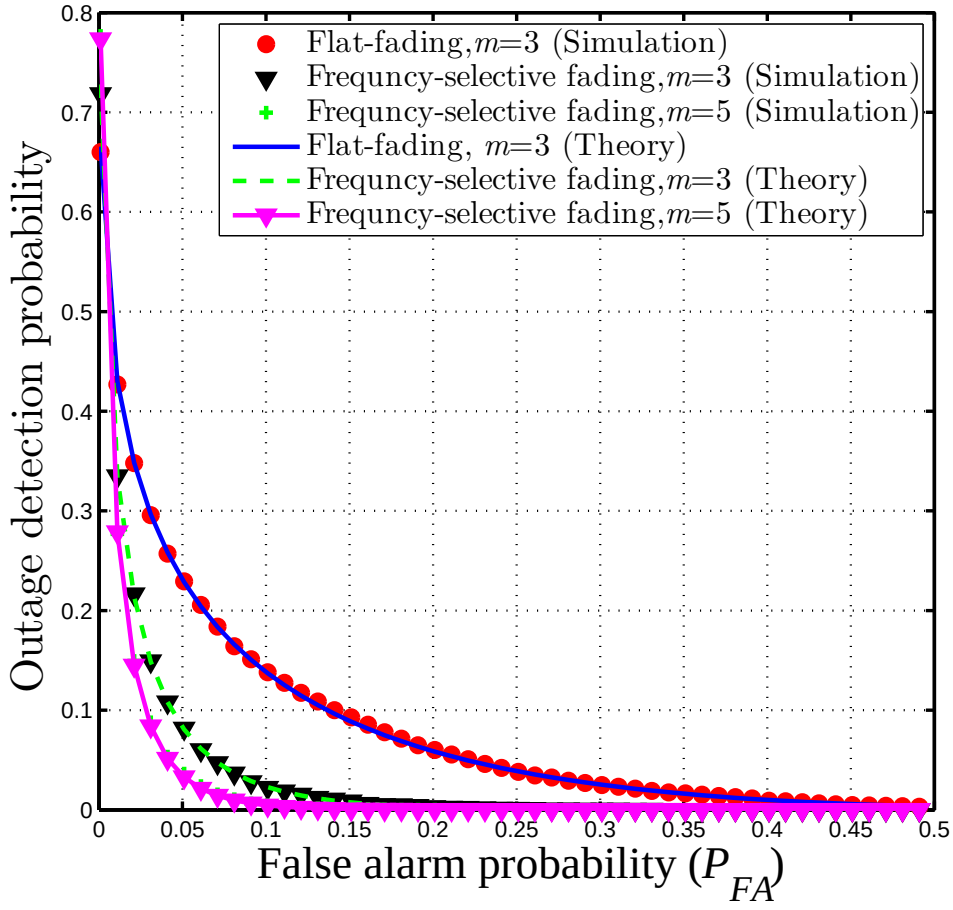

Figure 3.5: $\mathbb{P}_{\text{out}}$ versus P_{FA} for both an NFS channel (L=3) and an NFF channel. In all cases, δ=0.9 , N=550 and SNR=-10dB.

For NFF it is $\frac{|h_0|^2}{\sigma_w^2}$. And P_D improves with increasing m because as m increases as the channel gets better.

Result 2: Theoretical results verification for outage detection probability versus P_{FA} (Figure 3.5).

This figure shows $\mathbb{P}_{\text{out}}$ versus P_{FA}. Clearly the analytical derivations comply with the simulation results ((3.26)) and theory ((3.31)). It is obvious that $\mathbb{P}_{\text{out}}$ for an NFS channel is less than $\mathbb{P}_{\text{out}}$ for an NFF channel ((simulation - see (3.26)) and (theory - see (3.31) for L =1)), because of the multipaths.

Result 3: $\overline{P}_D$ versus L (Figure 3.6).

This Figure shows that when the channel between the primary user and the secondary user is NFS, the protection for the primary receiver is more guaranteed (because the $\overline{P}_D$ improves with L and m). It is clearly seen that $\overline{P}_D$ initially improves

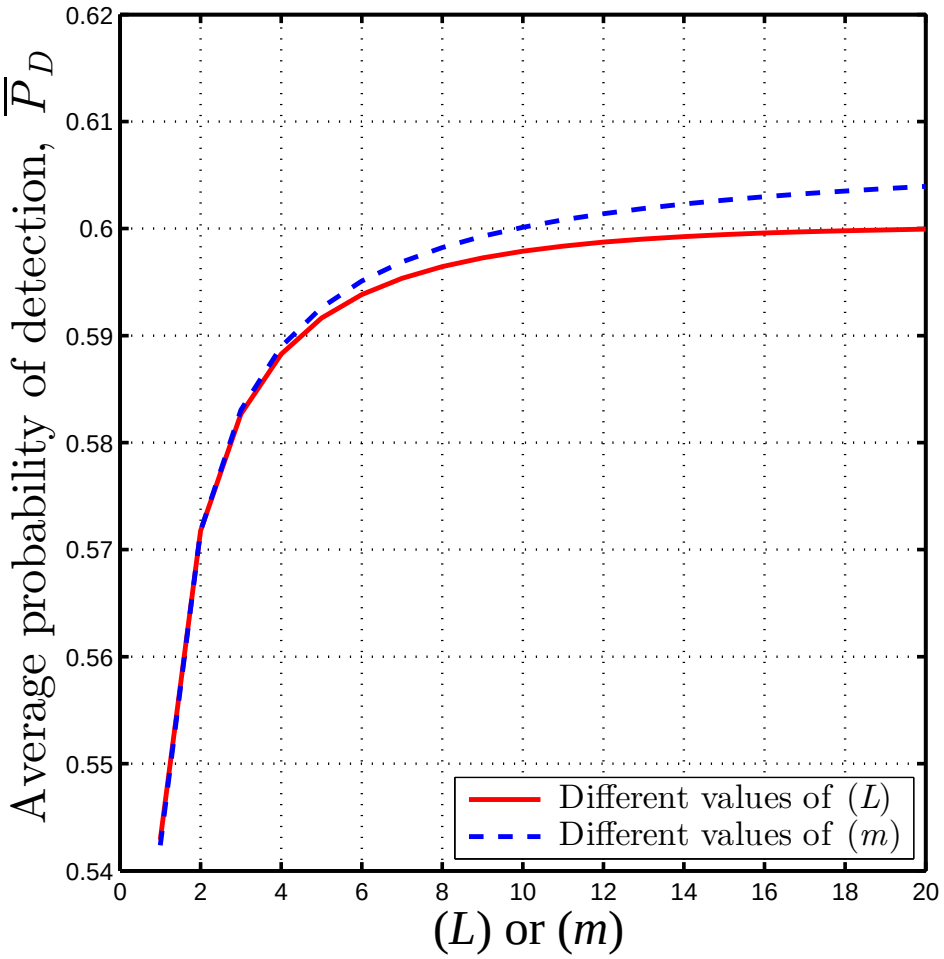

Figure 3.6: $\overline{P}_D$ versus Nakagami fading parameter (m) or (L). In all cases, ϵ=0.1, N=100 and SNR $= -7$dB.

significantly for $L = 1$ to 5 and $m = 1$ to 5 (see - (3.24)). After that it increases gradually and then levels out for high values of L and m. Also, it can be seen that the type of channel is more affected to the improvement of the detection performance compared with number of multitaps. Note that when L is increased, m is fixed to 2. Also, when m is increased, L is fixed to 2.

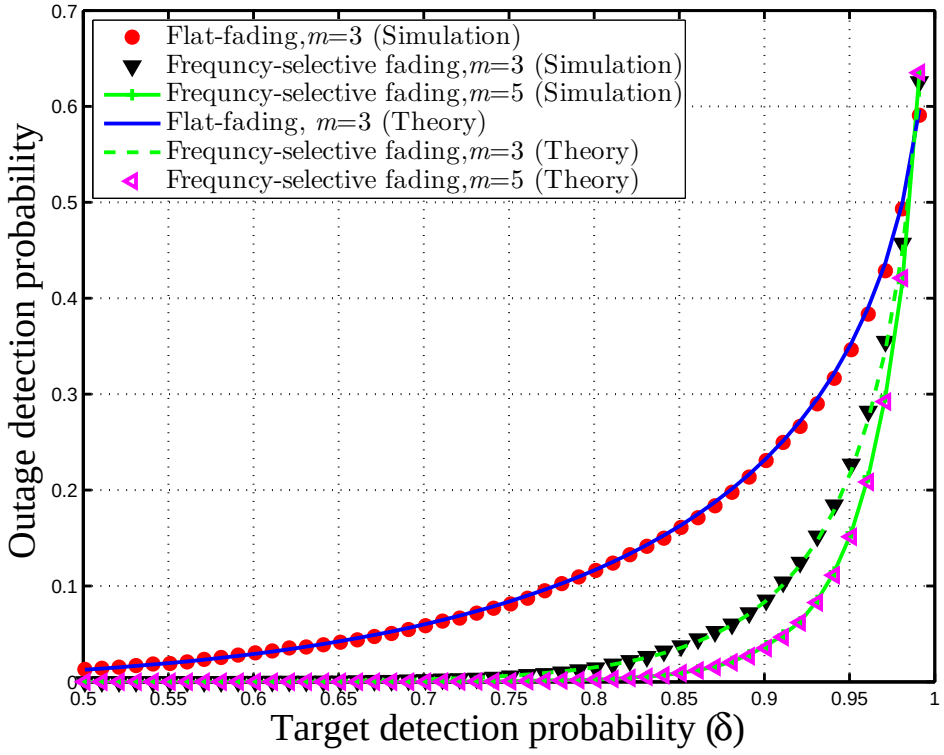

Figure 3.7: $\mathbb{P}_{\text{out}}$ versus δ for both NFS channel ($L = 3$) and NFF channel for different values of m. In all cases, $N = 550$, $\epsilon = 0.05$, and SNR = -10dB.

Result 4: $\mathbb{P}_{\text{out}}$ **versus** δ (Figure 3.7).

First, it can be seen the theory matches with the simulation ((simulation - see (3.26)) and (theory - see (3.31))). Also, it can be noticed the NFS channel gives a smaller outage detection probability compared to the NFF channel for different values of m, and this is because of the multipaths.

Result 5: $\mathbb{P}_{\text{out}}$ **versus** L (Figure 3.8).

Again the analytical derivation complies with the simulation results. For NFS channel (simulation - see (3.26)) and (theory - see (3.31)) and for NFF (simulation - see(3.26)) and (theory - see (3.31) for L=1). It is obvious that as the number of multipaths increases the $\mathbb{P}_{\text{out}}$ decreases then it levels out for high values of L. It is similar to the behavior of Figure 3.6. At the start $\mathbb{P}_{\text{out}}$ decreases rapidly then it decreases slowly. Also, the $\mathbb{P}_{\text{out}}$ has an added advantage due to the existence of the Nakagami parameter m (the $\mathbb{P}_{\text{out}}$ decreases when m increases).

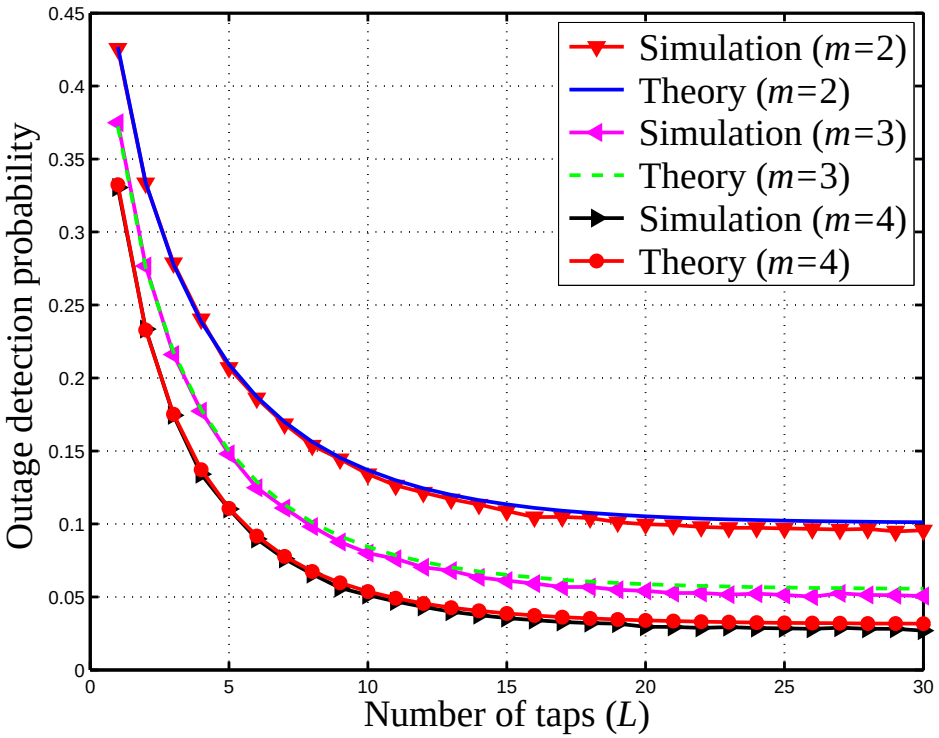

Figure 3.8: $\mathbb{P}_{\text{out}}$ versus Number of taps (L) for different number of m. In all cases, δ=0.9 , N=550 , ϵ=0.1 and SNR=-10dB.

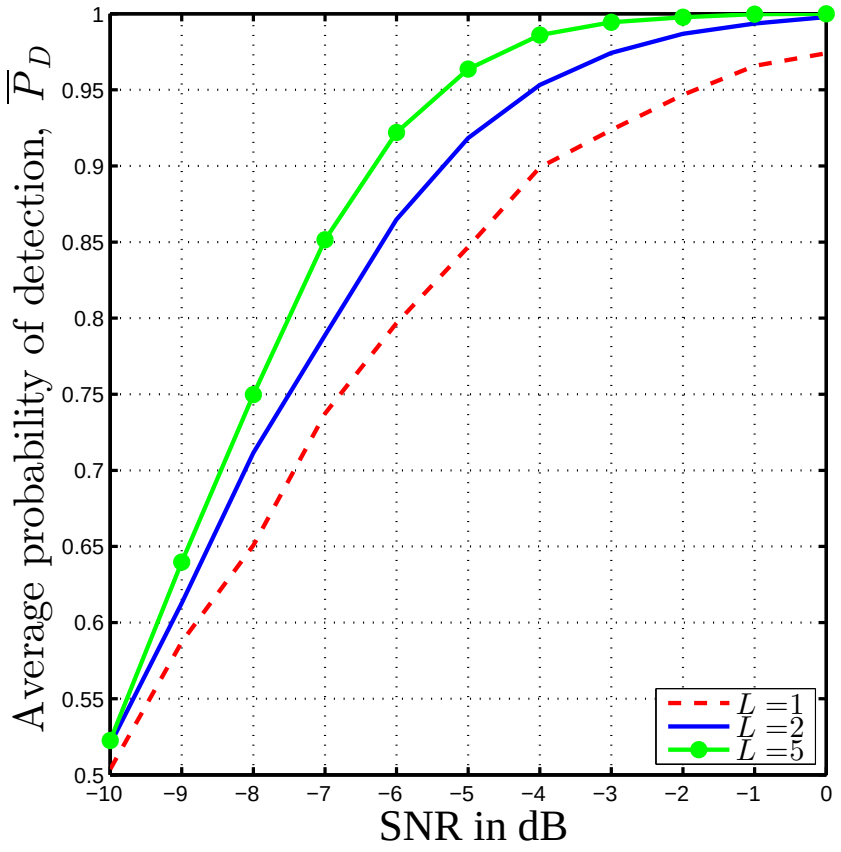

Figure 3.9: $\overline{P}_D$ versus the SNR for different number of L. In all cases, $m = 2$, $N = 200$ and $P_{FA} = 0.1$.

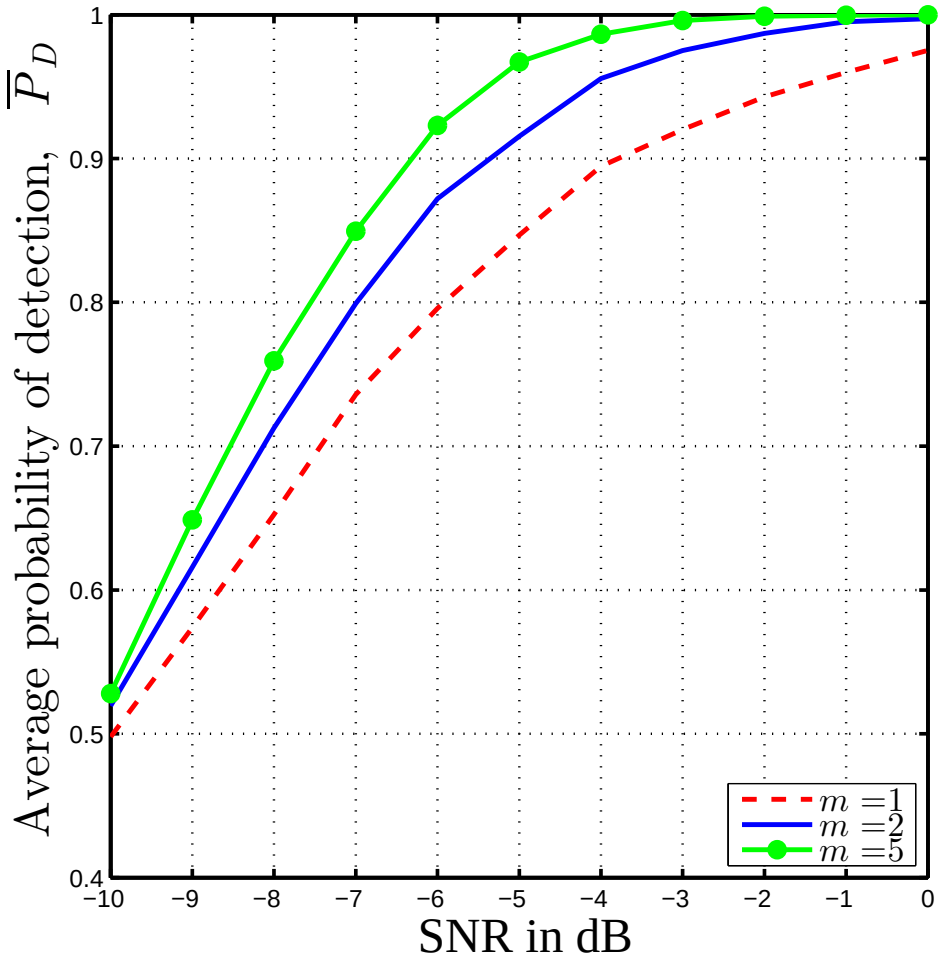

Figure 3.10: $\overline{P}_D$ versus the SNR for different values of m. In all cases, L=2, N=200 and P_{FA}=0.1 .

Result 6: $\overline{P}_D$ **versus** SNR **(different** L**)** (Figure 3.9).

It can be seen that as the SNR increases the performance improves for different values of L. And as L increases $\overline{P}_D$ also increases.

Result 7: $\overline{P}_D$ **versus** SNR **(different** m**)** (Figure 3.10).

Here it is obvious as the SNR increases the average detection probability improves for different values of m. Also, as m increases $\overline{P}_D$ improves.

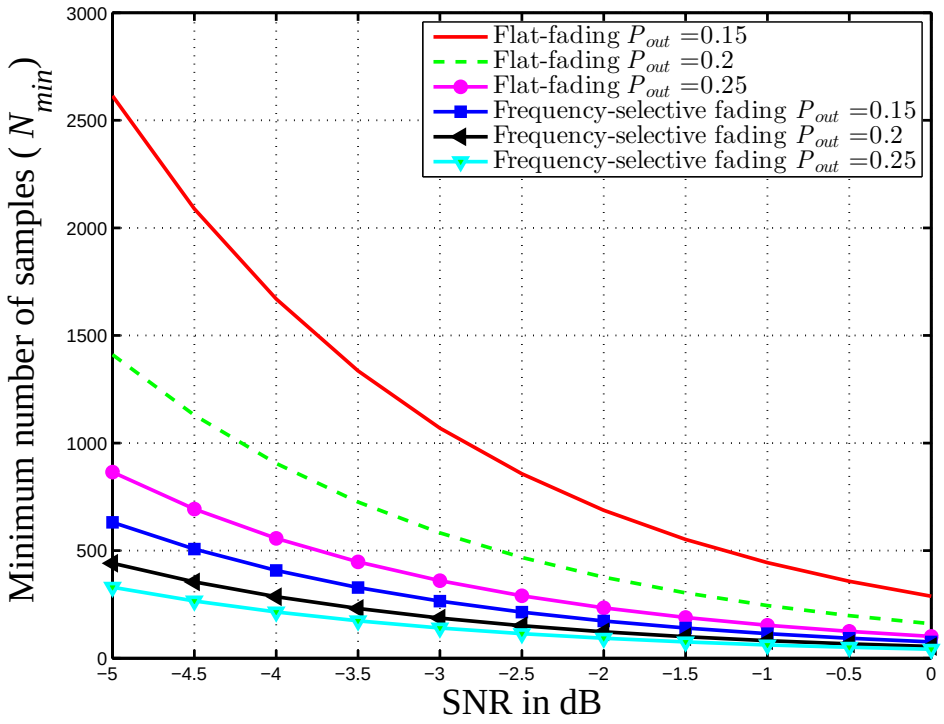

Figure 3.11: N_{min} versus SNR for NFS channel ($L = 2$) and NFF channel. In all cases, $\delta = 0.9$ and $\epsilon = 0.1$.

Result 8: N_{min} **versus** SNR (Figure 3.11).

Finally, this figure examines the minimum number of samples required to achieve ϵ, δ for different values of $\mathbb{P}_{out}$. Again the NFS channel needs less samples compared with the NFF channel because of the multipaths (theory - see (3.34)). Clearly, to make the performance of the ED more demanding (i.e., reduce $\mathbb{P}_{\text{out}}$) then N_{min} must be increased. Moreover, it can be seen that as the $\mathbb{P}_{out}$ increases the N_{min} decreases due to the restriction on the outage becomes less.

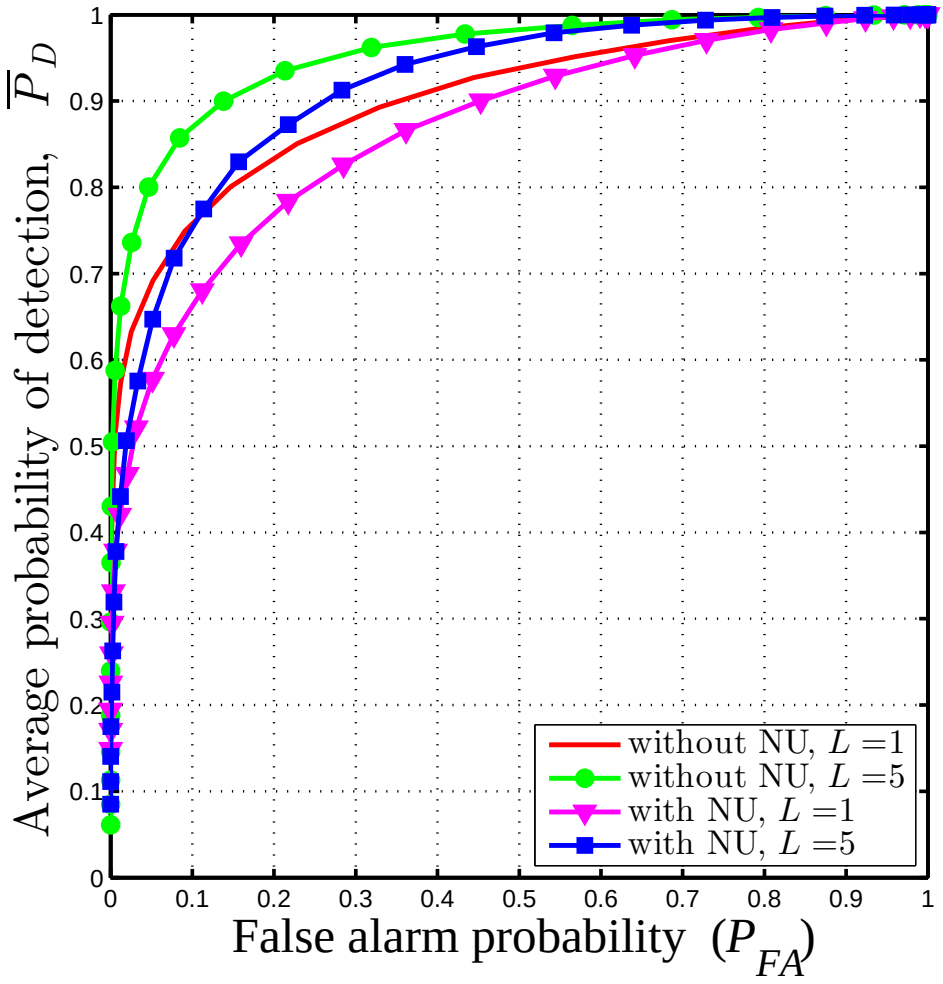

Figure 3.12: The $\overline{P}_D$ versus the P_{FA} in the presence of NU. In all cases, $\delta = 0.9$ and $\epsilon = 0.1$.

Result 9: $\overline{P}_D$ versus P_{FA} in the presence of NU (Figure 3.12).

This figure evaluates by simulation the detection performance of the ED in the presence of NU and over NFS. The NU has been generated according to the p.d.f. defined in (5.6). We can see from the figure that NU reduces the improvement of the performance. For L=5, the degradation due to the NU is approximately similar to the ED performance when L=1 without NU.

3.9 CHAPTER SUMMARY

This chapter studied the performance of the ED over an NFS channel by examining three different parameters. First, the average detection probability $(\overline{P}_D)$ was found theoretically and verified by simulation. Second, the outage detection probability $(\mathbb{P}_{\text{out}})$ was derived theoretically and confirmed via simulation. Third, the minimum number of samples (N_{min}) that satisfies a desired ROC was analytically derived through the outage detection probability. This outage detection probability gives the possibility for finding a closed-form expression for the minimum number of samples. All those parameters confirm that the ED over an NFS channel outperforms the ED over the NFF channels.

4

PERFORMANCE ANALYSIS OF COOPERATIVE SPECTRUM SENSING FOR COGNITIVE RADIO USING STOCHASTIC GEOMETRY

4.1 INTRODUCTION

In practice, several problems militate against effective and efficient spectrum sensing. These include the hidden primary user problem, fading, multipath and shadowing. As a result the secondary user cannot detect the primary user and when it accesses the primary's frequency band, hence it will cause interference to the primary receiver. Because of this, cooperative spectrum sensing has emerged to respond to these challenges [22, 51, 69, 70, 71, 72, 73, 74]. The energy detector (ED) is the simplest detector which can be implemented in practice, and so most research on cooperative spectrum sensing examines the ED.

In cooperative spectrum sensing, each secondary user reports its test statistic or measurement to the fusion center (FC). The reported or transmitted test statistics consume power and this power consumption might be significant if the number of secondary users is large. Thus power consumption needs to be considered in cooperative spectrum sensing design.

This chapter investigates the problem of cooperative spectrum sensing based energy efficiency. In addition, this chapter proposes a novel detection algorithm to reduce the energy overhead that results from sending test statistics to the FC.

4.1.1 *Literature review and motivation*

In the context of cooperative spectrum sensing many papers have dealt with the issue of power consumption. In the literature there are three main approaches regarding this matter.

A first approach (for example in [28, 75]) is the concept of a censoring or send/no send idea (i.e., only sending test statistics that are larger than a local threshold (ξ)). This was introduced to reduce the number of transmitted test statistics to the FC and thus save energy. This approach showed a slight performance degradation compared with uncensored cooperative spectrum sensing. Moreover, the authors used a cyclostationary detector to estimate the test statistic and also the threshold ξ was calculated depending on the local P_{FA}. Furthermore, when there is no test statistic sent to the FC, the FC assumes the primary user is absent. In addition, the detection performance at the FC was not derived theoretically. In [76], the authors suggested reducing the energy overhead by allowing the secondary users to randomly transmit their test statistics to the FC after comparing them with local thresholds. In [26], the transmitted test statistics were censored under the bandwidth constraints and they used an ED. They used two local thresholds ξ_1 and ξ_2, $(\xi_2 > \xi_1)$. When the test statistic is above ξ_2 the secondary user would send "1" to the FC, if it is below ξ_1 the secondary user sends "0" to the FC, and if it is in between ξ_1 and ξ_2 then it sends no message to the FC. However, the computation of the local threshold values were not taken into account and the final decision at the FC is dependent on what decision most of the secondary users have chosen. In addition, their results show that censoring cooperative spectrum sensing might be better than conventional cooperative sensing. In [32], censored cooperative spectrum sensing based on the ED was studied analytically and verified through simulation. The simulation results showed that censored cooperative sensing gave better performance compared with the conventional spectrum sensing when optimal values of ξ_1 and ξ_2 are used. In [29], the authors employed an autocorrelation detector for deciding the activity of the primary user and censored the test statistics sent to the FC by using only one local threshold, and this local threshold is calculated depending on the local P_{FA}.

In addition, the global test statistic at the FC consisted of two parts. The first part contained the test statistics that were above the local threshold, i.e, the test statistics were sent by the secondary users. The second part contained the average value of the test statistics in the no-send region under the null hypothesis.

A second approach for minimizing the energy overhead is a sequential detection [77]. This approach aims to reduce the average number of secondary users which send the test statistics to the FC and consequently the energy overhead is minimized. In this approach each secondary user computes its test statistic, and the FC sequentially accumulates the test statistic. If the accumulated test statistics falls between a certain region it continues to receive test statistics from the secondary users; if not, it stops receiving new test statistics. In [78] the concept of censoring and sequential detection are combined.

The last approach is presented in [27, 79], for which the idea of truncated censored sequential detection is used. This is where each secondary user might send its test statistic to the FC while not passing the limit of the number of the received samples.

In all aforementioned papers, the geometry of the secondary users (i.e., the spatial distribution of secondary users with respect to the primary user or the FC) was not considered. Also, the number of secondary users is assumed to be known. In addition, they do not consider the presence of the fading channels between the secondary users and the primary user and the fading channels between the secondary users and the FC. All of the above assumptions are of great importance and should really be considered in practice.

Motivated by the above explanations this chapter considers a more general secondary network model. This chapter introduces a random secondary network detection problem where the secondary network is modelled as a random geometric network. This random geometric network model is a generalization of the simple secondary model used in the existing literature. This model has not been employed for the above references (i.e., papers related to cooperative spectrum sensing based on energy saving).

For a random geometric secondary network, the implication of distance, pathloss exponent and the channel may make the transmit power of the *i*th secondary user (the transmit power needed to transmit the *i*th secondary user test statistic to the FC) too large in order to satisfy a certain signal to noise ratio at the FC. This transmit power might exceed the power budget of the secondary user equipment, in particular if the *i*th secondary user is far away from the FC and the pathloss exponent is high. That is, the secondary user must be inside a building or there is severe fading. Thus it is a good idea to "discard" those secondary users which require a transmit power exceeding a certain transmit power threshold for the following two reasons: (a) *minimizing energy overhead,* and (b) *the signal to noise ratio at the FC might not be satisfied due to the limited power budget of the secondary user equipment*. So in this work, to further reduce energy consumption, we will introduce a novel additional parameter (p_t), the transmit power threshold. This will be in addition to the conventional local threshold (ξ). The *i*th secondary user will only transmit the test statistic to the FC, if $T_{EDi} \geq \xi$ and $p_i \leq p_t$. Here T_{EDi} is the test statistic at the *i*th secondary user and p_i is the required transmit power for the *i*th secondary user to achieve a required signal to noise ratio (SNR) at the FC. Note that to minimize the power needed to send the test statistics to FC, the local threshold (ξ) and the transmit power threshold (p_t) must be chosen in an appropriate manner. To the best of author's knowledge, this idea has not been proposed in any previous research.

At FC problems can arise if the FC does not receive any test statistic from the secondary users because ξ is set too high or p_t is set too small. As a result, the detection performance at the FC might degrade. This issue will be taken into account in this study as well. To address this issue, we propose to examine the activity probability (P_{a1}) under $\mathcal{H}_1$. This is the probability that at least one test statistic is received by the FC. The objective is to find the optimum local threshold $(\xi = \xi_{opt})$ and the optimum transmit power threshold $(p_t = p_{topt})$ so that $P_{a1} \rightarrow 1$.

To enhance the detection performance at the FC, several combining techniques have been proposed in the literature such as an equal gain combining (EQ), a maximum ratio combining (MRC) and a selection combining (SC). Only, the SC is adopted in this work because it gives better detection performance compared to the

EQ[1]. However, MRC requires more information compared with SC, such as the channels between the secondary users and the primary user. Hence, it will complicate

For the conventional censoring, in this chapter the resulting detector is called a censored selection combining (CSC) scheme. But for the proposed censoring, the resulting detector is called a censored selection combining based power censoring (CSCPC) scheme.

4.2 CHAPTER CONTRIBUTION

The contributions of this chapter can be summarised as follows:

1. Most of the work in the literature assumes that the secondary users are distributed around the primary user, but this might not always be correct in practice. In some scenarios, the secondary users might be situated in a certain building such as a domestic area, company, hospital, etc., and the primary user may be located out side this area, i.e., a cellular network.

2. Theoretical derivation of the activity probability P_{a1} is carried out in order to find ξ_{opt} and p_{topt} such that $P_{a1} \to 1$.

3. The detection performance of the conventional CSC over small-scale fading and pathloss is derived analytically using the stochastic geometry tool and justified by simulation.

4. A novel CSCPC detector is proposed to alleviate the energy overhead. The detection performance of the CSCPC detector over small-scale fading and pathloss is derived theoretically using stochastic geometry and verified via simulation.

5. Finally, the average power that is needed to transmit the test statistics to the FC is obtained analytically using stochastic geometry and confirmed through simulation results.

1 Extensive simulation results have been done showing that the SC has a better performance.

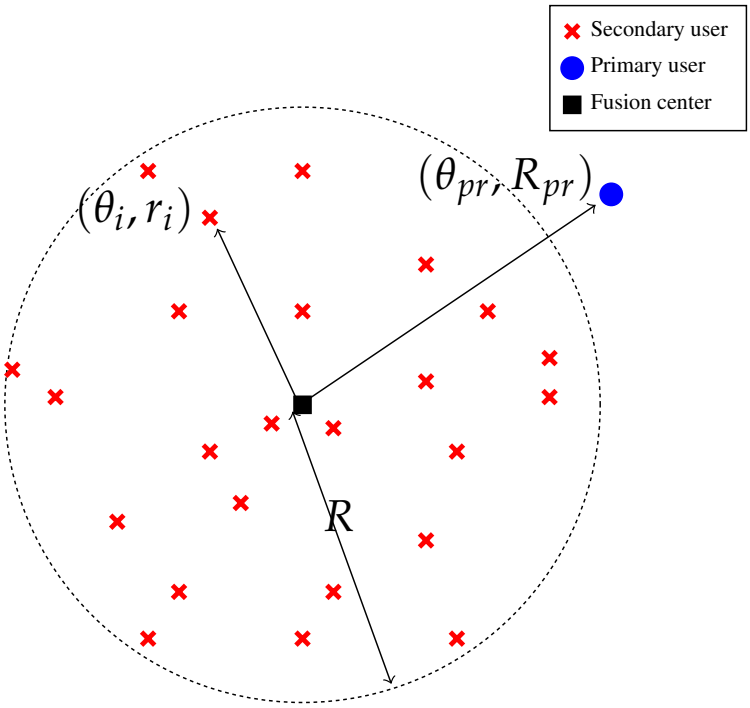

Figure 4.1: System model showing the secondary user, fusion center and the primary user.

Notice that the ED is used as the underlying strategy for all these contributions.

4.3 CHAPTER ORGANIZATION

The rest of this chapter is organized as follows. The system model is introduced in Section 4.4. Cooperative spectrum sensing is presented in 4.5. In Section 4.6, both P_{FA} and P_D are derived for the CSC scheme. The detection performance of the CSCPC detector is investigated in Section 4.7. Power consumption is analyzed in Section 4.8. Results and discussion are given in Section 4.9. Finally, a chapter summary is given in Section 4.10.

4.4 SYSTEM MODEL

A system model is illustrated in Figure 4.1. A detailed explanation of this model is given in the following subsections. Some notations from the previous chapter are re-defined for clarity.

4.4.1 *Secondary network model*

In this chapter, the secondary users are distributed uniformly in a circular area surrounding a FC located at the origin. The radius of the circle is denoted by R. The secondary users are supervised by the FC. The spatial distribution of the secondary users are modeled by a homogeneous Poisson point process (PPP) [38], i.e., Φ with intensity λ. The probability of m secondary users being inside an area $\mathcal{A}$ is characterized by

$$\text{Prob}\{m \text{ secondary users in } \mathcal{A}\} = \frac{(\lambda\mathcal{A})^m}{m!} e^{-\lambda\mathcal{A}}, \quad m \geq 0 \tag{4.1}$$

where $\mathcal{A} = \pi R^2$ is the total area in which the secondary users are located. The location of the ith secondary user is denoted by (θ_i, r_i), where θ_i is the angle between the ith secondary user and the positive x-axis and θ_i follows a uniform distribution between 0 and 2π. Finally, r_i is the distance between the ith secondary user and the FC and it is uniformly distributed between 0 and R.

4.4.2 *Primary network model*

For the primary network, we consider a fixed single primary user located at (θ_{pr}, R_{pr}). Here, θ_{pr} is a fixed angle between the primary user and the positive x-axis and R_{pr} is a fixed distance between the primary user and the FC. So the distance between the primary user and ith secondary user is given by

$$r_{pri} = \sqrt{r_i^2 + R_{pr}^2 - 2R_{pr}r_i\cos(\theta_i - \theta_{pr})}, \tag{4.2}$$

where the distance unit is in meter.

4.4.3 *Channel model between secondary users and primary user*

A Nakagami flat-fading channel is considered between the primary user and the ith secondary user. The overall channel power gain between the ith secondary user and the primary user is modeled by $h_i^2 q(\theta_i, r_i)$. h_i^2 represents the power gain of

the Nakagmai flat-fading channel $(f_{h^2}(t))$ (independent of i) with a shape parameter K_{h^2} and a scale parameter ϕ_{h^2} and is given by [67]

$$f_{h^2}(t) = \frac{t^{K_{h^2}-1}\exp(-\frac{t}{\phi_{h^2}})}{\phi_{h^2}^{K_{h^2}}\Gamma(K_{h^2})}. \tag{4.3}$$

And $q(\theta_i, r_i)$ is the path loss between the ith secondary user's location (θ_i, r_i) and the primary user's location (θ_{pr}, R_{pr}). This can also be written in terms of the path loss exponent (α) and a frequency dependent constant (κ), i.e.,

$$q(\theta_i, r_i) = \frac{\kappa}{r_{pri}^{\alpha}}. \tag{4.4}$$

For simplicity, κ is assumed to be 1.

4.4.4 *Channel model between the secondary users and the FC*

Similarly, the channel between the ith secondary user and the FC is assumed to be Nakagami flat-fading channel (g_i), thus the power of this channel (g_i^2) follows a Gamma distribution $(f_{g^2}(y))$ (independent of i) with a shape parameter K_{g^2} and a scale parameter ϕ_{g^2} and it is written as [67]

$$f_{g^2}(y) = \frac{y^{K_{g^2}-1}\exp(-\frac{y}{\phi_{g^2}})}{\phi_{g^2}^{K_{g^2}}\Gamma(K_{g^2})}. \tag{4.5}$$

The overall channel gain is given by $g_i^2 z(\theta_i, r_i)$, where $z(\theta_i, r_i)$ is the path loss between the ith secondary user and the FC with [64]

$$z(\theta_i, r_i) = \frac{1}{r_i^{\alpha}}. \tag{4.6}$$

4.4.5 *Received signal model*

The ith secondary user inside the area $\mathcal{A}$ receives either noise $(\mathcal{H}_0)$ or a primary signal plus noise $(\mathcal{H}_1)$, dependent upon the activity of the primary network:

$$\begin{aligned}\mathcal{H}_0: \quad x_i(n) &= w_i(n) \\ \mathcal{H}_1: \quad x_i(n) &= \sqrt{h_i^2 q(\theta_i, r_i)}s(n) + w_i(n)\end{aligned} \tag{4.7}$$

where $n = 0, 1, 2, ..., N-1$; N is the number of samples collected by the ith secondary user; $x_i(n)$ is the signal received by the ith secondary user; $w_i(n)$ is the ith secondary user's noise with distribution $\mathcal{CN}(0, \sigma_w^2)$; $s(n)$ is the primary signal which is randomly and independently drawn from a complex constellation. Finally, the average signal to noise ratio is defined at the FC by $SNR = 10\log_{10}\frac{P_p}{\sigma_w^2 R_{pr}^{\alpha}}$, where P_p is the primary transmit power.

4.5 COOPERATIVE SPECTRUM SENSING

In this section, the selection combining (SC) based cooperative spectrum sensing at the FC is investigated, in order to understand the activity probability, for two different censoring techniques: a received energy-based censoring (conventional censoring), and a required transmit power based censoring along with the conventional censoring[2].

4.5.1 *Received energy-based censoring*

The ith secondary user employs an ED and it compares the test statistic (T_{EDi}) with the local threshold ξ, where $T_{EDi} = \frac{1}{N}\sum_{n=0}^{N-1}|x_i(n)|^2$. Only if $(T_{EDi} > \xi)$ is satisfied, the test statistic will be sent to the FC. Thus a global test statistic (T_{max}) at FC will be chosen as follows:

$$T_{max} = \max_{\substack{(\theta_i, r_i)\in\Phi \\ T_{EDi}>\xi}} \left(T_{EDi}\right) \underset{\mathcal{H}_1}{\overset{\mathcal{H}_0}{\lessgtr}} \tau_{ED} \tag{4.8}$$

2 The first technique represents the conventional censoring scheme (CSC). The second technique represents the proposed scheme (CSCPC).

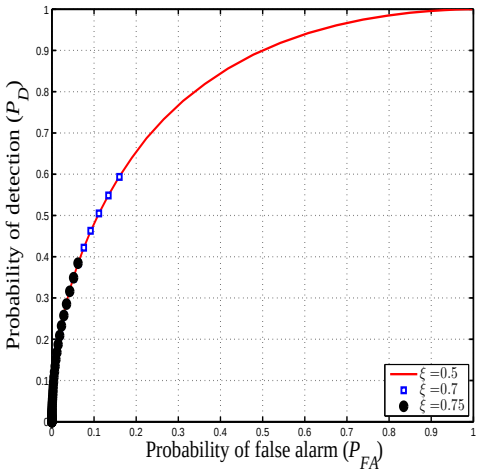

Figure 4.2: The probability of detection (P_D) versus the probability of false alarm (P_{FA}) for different values of ξ (simulation - see (4.8)). In all cases, $\alpha = 2$, $SNR = -11$dB, $R = 20$, $N = 50$, $R_{pr} = 25$, $\theta_{pr} = \frac{\pi}{2}$ and $\lambda = 0.1$.

where τ_{ED} is a global threshold at the FC. The idea behind the local threshold at each secondary user is to save power by transmitting only the most 'robust' test statistics to the FC.

4.5.2 *Required transmit power-based censoring*

In practice each secondary user faces a different signal to noise ratio at the FC. This means that the capability of sending the test statistics to the FC varies from one secondary user to another. The secondary users which are far away from the FC and those which are close to the FC (but in deep fading) will need significant transmit power to send their test statistics to the FC [3].

Motivated by the above discussion, a new parameter (transmit power threshold (p_t)) is introduced to save additional power. To send the test statistic T_{EDi} to the FC, the required transmit power p_i for the ith secondary user should satisfy $p_i \leq p_t$ where[4]

3 This power may be more than the budget power.

4 Here the p_{ref} and p_t

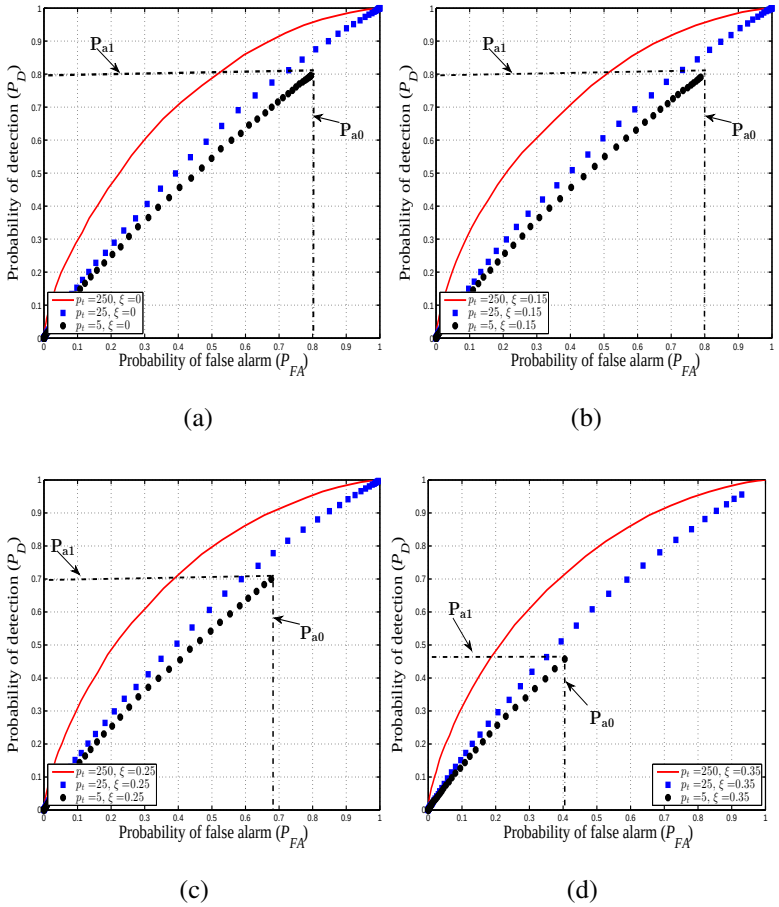

Figure 4.3: The P_D versus the P_{FA} for different values of p_t. (a) when $\xi = 0$. (b) when $\xi = 0.15$. (c) $\xi = 0.25$. (d) $\xi = 0.35$. In all cases, $SNR = -11$dB, $R = 20$, $N = 50$, $R_{pr} = 25$, $\theta_{pr} = \frac{\pi}{2}$ and $\lambda = 0.1$.

$$p_i = \frac{p_{ref}}{g_i^2 z(\theta_i, r_i)} \leq p_t. \tag{4.9}$$

Note that (4.9) is to guarantee that the received power at the FC equals p_{ref}. Now the test statistic in (4.8) with the condition in (4.9) becomes

$$T_{max} = \max_{\substack{(\theta_i, r_i)\in\Phi \\ T_{EDi}>\xi \\ p_i \leq p_t}} \left(T_{EDi} \right) \underset{\mathcal{H}_1}{\overset{\mathcal{H}_0}{\lessgtr}} \tau_{ED}. \tag{4.10}$$

4.5.3 *Idle network issue*

In cooperative spectrum sensing based on the global test statistics defined in (4.8) and (4.10), when the local threshold ξ is set too high or the transmit power threshold p_t is set too low, then the FC will not receive any test statistic (it will assume that the primary user is absent) and the detection performance at FC will deteriorate as will be seen next.

Figure 4.2 illustrates the detection performance of the global test statistic defined in (4.8). This figure is plotted by simulation for different values of ξ. We can see that as ξ increases the maximum achievable P_D reduces. The reason for that behaviour is because the FC has not received any test statistic. For example, when $\xi = 0.7$, $(P_{FA}, P_D) \leq (0.17, 0.6)$.

Now Figure 4.3 shows the detection performance of the global test statistic defined in (4.10) for different values of ξ and p_t. First, Figure 4.3 shows that as the p_t decreases so also does P_D. Also from figures 4.3a and 4.3b, it can be noticed that the detection performance is not affected by ξ. In addition, the worst scenario is when $p_t = 5$, for which $(P_{FA}, P_D) \leq (0.8, 0.8)$.

Figures 4.3c and 4.3d show that as the ξ increases as the maximum achievable P_D reduces rapidly. For example, when $\xi = 0.25$, (P_{FA}, P_D) stops at approximately $(0.68, 0.7)$ and when $\xi = 0.35$, $(P_{FA}, P_D) \leq (0.41, 0.46)$. The interpretation of the behavior of Figures 4.2 and 4.3 are discussed next.

Behavior explanation

The false alarm and detection probabilities at the FC are basically determined by the global threshold τ_{ED}. When the FC receives at least one test statistic, for $\tau_{ED} = 0$, then $P_D = P_{FA} = 1$. However, when the FC does not receive any test statistic the maximum values of P_D and P_{FA} depend on the availability of the test statistics at the FC [5]. As a result, P_D and P_{FA} at $\tau_{ED} = 0$ will be the probabilities that at least one test statistic is received by the FC under $\mathcal{H}_1$ and $\mathcal{H}_0$ respectively. Mathematically

5 In this scenario, the FC more likely decides that there is no primary user.

	$P_{FA} \approx$	$P_{a0} \approx$	$P_D \approx$	$P_{a1} \approx$
$\xi = 0.25,\ p_t = 5$	0.69	0.69	0.71	0.71
$\xi = 0.35,\ p_t = 5$	0.41	0.41	0.46	0.46
$\xi = 0.25,\ p_t = 25$	1	1	1	1
$\xi = 0.35,\ p_t = 25$	0.94	0.94	0.94	0.94

Table 4.1: P_{FA}, P_D, P_{a0} and P_{a1} for different values of ξ and p_t for $\tau_{ED} = 0$.

speaking, P_D and P_{FA} will be P_{a1} and P_{a0} instead of 1 and 1 respectively and are written as

$$\begin{aligned} P_D(\xi, p_t, \tau_{ED} = 0) &= P_{a1} \\ P_{FA}(\xi, p_t, \tau_{ED} = 0) &= P_{a0}. \end{aligned} \tag{4.11}$$

Here P_{a1} and P_{a0} are the probabilities that at least one test statistic is received by the FC under $\mathcal{H}_1$ and $\mathcal{H}_0$ respectively at $\tau_{ED} = 0$. Now P_D and the P_{FA} for any value of τ_{ED} are bounded by the following inequalities

$$\begin{aligned} P_D(\xi, p_t) &\leq P_{a1} \\ P_{FA}(\xi, p_t) &\leq P_{a0}. \end{aligned} \tag{4.12}$$

The previous results can be verified as follows. Figures 4.4 and 4.5 show P_{a1} and P_{a0} for different values of ξ and p_t respectively. Using Figures 4.3, 4.4 and 4.5, P_{FA}, P_D, P_{a0} and P_{a1} for different values of ξ and p_t are recorded in Table 4.1. The results in Table 4.1 confirm (4.11).

One commitment of cognitive radio is to protect the primary receiver from any potential interference form the cognitive network. This protection is related to the detection probability, so it is mandatory to guarantee $P_{a1} = 1$. Consequently, P_{a1} is considered instead of P_{a0}, the derivation of P_{a1} will be discussed in the next subsection.

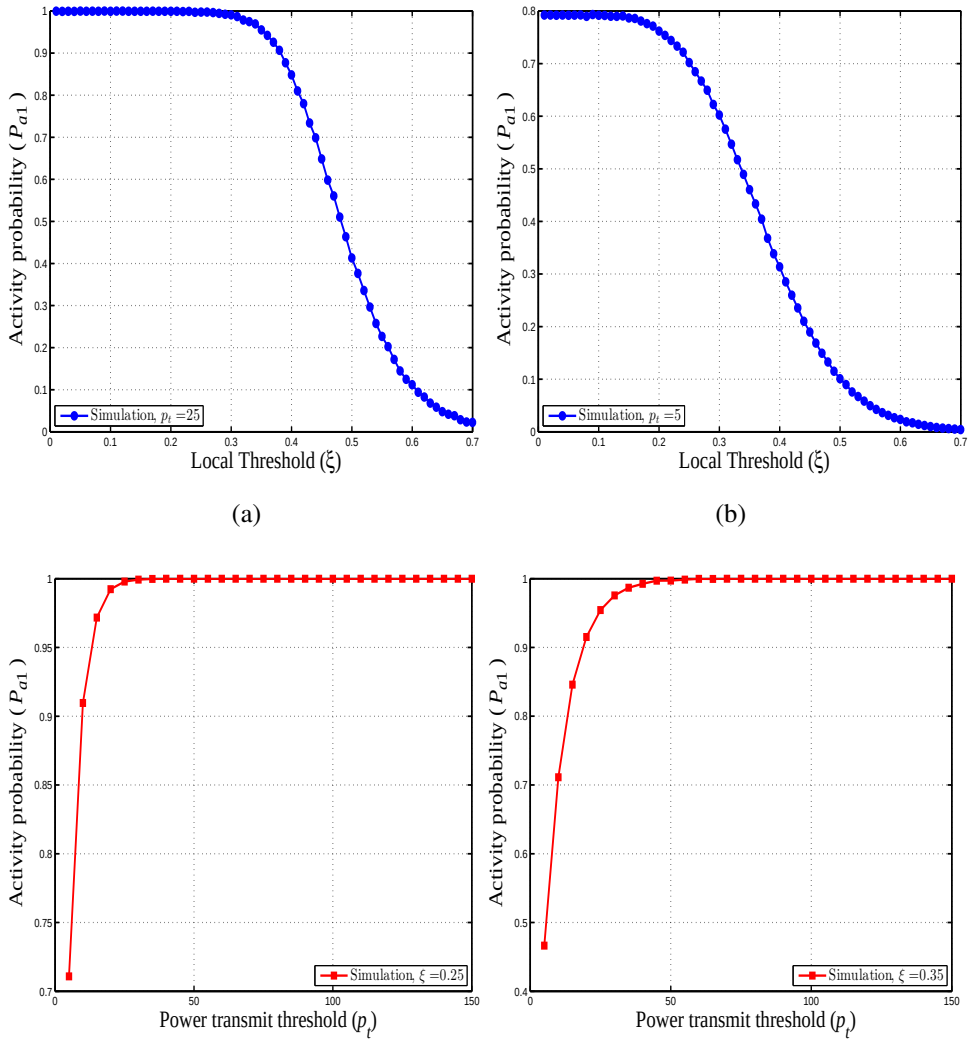

Figure 4.4: (a) P_{a1} versus ξ for $p_t = 25$. (b) P_{a1} versus ξ at $p_t = 5$. (c) P_{a1} versus p_t for $\xi = 0.25$. (d) P_{a1} versus p_t for $\xi = 0.35$. In all cases, $SNR = -11$dB, $R = 20$, $N = 50$, $R_{pr} = 25$, $\theta_{pr} = \frac{\pi}{2}$ and $\lambda = 0.1$.

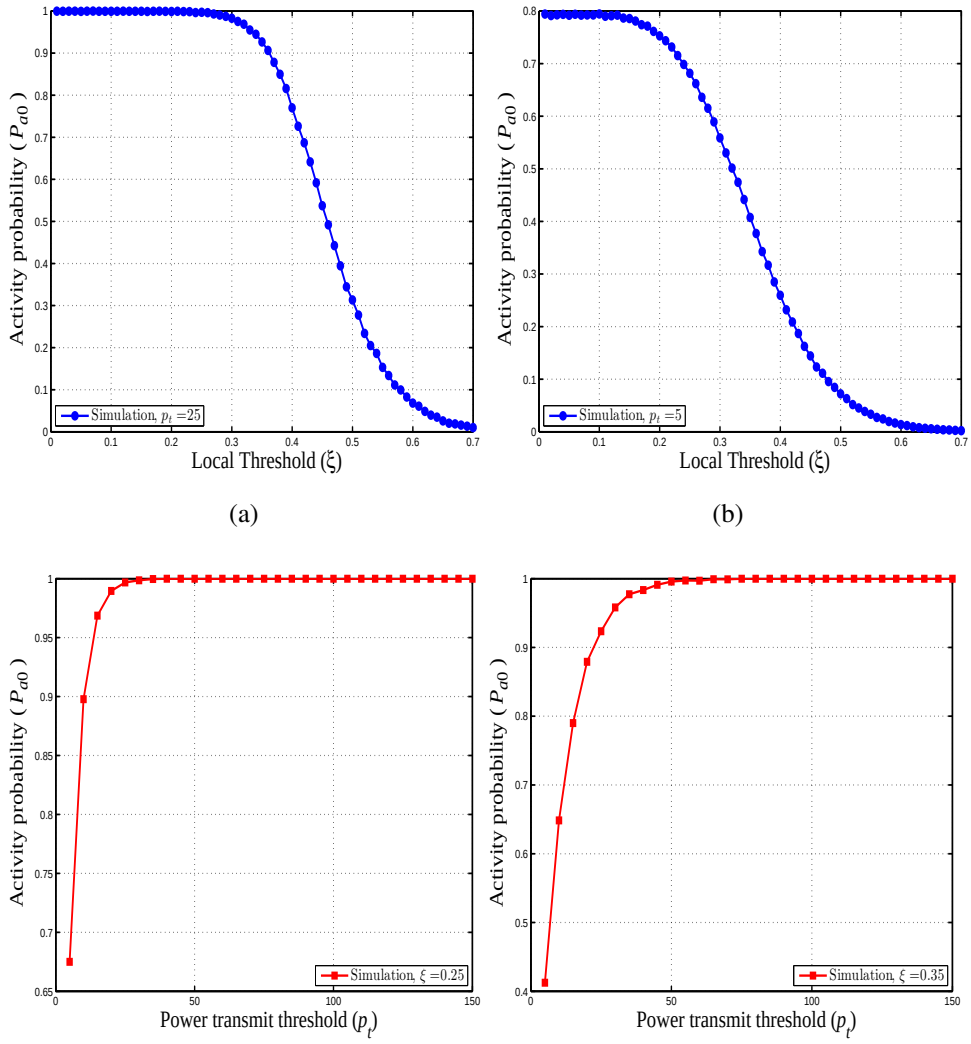

Figure 4.5: (a) The P_{a0} versus the ξ at $p_t = 25$. (b) The P_{a0} versus the ξ at $p_t = 5$. (c) The P_{a0} versus the p_t at $\xi = 0.25$. (d) The P_{a0} versus the p_t at $\xi = 0.35$. In all cases, $SNR = -11$dB, $R = 20$, $N = 50$, $R_{pr} = 25$, $\theta_{pr} = \frac{\pi}{2}$ and $\lambda = 0.1$.

4.5.4 *Activity probability*

As it is mentioned earlier, there exists a probability (because of the choice of ξ and p_t) that no test statistic may be sent to the FC and subsequently the detection performance may be degraded. Thus the activity probability (P_{a1}) is introduced, which is defined as *the probability that at least one test statistic is received by the*

FC under $\mathcal{H}_1$. Here we require $P_{a1} \approx 1$ to avoid any degradation in the detection performance and so we will examine how the choice of ξ and p_t affects P_{a1}.

Figures 4.4a and 4.4b show a plot of P_{a1} versus the ξ for different values of p_t. First it can be easily seen as p_t decreases from 25 to 5 the P_{a1} decreases. Also from Figures 4.4a and 4.4b, if ξ is very large (no test statistics will be sent to the FC). This means $P_{a1} \approx 0$ and this is desirable from a power saving point of view but it is undesirable from a detection performance point of view. Thus ξ should be chosen as large as possible to ensure that $P_{a1} \approx 1$. This maximum threshold will be called an optimum local threshold $(\xi = \xi_{opt})$.

The choice of parameter p_t also affects P_{a1}. This can also be seen in Figures 4.4c and 4.4d which show a plot of P_{a1} versus the p_t for different values of ξ. It can be seen that when p_t is small P_{a1} is also small. In terms of saving power this is desirable but in terms of detection performance it is not. However, if p_t is large, then $P_{a1} \approx 1$ and this will increase the power consumption which is desirable for the detection performance and not for saving power. Therefore, p_t should be chosen as small as possible such that $P_{a1} \approx 1$. This minimum transmit power threshold will be called the optimum transmit power threshold $(p_t = p_{topt})$.

Motivated by the above explanation we seek to find both ξ_{opt} and p_{topt} that satisfy the following condition:

$$(\xi_{opt}, p_{topt}) = \{\max \xi \text{ and } \min p_t \text{ such that } P_{a1}(\xi_{opt}, p_{topt}) = 1\}. \tag{4.13}$$

To compute (4.13) it is needed to derive the activity probability (P_{a1}) through the following proposition.

Proposition 1. The probability that at least one test statistic is received by the FC under $\mathcal{H}_1$ is given by:

$$P_{a1}(\xi, p_t) = 1 - \exp\Big(-\frac{\lambda}{\Gamma(K_{g^2})}\int_0^{2\pi}\int_0^{R} Q_{Nak}(\theta, r)\Gamma(K_{g^2}, \frac{p_{ref} r^{\alpha}}{p_t \phi_{g^2}})rdrd\theta\Big) \tag{4.14}$$

Proof. The probability that the test statistic T_{EDi} is not received by the FC (P_{ni}) occurs when the ξ and p_t are sufficiently high or low respectively. Mathematically speaking it is given by

$$P_{ni} = \text{Prob}\{T_{EDi} < \xi \text{ or } p_i > p_t\}. \tag{4.15}$$

Because T_{EDi} and p_i are independent, thus (4.15) can be written as

$$P_{ni} = 1 - \text{Prob}\{T_{EDi} > \xi | \mathcal{H}_1\}\text{Prob}\{p_i < p_t\}. \tag{4.16}$$

Because the secondary users are independent, thus the probability that no test statistic is received by the FC $(\overline{P}_n)$ under $\mathcal{H}_1$ is given by

$$\overline{P}_n = \mathbb{E}_{\Phi,h_i^2}\left[\prod_{(\theta_i,r_i)\in\Phi}\left[1 - \text{Prob}(T_{EDi} > \xi|\mathcal{H}_1)\text{Prob}(p_i < p_t)\right]\right]. \tag{4.17}$$

Then the probability that at least one test statistic is received by the FC is given by

$$P_{a1} = 1 - \overline{P}_n. \tag{4.18}$$

Now when $\text{Prob}(T_{EDi} > \xi|\mathcal{H}_1)$ is evaluated, the test statistic T_{EDi} under $\mathcal{H}_1$ will have a noncentral chi-square distribution with $2N$ degrees of freedom and a non centrality parameter $v_i = \frac{2Nh_i^2}{\sigma_w^2 r_{pri}^{\alpha}}$. Thus $\text{Prob}\{T_{EDi} > \xi|\mathcal{H}_1)$, conditioned on the channel and path loss is given by

$$\text{Prob}\{T_{EDi} > \xi|\mathcal{H}_1\} = Q_N(\sqrt{v_i}, \sqrt{\frac{2N\xi}{\sigma_w^2}}) \tag{4.19}$$

where $Q_N(.,.)$ is the generalized Marcum Q-function (conditioned on the channels and the pathloss) defined as follows,

$$Q_N(a,b) = \int_b^{\infty} \frac{x^N}{a^{N-1}}\exp\left(\frac{x^2+a^2}{2}\right) I_{N-1}(ax)dx.$$

Also, $\text{Prob}(p_i < p_t)$ after substituting $p_i = \frac{p_{ref}}{g_i^2 z(\theta_i,r_i)}$, can be written as

$$\text{Prob}\{p_i < p_t\} = \text{Prob}\{g^2 > \frac{p_{ref} r^{\alpha}}{p_t}\} \tag{4.20}$$

the subscript 'i' is dropped from g_i^2 and r_i^{α}, because the random variable g_i^2 follows a Gamma distribution. Thus (4.20) conditioned on the pathloss is

$$\text{Prob}\{p_i < p_t\} = \frac{\Gamma(K_{g^2}, \frac{p_{ref} r^{\alpha}}{p_t \phi_{g^2}})}{\Gamma(K_{g^2})}. \tag{4.21}$$

By substituting (4.19) and (4.21) into (4.18), then by applying the generating functional of the Poisson process [see [38], eq (4.3.8)]

$$P_{a1}(\xi, p_t) = 1 - \exp\Bigg(-\frac{\lambda}{\Gamma(K_{g^2})}\int_0^{2\pi}\int_0^{R}\Big[\int_0^{\infty} Q_N\Big(\sqrt{\frac{2Nh^2}{\sigma_w^2 r_{pr}^{\alpha}}}, \sqrt{\frac{2N\xi}{\sigma_w^2}}\Big) \times f_{h^2}(t)dt\Big] \times \Gamma\Big(K_{g^2}, \frac{p_{ref} r^{\alpha}}{p_t \phi_{g^2}}\Big) r dr d\theta\Bigg). \tag{4.22}$$

The inner integral in (4.22) represents the detection probability for a local secondary user over a Nakagmai fading channel and it is derived in [[22], equation (20)]. This inner integral is denoted by $Q_{Nak}(\theta, r)$. After substituting $Q_{Nak}(\theta, r)$ into (4.22) then (4.14) is obtained. Then after finding the activity probability (P_{a1}), the ξ_{opt} and the p_{opt} can be found numerically such that (4.13) is satisfied.

4.6 DETECTION PERFORMANCE ANALYSIS FOR THE CSC SCHEME

In this section closed-form expressions for P_{FA} and P_D are derived for the conventional censored selection combining (CSC) detector (see - (4.8)). For this detector, it is assumed that (4.13) is satisfied. Notice that, this detector does not depend on the p_i.

4.6.1 *False alarm probability derivation*

When each secondary user sends its test statistic $(T_{EDi} > \xi_{opt})$ to the FC then the FC selects the maximum test statistic. Thus

$$P_{FA} = \text{Prob}\{T_{max} > \tau_{ED} | \mathcal{H}_0\}. \tag{4.23}$$

Because all the secondary users are independent (4.23) can be written as

$$\begin{aligned} P_{FA} &= 1 - \text{Prob}\{T_{max} < \tau_{ED} | \mathcal{H}_0\} \\ P_{FA} &= 1 - \mathbb{E}_{\Phi, h_i^2}\Big[\prod_{\substack{(\theta_i, r_i)\in\Phi \\ T_{EDi} > \xi_{opt}}} \text{Prob}(T_{EDi} < \tau_{ED} | \mathcal{H}_0, \Phi, h_i^2)\Big]. \end{aligned} \tag{4.24}$$

As mentioned above, when (4.13) is satisfied, this means that at least one test statistic is received by the FC. Therefore, the selection combining at the FC will not be affected by the local threshold ξ_{opt} (as will be seen in the simulation section). Thus the local threshold ξ_{opt} could be omitted from (4.24). Now (4.24) can be written as

$$P_{FA} = 1 - \mathbb{E}_{\Phi,h_i^2}\Big[\prod_{(\theta_i,r_i)\in\Phi} \text{Prob}(T_{EDi} < \tau_{ED}\big|\mathcal{H}_0,\Phi,h_i^2)\Big]. \tag{4.25}$$

T_{EDi} under $\mathcal{H}_0$ is a sum of the squares of $2N$ Gaussian random variables with zero mean. Therefore, T_{EDi} follows a central chi-square distribution with $2N$ degrees of freedom. So $\text{Prob}\{T_{EDi} < \tau_{ED}\big|\mathcal{H}_0\} = 1 - \frac{\Gamma(N,\frac{N\tau_{ED}}{\sigma_w^2})}{\Gamma(N)}$ and (4.25) reduces to

$$P_{FA} = 1 - \mathbb{E}_{\Phi,h_i^2}\Big[\prod_{(\theta_i,r_i)\in\Phi}\Big(1 - \frac{\Gamma(N,\frac{N\tau_{ED}}{\sigma_w^2})}{\Gamma(N)}\Big)\Big]. \tag{4.26}$$

By applying the generating functional of the Poisson process in (4.26) [see [38], eq. (4.3.8)], the false alarm probability can be written as

$$\begin{aligned} P_{FA} &= 1 - \exp\Big(-\frac{\lambda\Gamma(N,\frac{N\tau_{ED}}{\sigma_w^2})}{\Gamma(N)}\int_0^{2\pi}\int_0^R rd\theta dr\Big) \\ P_{FA} &= 1 - \exp\Big(-\frac{\lambda\pi R^2\Gamma(N,\frac{N\tau_{ED}}{\sigma_w^2})}{\Gamma(N)}\Big). \end{aligned} \tag{4.27}$$

Note that (4.27) is independent from ξ_{opt} and so it will not affect the detection performance as will be seen in the simulation results.

4.6.2 *Detection probability derivation*

Now P_D, it can be derived in a similar manner to the P_{FA}. When each secondary user sends its test statistic $(T_{EDi} > \xi_{opt})$ to the FC, then the FC selects the maximum test statistic. Thus P_D is formulated as

$$P_D = \text{Prob}\{T_{max} > \tau_{ED}\big|\mathcal{H}_1\}. \tag{4.28}$$

Because the secondary users are independent and the selection combining at the FC is independent of the local threshold (ξ_{opt}) when (4.13) is satisfied, similar to P_{FA}, then (4.28) is given by

$$P_D = 1 - \mathbb{E}_{\Phi,h_i^2}\Big[\prod_{(\theta_i,r_i)\in\Phi} \text{Prob}\{T_{EDi} < \tau_{ED}\big|\mathcal{H}_1,\Phi,h_i^2\}\Big]. \tag{4.29}$$

$\text{Prob}(T_{EDi} < \tau_{ED}|\mathcal{H}_1)$ can be evaluated by 1-$Q_N(\sqrt{\frac{2Nh_i^2}{\sigma_w^2 r_{pri}^{\alpha}}}, \sqrt{\frac{2N\tau_{ED}}{\sigma_{w_i}^2}})$. Thus by substituting $\text{Prob}(T_{EDi} < \tau_{ED}|\mathcal{H}_1)$ into (4.29)

$$P_D = 1 - \mathbb{E}_{\Phi,h_i^2}\Big[\prod_{(\theta_i,r_i)\in\Phi}\Big(1 - Q_N\Big(\sqrt{\frac{2Nh_i^2}{\sigma_w^2 r_{pri}^{\alpha}}}, \sqrt{\frac{2N\tau_{ED}}{\sigma_w^2}}\Big)\Big)\Big]. \tag{4.30}$$

The transmitting secondary users constitutes a marked PPP with an intensity

$$\lambda_1(h^2) = \lambda f_{h^2}(t). \tag{4.31}$$

Then by applying the generating functional of the Poisson process in (4.30) [see [38], eq. (4.3.8)] and with an intensity defined in (4.31), the detection probability can be written as

$$P_D = 1 - \exp\Big(-\lambda \int_0^{2\pi}\int_0^{R}\Big[\int_0^{\infty} f_{h^2}(t) Q_N\Big(\sqrt{\frac{2Nh^2}{\sigma_w^2 r_{pr}^{\alpha}}}, \sqrt{\frac{2N\tau_{ED}}{\sigma_w^2}}\Big)dt\Big] \times r d\theta dr\Big). \tag{4.32}$$

By using [[22], equation (20)] in (4.32), then (4.32) becomes

$$P_D = 1 - \exp\Big(-\lambda \int_0^{2\pi}\int_0^{R} Q_{Nak}(\theta, r) r dr d\theta\Big), \tag{4.33}$$

where $Q_{Nak}(\theta, r)$ is defined in subsection 4.5.4.

4.7 DETECTION PERFORMANCE ANALYSIS FOR THE CSCPC SCHEME

In this section closed-form expressions for P_{FA} and P_D are derived for the censored selection combining detector based on power censoring (CSCPC) (see - (4.10)). This detector is evaluated analytically when (4.13) is satisfied and p_i is considered.

4.7.1 *False alarm probability derivation*

When each secondary user sends its test statistic ($T_{EDi} > \xi_{opt}$ and $p_i \leq p_{topt}$) to the FC, then the FC selects the maximum test statistic, and

$$P_{FA} = \text{Prob}\{T_{max} > \tau_{ED}|\mathcal{H}_0\}. \tag{4.34}$$

Because all the secondary users are independent, then (4.34) can be written as

$$P_{FA} = 1 - \mathbb{E}_{\Phi_p, h_i^2}\Big[\prod_{(\theta_i, r_i)\in\Phi_p} \text{Prob}\big\{T_{EDi} < \tau_{ED}\big|\mathcal{H}_0, \Phi_p, h_i^2\big\}\Big]. \tag{4.35}$$

Again, (4.35) does not rely on the local threshold ξ_{opt} and $\text{Prob}\big\{T_{EDi} < \tau_{ED}\big|\mathcal{H}_0\big\} = 1 - \frac{\Gamma(N, \frac{N\tau_{ED}}{\sigma_w^2})}{\Gamma(N)}$. Thus (4.35) can be written as

$$P_{FA} = 1 - \mathbb{E}_{\Phi_p, h_i^2}\Big[\prod_{(\theta_i, r_i)\in\Phi_p} \Big(1 - \frac{\Gamma(N, \frac{N\tau_{ED}}{\sigma_w^2})}{\Gamma(N)}\Big)\Big], \tag{4.36}$$

where Φ_p is the set of transmitting secondary users that satisfy $p_i \leq p_{topt}$. The transmitting secondary users Φ_p constitute a non-homogeneous/inhomogeneous in PPP with an intensity

$$\lambda_0(y, r) = \lambda \mathbf{1}\Big(\frac{p_{ref} r^\alpha}{y} < p_{topt}\Big) f_{g^2}(y), \tag{4.37}$$

where the subscript 'i' is dropped from g_i^2 and r_i^α and $\mathbf{1}\Big(\frac{p_{ref} r^\alpha}{y} < p_{topt}\Big)$ is an indicator which is defined as

$$\mathbf{1}\Big(\frac{p_{ref} r^\alpha}{y} < p_{topt}\Big) = \begin{cases} 1 & \frac{p_{ref} r^\alpha}{y} < p_{topt} \\ 0 & \frac{p_{ref} r^\alpha}{y} > p_{topt}. \end{cases} \tag{4.38}$$

By applying the generating functional of the Poisson process in (4.36) [see [38], eq. (4.3.8)] and with (4.37), then

$$\begin{aligned} P_{FA} &= 1 - \exp\Big(-\Lambda \int_0^\infty \int_0^{2\pi} \int_0^R \mathbf{1}(\frac{p_{ref} r^\alpha}{y} < p_{topt}) f_{g^2}(y) r dy d\theta dr\Big) \\ &= 1 - \exp\Big(-\frac{\Lambda}{\phi_{g^2}^{K_{g^2}} \Gamma(K_{g^2})} \int_0^\infty \int_0^{2\pi} \int_0^R \mathbf{1}(y > \frac{p_{ref} r^\alpha}{p_{topt}}) \\ &\times y^{K_{g^2}-1} \exp(-\frac{y}{\phi_{g^2}}) r dy d\theta dr\Big) \\ &= 1 - \exp\Big(-\frac{2\pi\Lambda}{\phi_{g^2}^{K_{g^2}} \Gamma(K_{g^2})} \int_0^R r \int_{\frac{p_{ref} r^\alpha}{p_{topt}}}^\infty y^{K_{g^2}-1} \exp(-\frac{y}{\phi_{g^2}}) dy dr\Big) \\ P_{FA} &= 1 - \exp\Big(-\frac{2\pi\Lambda}{\Gamma(K_{g^2})} \int_0^R \Gamma(K_{g^2}, \frac{p_{ref} r^\alpha}{\phi_{g^2} p_{topt}}) r dr\Big), \end{aligned} \tag{4.39}$$

where $\Lambda = \frac{\lambda \Gamma(N, \frac{N\tau_{ED}}{\sigma_w^2})}{\Gamma(N)}$.

4.7.2 *Detection probability derivation*

Now P_D can be obtained in a similar manner as P_{FA}. When each secondary user sends its test statistic ($T_{EDi} > \xi_{opt}$ and $p_i \leq p_{topt}$) to the FC, then the FC selects the maximum test statistic. Thus P_D can be written as

$$P_D = \text{Prob}\{T_{max} > \tau_{ED} | \mathcal{H}_1\}, \tag{4.40}$$

and because all the secondary users are independent, so

$$P_D = 1 - \mathbb{E}_{\Phi_p, h_i^2}\Big[\prod_{(\theta_i, r_i)\in\Phi_p} \text{Prob}\{T_{EDi} < \tau_{ED} | \mathcal{H}_1, \Phi_p, h_i^2\}\Big], \tag{4.41}$$

where $\text{Prob}\{T_{EDi} < \tau_{ED} | \mathcal{H}_1\} = 1 - Q_N(\sqrt{\frac{2Nh^2}{\sigma_w^2 r_{pr}^{\alpha}}}, \sqrt{\frac{2N\tau_{ED}}{\sigma_w^2}})$ and Φ_p is the set of transmitting secondary users that satisfy $p_i \leq p_{topt}$. Thus

$$P_D = 1 - \mathbb{E}_{\Phi_p, h_i^2}\Big[\prod_{(\theta_i, r_i)\in\Phi_p} \Big(1 - Q_N(\sqrt{\frac{2Nh^2}{\sigma_w^2 r_{pr}^{\alpha}}}, \sqrt{\frac{2N\tau_{ED}}{\sigma_w^2}})\Big)\Big]. \tag{4.42}$$

The transmitting secondary users Φ_p constitutes a non-homogeneous/inhomogeneous PPP with an intensity

$$\lambda_1(y, t, r) = \lambda \mathbf{1}(\frac{p_{ref} r^{\alpha}}{y} < p_{topt}) f_{h^2}(t), \tag{4.43}$$

where $\mathbf{1}(\frac{p_{ref} r^{\alpha}}{y} < p_{topt})$ is defined in (4.38). Then by applying the generating functional of the Poisson process in (4.42) [see [38], eq. (4.3.8)] and with (4.43), then P_D is modified as follows

$$P_D = 1 - \exp\Big(-\triangle \int_0^{\infty}\int_0^{\infty}\int_0^{2\pi}\int_0^{R} Q_N(\sqrt{\frac{2Nt}{\sigma_w^2 r_{pr}^{\alpha}}}, \sqrt{\frac{2N\tau_{ED}}{\sigma_w^2}})$$
$$\mathbf{1}(y > \frac{p_{ref} r^{\alpha}}{p_{topt}}) \times t^{K_{h^2}-1}\exp(-t/\phi_{h^2}) \times y^{K_{g^2}-1}$$
$$\times \exp(-y/\phi_{g^2}) r dr d\theta dt dy\Big)$$

$$P_D = 1 - \exp\Bigg(-\triangle \int_0^{2\pi}\int_0^{R}\Bigg[r\Big[\int_0^{\infty} Q_N\Big(\sqrt{\frac{2Nt}{\sigma_w^2 r_{pr}^{\alpha}}}, \sqrt{\frac{2N\tau_{ED}}{\sigma_w^2}}\Big)t^{K_{h^2}-1} \times \exp(-t/\phi_{h^2})dt\Big]\int_{\frac{p_{ref}r^{\alpha}}{p_{topt}}}^{\infty} y^{K_{g^2}-1}\exp(-y/\phi_{g^2})dy\Bigg]drd\theta\Bigg)$$

$$= 1 - \exp\Bigg(-\triangle\phi_{g^2}^{K_{g^2}}\int_0^{2\pi}\int_0^{R}\Bigg[r\Gamma\Big(K_{g^2}, \frac{p_{ref}r^{\alpha}}{p_{topt}\phi_{g^2}}\Big) \times \Big[\int_0^{\infty} Q_N\Big(\sqrt{\frac{2Nh^2}{\sigma_w^2 r_{pri}^{\alpha}}}, \sqrt{\frac{2N\tau_{ED}}{\sigma_w^2}}\Big)t^{K_{h^2}-1}\exp(-t/\phi_{h^2})dt\Big]\Bigg]drd\theta\Bigg),$$

where $\Delta = \frac{\lambda}{\Gamma(K_{h^2})\phi_{h^2}^{K_{h^2}}\phi_{g^2}^{K_{g^2}}\Gamma(K_{g^2})}$. Finally the detection probability is given by

$$P_D = 1 - \exp\Bigg(-\Delta\phi_{g^2}^{K_{g^2}}\int_0^{2\pi}\int_0^{R}\Big[rQ_{Nak}(\theta, r)\Gamma\Big(K_{g^2}, \frac{p_{ref}r^{\alpha}}{p_{topt}\phi_{g^2}}\Big)\Big]drd\theta\Bigg). \tag{4.44}$$

where $Q_{Nak}(\theta, r)$ is defined in subsection 4.5.4.

4.8 AVERAGE TOTAL POWER CONSUMPTION

In this section, the average total power $\mathbb{E}[\triangle(\xi, p_t)]$ consumption is derived. Here $\triangle(\xi, p_t)$ is the secondary network's total power needed to transmit the test statistics to the FC. The average total power consumption is derived for two different scenarios.

Scenario I: The first scenario is when the primary user is absent $(\mathcal{H}_0)$. In this case, the total power needed to transmit the test statistics to the FC is given by

$$\begin{aligned}\Delta_0(\xi, p_t) &= \sum_{\substack{(\theta_i, r_i)\in\Phi_p \\ T_{EDi}\big|\mathcal{H}_0>\xi}} p_i \\ &= \sum_{\substack{(\theta_i, r_i)\in\Phi_p \\ T_{EDi}\big|\mathcal{H}_0>\xi}} \frac{p_{ref}r_i^{\alpha}}{g_i^2},\end{aligned} \tag{4.45}$$

notice that the transmitted test statistic should satisfy ($T_{EDi} > \xi$ and $p_i \leq p_t$). The transmitting secondary users Φ_p constitute a non-homogeneous PPP with an intensity

$$\begin{aligned}\lambda_0(y,r) &= \lambda \text{Prob}\{T_{EDi} > \xi | \mathcal{H}_0\} \mathbf{1}(\frac{p_{ref} r^\alpha}{y} < p_t) f_{g^2}(y) \\ \lambda_0(y,r) &= \frac{\lambda \Gamma(N, \frac{N\xi}{\sigma_w^2})}{\Gamma(N)} \mathbf{1}(\frac{p_{ref} r^\alpha}{y} < p_t) f_{g^2}(y),\end{aligned} \tag{4.46}$$

where $\mathbf{1}(\frac{p_{ref} r^\alpha}{y} < p_t)$ is defined in (4.38). Thus the average total power when the primary user is absent is given by

$$\mathbb{E}\left[\triangle_0(\xi, p_t)\right] = \sum_{\substack{(\theta_i, r_i) \in \Phi_p \\ T_{EDi} | \mathcal{H}_0 > \xi}} \mathbb{E}[\frac{p_{ref} r_i^\alpha}{g_i^2}]. \tag{4.47}$$

Now by applying Campbell's theorem [38] with (4.46)

$$\begin{aligned}\mathbb{E}\left[\triangle_0(\xi, p_t)\right] &= \frac{\lambda p_{ref} \Gamma(N, \frac{N\xi}{\sigma_w^2})}{\Gamma(N)} \int_0^\infty \int_0^{2\pi} \int_0^R \frac{r^\alpha}{y} \frac{y^{K_{g^2}-1}}{\Gamma(K_{g^2}) \phi_{g^2}^{K_{g^2}}} \\ &\times \mathbf{1}(\frac{p_{ref} r^\alpha}{y} < p_t) \exp(-y/\phi_{g^2}) r dr d\theta dy \\ &= \frac{2\pi \lambda p_{ref} \Gamma(N, \frac{N\xi}{\sigma_w^2})}{\phi_{g^2}^{K_{g^2}} \Gamma(K_{g^2}) \Gamma(N)} \int_0^\infty \int_0^R r^{\alpha+1} y^{K_{g^2}-2} \exp(-y/\phi_{g^2}) \\ &\times \mathbf{1}\left(r < \left(\frac{p_t y}{p_{ref}}\right)^{1/\alpha}\right) dr dy.\end{aligned} \tag{4.48}$$

And by substituting $u = y/\phi_{g^2}$ into (4.48)

$$\begin{aligned}\mathbb{E}\left[\triangle_0(\xi, p_t)\right] &= \vartheta \left[\int_0^\infty \int_0^{(u p_t \phi_{g^2}/p_{ref})^{1/\alpha}} r^{\alpha+1} u^{K_{g^2}-2} \exp(-u) du dr\right] \\ &= \vartheta \left[\int_0^\infty u^{K_{g^2}-2} \exp(-u) \left[\int_0^{(u p_t \phi_{g^2}/p_{ref})^{1/\alpha}} r^{\alpha+1} \, \mathrm{d}r\right] du\right] \\ &= \frac{\vartheta (\frac{p_t \phi_{g^2}}{p_{ref}})^{\frac{\alpha+2}{\alpha}}}{(\alpha+2)} \left[\int_0^\infty u^{K_{g^2}+\frac{2}{\alpha}-1} \exp(-u) du\right] \\ &= \frac{\vartheta (\frac{p_t \phi_{g^2}}{p_{ref}})^{\frac{\alpha+2}{\alpha}}}{(\alpha+2)} \Gamma(K_{g^2} + \frac{2}{\alpha}),\end{aligned} \tag{4.49}$$

where $\vartheta = \frac{2\pi\lambda p_{ref}\Gamma(N,\frac{\xi}{\sigma_w^2})}{\phi_{g^2}\Gamma(K_{g^2})\Gamma(N)}$.

Scenario II: The second scenario is when the primary user is present $(\mathcal{H}_1)$. In this case, the total power needed to transmit the test statistics to the FC is given by

$$\begin{aligned}\Delta_1(\xi, p_t) &= \sum_{\substack{(\theta_i,r_i)\in\Phi_p \\ T_{EDi}\left|\mathcal{H}_1>\xi\right.}} p_i \\ &= \sum_{\substack{(\theta_i,r_i)\in\Phi_p \\ T_{EDi}\left|\mathcal{H}_1>\xi\right.}} \frac{p_{ref} r_i^{\alpha}}{g_i^2},\end{aligned} \tag{4.50}$$

and again Φ_p is the set of transmitting secondary users that satisfy $p_i \leq p_t$. Also, Φ_p constitutes a non-homogeneous PPP with an intensity

$$\begin{aligned}\lambda_1(y,t,r) &= \lambda \text{Prob}\{T_{EDi} > \xi \left| \mathcal{H}_1 \right.\} \mathbf{1}(\frac{p_{ref} r^{\alpha}}{y} < p_t) f_{g^2}(y) \\ &= \lambda Q_N(\sqrt{\frac{2Nt}{\sigma_w^2 r_{pr}^{\alpha}}}, \sqrt{\frac{2N\xi}{\sigma_w^2}}) \mathbf{1}(\frac{p_{ref} r^{\alpha}}{y} < p_t) f_{g^2}(y).\end{aligned} \tag{4.51}$$

Thus the average total power when the primary user is present is given by

$$\mathbb{E}\left[\triangle_1(\xi, p_t)\right] = \sum_{\substack{(\theta_i,r_i)\in\Phi_p \\ T_{EDi}\left|\mathcal{H}_1>\xi\right.}} \mathbb{E}[\frac{p_{ref} r_i^{\alpha}}{g_i^2}]. \tag{4.52}$$

By using (4.51) and Campbell's theorem

$$\begin{aligned}\mathbb{E}\left[\triangle_1(\xi, p_t)\right] &= \vartheta_1 \int_0^{\infty}\int_0^{\infty}\int_0^{2\pi}\int_0^{R} \frac{r^{\alpha}}{y} y^{K_{g^2}-1} t^{K_{h^2}-1} \\ &\quad \times Q_N(\sqrt{\frac{2Nt}{\sigma_w^2 r_{pr}^{\alpha}}}, \sqrt{\frac{2N\xi}{\sigma_w^2}}) \mathbf{1}(\frac{p_{ref} r^{\alpha}}{y} < p_t) \\ &\quad \times \exp(-y/\phi_{g^2}) \exp(-t/\phi_{h^2}) r dy dt d\theta dr \\ &= \vartheta_1 \int_0^{2\pi}\int_0^{R} r^{\alpha+1} \Bigg[[\int_0^{\infty} t^{K_{h^2}-1} \exp(-t/\phi_{h^2}) \\ &\quad Q_N(\sqrt{\frac{2Nt}{\sigma_w^2 r_{pr}^{a}}}, \sqrt{\frac{2N\xi}{\sigma_w^2}}) dt] \\ &\quad \times [\int_0^{\infty} y^{K_{g^2}-2} \mathbf{1}(y > \frac{p_{ref} r^{\alpha}}{p_t}) \exp(-y/\phi_{g^2}) dy] \Bigg] \mathrm{d}r\end{aligned}$$

$$
\begin{aligned}
&= \vartheta_1 \int_0^{2\pi} \int_0^{R} r^{\alpha+1} Q_{Nak}(\theta, r) \\
&\times \int_{\frac{p_{ref} r^{\alpha}}{p_t}}^{\infty} y^{K_{g^2}-2} \exp(-y/\phi_{g^2}) dy dr \\
&= \vartheta_1 \phi_{g^2}^{K_{g^2}-1} \int_0^{2\pi} \int_0^{R} r^{\alpha+1} Q_{Nak}(\theta, r) \Gamma(K_{g^2} - 1, \frac{p_{ref} r^{\alpha}}{p_t \phi_{g^2}}),
\end{aligned}
\tag{4.53}
$$

where $\vartheta_1 = \frac{\lambda p_{ref}}{\Gamma(K_{h^2}) \phi_{h^2}^{K_{h^2}} \Gamma(K_{g^2}) \phi_{g^2}^{K_{g^2}}}$. By evaluating (4.53) numerically, the average total power of the secondary network for sending the test statistics to the FC is given by

$$
\mathbb{E}[\triangle(\xi, p_t)] = P(\mathcal{H}_0) \mathbb{E}\left[\triangle_0(\xi, p_t)\right] + P(\mathcal{H}_1) \mathbb{E}\left[\triangle_1(\xi, p_t)\right], \tag{4.54}
$$

where $P(\mathcal{H}_0)$ is the activity of the secondary network and $P(\mathcal{H}_0) = 1 - P(\mathcal{H}_1)$.

4.9 RESULTS AND DISCUSSION

This section presents some simulation results to validate the theoretical analysis that has been coppied out in the last sections for the following system parameters: $m = 2$, $P_p = 1$, and $p_{ref} = 1$. In addition, it provides some results regarding the CSC and CSCPC schemes, showing the advantage of CSCPC over CSC in terms of reducing the energy overhead while the detection performance loss is negligible. The number of Monte Carlo iterations is set to 10^5. The ξ_{opt} and p_{topt} are found using (4.14) by grid search.

Result 1: Theoretical results verification for activity probability (Figures 4.6 and 4.7).

Here the activity probability under $\mathcal{H}_1$ (P_{a1}) is plotted analytically using (4.22). The simulation result is plotted by counting how many times the FC receives any test statistic out of the total number of iterations. First, Figure 4.6 shows P_{a1} versus the local threshold, ξ, for $p_t = 100$. It is obvious the simulation matches closely the analytical result. Second, Figure 4.7 plots P_{a1} versus the transmit power threshold, p_t, for $\xi = 0.05$. Again the simulation complies with the analysis. It is observed in

both figures that for a high value of ξ and a low value of p_t there is no test statistic at the FC and this makes the final decision at the FC uncertain.

Result 2: Theoretical results verification for detection performance analysis for the CSC and CSCPC schemes (Figures 4.8, 4.9, 4.10 and 4.11)

Figure 4.8 shows the detection performance of the censored selection combining (CSC) scheme at the FC without power constraint (theory - see (4.27) and (4.33), simulation - see (4.8)) for different values of signal to noise ratio. It is clear that the theoretical derivations match the simulation results. Now Figure 4.9 illustrates the detection performance of the CSC scheme for different values of λ. Again the simulation results verify the theoretical derivations. In Figure (4.10), the detection performance for different values of ξ is shown (the simulation and the theoretical results are virtually the same and therefore only the theoretical results are presented). Here, it is obvious from the simulation that the detection performance is not sensitive to the local threshold conditioned for $\xi \leq \xi_{opt}$, where in this scenario $\xi_{opt} = 0.55$.

Now we examine a validation for the theoretical analysis of the detection performance of the censored selection combining based power censoring (CSCPC) scheme (theory - see (4.39) and (4.44), simulation - see (4.10)) as plotted in Figure 4.11. As can be seen from Figure 4.11, both the simulation and the analytical results are identical for different values of p_t. In this figure it can easily be seen that as p_t decreases the detection performance degrades since not a lot of test statistics are being transmitted to the FC.

Result 3: Theoretical results verification for the average transmitted power (Figures (4.12) and (4.13))

Figure 4.12 presents both the simulation and the theoretical results of the power needed to transmit the test statistics to the FC versus the power transmit threshold (p_t), for different values of ξ. We can see that the theory and the simulation are identical. In addition, it can be observed that the total power can be reduced by decreasing p_t and increasing ξ. Now Figure 4.13 manifests the power needed to transmit the test statistics to the FC versus the local threshold (ξ), for different values of p_t. Again the simulation matches the theory and the total power increases with increasing p_t. For theory - see (4.54) and for simulation - see (4.45) and (4.50).

The next results (Figures 4.14, 4.15 and 4.16) show the advantage of the CSCPC scheme over the CSC scheme in terms of detection performance and power saving.

Result 4: The detection performance versus p_t (CSCPC scheme), $\mathbb{E}[\triangle(\xi, p_t)]$ versus ξ, and P_D versus P_{FA} (Figures 4.14, **4.15** and **4.16**)

In Figure 4.14, the detection performance against the power transmit threshold for the CSCPC scheme is shown. This figure shows that the improvement of the detection performance increases dramatically with increasing p_t and then it levels out for different values of P_{FA}. The power transmit threshold can be chosen such that the target detection is met. For example, for a target detection probability $\delta = 0.9$ at $P_{FA} = 0.01$, $p_t = 750$ is a good choice.

Now Figure 4.15 shows the total power needed to send the test statistics to the FC versus the local threshold for the CSC and the CSCPC schemes. Here it can be seen that the proposed technique CSCPC can save a lot of power compared with the CSC. It can be observed that the power needed for the CSC can be reduced approximately by half for CSCPC at $\xi < (\xi_{opt} = 0.1)$ and $p_t = 750$. Theory - for the CSC scheme see (4.27), (4.33) and (4.54), for the CSCPC scheme see (4.39), (4.44) and (4.54).

To be more rigorous, we have to examine the detection performance for the CSC and the CSCPC schemes for a certain value of p_t such that a target P_{FA} and a target P_D are met and $P_{a1}(\xi_{opt}, p_{t_{opt}}) = 1$. For example for $(P_{FA}, P_D) = (0.01, 0.9)$, $p_t = 750$ is a suitable choice to satisfy the target P_{FA} and P_D as shown in Figure 4.14. In addition, the choice of $p_t = 750$ can satisfy $P_{a1}(\xi_{opt}, p_{t_{opt}}) = 1$ (where $\xi_{opt} = 0.1$, $p_{topt} = 30$ are found using (4.14) by grid search).

For these requirements, Figure 4.16 plots the detection performance for the CSC and the CSCPC schemes. It can be observed that both are approximately the same. Thus it can be confirmed that the CSCPC scheme has achieved its purpose which is to save power with a negligible loss to the detection performance.

Finally, from Figures 4.14, 4.15 4.16 we can see that the total power needed to transmit the test statistics to the FC is decreased while the detection performance remains unchanged.

Result 5: P_D **versus** P_{FA} **in the presence of NU** (Figure **4.17**)

This figure evaluates by simulation the detection performance of the CSC and the CSCPC schemes in the presence of NU. The NU has been generated according to the p.d.f. defined in (5.6). It can be seen that the effect of NU on the detection performance is negligible compared to the local sensing as shown in Figure 5.2.

Result 6: P_D **versus** R **for different values of** λ Figure (**4.18**).

Figure 4.18 depicts the P_D versus R for different values of λ. It shows that as λ increases as the performance improves. However for CSCPC the performance improvement stops at a certain value of R due to the power constraint.

Result 7: P_D **versus SNR and** $\mathbb{E}[\triangle(\xi, p_t)]$ **versus SNR for different values of** p_t (Figures **4.19** and 4.20).

From Figure 4.19 it is easily be seen that the detection performance of the CSCPC scheme for $p_t = 1500$ approaches to the detection performance of the CSC scheme. Also, it is observed that the detection performance of CSCPC deteriorates for $p_t = 750$ and $p_t = 1000$. The reason is that the secondary users which are far away from the FC do not participate in the detection problem because of the constraint on p_t . In Figure 4.20, it can be seen how much power can be kept for the case of $p_t = 750,\ 1000$. Also, the figure shows that the CSCPC scheme for $p_t = 1500$ approximately dissipates half the power needed for the CSC scheme. Moreover, from Figures 4.19 and 4.20, it is noticeable that as the SNR increases, the P_D and the average power tend to 1 and 0 respectively. Thus from Figures 4.19 and 4.20, we can say that the CSCPC scheme for $p_t = 1500$ maintains the detection performance unaffected while reducing the power consumption to the half.

Result 8: P_D **versus** R **and** $\mathbb{E}[\triangle(\xi, p_t)]$ **versus** R **and for different values of** p_t (Figures **4.21** and 4.22)

Figure 4.21 shows that the performance of the CSCPC detector for $p_t = 1500$ approaches the performance of the CSC detector. Also, it is observed that the CSCPC detector for $p_t = 750$ and $p_t = 1000$ (after a certain value of R) maintains unaffected. The reason for that is that the secondary users which are far away from the FC cannot send their test statistics to the fusion center due to the small values of p_t. Figure 4.22 shows how much of power can be reduced by employing the CSCSP

scheme compared to the CSC scheme. So the the proposed detector (CSCSP) can save a huge power with a small distortion to the detection performance.

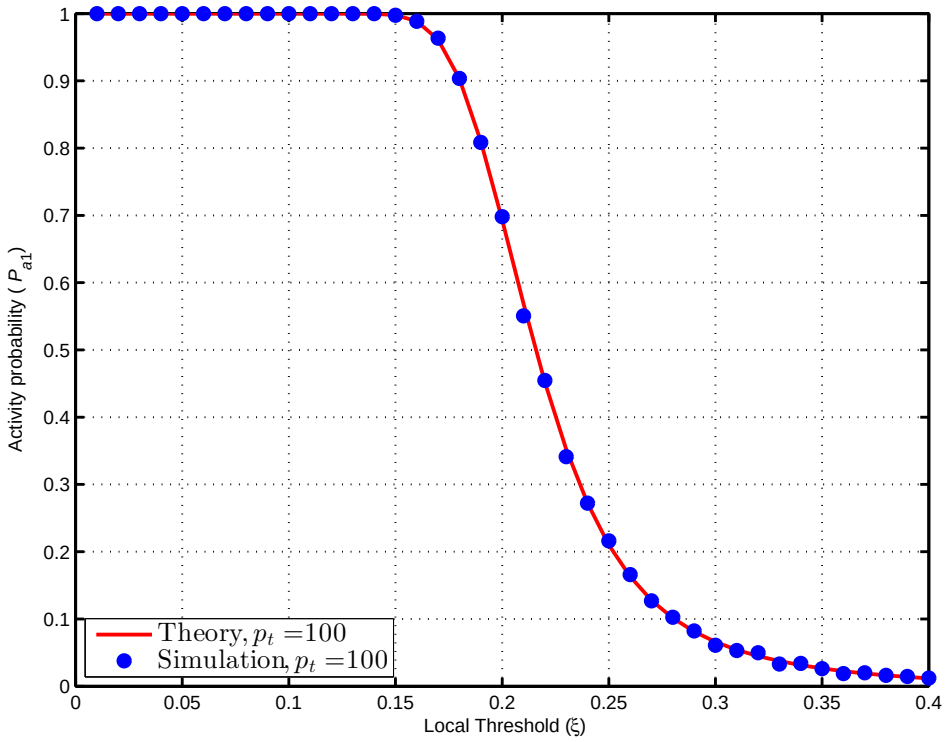

Figure 4.6: The activity probability (P_{a1}) versus the local threshold (ξ) for $p_t = 100$. In all cases, $N = 10$, $R = 20$, $\theta_{pr} = \frac{\pi}{2}$, $R_{pr} = 25$, $\alpha = 2$ and $SNR = -8$dB.

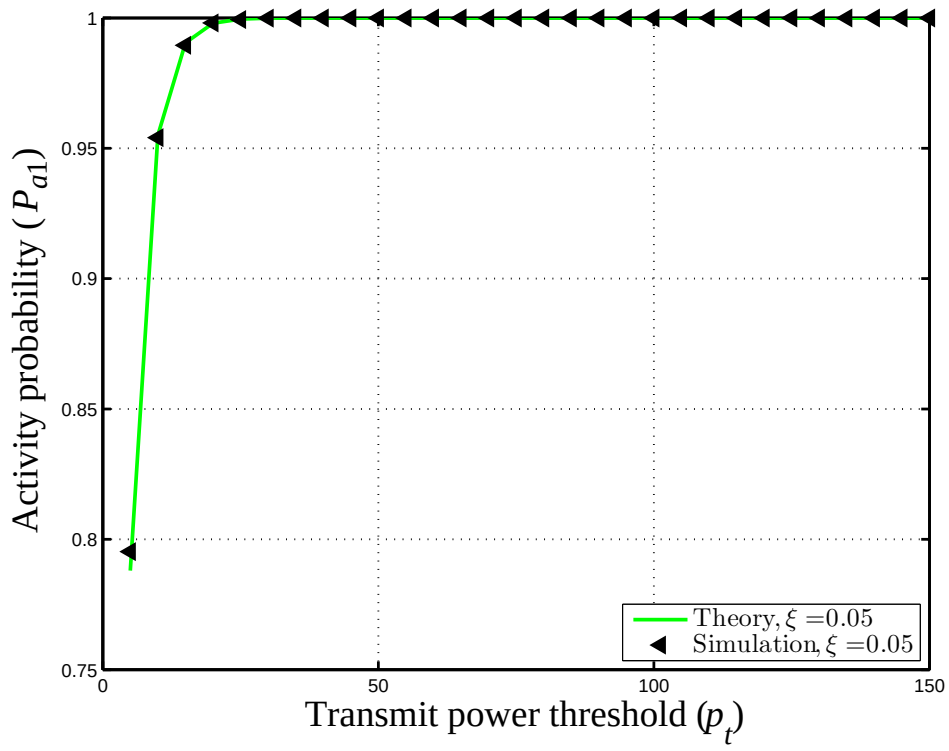

Figure 4.7: The activity probability (P_{a1}) versus the transmit power threshold (p_t) for $\xi = 0.05$. In all cases, $N = 10$, $R = 20$, $\theta_{pr} = \frac{\pi}{2}$, $R_{pr} = 25$, $\alpha = 2$ and $SNR = -8$dB.

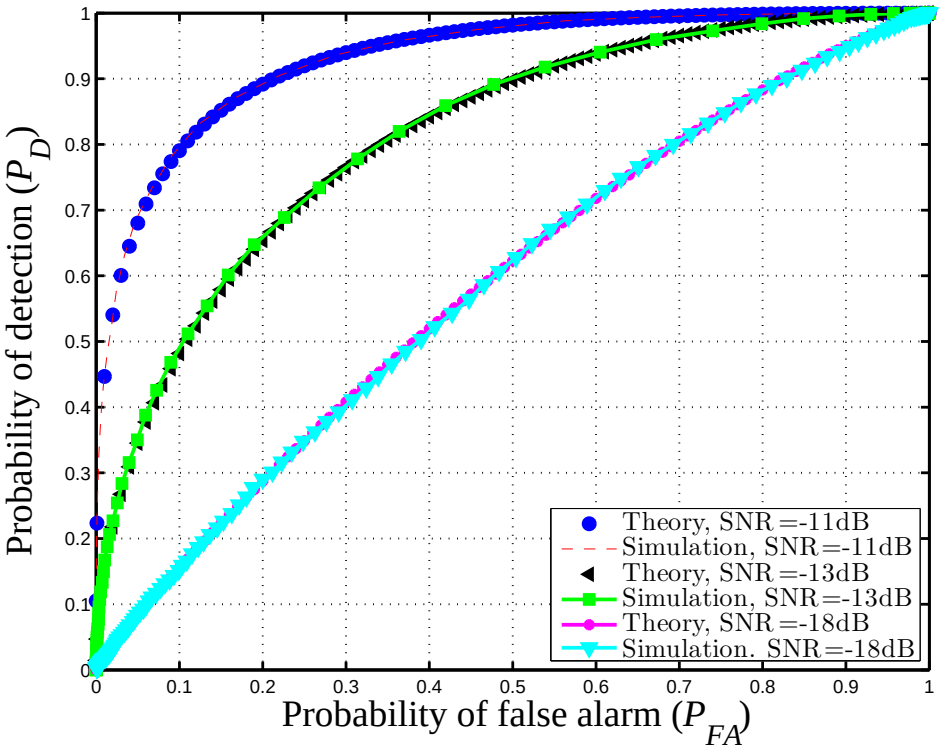

Figure 4.8: The P_D versus the P_{FA} for the CSC for different values of SNR (no power constraint). In all cases, $N = 10$, $R = 20$, $R_{pr} = 25$, $\theta_{pr} = \frac{\pi}{2}$, $\alpha = 2$ and $\lambda = 0.1$.

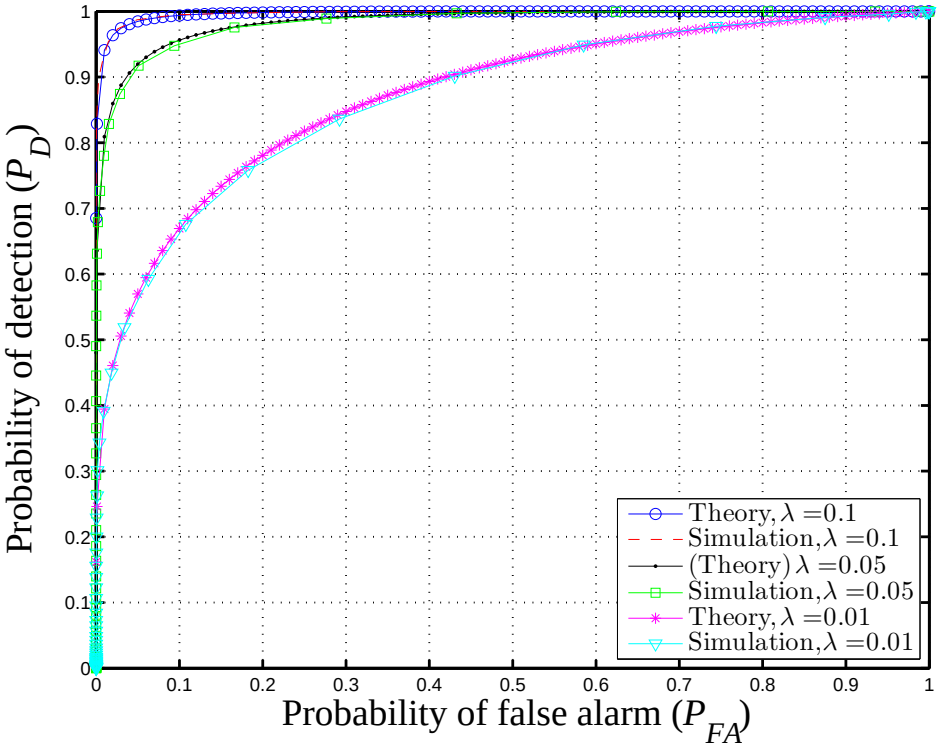

Figure 4.9: The P_D versus the P_{FA} for the CSC for different values of λ (no power constraint). In all cases, $N = 10$, $R = 20$, $R_{pr} = 25$, $\theta_{pr} = \frac{\pi}{2}$ and $SNR = -6$dB.

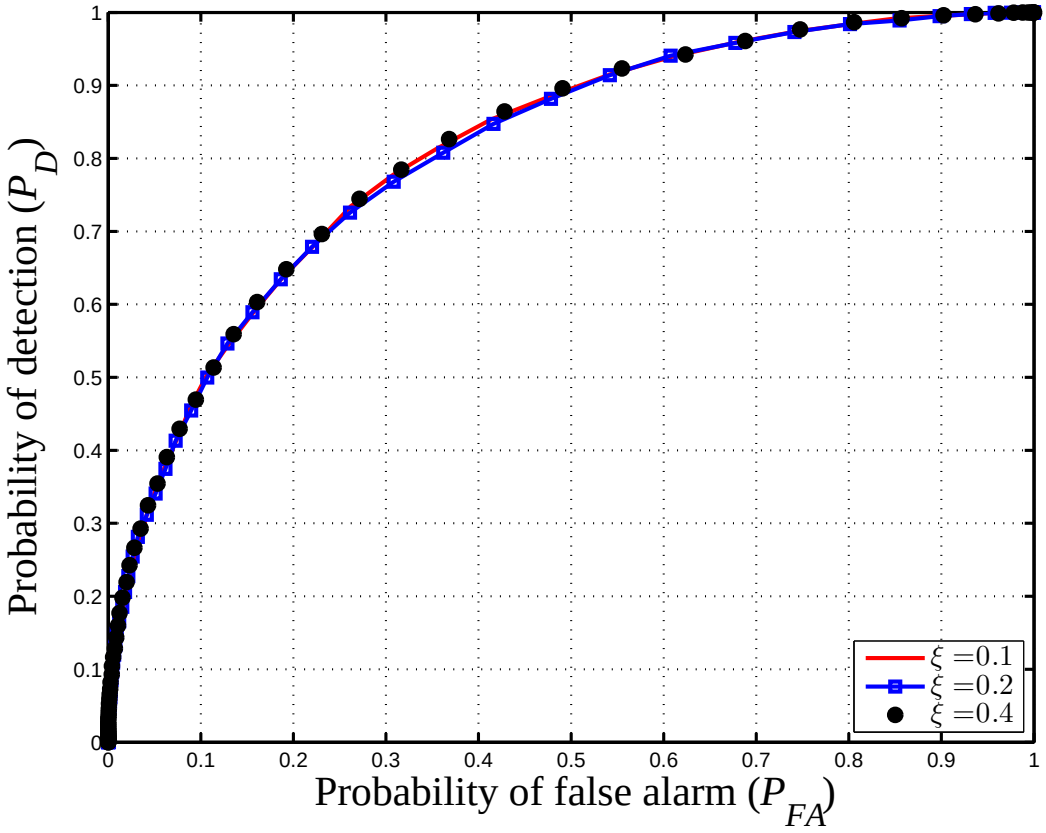

Figure 4.10: The P_D versus the P_{FA} for the CSC scheme for different values of ξ. In all cases, $N = 10$, $R = 20$, $R_{pr} = 25$, $\theta_{pr} = \frac{\pi}{2}$, $\alpha = 2$, $\lambda = 0.1$ and $SNR = -13$dB.

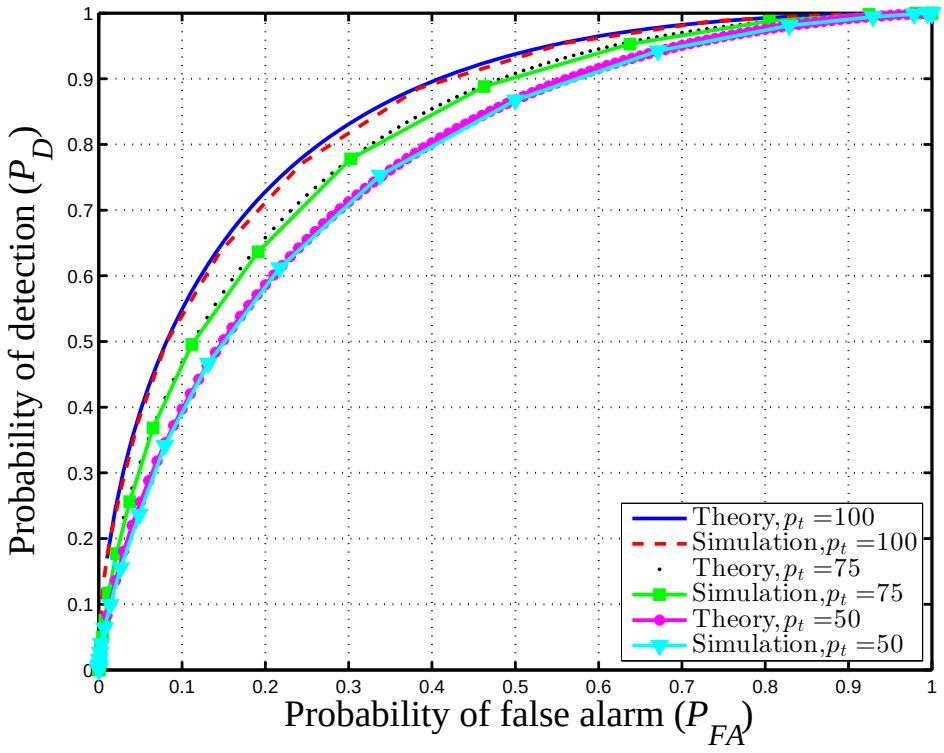

Figure 4.11: The P_D versus the P_{FA} for different values of P_t. In all cases, $N = 10$, $R = 20$, $R_{pr} = 25$, $\theta_{pr} = \frac{\pi}{2}$, $\alpha = 2$, $\lambda = 0.1$ and SNR $= -6$dB.

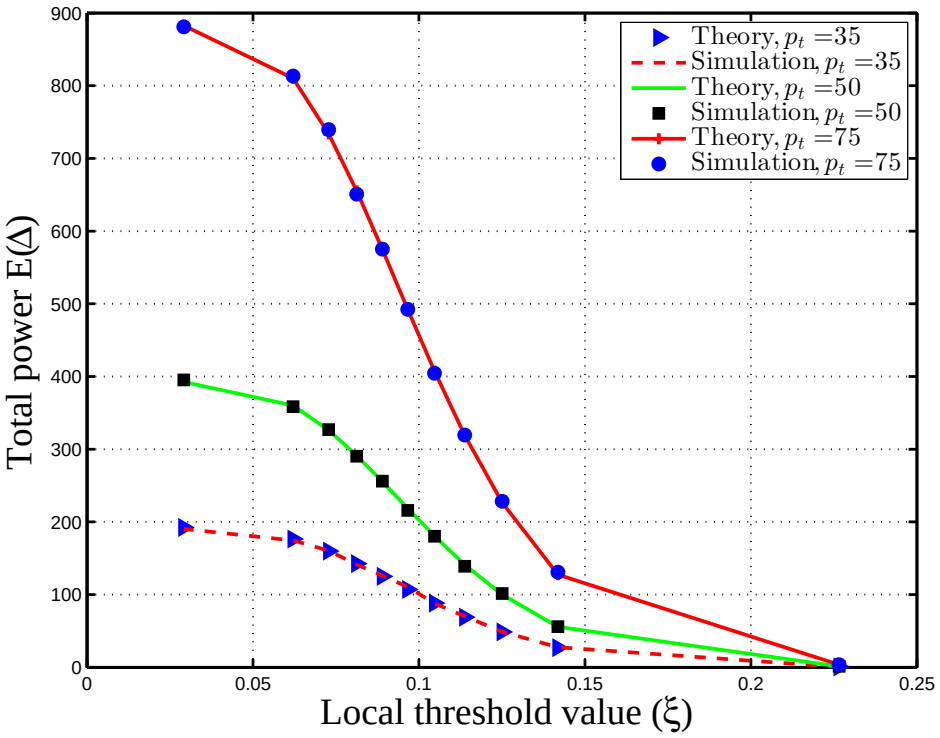

Figure 4.12: The $\mathbb{E}[\triangle]$ to the FC versus the ξ, for different values of p_t. In all cases, $N = 10$, $R = 20$, $R_{pr} = 25$, $\theta_{pr} = \frac{\pi}{2}$, $\alpha = 2$, $\lambda = 0.1$ and SNR $= -8$dB.

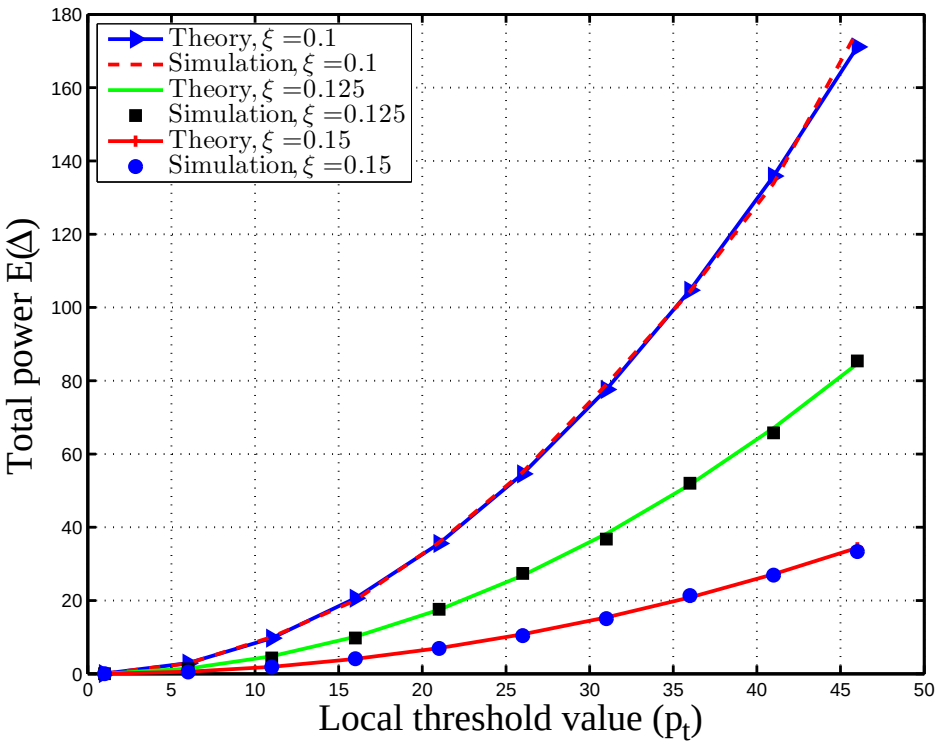

Figure 4.13: The $\mathbb{E}[\triangle]$ to the FC versus the p_t, for different values of ξ. In all cases, $N = 10$, $R = 20$, $R_{pr} = 25$, $\theta_{pr} = \frac{\pi}{2}$, $\lambda = 0.1$, $\alpha = 2$ and SNR $= -8$dB.

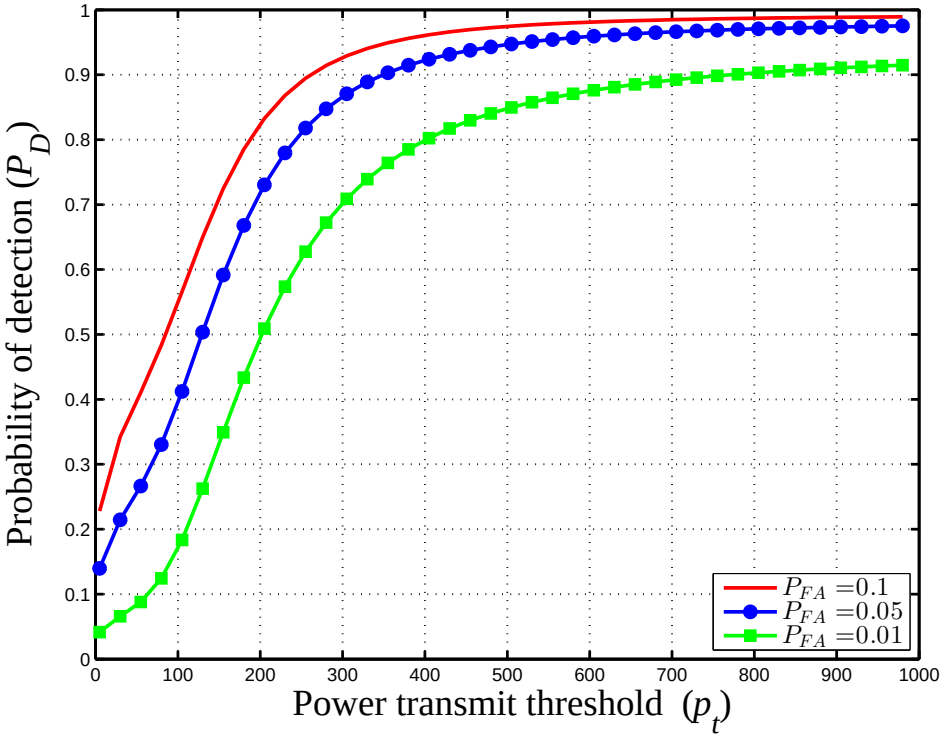

Figure 4.14: The P_D versus the power transmit threshold for the CSCPC. In all cases, $N = 10$, $R = 20$, $R_{pr} = 25$, $\theta_{pr} = \frac{\pi}{2}$, $\alpha = 2$, $\lambda = 0.1$ and SNR $= -8$dB.

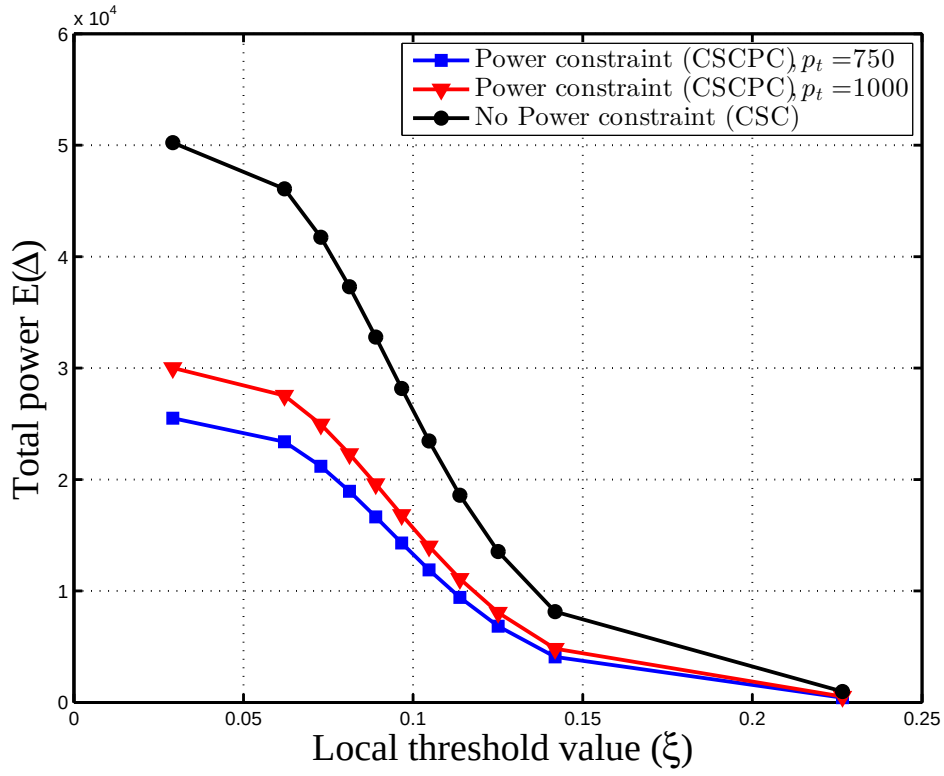

Figure 4.15: The average total power $\mathbb{E}[\triangle(\xi, p_t)]$ versus the local threshold (ξ). In all cases, $m = 2$, $R = 20$, $R_{pr} = 25$, $\theta_{pr} = \frac{\pi}{2}$, $\alpha = 2$, $\lambda = 0.1$ and SNR $= -8$dB.

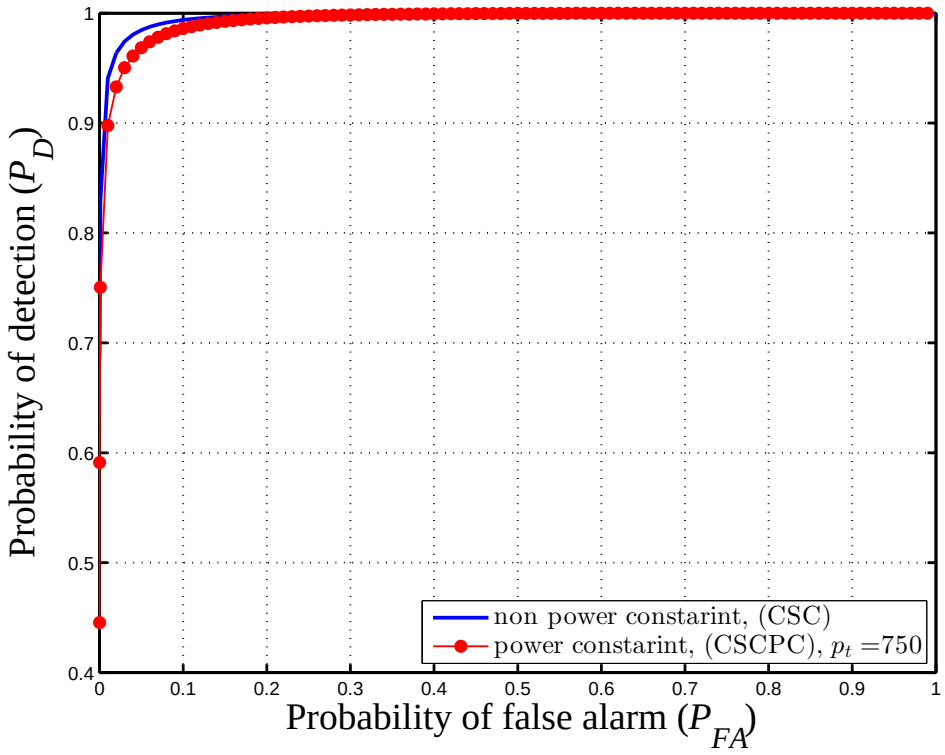

Figure 4.16: The P_D versus the P_{FA} for the CSC and the CSCPC. In all cases, $\xi_{opt} = 0.1$, $p_{t_{opt}} = 30$, $R = 20$, $R_{pr} = 25$, $\theta_{pr} = \frac{\pi}{2}$, $\alpha = 2$, $\lambda = 0.1$ and SNR $= -8$dB.

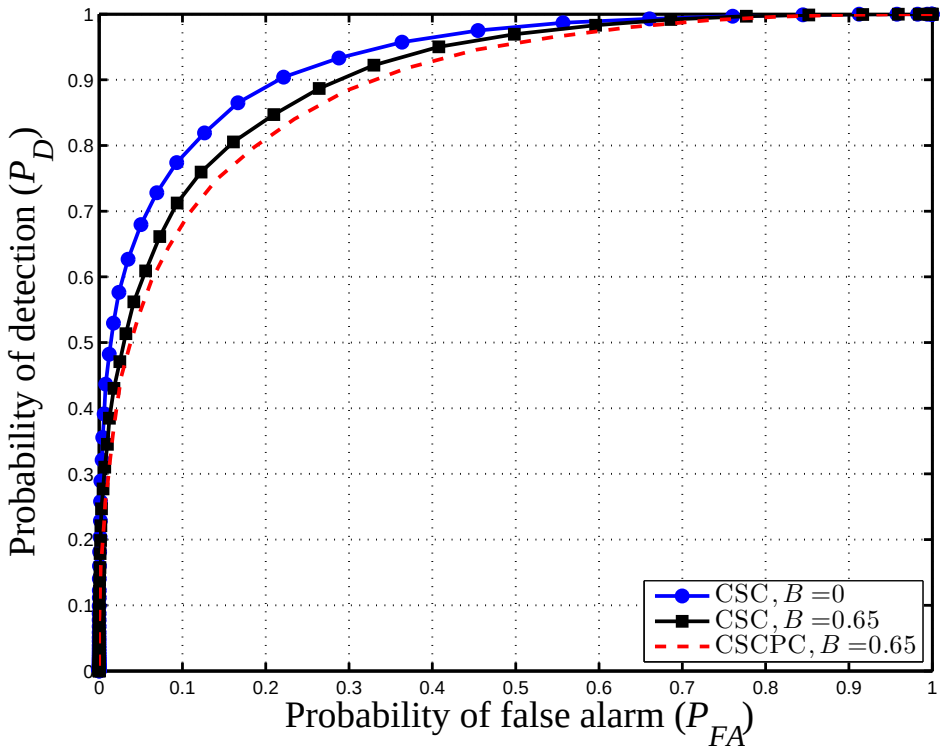

Figure 4.17: The P_D versus the P_{FA} for the CSC and the CSCPC in the presence of NU. In all cases, $\xi_{opt} = 0.1$, $R = 20$, $R_{pr} = 25$, $\theta_{pr} = \frac{\pi}{2}$, $\alpha = 2$, $\lambda = 0.1$ and SNR $= -8$dB.

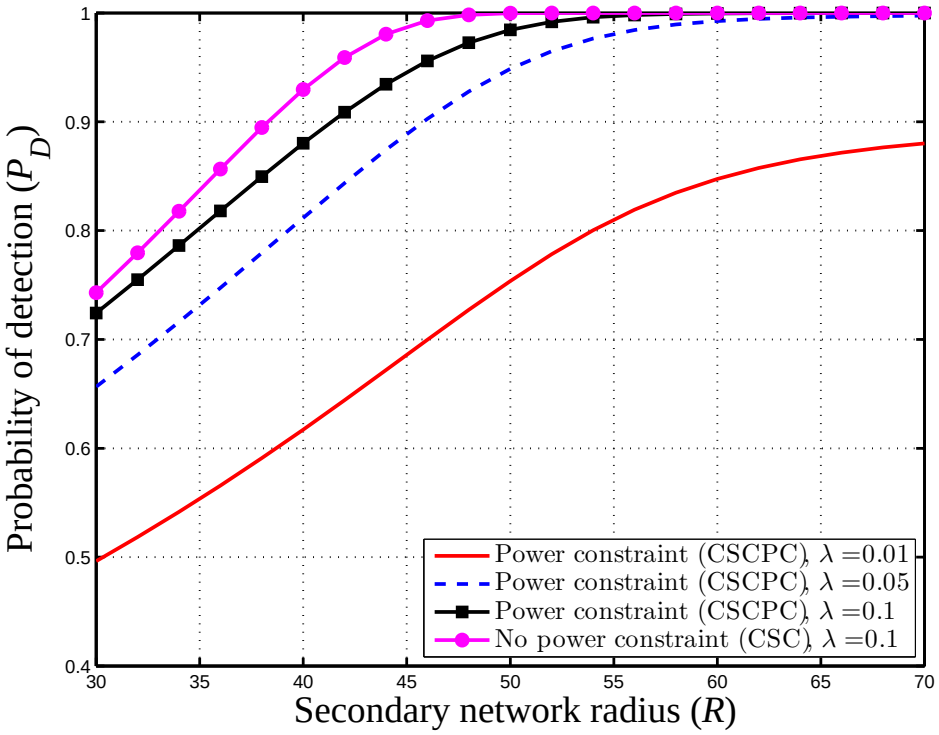

Figure 4.18: The P_D versus the secondary network radius (R) for different values of λ. In all cases, $P_{FA} = 0.1$, $R_{pr} = 75$, $\theta_{pr} = \frac{\pi}{2}$, $\alpha = 2$, and SNR $= -8$dB. For the CSCPC scheme $p_t = 1000$.

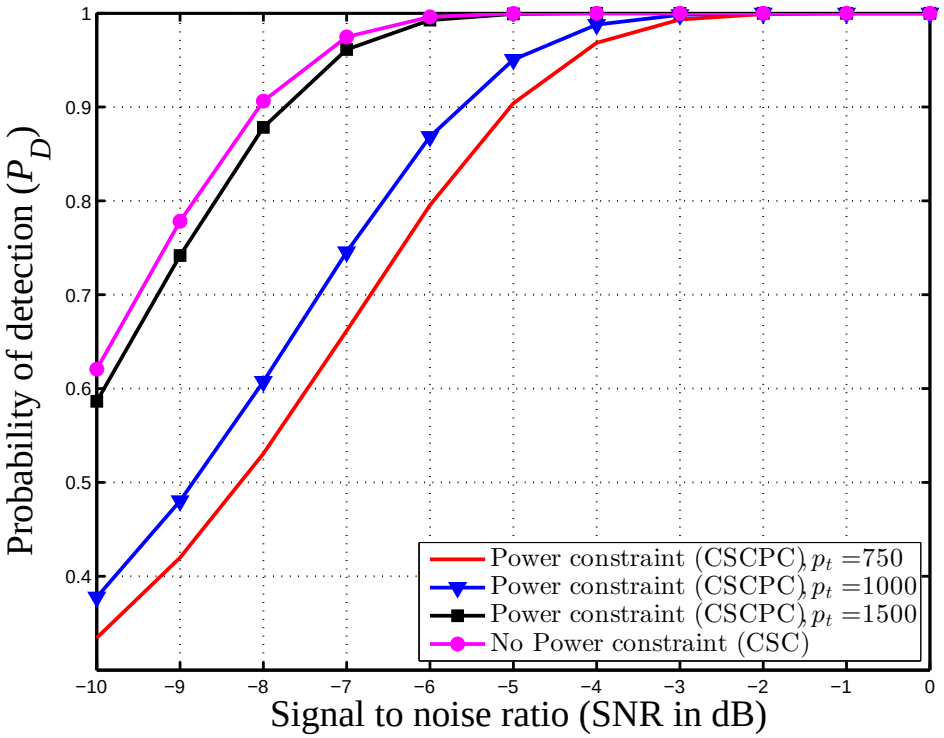

Figure 4.19: The P_D versus the SNR for different values of p_t. In all cases, $P_{FA} = 0.1$, $R_{pr} = 75$, $\theta_{pr} = \frac{\pi}{2}$, and $\alpha = 2$.

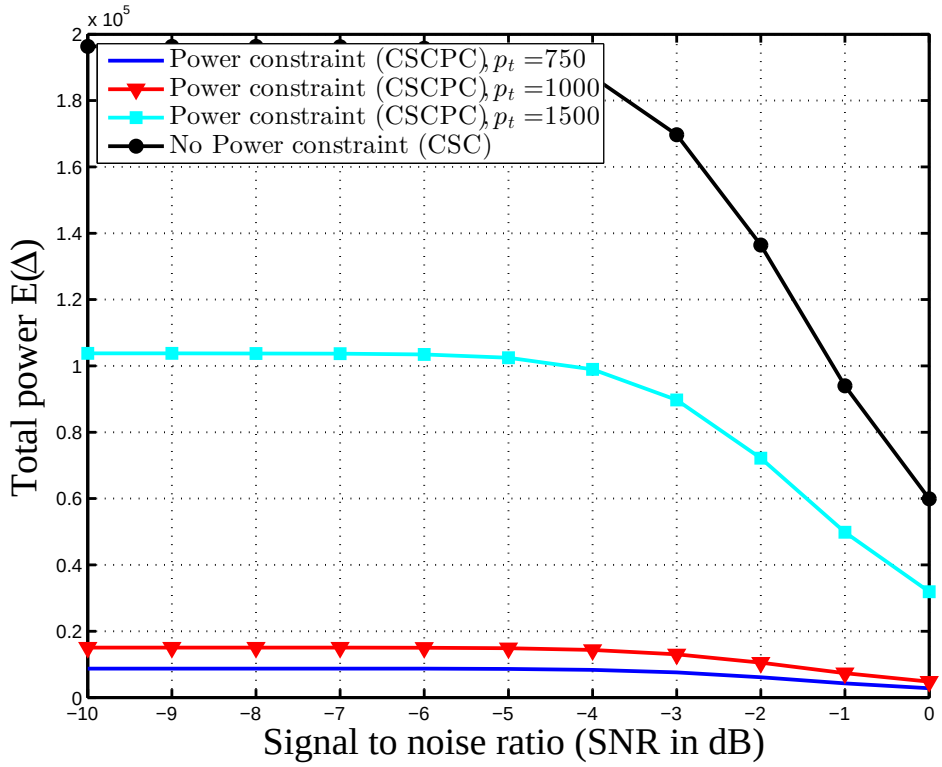

Figure 4.20: The average total power $\mathbb{E}[\triangle(\xi, p_t)]$ versus the SNR for different values of p_t. In all cases, $R_{pr} = 75$, $\theta_{pr} = \frac{\pi}{2}$, $\alpha = 2$, and SNR $= -8$dB.

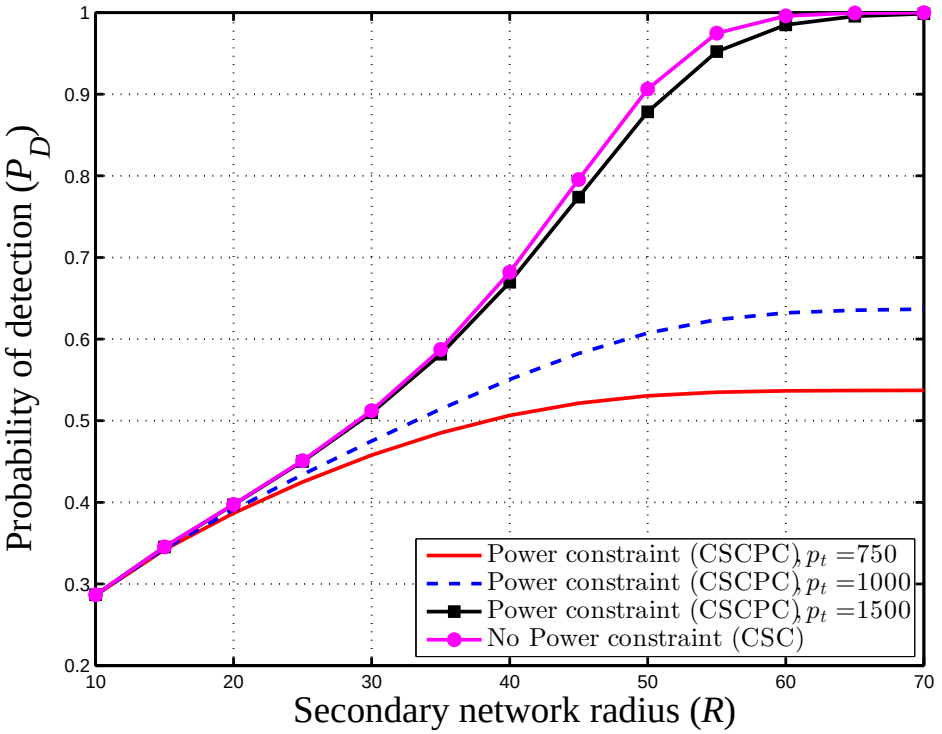

Figure 4.21: The average total power $\mathbb{E}[\triangle(\xi, p_t)]$ versus R for different values of p_t. In all cases, $R_{pr} = 75$, $\theta_{pr} = \frac{\pi}{2}$, $\alpha = 2$, and SNR $= -8$dB.

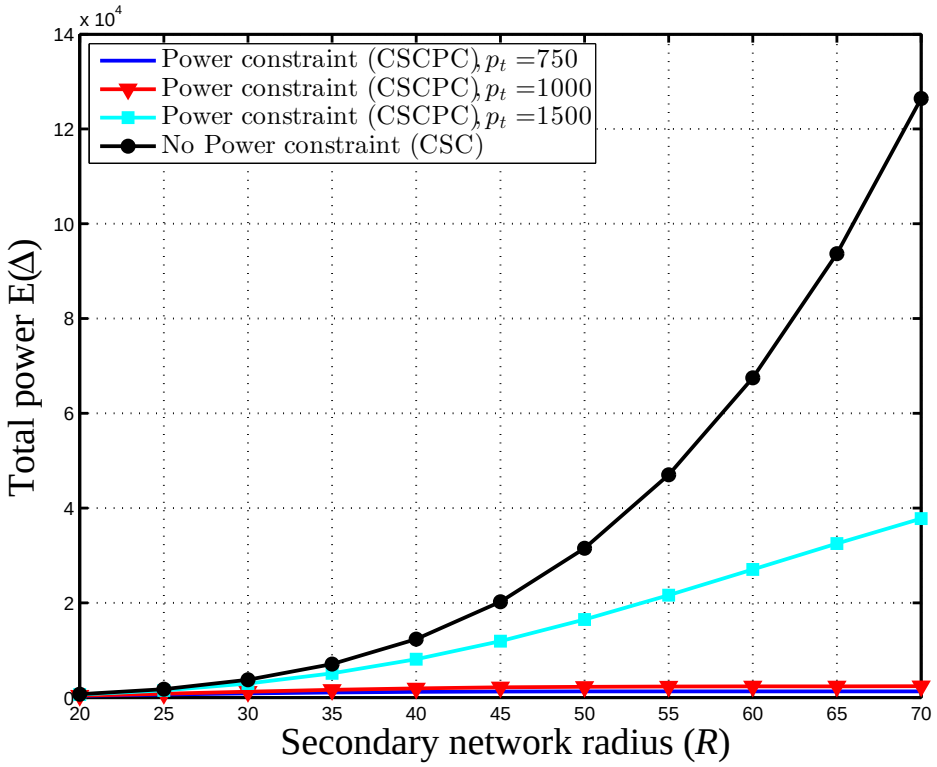

Figure 4.22: The P_D versus the secondary user radius (R) for the CSC and the CSCPC. In all cases, $P_{FA} = 0.1$, $R_{pr} = 75$, $\theta_{pr} = \frac{\pi}{2}$, $\alpha = 2$, $\lambda = 0.01$ and SNR $= -8$dB.

4.10 CHAPTER SUMMARY

The main goal of this chapter is to save energy when sending the test statistics to the FC, but not at the expense of significant performance degradation[6]. Firstly, an analytical expression for the activity probability is proposed so that the idle network issue is tackled. Secondly, the conventional censored selection combining (CSC) scheme is investigated analytically, where CSC is based on the local sensing threshold (ξ). Thirdly, a novel detector is proposed to reduce the energy overhead. The proposed scheme is named censored selection combining based power constraint (CSCPC). It relies on the local threshold (ξ) and the transmit power threshold (p_t). The main idea behind introducing the p_t is to have more degrees of freedom to decrease the overhead energy that is needed to send the test statistics to the FC. More-

6 Notice that saving the energy will decrease the potential interference at primary user receiver.

over, the total power required is derived analytically. The CSC, CSCPC schemes and total power are derived using the stochastic geometry tool and verified by simulation. Finally it is shown by simulation how the proposed CSCPC detector can alleviate the power consumption while the detection performance distortion is negligible compared with the conventional censoring case (CSC).

5

SENSING-THROUGHPUT TRADEOFF IN THE PRESENCE OF NOISE UNCERTAINTY AND OVER NAKAGAMI-*M* FREQUENCY-SELECTIVE CHANNELS

5.1 INTRODUCTION

To complete the picture of cognitive radio, this chapter examines the secondary user's throughput. Performance analysis of secondary user is very useful when designing practical systems. For example, one of aims of cognitive radio is to increase the data rate, but in some uncertain environments, such as channel fading, a secondary user cannot achieve the required data rate.

The objective of this chapter is to evaluate the performance of the secondary user when the sensing (the primary-transmitter secondary-transmitter link), interference (the primary-transmitter secondary-receiver link) and communicating[1] (the secondary-transmitter secondary-receiver link) channels are Nakagami-*m* frequency-selective (NFS) as shown in Figure 5.1. Moreover, the chapter includes the issue of noise uncertainty (NU) at the sensing stage. Sensing-throughput tradeoff is considered as a performance metric in the evaluation. In order to formulate the secondary throughput this chapter evaluates two parameters. Firstly[2], we have a closed-form expression for the sensing threshold that takes into consideration NU and an NFS channel. Secondly, we derive closed-form expressions for success probabilities in

1 Throughout this chapter we use communicating channel and secondary link interchangeably.

2 The secondary throughput relies on the results of spectrum sensing which is strongly related to the sensing threshold.

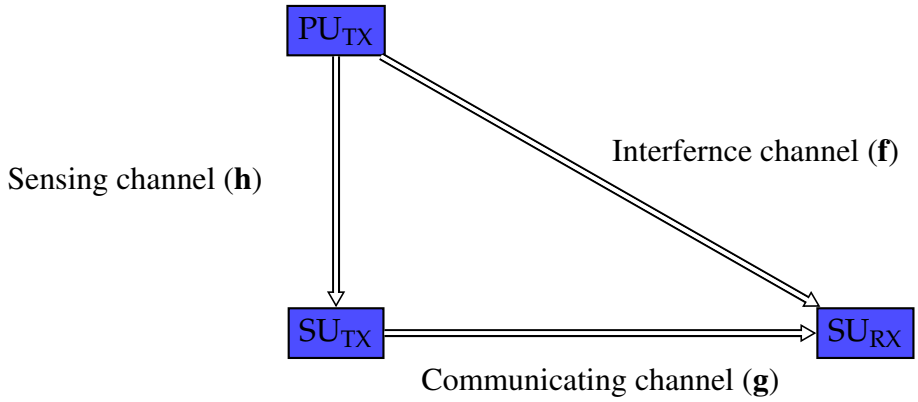

Figure 5.1: System model showing the sensing, communicating and interference channels.

the presence and absence of the primary user. Finally, we look at the effect of spectrum sensing on the secondary throughput.

The investigation also includes the autocorrelation detector (AD) which is not sensitive to NU. The AD is included in the investigation for a comparison purpose. Because the AD depends on an OFDM signal, the OFDM is chosen as a candidate for the primary user's signal.

To the best of author's knowledge, the analytical study of sensing-throughput tradeoff in the presence of NU and over an NFS channel has not been examined in any previous research.

5.1.1 *Background*

5.1.1.1 *Sensing-throughput tradeoff*

The fundamental functions of cognitive radio technology are spectrum sensing and data transmission. The secondary user frame in cognitive radio technology has a time slot divided into two parts [17]. The first part is allocated for spectrum sensing over the entire primary user band and the second part is reserved for data transmission. Both sensing and transmission are executed sequentially. This differs from traditional wireless communication systems which have only one part for transmission. Figure 5.2 illustrates the periodic spectrum sensing (N) and date transmission (W-N) in cognitive radio, where W represents the secondary frame duration. Once

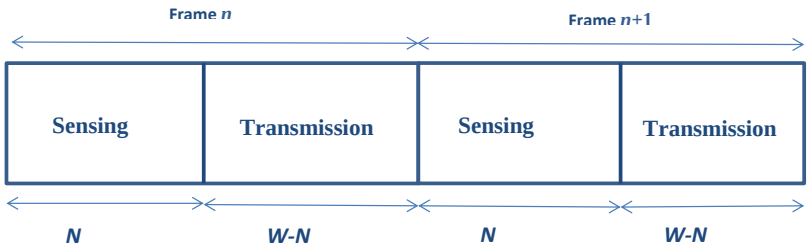

Figure 5.2: A periodic sensing/transmission structure for cognitive radio technology.

the secondary user declares the absence of the primary user, the secondary user accesses the primary user band in the rest part of the frame; otherwise, the secondary user switches off its transmission until it detects an unoccupied primary user band in the subsequent frames[3].

From Figure 5.2, a long sensing time reduces the time allocated for the secondary user to access the primary user band. This causes the secondary throughput to be very low but the primary user receiver is kept safe form any potential interference. On the other hand, a short sensing time maximises the secondary throughput but the primary user is more vulnerable to be interference from the secondary user. This can be interpreted in terms of the false alarm probability and the detection probability. As the sensing time increases the false alarm probability increases (this means a low secondary transmission) and the detection probability increases (makes the primary user less exposed to secondary interference). From the secondary user's perspective, the false alarm probability is required to be low, so the utilization of the spectrum by the secondary user is more likely. However, from the primary user's perspective, the detection probability is required to be high, so that the interference to the primary user may be minimized. Capitalizing from this discussion, the sensing and communicating channels are strictly intertwined with each other and clearly there exists a tradeoff between the spectrum sensing and the secondary user's throughput [17].

3 Notice this model works only when the primary user is active or absent during the whole secondary user frame.

The possible interference at the primary receiver, because of missed detection, is related to the detection probability. By choosing appropriate sensing threshold value such that the detection probability is larger than a target detection probability within the sensing interval, a sufficient protection to the primary user might be obtained.

5.1.1.2 *Noise uncertainty*

The main disadvantage of ED is the susceptibility to the noise uncertainty (NU) phenomena. It is well known that the ED severely degrades due to NU, i.e., the *noise power does actually change with time and location, which is called noise uncertainty*[4]*,* because of the following reasons [41, 80]:

- thermal noise;
- receiver nonlinearity;
- initial calibration error;
- due to interference.

In the presence of NU the ED does not work below certain values of signal to noise ratio.

5.1.2 *Literature review and motivation*

5.1.2.1 *Sensing-throughput tradeoff over a fading channel*

There exists plenty of works related to the sensing-throughput tradeoff. In [17], Liang *et al.* have formulated the sensing-throughput tradeoff problem for a cognitive network. In [17] the authors studied the sensing-throughput tradeoff when sensing, interference and communicating channels are subjected to an additive white Gaussian noise (AWGN). The optimal sensing time that maximises the secondary

4 In this thesis we assume that the actual noise power is invariant in the duration of the detection but changes randomly from one detection period to another.

throughput subject to a certain detection probability has been found via simulation. In [36] the authors studied the sensing-throughput tradeoff problem using double thresholds over AWGN channels. In [81], the sensing-throughput tradeoff was investigated by optimizing the optimal sensing time that maximizes the average throughput of a secondary link when there exists a Rayleigh flat-fading channel. The authors assumed a AWGN for the sensing channel.

In [33], the sensing-throughput tradeoff was investigated for sensing-based spectrum sharing over AWGN channels. In [37], the same scenario in [33] has been have studied based for an outage capacity over Rayleigh and Nakagami-*m* flat-fading channels. For evaluating the outage capacity, the authors assume there exists a fading channel for the secondary link and for the interference link. However, the sensing channel is just considered for AWGN.

For wideband secondary access, in [35, 82], the sensing-throughput tradeoff was evaluated by optimizing the sensing time. In [35], the study assumed that all channels are AWGN. In [82], the secondary and the interference links are considered flat-fading and the sensing channel is assumed to be AWGN.

It appears from the above literature review that there exists an important gap that is missing and needs to be explored further. The multipath impairment process is not considered for the sensing channel in all the above papers and this can significantly change performance. Indeed, considering fading channels for both secondary and interference links but not taking into account the fading in the sensing channel is not a realistic assumption. The authors in the above papers resort to finding the sensing threshold only for AWGN to overcome the analytical difficulties that arise from the presence of the averaging of Q-function or Marcum Q-function over the distribution of the signal to noise ratio[5] at the secondary user transmitter. And this (calculating the sensing threshold value for a AWGN) does not reflect the actual scenario in a cognitive network. Indeed, ignorance of the sensing fading channel is due to the existence of averaging the conditional detection probability over the signal to noise ratio distribution. This averaging means that the corresponding sensing threshold

5 The signal to noise ratio is a function in the sensing instantaneous channel.

for a target detection probability needs to be determined by an iterative trial-based approach, which is computationally costly for the secondary user.

In the presence of a fading channel, the probability of detection itself becomes a random variable. Hence, the sensing process should be designed in such a way that the detection can still be provided for the primary system. In [83], the authors proposed the detection outage probability as a suitable criteria for achieving such a design. The authors obtained an optimal sensing threshold by bounding the detection outage probability with a reliability constraint when a target detection probability is required.

Notice that not only the detection process of the primary user is influenced by the fading but also the achievable capacity of the missed detecting secondary user is also affected by the fading. The missed detecting secondary user encounters an additional interference from the active primary user which also suffers from fading uncertainty. This necessitates the consideration of communicating and interference channels while studying the optimization of the secondary throughput under a detection outage constraint. However in [83], the authors have considered the impact of fading in the sensing channel and they have ignored the fading channel in the communicating and interference channels. In other words while the channel between primary transmitter and secondary transmitter is accommodated, the secondary and interference links are assumed to be perfect with only AWGN. In a practical situation, this assumption is not realistic as both the primary and secondary networks are collocated and all links suffer from the fading process. So, here the fading channels for the interference and the secondary links must be taken into account.

5.1.2.2 *Noise uncertainty*

This part covers a review on cognitive radio where NU exists. Several research directions have been found in the literature.

The first direction concentrates on proposing new detectors which mitigate the NU issue. For example, in [84] the authors proposed a detector which depends on the kth moment of the received signal. The effects of both NU and the Rayleigh fading channel on the detection performance of the proposed detector was evaluated

by simulation. In [85], a generalized energy detector was analysed [6] under the worst case scenario of NU. Only upper and lower NU bounds are known, and under the assumption that the NU follows a uniform distribution. In [86], the authors have proposed a covariance detector to tackle the NU problem and applied a generalized likelihood ratio test to formulate the test statistic. The detection performance was only evaluated by simulation. In [87, 88, 89], some algorithms have been proposed for the primary user based OFDM signal which depends on the cyclic prefix. In [86, 90], the authors have proposed algorithms based on multi antennas at secondary user.

The second direction is based on noise power estimation. The main idea is based on estimating the noise power and subsequently the NU can be accounted for. In [91], the authors discussed employing an autoregressive model to estimate the noise power. The proposed algorithm was evaluated by simulation. In [92], the noise power was estimated by a maximum likelihood estimator. In [93], the authors proposed a detector for wireless microphone signals that exploits the advantages of both the power spectrum density detector based sensing and the eigenvalue detector based sensing. The study was only conducted by simulation.

The third direction is based on studying the performance of the ED in the presence of NU for different scenarios. In [94], the authors have assumed that NU follows a log normal distribution with a certain variance. In [95], the ED performance under both discrete and continuous models of NU was investigated. Also in [95], the authors demonstrated that by selecting different threshold values different detection performances can be achieved. Moreover, they illustrated that when the distribution of NU is known the threshold value can be chosen such that the detection performance is improved. In [96], a cooperative spectrum sensing using ED was studied in the presence of NU. In [97], a cooperative spectrum sensing using OR, AND and majority rule was investigated by considering both NU and Rayleigh fading channels. The work was based on simulation, the results showed that the AND rule yields better performance over AWGN channels while in Rayleigh channels the OR rule is a preferable choice. In [98], a cooperative spectrum sensing in the presence of

6 A generalized energy detector uses $\mathbb{E}[|x(n)|^p]$ instead of $\mathbb{E}[|x(n)|^2]$.

the worst-case impact of NU and over log-normal shadowing channels was studied through simulation. The results illustrated that the cooperation mitigates the problem of NU. In [99], the effect of noise power uncertainty on the detection performance at the fusion center was examined for equal combining, weighted combining and the likelihood ratio test. In [100] the authors proposed a cooperative spectrum sensing with adaptive thresholds to enhance the detection performance in the presence of NU. Furthermore, in [100] the authors proposed an Ad-hoc method that depends on the NU factor and the results demonstrated that the proposed detector is more robust to the NU compared with the equal combining, weighted combining and likelihood ratio test.

The fourth direction looks at the effect of noise uncertainty on other aspects such as secondary throughput. In [101], the authors examined by simulation the throughput of the secondary user using ED, the maximum minimum eigenvalue detector and the maximum eigenvalue detector in the presence of NU. However in [101] there are two research gaps that need to be filled in: The first gap is that the channel fading was not considered. The second gap is that the threshold value, that satisfies the target detection probability, was determined[7] numerically by integrating the detection probability over the p.d.f of the NU distribution for each value of the number of received samples. This threshold is very complex to evaluate.

Now it is obvious that the effect of spectrum sensing (using the ED) on the secondary user throughput in the presence of NU and over an NFS channel has not been investigated yet. Therefore, motivated by the above discussion, this chapter evaluates analytically the secondary throughput[8] while assuming that the sensing, communicating and interference links suffer from fading channels. Furthermore, a more generic model is adopted for the sensing, communicating and interference links which is the NFS channel (for more details about NFS channel please refer to chapter 3). Moreover, this chapter takes into consideration NU at the sensing stage.

7 In the literature when the secondary throughput is studied the spectrum sensing threshold should be found such that it satisfies a target probability of detection.

8 Secondary performance, secondary throughput and sensing-throughput tradeoff are interchangeably used throughout this chapter.

Motivation behind choice of the AD:

It is well known that the ED is the optimum detector (when the noise variance is known and for an i.i.d signal) and when there is no information about the primary user. However, when there exists NU, the detection performance of the ED degrades. Consequently, other techniques have been proposed to tackle the NU issue. Some of those algorithms depend on multi antennas at secondary user such as [86, 90]. Other detectors are based on OFDM signals. For example, in [87, 88, 89] the authors have proposed detectors that can exploit the autocorrelation property (due to the existence of a cyclic prefix) in order to detect the presence of the primary user. In all the mentioned papers their detectors outperform the ED in the presence of NU [86, 90, 87].

In our scenario, the proposed algorithms in [86, 90] cannot be compared with an ED because they depend on MIMO technology. For other algorithms in [87, 88, 89], the proposed detector in [87] (AD) is chosen for a comparison because it has closed-form expressions for the probabilities of both false alarm and detection and it is less complex compared with other techniques [102].

Figure 5.3 shows a comparison between the ED and the AD for different values of NU bound (B) (it will be defined in the next section). As can be seen from this figure, the AD outperforms the ED when there exists NU.

In this context, two questions arise:

1. Does the NU degrade the secondary throughput when the ED is used for spectrum sensing?

2. Is the secondary throughput when the AD is used for spectrum sensing better than the secondary throughput when the ED is used for spectrum sensing?

5.2 CHAPTER CONTRIBUTIONS

The contributions of this chapter can be summarized as follows.

1. First, a closed-form upper bound of the sensing threshold is derived analytically for the ED. The sensing threshold takes into account both the effects of

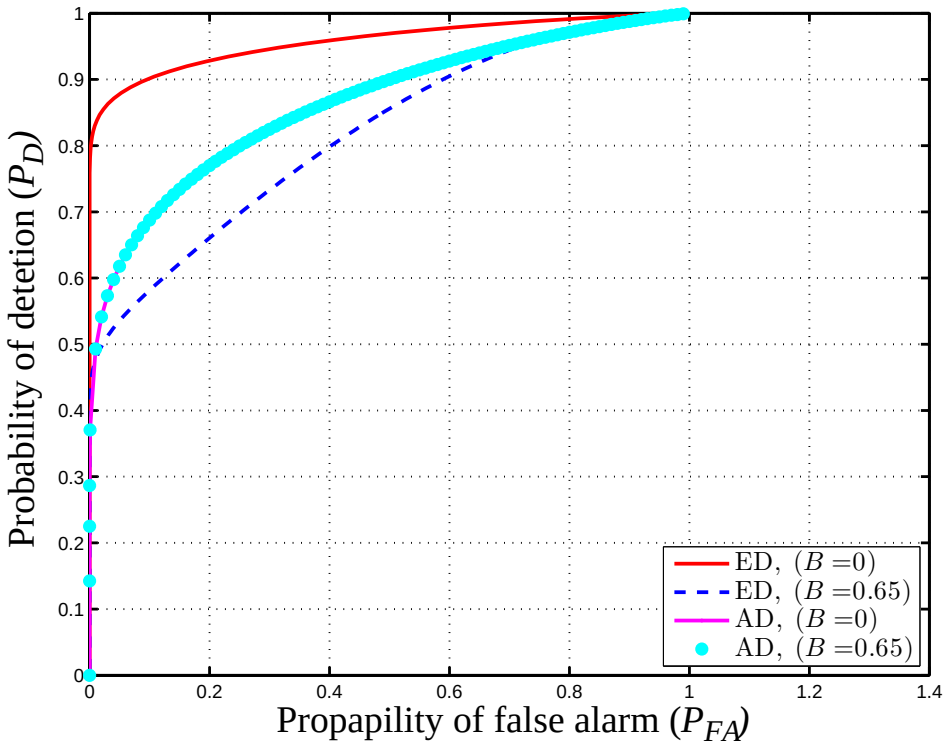

Figure 5.3: Probability of detection versus probability of false alarm for different values of NU factor (B). In all cases, $L = 1$, $N = 200$, and SNR $= -10$dB.

NU as well as the NFS channel. Second, a tight closed-form expression for the sensing threshold for the ED, under NU and over a Nakagami-*m* flat-fading (NFF) channel, is theoretically obtained.

2. Second, a closed-form expression for the sensing threshold, for the AD over an NFS channel is derived theoretically.

3. Closed form expressions for success probabilities in the absence/presence of the primary user are then derived.

4. Analytical expressions are derived for the secondary throughput while both the ED and the AD are used for spectrum sensing. The analytical expressions are in terms of the sensing threshold derived in 1 (for the ED) and 2 (for the AD). Moreover, it is a function in the success probabilities derived in 3.

5.3 CHAPTER ORGANIZATION

The rest of this chapter is organized as follows. In Section 5.4, the system model is introduced. Section 5.5 presents spectrum sensing using both an ED and an AD. Section 5.6 shows the problem formulation. Section 5.7 presents the outage detection probability in the presence of NU and over an NFS channel for the ED and the AD. In Section 5.8 the sensing-throughput problem is examined. In Section 5.9, the simulation results are discussed. Finally, the chapter summary is given in Section 5.10.

5.4 SYSTEM MODEL

5.4.1 *Chanel model*

Here we consider a cognitive network which consists of a primary transmitter (PU_{TX}) and a primary receiver (PU_{RX}) which operate in the presence of a collocated secondary link. The secondary link consists of a secondary transmitter (SU_{TX}) and its receiver (SU_{RX}), Figure 5.1 shows this scenario. It is assumed that all the channels suffer are NFS channels which are modeled as a finite impulse response (FIR) filter. These channels are described as follows. First, the impulse response for the $PU_{TX} \rightarrow SU_{TX}$ (sensing) link is denoted by

$$\mathbf{h} = [h_0\ h_1\ h_2\ ...\ h_{L-1}]^T. \tag{5.1}$$

Then the impulse response for the $SU_{TX} \rightarrow SU_{RX}$ (communicating) link is denoted by

$$\mathbf{g} = [g_0\ g_1\ g_2\ \cdots\ g_{L-1}]^T. \tag{5.2}$$

Finally the impulse response for the $PU_{TX} \rightarrow SU_{RX}$ (interference) link is denoted by

$$\mathbf{f} = [f_0\ f_1\ f_2\ ...\ f_{L-1}]^T. \tag{5.3}$$

All elements of the above mentioned channels are i.i.d. Also, it is assumed that all the channels have an exponential power delay profile.

5.4.2 *Primary user signal*

As the investigation in this chapter is based on the AD as well, thus it is assumed that the primary network employs OFDM technology. Let $\mathbf{S_m} = [S_m(0)\ S_m(1)\ S_m(2)\ ...\ S_m(N_d-1)]$ represents the N_d complex PSK symbols of the mth OFDM symbol. After the IFFT, the OFDM symbol is described by the following N_d complex values:

$$s_m(n) = \frac{1}{\sqrt{N_d}} \sum_{k=0}^{N_d-1} S_m(k) e^{\frac{j2\pi nk}{N_d}}, \quad n = 0, ..., N_d - 1 \tag{5.4}$$

where n and k are discrete-time and frequency indexes respectively. Adding the last N_c elements of $s_m(n)$ as a cyclic prefix the mth cyclic-prefixed OFDM symbol will be $[s_m(N_d - N_c)\ ...\ s_m(N_d-1)\ s_m(0)\ ...\ s_m(N_d-1)]$. An OFDM frame consists of several OFDM symbols which are transmitted sequentially. For notational simplicity, each element of the transmitted OFDM frame will be denoted by $s(n)$. For a large IFFT size, then by the central limit theorem, $s(n) \sim \mathcal{CN}(0, P_p)$ [88], where P_p is the primary user's transmit power.

5.4.3 *Model of noise uncertainty*

As before:

$$\begin{aligned} \mathcal{H}_0: \quad x(n) &= w(n) \\ \mathcal{H}_1: \quad x(n) &= \sum_{l=0}^{L-1} h_l s(n-l) + w(n). \end{aligned} \tag{5.5}$$

Now $(w(n))$ is i.i.d. circularly symmetric complex Gaussian noise with zero-mean and $\mathbb{E}\left[|w(n)|^2\right] = \sigma_w^2$; but the estimate of σ_w^2 will be $\hat{\sigma}_w^2 = \rho\sigma_w^2$ where ρ is called the NU factor [41][9]. Note that ρ (in dB) can be modeled as a uniform distribution in the interval $[-B,\ B]$, where B (in dB) is the NU bound and $B = \sup[10\log_{10}(\rho)]$[10].

9 Noise uncertainty means that the secondary user does not know the true noise variance.

10 There is an ongoing debate about which distribution should be considered for the NU [41].

This is the most commonly used model for NU in the literature [99, 86, 90, 101] and the probability density function (p.d.f.) for the NU factor (ρ) is [80]:

$$f_\rho(t) = \begin{cases} 0, & t < 10^{-B/10}, \\ \frac{5}{\ln(10)Bt}, & 10^{-B/10} \leq t \leq 10^{B/10}, \\ 0, & t > 10^{B/10}. \end{cases} \tag{5.6}$$

Finally, the instantaneous signal to noise ratio (at the $\mathrm{SU_{TX}}$) is defined as $\gamma = P_p \sum_{l=0}^{L-1} |h_l|^2 \Big/ \rho\sigma_w^2$.

5.5 SPECTRUM SENSING TECHNIQUES

This section looks at the detection performance of both the ED and the AD.

5.5.1 *Energy detector (ED) performance*

This subsection shows the analysis of spectrum sensing using the ED. From Section 5.4.2, the primary signal follows a complex Gaussian distribution, so the test statistic (T_{ED}) can be modeled under two hypothesis as follows

$$T_{ED} \sim \begin{cases} \mathcal{N}(\mu_0, \sigma_0^2), \text{ under } \mathcal{H}_0, \\ \mathcal{N}(\mu_1, \sigma_1^2), \text{ under } \mathcal{H}_1, \end{cases} \tag{5.7}$$

where $\mu_0 = \rho\sigma_w^2$, $\sigma_0^2 = \frac{\rho^2\sigma_w^4}{N}$,

$$\mu_1 = \rho\sigma_w^2 + P_p \sum_{l=0}^{L-1} |h_l|^2, \tag{5.8}$$

and

$$
\begin{aligned}
\sigma_1^2 &= \mathbb{E}[T_{ED}^2] - \mu_1^2 \\
&2P_p^2 \sum_{l=0}^{L-1} |h_l|^4 + (1+\frac{1}{N}) P_p^2 \sum_{\substack{l_1,l_2=0 \\ l_1 \neq l_2}}^{L-1} |h_{l_1}|^2 |h_{l_2}|^2 + \rho^2 \sigma_w^4 \\
&+ \rho^2 \sigma_w^4 / N + \frac{2}{N} P_p \rho \sigma_w^2 \sum_{l=0}^{L-1} |h_l|^2 + 2P_p \rho \sigma_w^2 \sum_{l=0}^{L-1} |h_l|^2 \\
&- \Big[2P_p \rho \sigma_w^2 \sum_{l=0}^{L-1} |h_l|^2 + P_p^2 \sum_{l=0}^{L-1} |h_l|^4 + P_p^2 \sum_{\substack{l_1 \& l_2=0 \\ l_1 \neq l_2}}^{L-1} |h_{l_1}|^2 |h_{l_2}|^2 \\
&+ \rho^2 \sigma_w^4 \Big] \\
&= \frac{1}{N} \Big(P_p \sum_{l=0}^{L-1} |h_l|^2 + \rho \sigma_w^2 \Big)^2 .
\end{aligned}
\tag{5.9}
$$

So the detection probability conditioned on channel and ρ can be written as

$$
P_D = Q\left(\frac{\tau_{ED} - \rho\sigma_w^2 - P_p \sum_{l=0}^{L-1} |h_l|^2}{\frac{1}{\sqrt{N}} \left(P_p \sum_{l=0}^{L-1} |h_l|^2 + \rho \sigma_w^2 \right)} \right). \tag{5.10}
$$

5.5.2 *Autocorrelation detector (AD) performance*

As mentioned earlier in Section 5.1 (see - Figure 5.3), the detection performance of the AD is not affected by the NU. Thus the estimate of σ_w^2 will be $\hat{\sigma}_w^2 = \sigma_w^2$ and $\gamma = \frac{P_p}{\sigma_w^2} \sum_{l=0}^{L-1} |h_l|^2$. The proposed detector follows the approach of [88] which exploits the property of OFDM signals (provided by the cyclic prefix (CP)) such that the autocorrelation coefficients are non-zero at lags $\pm N_d$ and they are also the log-likelihood ratio test (*LLRT*) statistic for a low signal to noise ratio (SNR). So the test statistic is [88]

$$
T_{AD} = \frac{\frac{1}{N} \sum_{n=0}^{N-1} \Re\{x(n) x^*(n+N_d)\}}{\frac{1}{2(N+N_d)} \sum_{n=0}^{N+N_d-1} |x(n)|^2} \underset{\mathcal{H}_0}{\overset{\mathcal{H}_1}{\gtrless}} \tau_{AD}, \tag{5.11}
$$

where N ($N >> N_d$) is the number of samples used in the autocorrelation estimation, $\Re\{.\}$ denotes the real part of a complex number and τ_{AD} is a threshold value used to determine whether the primary user is present ($T_{AD} \geq \tau_{AD}$) or not

($T_{AD} < \tau_{AD}$). The distribution of the test statistic in (5.11) can be approximated (for sufficiently large N) as [88]

$$\begin{aligned} \mathcal{H}_0: \quad T_{AD} &\sim \mathcal{N}\Big(0, \frac{1}{2N}\Big), \\ \mathcal{H}_1: \quad T_{AD} &\sim \mathcal{N}\Big(\alpha, \frac{(1-\alpha^2)^2}{2N}\Big), \end{aligned} \tag{5.12}$$

where $\alpha = (N_c P_p/(N_d + N_c)) \times \sum_{l=0}^{L-1} |h_l|^2 / (P_p \sum_{l=0}^{L-1} |h_l|^2 + \sigma_w^2)$. Therefore, the probabilities of false alarm P_{FA} and detection P_D, conditioned on the channel, are given by:

$$P_{FA} = P\{T_{AD} > \tau_{AD} | \mathcal{H}_0\} = \frac{1}{2}\text{erfc}\Big(\sqrt{N}\tau_{AD}\Big), \tag{5.13}$$

$$P_D = P\{T_{AD} > \tau_{AD} | \mathcal{H}_1\} = \frac{1}{2}\text{erfc}\Big(\sqrt{N}\frac{\tau_{AD} - \alpha}{1-\alpha^2}\Big), \tag{5.14}$$

where $\text{erfc}(z) = \frac{2}{\sqrt{\pi}} \int_z^\infty \exp(-t^2) dt$ is the complementary error function.

5.6 PROBLEM FORMULATION

One of the most important parameter designs in spectrum sensing is τ_{ND} where $ND = \{ED, AD\}$. In the context of cognitive radio, the calculation of the τ_{ND} is generally determined by targeting a fixed false alarm probability while maximising the detection probability. When the secondary user throughput is evaluated, τ_{ND} is determined by targeting a fixed detection probability (δ). Indeed, in this context, the secondary users should not disturb the primary user up to a pre-defined detection probability (δ) and this means that the secondary user would not cause any interference to the primary receiver. For example, the τ_{ED} must be calculable in an efficient way and this can be done only by approximating the test statistic distribution of the ED by a Gaussian distribution. For an AWGN (neglecting the channel term and NU in (5.10)) then

$$\tau_{ED} = \sigma_w^2 + P_p + \frac{Q^{-1}(\delta)}{\sqrt{N}}(P_p + \sigma_w^2). \tag{5.15}$$

But when the channel is incorporated, then τ_{ED} is calculated such that the average detection probability $(\overline{P}_D)$ is satisfied.

$$\overline{P}_D = \int_0^\infty Q(\mathbb{T}_h, \sigma_w^2, N, \delta, \tau_{ED}) f(\mathbb{T}_h) d\mathbb{T}_h \geq \delta, \tag{5.16}$$

where $\mathbb{T}_h = \sum_{l=0}^{L-1} |h_l|^2$ and $f(.)$ is the p.d.f of $\mathbb{T}_h$. The τ_{ED} that satisfies (5.16) (for each σ_w^2, N and δ) can only be calculated by an iterative method which is a computationally inefficient solution. When there are two random variables, for example channel and NU, the τ_{ED} should satisfy the following inequality

$$\overline{P}_D = \int_0^{\infty} \int_{10^{-0.1B}}^{10^{0.1B}} Q\big(\mathbb{T}_h, \rho\sigma_w^2, B, N, \tau_{ED}\big) f(\rho) f(\mathbb{T}_h) d\rho d\mathbb{T}_h \geq \delta. \tag{5.17}$$

The determination of a τ_{ED} that satisfies (5.17) (for each σ_w^2, B, N and δ) is not an easy task, especially in context of the cognitive radio which has to find the τ_{ED} value as quickly as possible.

One goal of this chapter is to determine the τ_{ED} in a closed-form expression in the presence of NU and over NFS channel for any value of σ_w^2, B, N and δ. Mathematically speaking, the τ_{ED} has to be found analytically in a closed-form expression such as

$$\tau_{ED} = \Xi(\sigma_w^2, B, N, \delta), \tag{5.18}$$

where $\Xi(\sigma_w^2, B, N, \delta)$ is a function resulting from an integration for the detection probability over channel and NU p.d.f.'s. This calculation of τ_{ED} can be only found through the outage detection probability $(\mathbb{P}_{\text{out}})$ which is written as follows

$$\mathbb{P}_{\text{out}} = \text{Prob}\{P_D < \delta\}. \tag{5.19}$$

The next section shows how by using (5.19) the sensing threshold or decision threshold can be built into a theoretical expression for both the ED and the AD detectors.

5.7 THRESHOLD DETERMINATION

The channel in the $\text{PU}_{\text{TX}} \rightarrow \text{SU}_{\text{TX}}$ link is NFS and there also exists NU at SU_{TX}. Therefore, the estimated SNR ratio is defined at SU_{Tx} as $\gamma = \frac{P_p}{\rho\sigma_w^2} \sum_{l=0}^{L-1} |h_l|^2$, where γ is a random variable. Due to both the NU and the NFS channel there is a probability that the random variable P_D at SU_{TX} may fall below δ, and so an outage could occur. The objective is to upper bound the outage as follows:

$$\mathbb{P}_{\text{out}} = \text{Prob}\{P_D < \delta\} \leq \theta, \tag{5.20}$$

where θ is the upper outage detection probability bound determined by the primary user. Next we discuss the derivation of the sensing threshold for both the ED and the AD such that (5.20) is satisfied.

5.7.1 *Energy detector*

The derivation of the sensing threshold for the ED will be done for two different channel scenarios: i.e., the NFS channel and then the NFF channel.

5.7.1.1 *Nakagami-*m *frequency-selective channel*

In order to satisfy (5.20) for a given δ, it is necessary to compute the upper sensing threshold ($\tau_{ED} = \tau_{ED\theta}$) that sets $\mathbb{P}_{\text{out}} = \theta$. What is now needed is to calculate the sensing threshold ($\tau_{ED\theta}$) so that ($\tau_{ED} \leq \tau_{ED\theta}$) values will satisfy (5.20). To do this, we re-write ($\mathbb{P}_{\text{out}} = \text{Prob}\{P_D < \delta\}$) in terms of the SNR γ at SU_{TX} in the $\text{PU}_{\text{TX}} \rightarrow \text{SU}_{\text{TX}}$ link, i.e.,

$$\mathbb{P}_{\text{out}} = \left(\sum_{l=0}^{L-1} |h_l|^2 \leq \frac{\tau_{ED} - \rho\sigma_w^2 A_1}{P_p A_1}\right), \tag{5.21}$$

where $A_1 = 1 + \frac{Q^{-1}(\delta)}{\sqrt{N}}$. From chapter 3, the random variable $\mathbb{T}_h = \sum_{l=0}^{L-1} |h_l|^2$ can be approximated by a Gamma distribution function. Thus (5.21) becomes

$$\mathbb{P}_{\text{out}} = \mathbb{E}_\rho \left[1 - \frac{1}{\Gamma(K_{\mathbb{T}_h})} \Gamma(K_{\mathbb{T}_h}, \frac{\tau_{ED} - \rho\sigma_w^2 A_1}{\phi_{\mathbb{T}_h} P_p A_1})\right], \tag{5.22}$$

where $K_{\mathbb{T}_h}$ and $\phi_{\mathbb{T}_h}$ are defined in subsection 3.6.1.2. To find a closed-form expression for the threshold value ($\tau_{ED} = \tau_{ED\theta}$) that satisfies $\mathbb{P}_{\text{out}} = \theta$ using (5.22) is intractable. Thus it is desirable to seek to use some upper bounds or lower bounds for the upper incomplete Gamma function. We will use the following inequality [103]

$$(1 - \exp(-ay))^{K_{\mathbb{T}_h}} \leq 1 - \frac{\Gamma(K_{\mathbb{T}_h}, y)}{\Gamma(K_{\mathbb{T}_h})}, \tag{5.23}$$

where

$$a = \begin{cases} 1, & \text{if } 0 < K_{\mathbb{T}_h} < 1 \\ \Gamma(1 + K_{\mathbb{T}_h}), & \text{if } K_{\mathbb{T}_h} > 1. \end{cases}^{-\frac{1}{K_{\mathbb{T}_h}}}$$

By substituting (5.23) into (5.22), then (5.22) becomes

$$\mathbb{P}_{\text{out}} \geq \mathbb{E}_{\rho}\left[\left(1-\exp(-a\big[\frac{\tau_{ED}}{\phi_{\mathbb{T}_h}P_p(1+A_1)}-\frac{\rho\sigma_w^2}{\phi_{\mathbb{T}_h}P_p}\big])\right)^{K_{\mathbb{T}_h}}\right]. \tag{5.24}$$

To find the sensing threshold ($\tau_{ED} = \tau_{ED\theta}$) that satisfies $\mathbb{P}_{\text{out}} = \theta$ using (5.24) is still intractable. Thus some other approximation methods can be exploited. By examining the expression inside the expectation in (5.24) it is seen that it is a monotonically decreasing function in ρ and so Jensen's Inequality can be applied:

$$\begin{aligned}
&\mathbb{E}_{\rho}\left[\left(1-\exp(-a\big[\frac{\tau_{ED}}{\phi_{T_h}P_pA_1}-\frac{\rho\sigma_w^2}{\phi_{\mathbb{T}_h}P_p}\big])\right)^{K_{\mathbb{T}_h}}\right]\\
&\geq \left(1-\mathbb{E}_{\rho}\exp(-a\big[\frac{\tau_{ED}}{\phi_{\mathbb{T}_h}P_pA_1}-\frac{\rho\sigma_w^2}{\phi_{\mathbb{T}_h}P_p}\big])\right)^{K_{\mathbb{T}_h}}\\
&= \left(1-\exp(\frac{-a\tau_{ED}}{\phi_{\mathbb{T}_h}P_pA_1})\mathbb{E}_{\rho}\big[\exp(\frac{\rho\sigma_w^2}{\phi_{\mathbb{T}_h}P_p})\big]\right)^{K_{\mathbb{T}_h}}.
\end{aligned} \tag{5.25}$$

By substituting (5.25) into (5.24) then after some manipulation, the threshold value $\tau_{ED\theta}$ that satisfies $\mathbb{P}_{\text{out}} = \theta$ is given by

$$\tau_{ED\theta} = -\Big(\frac{\phi_{\mathbb{T}_h}P_p(1+A_1)}{a}\Big)\times\log_2\Big[\frac{1-\theta^{\frac{1}{K_{\mathbb{T}_h}}}}{\mathbb{E}_{\rho}\big[\exp(\frac{a\rho\sigma_w^2}{\phi_{\mathbb{T}_h}})\big]}\Big]. \tag{5.26}$$

Notice that, when there exists only NFF (5.22) reduces to

$$\mathbb{P}_{\text{out}} = 1-\frac{1}{\Gamma(K_{\mathbb{T}_h})}\Gamma(K_{\mathbb{T}_h},\frac{\tau_{ED}-\sigma_w^2(1+A_1)}{\phi_{\mathbb{T}_h}P_p(1+A_1)}). \tag{5.27}$$

Consequently, $\tau_{ED\theta}$ is given by

$$\tau_{ED\theta} = \sigma_w^2(1+A_1)+\phi_{\mathbb{T}_h}P_p(1+A_1)\Gamma^{-1}(K_{\mathbb{T}_h},\Gamma(K_{\mathbb{T}_h})(1-\theta)). \tag{5.28}$$

Also, when there is only NU then (5.20) becomes

$$\begin{aligned}
\mathbb{P}_{\text{out}} &= \text{Prob}\{P_D<\delta\}\\
&= \text{Prob}\{10^{\frac{-B}{10}}<\rho<\frac{\tau_{ED}}{\sigma_w^2A_1}-1\}\\
&= \frac{5}{B\ln(10)}\ln(\frac{\tau_{ED}}{\sigma_w^2A_1}-1)+\frac{B\ln(10)}{10},
\end{aligned} \tag{5.29}$$

and so

$$\tau_{ED\theta} = A_1\big[\sigma_w^2\exp(0.5\theta B\ln(10)-0.1B\ln(10))+1\big], \tag{5.30}$$

where $A_1 = 1+\frac{Q^{-1}(\delta)}{N}$.

5.7.1.2 *Rayleigh flat-fading channel*

For a Rayleigh fading channel (set m=1 for a Nakgami fading channel), then (5.22) is written as

$$\mathbb{P}_{\text{out}} = \mathbb{E}_{\rho}\left[1 - \exp(-\frac{\tau_{ED\theta}}{P_p(1+A_1)} + \frac{\rho\sigma_w^2}{P_p})\right], \tag{5.31}$$

by examining the expression inside the expectation in (5.31) we can see that it is a monotonically decreasing function in ρ and so Jensen's Inequality can be applied. Thus the threshold value $\tau_{ED\theta}$ that satisfies $\mathbb{P}_{\text{out}} = \theta$ is given by

$$\tau_{ED\theta} = -\Big(\phi_{\mathbb{T}_h} P_p(1+A_1)\Big) \times \log_2\Big[\frac{1-\theta}{\mathbb{E}_{\rho}\big[\exp(a\rho\sigma_w^2)\big]}\Big]. \tag{5.32}$$

5.7.2 *Autocorrelation detector*

This subsection derives the $\mathbb{P}_{\text{out}}$ for the AD over NFS. By substituting (5.14) into (5.20) then the outage detection probability is given as

$$\mathbb{P}_{\text{out}} = \text{Prob}\left\{\frac{1}{2}\text{erfc}\left(\sqrt{N}\frac{\tau_{AD}-\alpha}{1-\alpha^2}\right) \leq \delta\right\}. \tag{5.33}$$

Notice that (5.33) does not depend on the NU as shown in Figure 5.3. If we let $\alpha = \frac{\kappa\gamma}{\gamma+1}$ where $\kappa = \big(N_c/(N_d+N_c)\big)$, then the outage detection probability is given by

$$\mathbb{P}_{\text{out}} = \text{Prob}\left\{\frac{1}{2}\text{erfc}\left(\sqrt{N}\frac{\tau_{AD}-\frac{\kappa\gamma}{\gamma+1}}{1-\left(\frac{\kappa\gamma}{\gamma+1}\right)^2}\right) \leq \delta\right\}. \tag{5.34}$$

Now (5.34) can be simplified to

$$\mathbb{P}_{\text{out}} = \text{Prob}\big\{\triangle \leq 0\big\}, \tag{5.35}$$

where

$$\triangle = \epsilon_1\gamma^2 + \epsilon_2\gamma + \epsilon_3,$$

and

$$\begin{aligned}\epsilon_1 =& \frac{-\kappa^2}{\sqrt{N}}\text{erfcinv}(2\delta) - \tau_{AD} + \left(\kappa + \frac{1}{\sqrt{N}}\right) + \text{erfcinv}(2\delta)\\ \epsilon_2 =& -2\tau_{AD} + \left(\kappa + \frac{2}{\sqrt{N}}\text{erfcinv}(2\delta)\right)\\ \epsilon_3 =& -\tau_{AD} + \frac{1}{\sqrt{N}}\text{erfcinv}(2\delta),\end{aligned}$$

where erfcinv(.) is the inverse complementary error function. Now $\triangle = \epsilon_1(\gamma - \gamma_1)(\gamma - \gamma_2)$, and choosing the largest solution (γ_2) then (5.35) can be written in terms of γ as

$$\mathbb{P}_{\text{out}} = \text{Prob}(\gamma \leq \gamma_2), \tag{5.36}$$

where

$$\gamma_2 = \left(1 + \frac{2\beta}{\kappa} + \sqrt{4\nu\beta + 1}\right) \Big/ \left(2(\kappa\nu - \frac{\beta}{\kappa} - 1)\right), \tag{5.37}$$

with $\nu = \frac{1}{\sqrt{N}}\text{erfcinv}(2\delta)$ and $\beta = \nu - \tau_{AD}$. Re-writing (5.36) in terms of the channel coefficients then

$$\mathbb{P}_{\text{out}} = \text{Prob}\left\{\sum_{l=0}^{L-1} |h_l|^2 \leq \frac{\sigma_w^2\gamma_2}{P_p}\right\}. \tag{5.38}$$

The p.d.f. of of the random variable $\mathbb{T}_h = \sum_{l=0}^{L-1} |h_l|^2$, as before, is approximated by a Gamma distribution with a shape parameter $K_{\mathbb{T}_h}$ and a scale parameter $\phi_{\mathbb{T}_h}$ (defined in subsection 3.6.1.2). Thus (5.38) is given by

$$\mathbb{P}_{\text{out}} = 1 - \frac{\Gamma(K_{\mathbb{T}_h}, \frac{\sigma_w^2\gamma_2}{P_p\phi_{\mathbb{T}_h}})}{\Gamma(K_{\mathbb{T}_h})}. \tag{5.39}$$

Then the γ_2 that satisfies $\mathbb{P}_{\text{out}} = \theta$ can be found as

$$\gamma_2 = \frac{P_p\phi_{\mathbb{T}_h}}{\sigma_w^2}\Gamma^{-1}(K_{\mathbb{T}_h}, (1-\theta)\Gamma(K_{\mathbb{T}_h})). \tag{5.40}$$

By substituting (5.37) into (5.40), and after some mathematics, then the $\tau_{AD\theta}$ that satisfies $\mathbb{P}_{\text{out}} = \theta$ is:

$$\tau_{AD\theta} = \nu\left(1 - \frac{1}{2\beta_1^2}\right) + \frac{\beta_2}{\beta_1}\left[1 - \sqrt{\frac{\nu^2}{4\beta_1^2\beta_2^2} + \frac{1}{4\beta_2^2} - \frac{\nu}{\beta_1\beta_2}}\right] \tag{5.41}$$

where $\beta_1 = -(\gamma_2 + 1)/\kappa$ and $\beta_2 = \kappa\nu\gamma_2 - (\gamma_2 + 0.5)$. Next the secondary throughput will be discussed for both the ED and the AD.

5.8 SECONDARY USER'S THROUGHPUT

5.8.1 *Nakagami*-m *frequency-selective channel*

In this section, the average throughput of the secondary link ($SU_{TX} \rightarrow SU_{TX}$) is derived. Here it is assumed that a secondary network employs orthogonal frequency division multiplexing (OFDM) technology. There are two reasons for adopting this technology. First, it is a practical assumption, which is employed in many applications such as WIMAX, digital television and audio broadcasting. Second, this assumption makes the analysis of the secondary throughput easier. The NFS channel of the secondary link ($SU_{TX} \rightarrow SU_{RX}$), $\mathbf{g}$ (channel gains), are written in the frequency domain as

$$\mathbf{G} = [|G(0)|^2|G(1)|^2 \dots |G(J-1)|^2], \tag{5.42}$$

where the complex channel coefficient at the kth subcarrier is expressed as

$$G(k) = \frac{1}{\sqrt{J}} \sum_{l=0}^{L-1} g_l \exp(i2\pi lk/J) \qquad k = 0, 1, \dots, J-1. \tag{5.43}$$

Here J is the size of the discrete Fourier transform (DFT) (or the number of subcarriers) and g_l is defined in (5.2). The amplitude of g_l follows a Nakagami distribution with a Nakagami parameter m and a spreading parameter $\Omega_{g_l} = \mathbb{E}[|g_l|^2]$. The phase of g_l follows a uniform distribution over $[0, 2\pi)$. The amplitude of $G(k)$ can be approximated by a Nakagami distribution with a new Nakagami parameter $\bar{m}_{|G(k)|}$ and a spreading parameter $\bar{\Omega}_{|G(k)|}$ which are given as [63, 104]

$$\begin{aligned} \bar{m}_{|G|} &= \frac{\bar{\Omega}_{|G|}^2}{\frac{1}{m}\sum_{l=0}^{L-1}\Omega_{g_l}^2 + \sum_{\substack{l_1,l_2=0 \\ l_1\neq l_2}}^{L-1}\Omega_{g_{l_1}}\Omega_{g_{l_2}}} \\ \bar{\Omega}_{|G|} &= \frac{1}{J}\sum_{l=0}^{L-1}\Omega_{g_l}. \end{aligned} \tag{5.44}$$

Because these parameters are independent with respect to the index k, so k is omitted from (5.44). The NFS channel of the interference link ($\mathrm{PU_{TX}} \rightarrow \mathrm{SU_{RX}}$), $\mathbf{f}$ (channel gains), can be described in frequency domain as

$$\mathbf{F} = [|F(0)|^2 |F(1)|^2 \ldots |F(J-1)|^2]. \tag{5.45}$$

The complex channel coefficient at the kth subcarrier is written as

$$F(k) = \frac{1}{\sqrt{J}} \sum_{l=0}^{L-1} f_l \exp(i2\pi lk/J) \qquad k = 0, 1, \ldots, J-1. \tag{5.46}$$

Again the amplitude of f_l follows a Nakagami distribution with a Nakagami parameter m and a spreading parameter $\Omega_{f_l} = \mathbb{E}[|f_l|^2]$. Also, the amplitude of $F(k)$ can be approximated by a Nakagami distribution with a new Nakagami parameter $\bar{m}_{|F(k)|}$ and a spreading parameter $\bar{\Omega}_{|F(k)|}$ [63, 104] which are written as

$$\begin{aligned} \bar{m}_{|F|} &= \frac{\bar{\Omega}^2_{|F|}}{\frac{1}{m}\sum_{l=0}^{L-1} \Omega^2_{f_l} + \sum_{\substack{l_1, l_2 = 0 \\ l_1 \neq l_2}}^{L-1} \Omega_{f_{l_1}} \Omega_{f_{l_2}}} \\ \bar{\Omega}_{|F|} &= \frac{1}{J} \sum_{l=0}^{L-1} \Omega_{f_l}. \end{aligned} \tag{5.47}$$

Again, because these parameters are independent of the index k, so k in (5.47) is omitted. Here the throughput of the secondary link is defined in terms of the success probability P_{succ} (i.e., probability of successful transmission times the bits/s/Hz capacity). So the throughput is given as:

$$C = P_{succ} \times \log_2(1 + \gamma_s) \quad \text{bits/s/Hz} \tag{5.48}$$

where γ_s is the secondary user's desired SNR threshold (or SINR when the primary is present). The success probability can be expressed in terms of the outage probability as

$$P_{succ} = 1 - P_{out}, \tag{5.49}$$

where P_{out} is the outage probability for the secondary link ($\mathrm{SU_{TX}} \rightarrow \mathrm{SU_{RX}}$). Thus, it is necessary to derive P_{out} to solve (5.49). In the literature the definition of the outage probability for an OFDM system is defined as follows. The OFDM system is considered in outage when at least one OFDM subcarrier is in outage [105, 106,

107]. This consideration comes because of the assumption of equal bit allocation for all OFDM subcarriers. In addition, after a careful literature review on the outage probability for an OFDM technology, the mathematical derivation of the outage probability assumes that the subcarriers of channels are independent and identically distributed random variables [105, 106, 107]. However, in practice the subcarriers are correlated and this is due to the common of impulse response between different subcarriers as shown in (5.43) and (5.46). This work takes into consideration the effects of that correlation in finding the success probability. This consideration is more realistic than in other works in [105, 106, 107].

Now, the average throughput of the secondary link ($\mathrm{SU_{TX}} \rightarrow \mathrm{SU_{RX}}$) may be analysed in two different scenarios (without consideration of spectrum sensing).

1. The first scenario is when there is no primary user transmitting $(\mathcal{H}_0)$. As an indication of a successful reception at the receiver side, we introduce a global signal to noise ratio $SNR_{global0}$ (where the subscript "0" means under $\mathcal{H}_0$) at the secondary receiver side $(\mathrm{SU_{RX}})$. This is conducted by the summation of the signal to noise ratio of all subcarriers at the secondary receiver side. When the $SNR_{global0} > \gamma_s$ then the reception at the secondary receiver side is successful. This $SNR_{global0}$ can be expressed (under $\mathcal{H}_0$) as

$$SNR_{global0} = \frac{P_s}{\sigma_v^2} \sum_{k=0}^{J-1} |G(k)|^2, \tag{5.50}$$

where P_s, σ_v^2 are the secondary transmit power and the noise variance respectively. Thus the success probability can be written as

$$P_{succ0} = \mathrm{Prob}\Big(\frac{P_s}{\sigma_v^2} \sum_{k=0}^{J-1} |G(k)|^2 > \gamma_s\Big). \tag{5.51}$$

But from Parseval's theorem,

$$\sum_{k=0}^{J-1} |G(k)|^2 = \sum_{l=0}^{L-1} |g_l|^2, \tag{5.52}$$

and so, (5.51) can be written as follows

$$P_{succ0} = \mathrm{Prob}\Big(\sum_{l=0}^{L-1} |g_l|^2 > \frac{\sigma_v^2 \gamma_s}{P_s}\Big). \tag{5.53}$$

The random variable $\mathbb{T}_g = \sum_{l=0}^{L-1} |g_l|^2$ in (5.53) follows a Gamma distribution with a shape parameter $K_{\mathbb{T}_g} = \frac{m(\sum_{l=0}^{L-1} \Omega_{g_l})^2}{\sum_{l=0}^{L-1} \Omega_{g_l}^2}$ and a scale parameter $\phi_{\mathbb{T}_g} = \frac{\sum_{l=0}^{L-1} \Omega_{g_l}^2}{m \sum_{l=0}^{L-1} \Omega_{g_l}}$. Thus the success probability under $\mathcal{H}_0$ is given by

$$P_{succ0} = \frac{\Gamma(K_{\mathbb{T}_g}, \frac{\sigma_v^2 \gamma_s}{\phi_{\mathbb{T}_g} P_s})}{\Gamma(K_{\mathbb{T}_g})}. \tag{5.54}$$

Now the throughput of the secondary link ($\mathrm{SU_{TX}} \rightarrow \mathrm{SU_{RX}}$) when there is no primary user is given by

$$C_0 = P_{succ0} \times \log_2(1+\gamma_s) \quad \text{bits/s/Hz}. \tag{5.55}$$

2. The second scenario is when there is a primary user ($\mathcal{H}_1$). In this scenario the global signal to noise ratio $SNR_{global1}$ (the subscript "1" means under $\mathcal{H}_1$) is written as

$$SNR_{global1} = \sum_{k=0}^{J-1} \frac{P_s |G(k)|^2}{\sigma_v^2 + P_p |F(k)|^2}. \tag{5.56}$$

Now the success probability is given by

$$P_{succ1} = \mathrm{Prob}\Big(\sum_{k=0}^{J-1} \frac{P_s |G(k)|^2}{\sigma_v^2 + P_p |F(k)|^2} > \gamma_s\Big). \tag{5.57}$$

Note that $|G(k)|^2$ and $|F(k)|^2$ follow Gamma distributions with the following parameters [104]

$$K_{|G|} = \bar{m}_{|G|}, \ \phi_{|G|} = \frac{\bar{\Omega}_{|G|}^2}{\bar{m}_{|G|}}, K_{|F|} = \bar{m}_{|F|} \text{ and } \phi_{|F|} = \frac{\bar{\Omega}_{|F|}^2}{\bar{m}_{|F|}}, \tag{5.58}$$

where ($\bar{m}_{|G|}$,$\bar{\Omega}_{|G|}^2$), ($\bar{m}_{|F|}$,$\bar{\Omega}_{|F|}^2$) are defined in (5.44) and (5.47) respectively. The distribution of $\mathbb{T}_{GF} = \sum_{k=0}^{J-1} \frac{P_s |G(k)|^2}{\sigma_v^2 + P_p |F(k)|^2}$ is difficult to derive due to the existence of the summation. During extensive simulations it is found that $\mathbb{T}_{GF}$ can be approximated using a Gamma distribution with a shape parameter $K_{\mathbb{T}_{GF}}$ and a scale parameter $\phi_{\mathbb{T}_{GF}}$.

To find $K_{\mathbb{T}_{GF}}$ and $\phi_{\mathbb{T}_{GF}}$, the mean and the variance of $\mathbb{T}_{GF}$ have to be found. Since the subcarriers are correlated, it is necessary to know the joint p.d.f. for two random

variables of a Nakagami distribution. By using this p.d.f then the shape parameter $K_{\mathbb{T}_{GF}}$ and the scale parameter $\phi_{\mathbb{T}_{GF}}$ are given by (see - Appendix A)

$$\begin{aligned} K_{\mathbb{T}_{GF}} &= \mu^2_{\mathbb{T}_{GF}}/\sigma^2_{\mathbb{T}_{GF}}, \\ \phi_{\mathbb{T}_{GF}} &= \sigma^2_{\mathbb{T}_{GF}}/\mu_{\mathbb{T}_{GF}}, \end{aligned} \tag{5.59}$$

where $\mu_{\mathbb{T}_{GF}}$ and $\sigma^2_{\mathbb{T}_{GF}}$ are defined in (A.4) and (A.8) respectively. Thus the success probability under $\mathcal{H}_1$ is given by

$$P_{succ1} = \frac{\Gamma(K_{\mathbb{T}_{GF}}, \frac{\gamma_s}{\phi_{\mathbb{T}_{GF}}})}{\Gamma(K_{\mathbb{T}_{GF}})}. \tag{5.60}$$

Finally, the secondary throughput when there exists a primary user, is

$$C_1 = P_{succ1} \times \log_2(1+\gamma_s) \quad \text{bits/s/Hz}. \tag{5.61}$$

5.8.2 *Nakagami*-m *flat-fading channel*

This subsection analytically characterizes the average throughput of the secondary link, $\text{SU}_{\text{TX}} \rightarrow \text{SU}_{\text{RX}}$ when the secondary network employs a non OFDM system and over flat-fading channels. The difference between this subsection and the previous subsection is that, this subsection derives the exact expression for the success probabilities under $\mathcal{H}_0$ and $\mathcal{H}_1$. As in the previous subsection two different scenarios have been considered

1. The first scenario is when there is no primary user transmitting $(\mathcal{H}_0)$. The channel in the $\text{SU}_{\text{TX}} \rightarrow \text{SU}_{\text{RX}}$ link now becomes

$$\mathbf{g} = |g|^2, \tag{5.62}$$

where the subscript 0 in g is omitted. Thus the success probability can be written as

$$P_{succ0} = 1 - \text{Prob}\{\frac{P_s|g|^2}{\sigma_v^2} < \gamma_s\}, \tag{5.63}$$

and the $|g|^2$ follows Gamma distribution with scaling parameter $K_g = m$ and shape parameter $\phi_g = \Omega_g/m$. As a result, (5.63) becomes

$$P_{succ0} = \frac{\Gamma(m, \frac{m\gamma_s\sigma_v^2}{\Omega_g P_s})}{\Gamma(m)}. \tag{5.64}$$

Now the throughput of the secondary link ($SU_{TX} \rightarrow SU_{RX}$) when there is no primary user is given by

$$C_0 = \frac{\Gamma(m, \frac{m\gamma_s\sigma_v^2}{\Omega_g P_s})}{\Gamma(m)} \times \log_2(1+\gamma_s) \quad \text{bits/s/Hz.} \tag{5.65}$$

2. The second scenario is when there is a primary user ($\mathcal{H}_1$). First, the channel between the primary transmitter and secondary receiver is written as

$$\mathbf{f} = |f|^2,$$

and again the subscript 0 in f is omitted. Therefore, the success probability in this scenario is given by

$$P_{succ1} = 1 - \text{Prob}\left(\frac{P_s|g|^2}{\sigma_v^2 + P_p|f|^2} < \gamma_s\right), \tag{5.66}$$

$$\Rightarrow \qquad P_{succ1} = \frac{1}{\Gamma(m)} \mathbb{E}_{|f|^2}\left[\Gamma\left(m, \frac{m\gamma_s\sigma_v^2 + m\gamma_s P_p|f|^2}{\Omega_g P_s}\right)\right]. \tag{5.67}$$

The distribution of f follows a Gamma distribution with scaling parameter $K_f = m$ and shape parameter $\phi_f = \Omega_f/m$. Using [[50], eq (1.111) and eq (8.352)] and averaging over the distribution of $|f|^2$ so (5.67) becomes

$$P_{succ1} = \Lambda\left[\sum_{r=0}^{m-1}\sum_{r_1=0}^{r} \frac{(\frac{m\gamma_s\sigma_v^2}{\Omega_f P_s})^{r-r_1}(\frac{m\gamma_s P_p}{\Omega_f P_s})^{r_1}}{(\frac{m}{\Omega_f} + \frac{m\gamma_s P_p}{\Omega_f P_s})^{m+r}} \times \frac{\Gamma(m+r_1)}{r_1!(r-r_1)!\Gamma(m)}\right], \tag{5.68}$$

where $\Lambda = \frac{(m-1)!\exp(\frac{m\gamma_s\sigma_v^2}{\Omega_g P_s})}{\Gamma(m)(\frac{\Omega_g}{m})^m}$. Thus the secondary throughput when there exists a primary user is given as

$$C_1 = P_{succ1} \times \log_2(1+\gamma_s) \quad \text{bits/s/Hz.} \tag{5.69}$$

5.8.3 *Energy detector*

This subsection evaluates the average throughput when the ED is used for spectrum sensing. When applying spectrum sensing and using (5.55) and (5.61), the average throughput of the secondary link $SU_{TX} \rightarrow SU_{RX}$ can be written as

$$\begin{aligned} C_{ED} = (1 - \frac{N}{W})[&P(\mathcal{H}_0)\text{Prob}(T_{ED} < \tau_{ED\theta}|\mathcal{H}_0)C_0 \\ &+ P(\mathcal{H}_1)\text{Prob}(T_{ED} < \tau_{ED\theta}|\mathcal{H}_1)C_1] \end{aligned} \tag{5.70}$$

where $\tau_{ED\theta}$ is defined in (5.26). Also, $\text{Prob}(T_{ED} < \tau_{ED\theta}|\mathcal{H}_0) = 1 - \bar{P}_{FA}$ and $\text{Prob}(T_{ED} < \tau_{ED\theta}|\mathcal{H}_1) = 1 - \overline{P}_D$. Note that $\bar{P}_{FA}$ is the average of P_{FA} over the p.d.f of the NU and it is given by

$$\bar{P}_{FA} = \int_{10^{-0.1B}}^{10^{0.1B}} Q\Big(\sqrt{N}(\frac{\tau_{ED\theta}}{\rho\sigma_v^2} - 1\Big) f_\rho(t)dt. \tag{5.71}$$

Now $\bar{P}_D = \mathbb{E}[P_D]$ is the average of P_D over the p.d.f.'s of $\mathbb{T}_h$ and the NU and it is given by

$$\begin{aligned}\bar{P}_D = &\int_{10^{-0.1B}}^{10^{0.1B}} f_\rho(z) \\ &\times \left[\int_0^\infty Q\left[\frac{\tau_{ED\theta} - \sigma_w^2 - P_p t}{\frac{1}{\sqrt{N}}\Big(P_p t + \rho\sigma_w^2\Big)}\right] \times f_{\mathbb{T}_h}(t)dt\right] dz\end{aligned} \tag{5.72}$$

where $\mathbb{T}_h = \sum_{l=0}^{L-1} |h_l|^2$. The inner integral in (5.72) is derived in chapter 3 for a Gaussian signal (see (3.25)). Thus (5.72) can be evaluated in one integral instead of two integrals. By substituting, (5.71) and (5.72) into (5.70), then (5.70) becomes

$$\begin{aligned}C_{ED} = (1 - \frac{N}{W})\Big[&P(\mathcal{H}_0)C_0(1 - \overline{P}_{FA}(\tau_{ED\theta})) \\ &+ P(\mathcal{H}_1)C_1(1 - \overline{P}_D(\tau_{ED\theta}))\Big].\end{aligned} \tag{5.73}$$

5.8.4 *Autocorrelation detector*

By employing the AD for spectrum sensing and using (5.55) and (5.61), the average throughput of the secondary link is given by

$$\begin{aligned}C_{AD} = (1 - \frac{N}{W})\Big[&P(\mathcal{H}_0)C_0\text{Prob}(T_{AD} < \tau_{AD\theta}|\mathcal{H}_0) \\ &+ P(\mathcal{H}_1)C_1\text{Prob}(T_{AD} < \tau_{AD\theta}|\mathcal{H}_1)\Big]\end{aligned} \tag{5.74}$$

where $\tau_{AD\theta}$ is defined in (5.41) and $\text{Prob}(T_{ED} < \tau_{AD\theta}|\mathcal{H}_0) = 1 - \bar{P}_{FA}$ and $\bar{P}_{FA}$ is given by

$$\bar{P}_{FA} = P_{FA} = P(T_{AD} < \tau_{AD\theta}|\mathcal{H}_0) = \frac{1}{2}\text{erfc}\Big(\sqrt{N}\tau_{AD\theta}\Big). \tag{5.75}$$

Notice that $\bar{P}_{FA} = P_{FA}$ because the false alarm probability is independent from the noise variance. Also, $(T_{AD} < \tau_{AD\theta} | \mathcal{H}_1) = 1 - \overline{P}_D$, where $\bar{P}_D = \mathbb{E}[P_D]$ is the average over the p.d.f. of $\mathbb{T}_h$ and it is given by

$$\begin{aligned}\bar{P}_D &= P(T_{AD} > \tau_{AD\theta} | \mathcal{H}_1) \\ &= \frac{1}{2}\left[\int_0^{\infty} \operatorname{erfc}\left(\sqrt{N}\frac{\tau_{AD\theta} - \kappa_1 t/(P_p t + \sigma_w^2)}{1 - \left[\kappa_1 t/(P_p t + \sigma_w^2)\right]^2}\right) \times f_{\mathbb{T}_h}(t)dt\right]\end{aligned} \tag{5.76}$$

where $\kappa_1 = (N_c \big/ (N_d + N_c))P_p$ and $\mathbb{T}_h = \sum_{l=0}^{L-1} |h_l|^2$. The integral can be evaluated numerically, and by substituting (5.75) and (5.76) into (5.74), then

$$\begin{aligned}C_{AD} = (1 - \frac{N}{W})\Big[&P(\mathcal{H}_0)C_0(1 - P_{FA}(\tau_{AD\theta}) \\ &+ P(\mathcal{H}_1)C_1(1 - \bar{P}_D(\tau_{AD\theta})\Big].\end{aligned} \tag{5.77}$$

Next the simulation results are discussed.

5.9 SIMULATION AND DISCUSSION

In this section, some simulation results are presented to justify the analytical results and to show the effect of both NU and the NFS channel on the secondary throughput under outage constraint using the ED and AD. The system parameters that have been used are as follows. For the NFS channel of $\text{PU}_{\text{TX}} \rightarrow \text{SU}_{\text{TX}}$ link $(\mathbf{h})$, $\text{SU}_{\text{TX}} \rightarrow \text{SU}_{\text{RX}}$ link $(\mathbf{g})$ and $\text{PU}_{\text{TX}} \rightarrow \text{SU}_{\text{RX}}$ $(\mathbf{f})$ link, the channels taps are generated according to an exponential power delay profile. The signal to noise ratios at the $\text{SU}_{\text{TX}} \rightarrow \text{SU}_{\text{RX}}$ link and $\text{PU}_{\text{TX}} \rightarrow \text{SU}_{\text{RX}}$ link are set to $\frac{P_s \sum_{l=0}^{L-1} \mathbb{E}|g_l|^2}{\sigma_v^2} = 20\text{dB}$ and $\frac{P_p \sum_{l=0}^{L-1} \mathbb{E}|f_l|^2}{\sigma_v^2} = -10\text{dB}$, respectively. γ_s =10dB, $P(H_0)$=0.7, $P(H_1)$=0.3, $\delta = 0.9$, N_c= 8, $N_d = 32$, and W =$100(N_c + N_d)$ samples. The number of iterations that is used for the simulation is 10^5.

Result 1: Theoretical results verification for threshold values (ED) in the presence of NU and over NFS and NFF channels (Figures 5.4, 5.5, 5.6 and 5.7).

Figures 5.4 (for different SNR values) and 5.5 (for different N values) show the outage detection probability bound (θ) versus the sensing threshold $(\tau_{ED\theta})$ for the

exact threshold (found via (5.22)) and the approximate threshold using Jensen's Inequality (see (5.26)) for L=2 and m=2. It is easily seen that this approximation is almost tight for small values of θ and it is a lower bound for high values of θ.

Figures 5.6 and 5.7 show θ versus the $\tau_{ED\theta}$ for both the exact threshold (found via (5.31)) and and the approximate threshold using Jensen's Inequality (see - (5.32)) for L=1 and m=1. It is evidenced from the simulation that both curves are almost identical.

Result 2: Theoretical results verification for secondary throughput (ED) in the presence of NU and over NFS channel (Figures **5.8** and 5.9).

Figure 5.8 depicts the theoretical result for the secondary throughput while the ED used for sensing (for NFS, please see (5.26) and (5.73). For NFF, see (5.32) and for (5.73)) and the simulation result (for both NFF and NFS see (5.21) and (5.73)). The figure shows that the theoretical result is an upper bound for the simulation result. Since $\tau_{ED\theta}$ is a lower bound this implies that it is larger than the exact threshold for a specific θ, as shown from Figures 5.4 and 5.5. This gives a small $\overline{P}_{FA}$ and $\overline{P}_{D}$. Subsequently, the resulting throughput becomes an upper bound for the exact throughput.

Moreover, the figure illustrates that as L increases the secondary throughput improves. This behavior can be interpreted as follows. As the $\tau_{ED\theta}$ increases with L for the same value of θ, as shown in Figure 5.9, reducing the $\overline{P}_{FA}$ and $\overline{P}_{D}$ and accordingly the throughput improves.

Result 3: Secondary throughput (ED) in the presence of NU and over NFS channel with different values of θ, L and m (Figures 5.10, **5.11,** and 5.12)**.**

Firstly, from Figure 5.10 it is easily seen that as θ increases the secondary throughput increases (theory - see (5.26) and (5.73)). Moreover, it can be seen that as the θ increases the optimum sensing time (i.e., the $N = N_{opt}$ that maximizes the throughput) decreases due to more outage being allowable

Secondly, Figure 5.11 shows that as the L increases, we initially get a considerable improvement in the secondary throughput $(L = 1, 2, 3)$ and then this gain levels off for large values of L $(L = 14, 15)$ (for the interpretation, see Result 2).

Thirdly, Figure 5.12 shows that the secondary throughput initially improves significantly for m= 1 (Rayleigh fading channel) and m=2. After that it increases gradually and then the throughput flattens out for m = 14 and 15. This can be explained since as m increases the channel becomes less severe and then the effect of the channel eventually disappears for a very large value of m which is the case of an AWGN channel.

Result 4: Secondary throughput (ED) in the presence of NU and over an NFS channel with different values of B (Figure 5.13)**.**

This figure plots secondary throughput (C_{ED}) against the sensing time (N) for different values of B (theory - see (5.26) and (5.73)). It can be seen that as B increases the secondary throughput decreases[11]. Moreover, it is observed that as B increases the optimum sensing time (i.e., the $N = N_{opt}$ that maximizes the throughput) increases and then it decreases for $B = 0.75$. This can be explained as follows. When B increases and reaches a certain value, the sensing is not beneficial and the secondary user is less confident about any sensing decision. Therefore, it is advantageous to reduce sensing time (as regards maximising the secondary throughput).

Result 5: Maximum throughput versus γ_s (Figure **5.14**)**.**

Now Figure 5.14 illustrates the relationship between the maximum secondary throughput and γ_s. We can see from the figure that there exists an optimum γ_s^* that maximizes the secondary throughput. This is because $\log_2(1+\gamma_s)$ is an increasing function and P_{succ0} or P_{succ1} is a decreasing function. Notice that the θ does not have any effect on the optimum γ_s^*.

Result 6: Secondary throughput (AD) in both the presence and the absence of NU (Figure **5.15**)**.**

Figure 5.15 presents the secondary throughput for the AD in both the presence and the absence of NU and over the NFS channel (theory - see (5.41) and (5.77), simulation - see (5.33) and (5.77)). It is noticeable that NU has no affect on the

11 Notice that for small number of N, the secondary throughput is better for high values of B. This is because the approximation of calculating the threshold value does not work well for high values of B.

secondary throughput and this is why the NU was not taken into account in the analysis.

Result 7: Secondary throughput (AD) over NFS channel with different values of θ, L, and m (Figures 5.16, 5.17 and 5.18)**.**

Figure 5.16 shows the sensing-throughput tradeoff while the AD is used for sensing for different values of θ. Here, it can be clearly seen that as the θ increases the secondary throughput increases and this is because the restriction is less for high values of θ.

Now Figure 5.17 depicts that by increasing the number of multipaths (L) the secondary throughput is initially getting a considerable improvement (L=1,3,5) and then this gain levels off for large values of L (L=14,15).

Here Figure 5.18 illustrates the secondary-throughput tradeoff for different values of m. It is clear from the figure that the secondary throughput initially improves rapidly as m increases and then the improvement increases gradually until it flattens out for high values of m (m=14,15). Notice that all the aforementioned figures in Result 7 are plotted using (5.41) and (5.77).

Result 8: Sensing-throughput tradeoff comparison between the ED and the AD in the presence of NU and over NFS channel (Figure 5.19)**.**

Lastly, this figure shows a comparison between the ED and the AD in terms of sensing-throughput tradeoff. It is shown in Figure 5.3 that the NU affects badly on the detection performance of the ED and does not affect on the performance of AD. However, this massive deterioration in the detection performance does not appear on the secondary throughput. In other wards, the secondary throughput (when the ED is used for sensing) is better compared with the AD. But the detection performance of the ED is very sensitive to the NU (unlike an AD).

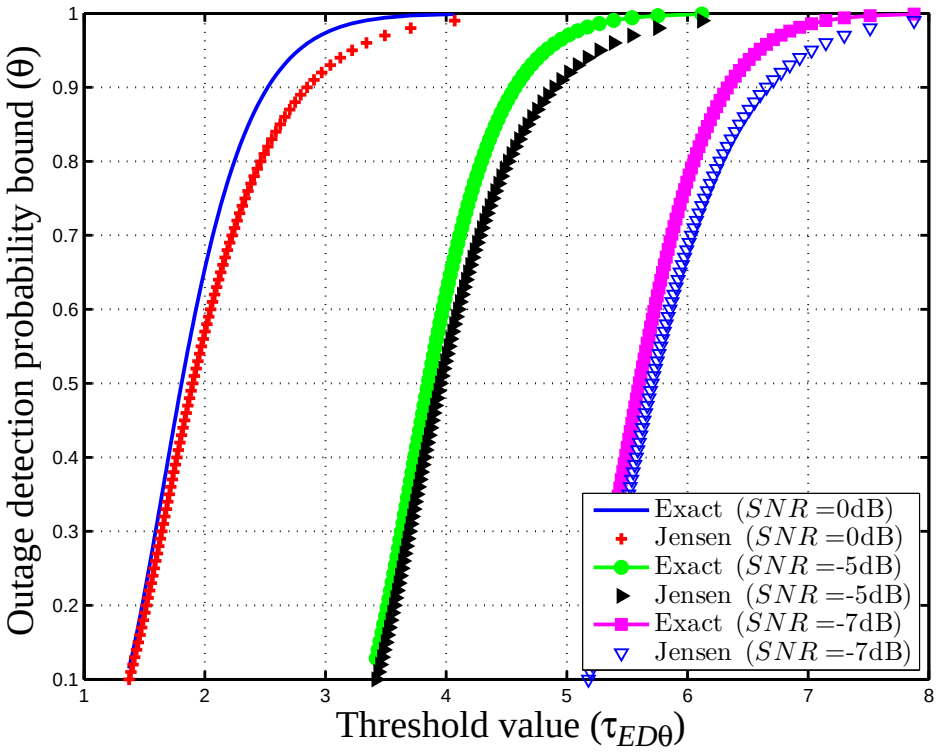

Figure 5.4: θ versus the $\tau_{ED\theta}$ over NU and NFS channels for the exact threshold and the approximate threshold using Jensen's Inequality, for different values of SNR. In all cases, L=2, m=2, $N = 500$ and $B = 0.25$.

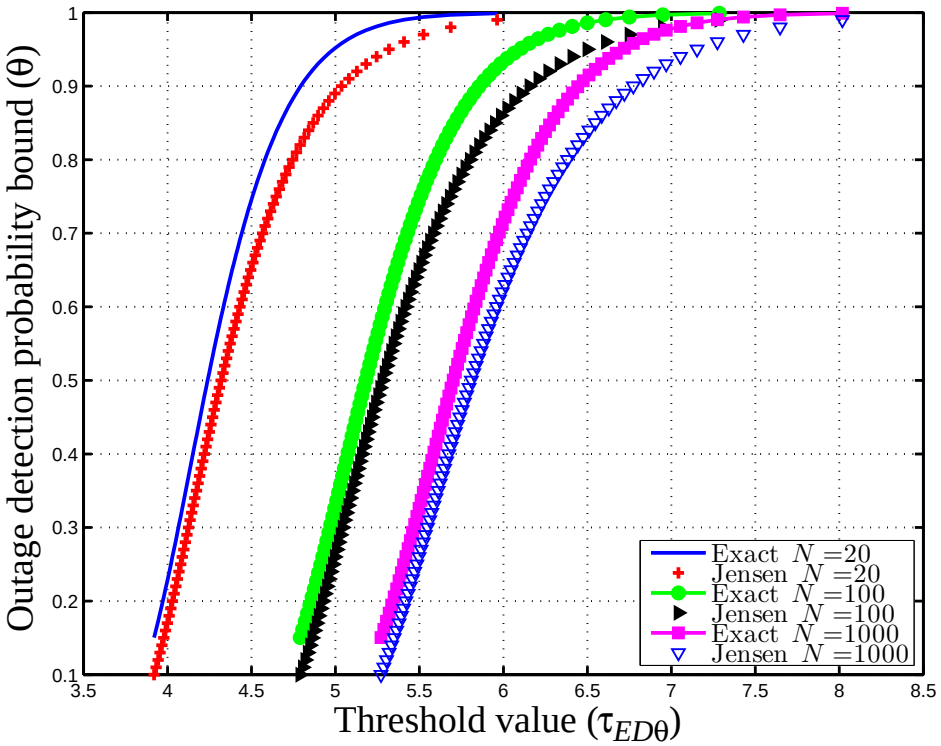

Figure 5.5: θ versus the $\tau_{ED\theta}$ over NU and NFS channels for the exact threshold and the approximate threshold using Jensen's Inequality, for different values of N. In all cases, $SNR = 10\log\frac{P_p}{\sigma_w^2} = -7$dB, L=2, m=2 and $B = 0.25$.

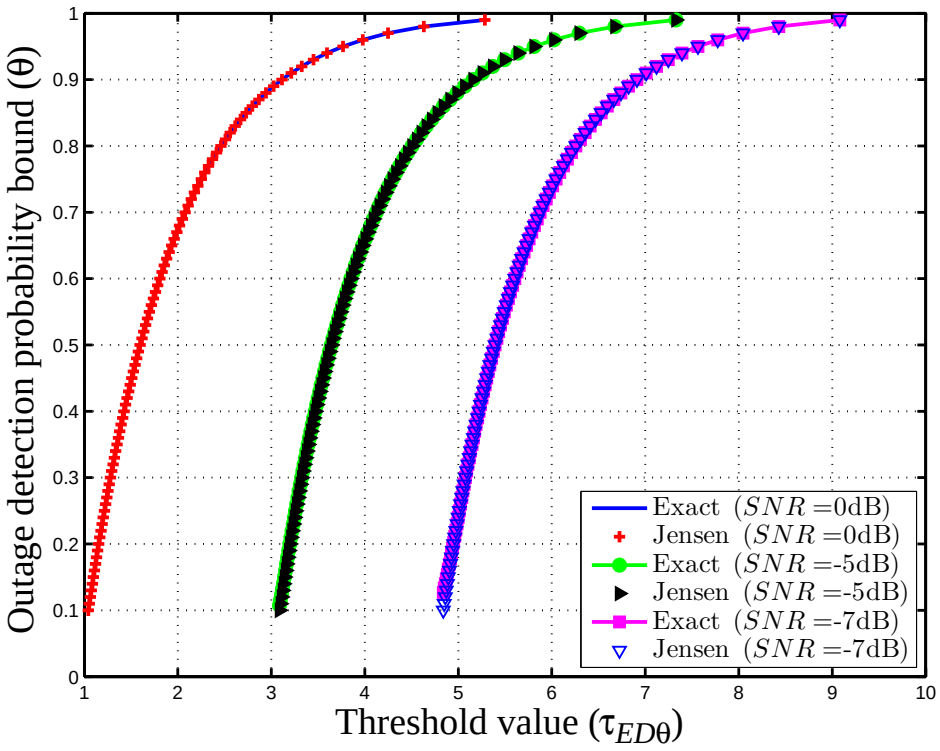

Figure 5.6: θ versus the $\tau_{ED\theta}$ over NU and NFF channels for the exact threshold and the approximate threshold using Jensen's Inequality, for different values of SNR. In all cases, L=1 , m=1, N=500 and $B = 0.25$dB.

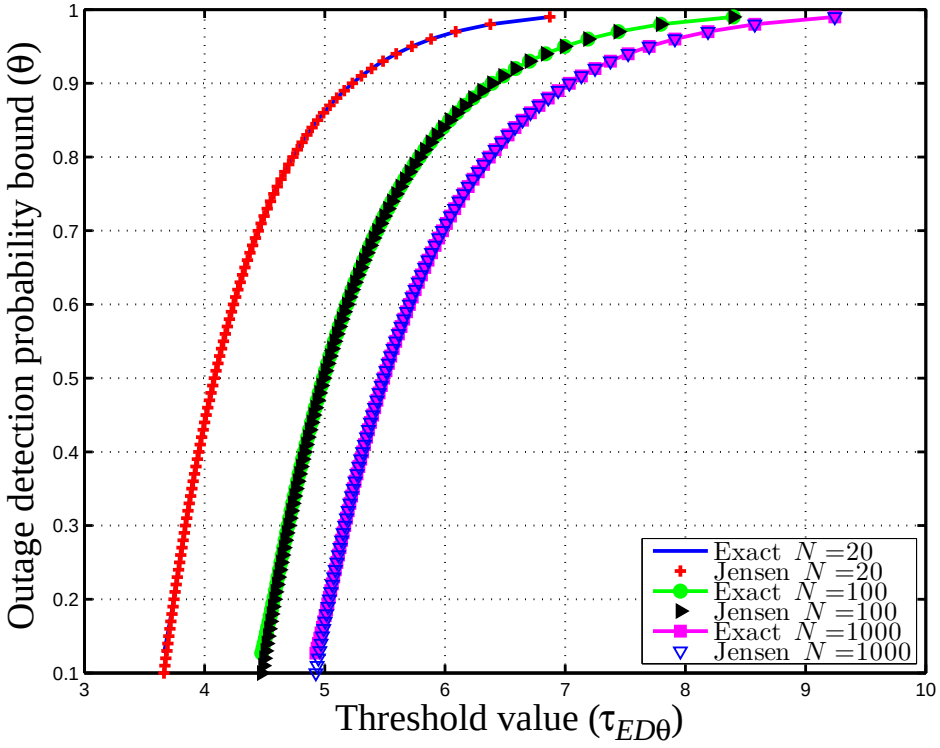

Figure 5.7: θ versus the $\tau_{ED\theta}$ over NU and NFF channels for the exact threshold and the approximate threshold using Jensen's Inequality, for different values of N. In all cases, $SNR = 10\log\frac{P_p}{\sigma_w^2} = -7$dB, L=1 , m=1 and $B = 0.25$dB.

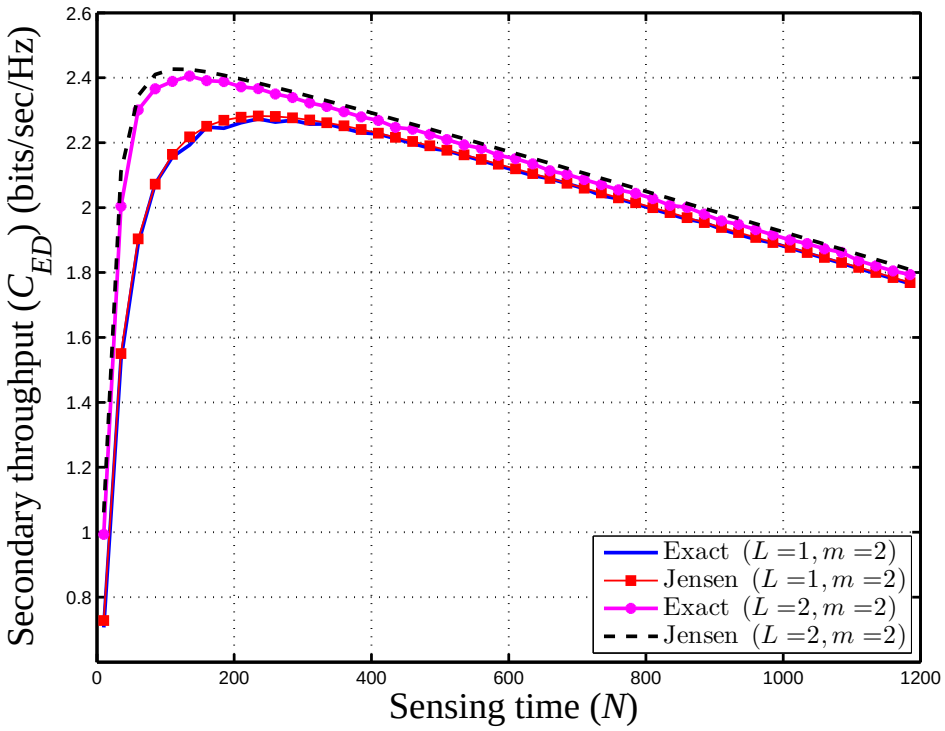

Figure 5.8: The achievable throughput, C_{ED}, versus the sensing time, N, in the presence of NU and over NFS. In all cases, $B = 0.75$dB, $\theta = 0.15$ and $\gamma_{ave} = 0$dB.

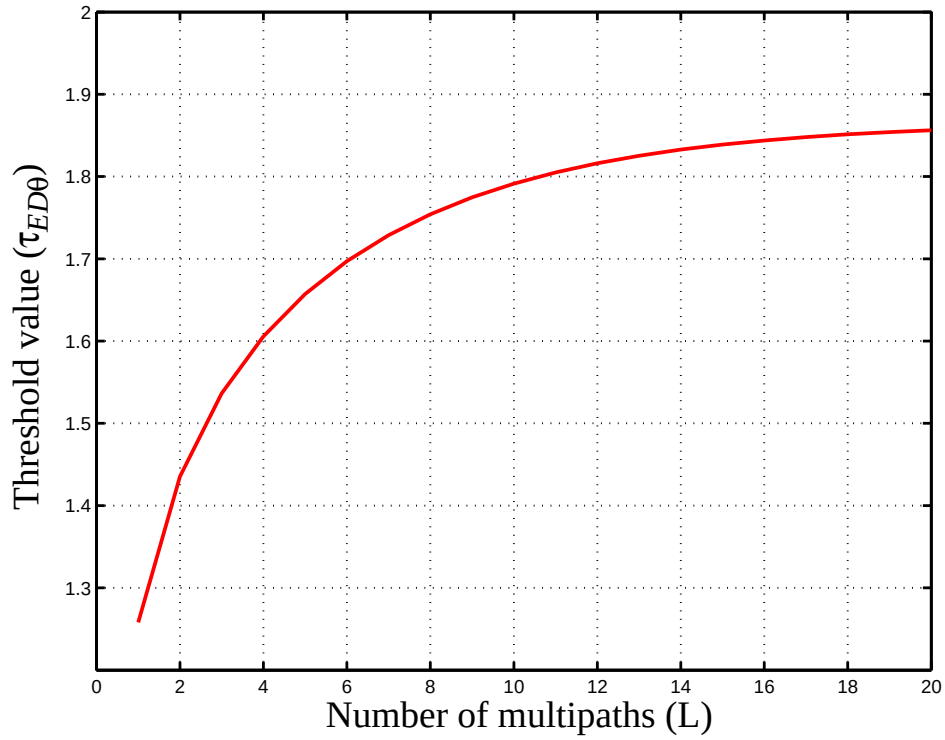

Figure 5.9: The threshold value, $\tau_{ED\theta}$, versus the number of multipaths L, where m=2, N=300, B=0.75dB, $\theta = 0.15$ and $\gamma_{ave} = 0$dB.

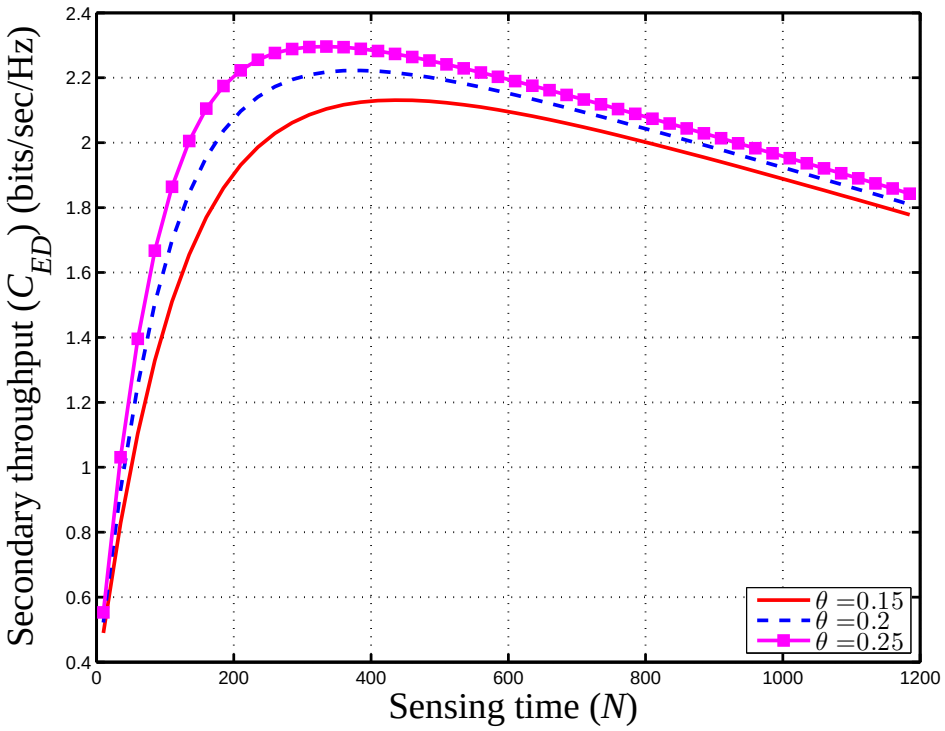

Figure 5.10: The secondary throughput,C_{ED}, versus sensing time, N. In all cases, $L = 2$, $m = 2$, B=0.25dB and γ_{ave}(in dB) $= -5$.

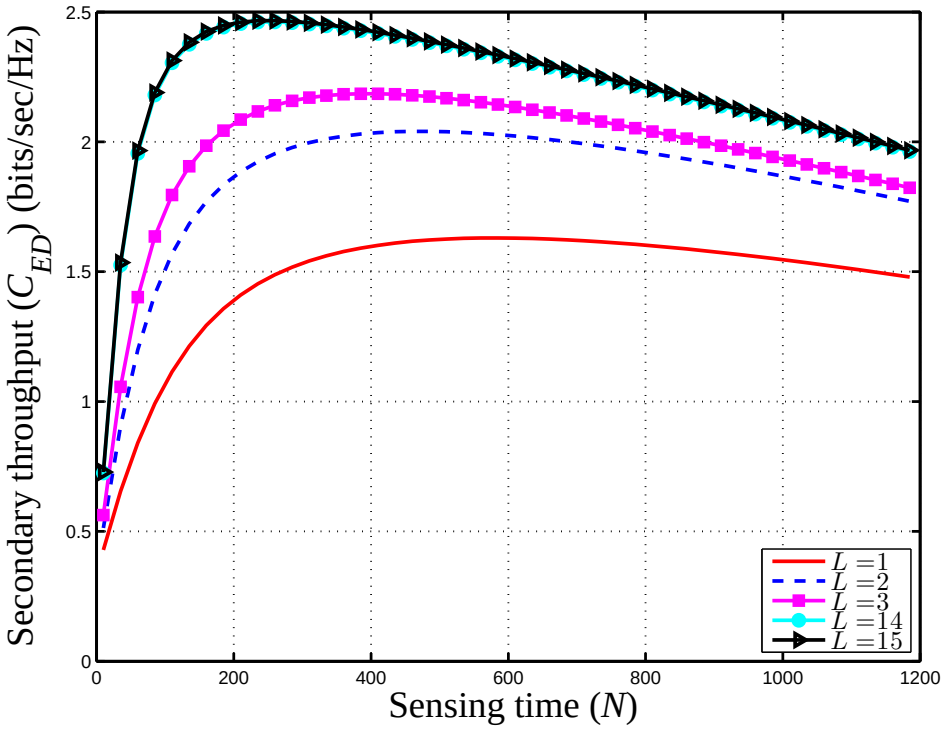

Figure 5.11: The secondary throughput, C_{ED}, versus sensing time, N. In all cases, $m = 2$, $B = 0.5$dB, $\theta = 0.15$ and $\gamma_{ave} = -5$dB.

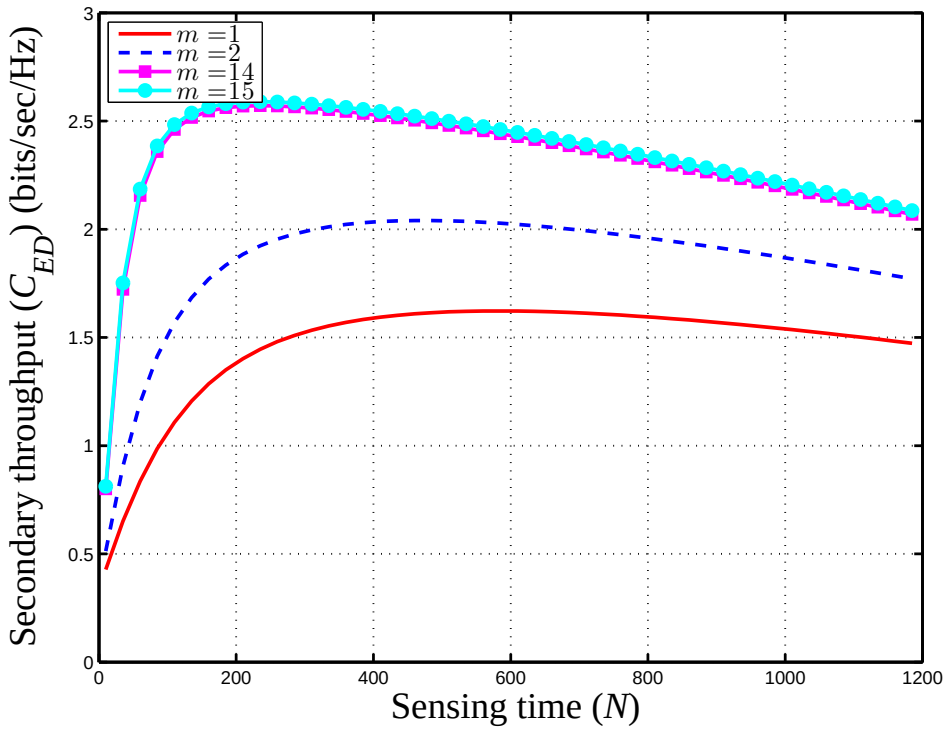

Figure 5.12: The secondary throughput, C_{ED}, versus sensing time, N. In all cases, $L = 2$, $B = 0.5$dB, $\theta = 0.15$ and $\gamma_{ave} = -5$dB.

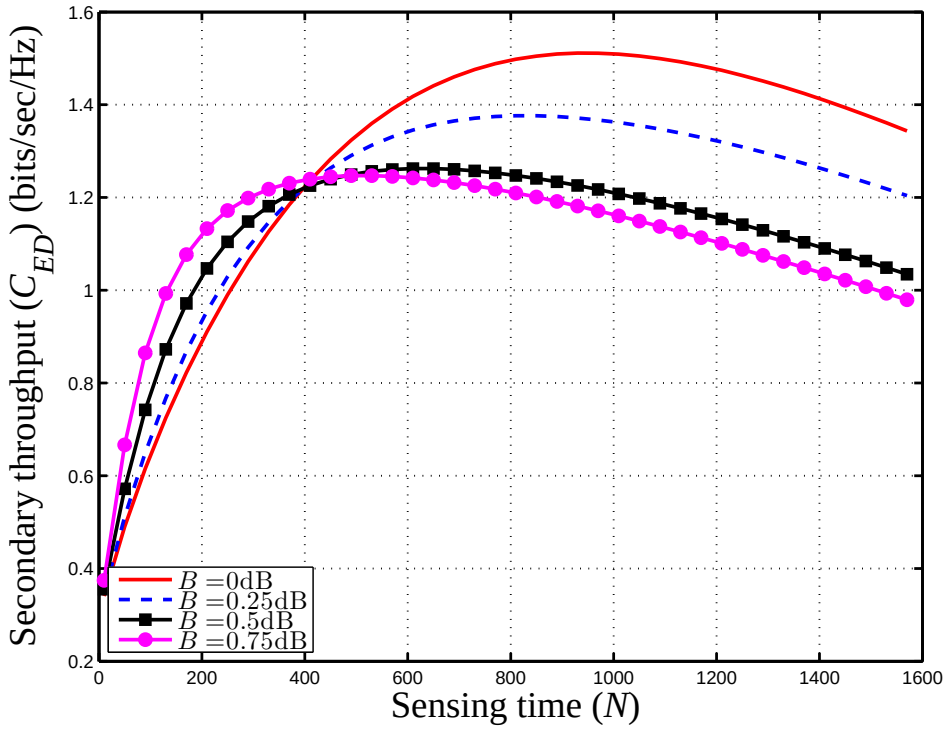

Figure 5.13: The secondary throughput, C_{ED}, versus sensing time, N, for different values of B. In all cases, $L = 1$, $m = 1$, $\theta = 0.15$ and $\gamma_{ave} = -5$dB.

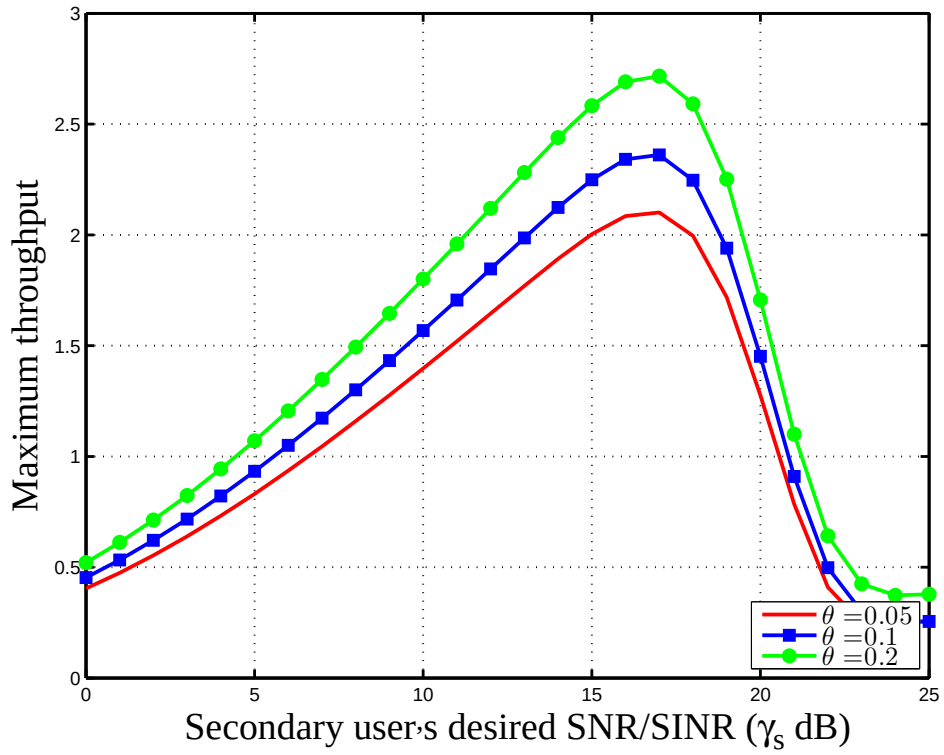

Figure 5.14: The maximum secondary throughput, $\max[C_{ED}]$, versus the secondary user's desired SNR/SINR,(γ_s), for different values of θ. In all cases, L =3 m=2, B=0.5dB and γ_{ave} (in dB) = 0dB.

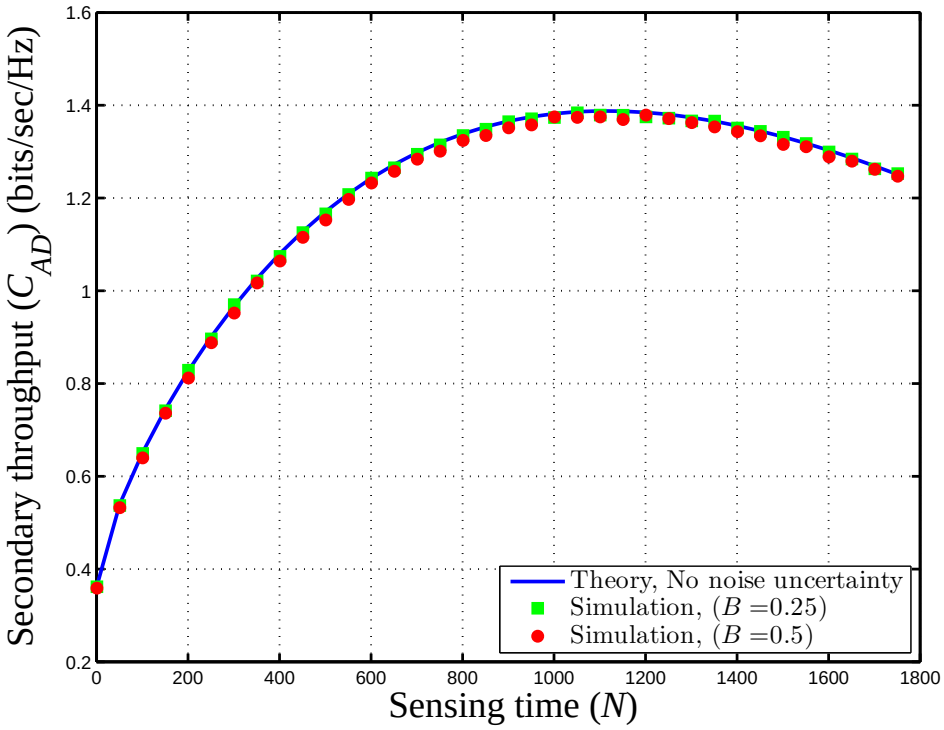

Figure 5.15: The secondary throughput, C_{AD}, versus sensing time, N. In all cases, $L = 2$, $m = 2$, $\theta = 0.15$ and $\gamma_{ave} = -5$dB.

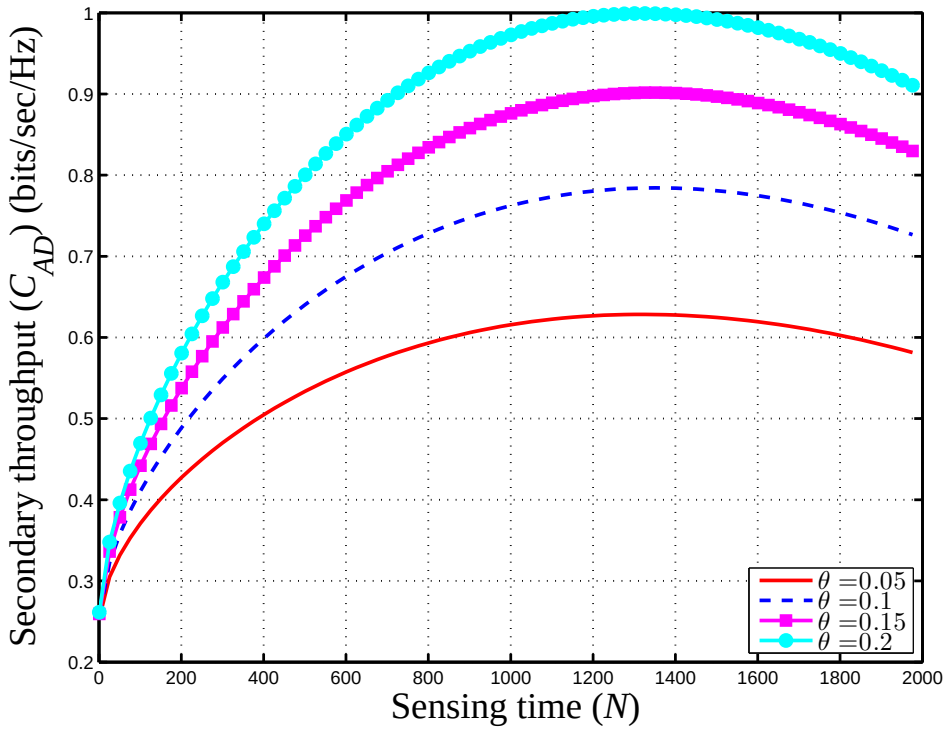

Figure 5.16: The secondary throughput, C_{AD}, versus sensing time, N. In all cases, $L = 2$, $m = 2$, and $\gamma_{ave}(\text{in dB}) = -5$.

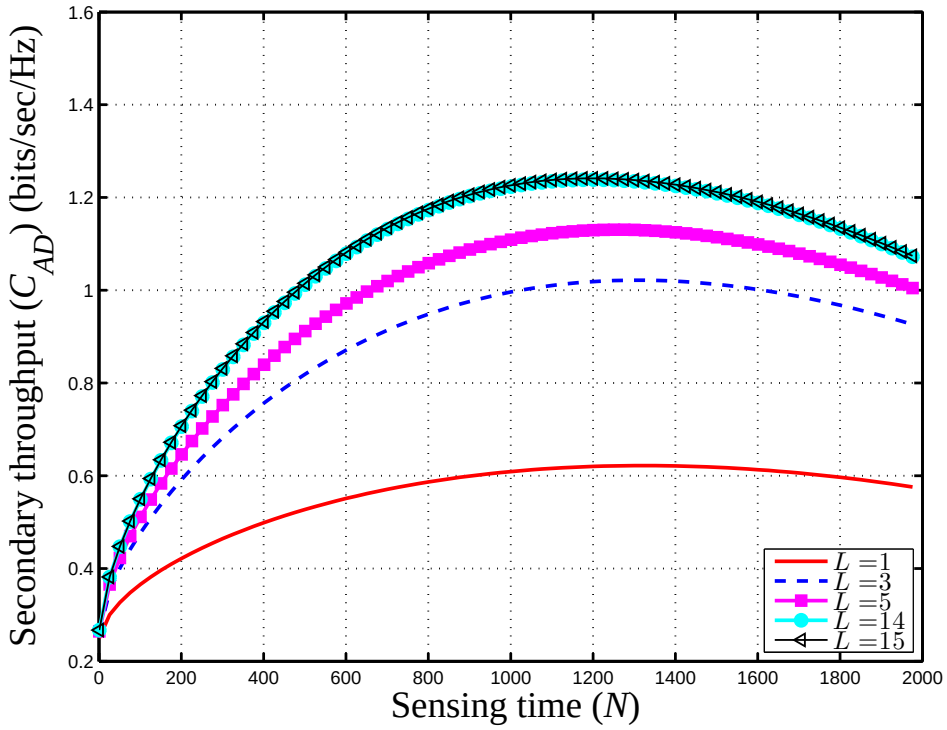

Figure 5.17: The secondary throughput, C_{AD}, versus sensing time, N. In all cases, $m = 2$, $\theta = 0.15$, and $\gamma_{ave}(\text{in dB}) = -5$.

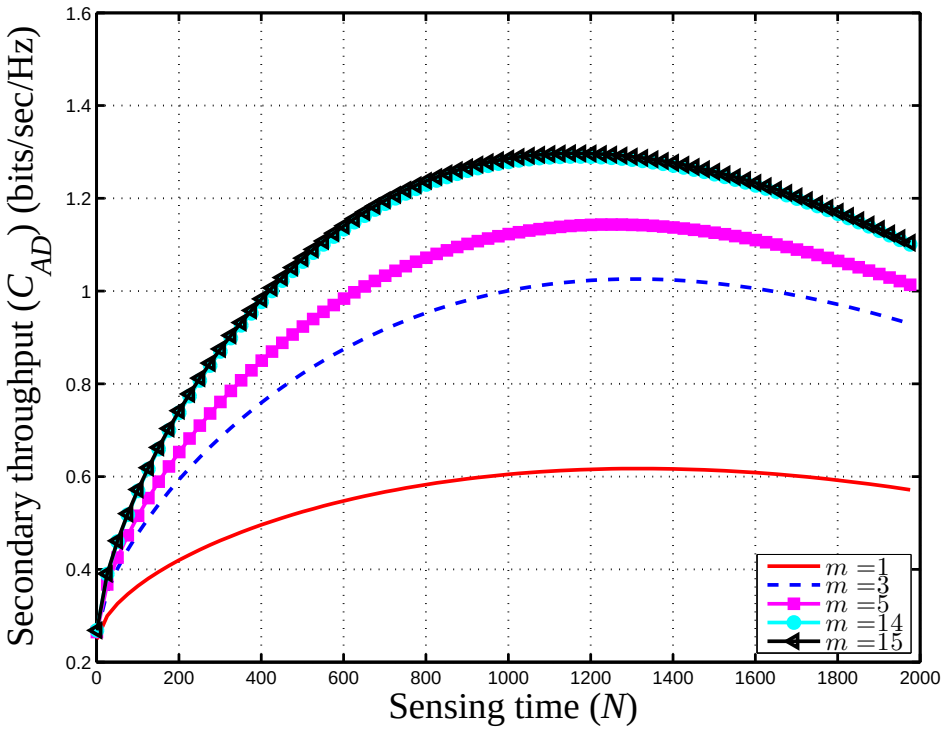

Figure 5.18: The secondary throughput, C_{ED}, versus sensing time, N. In all cases, L=2, $\theta = 0.15$ and $\gamma_{ave} = -5$dB.

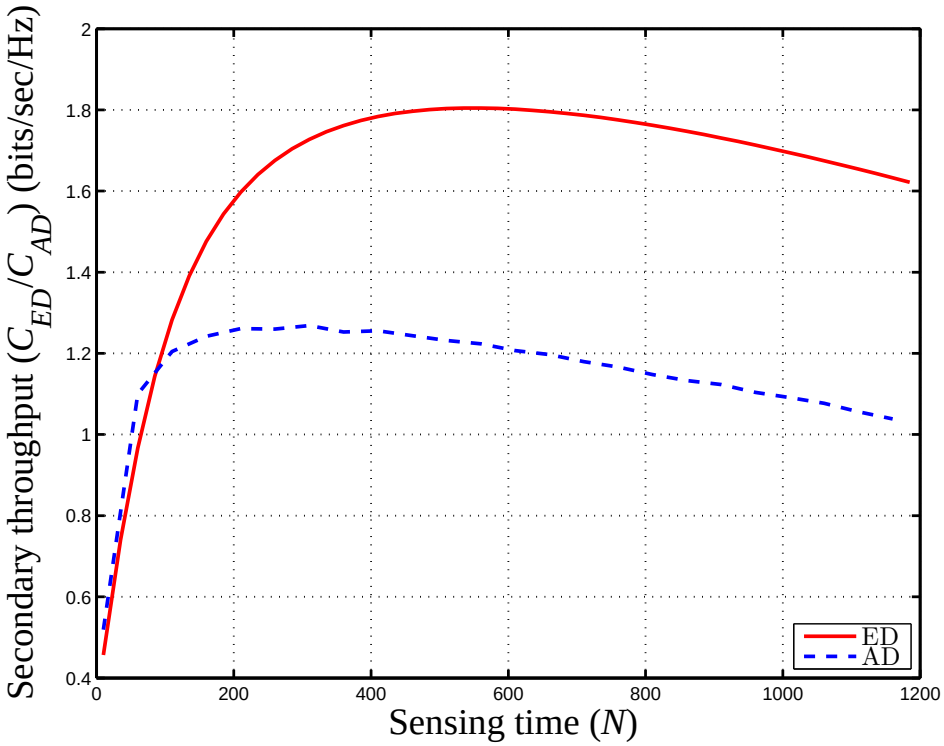

Figure 5.19: The secondary throughput for ED (C_{ED}) and for the AD (C_{AD}) versus sensing time, N. In all cases, $m = 1$, $L = 2$, $B = 0.5$dB, $\gamma_{ave}(\text{in dB}) = -5$, and $\theta = 0.15$.

5.10 CHAPTER SUMMARY

The sensing-throughput tradeoff under outage constraints has been studied in the presence of NU and over NFS channel. This work consideres an NFS channel for the sensing channel, the communicating channel (secondary link) and the interference channel (caused by the primary user). Moreover, this study was based on two different detectors, the ED and the AD.

Rigurous performance analyses have been done throughout the chapter. First, a closed form expression for the sensing threshold under an outage constraint on the detection probability is found. Second a closed form expression for the secondary throughput is derived analytically. To derive the secondary throughput, success probabilities for the secondary link under both the presence and the absence of a primary user are derived theoretically.

Firstly, using the concept of outage detection probability, a closed form expression for the sensing threshold has been derived for the ED under NU and over the NFS. Moreover, another closed form expression for the sensing threshold has been found for the AD over NFS. Secondly, success probabilities for the secondary link under both the presence and the absence of a primary user are derived theoretically. Thirdly, closed form expressions for the secondary throughput for both the ED and the AD are derived analytically in terms of the sensing threshold and the success probabilities. In addition, all the theoretical results are verified by simulation.

The results have shown that the secondary throughput, when the ED and the AD are used for sensing, improves with an initial increase for the number of multipaths and then this improvement levels out. Also, for both the ED and the AD, when the Nakagami fading parameter (m) increases the secondary throughput initially dramatically improves and then for high values of m the improvement it levels off. Moreover, the simulation results have shown that the secondary throughput for the ED case is sensitive to the NU. Furthermore, the simulation results show that there exists a quality of service (the secondary user's desired SNR threshold) that maximizes the secondary throughput. For the AD, the results have shown that the AD detector is not affected by the NU and so the detection performance of the ED be-

comes worst than the AD detection performance in the presence of NU. But even if the ED is used for sensing, the secondary throughput is still superior compared to using the AD for sensing.

6

CONCLUSIONS AND FUTURE WORK

6.1 CONCLUSIONS

An important constraint in cognitive radio network is the lack of coordination and cooperation with the primary network and this renders synchronization with the primary network unrealistic. In practical cognitive systems, durable sensing techniques are a mandatory requirement to protect the primary receiver. Accordingly, Chapter 2 presents novel robust spectrum sensing algorithms such as $\frac{N}{2}$-BLCD, SOMF-I and SOMF-II which (in contrast with the MF) are insensitive to PN and CFO.

In reality, having a closed-form expression for detection probability may provide a rigorous understanding of the principles of system design. This understanding guides the designer to predict behavioural changes in cognitive or primary networks without the need for carrying through many Monte Carlo simulations for each choice of parameters. So, unlike some previous work in the literature, chapter 3 investigates the performance of the ED over NFS channels in terms of three different considerations, namely; the average detection probability, outage detection probability and the minimum number of samples which satisfy a desired ROC condition.

An important stage in cooperative spectrum sensing is sending measurements to the FC which can deplete valuable energy resources. Most existing solutions in cooperative spectrum sensing use censoring techniques. However, not all the degrees of freedom have been exploited here to reduce the energy overhead. Consequently, chapter 4 proposes the CSCPC approach as an energy-efficient cooperative spec-

trum sensing algorithm while taking into consideration the transmit power (the required power to send the measurements to the FC) along with the censored threshold. Our results have shown that we can economise on transmit power and the primary user's protection is still guaranteed when compared to the conventional censoring cooperative spectrum sensing (CSC).

To fully understand cognitive radio techniques, it is necessary to evaluate the cognitive performance under practical scenarios. This provides a useful guideline for the future design of a cognitive radio network. So, a comprehensive evaluation has been conducted in terms of sensing-throughput tradeoff. In chapter 5, the sensing-throughput tradeoff has been derived in the presence of NU and over NFS under outage constraints for the ED and AD based on OFDM primary user signal. The evaluation has been derived in terms of two parameters. The first considers a closed-form equation for the sensing threshold while taking into consideration the NU and the NFS while the second evaluates success probabilities under $\mathcal{H}_0$ and $\mathcal{H}_1$. The simulation results have shown that the secondary throughput for the ED is very sensitive to the NU and it degrades rapidly with a small change in NU bound. The amount of the performance degradation depends on the NU bound. The secondary user's throughput is however not affected when the AD is used for spectrum sensing. Furthermore, simulation results have shown that while the NFS degrades the secondary user's performance, the degradation may be mitigated with an initial increase in L and m and then the improvement levels out.

Moreover, the results have shown that the ED (in the presence of NU) provides a better secondary user throughput compared to the AD. The ED detection performance however, deteriorates compared to the AD in the presence of NU. Finally, the results show that there exists a secondary user's desired SNR threshold that maximises the secondary throughput.

6.2 FUTURE WORK AND OPEN DIRECTIONS

All the previous work has stimulated thought about existing practices and provoked discussion about future research directions. A few of these are listed below.

First approach

Regarding the CFO in chapter 2, the study may be extended for cooperative spectrum sensing with different CFO's. The analysis may start by examining in depth the behavior of the cooperative spectrum sensing at the FC. Then the study might include some different CFO estimators (e.g., ML).

Furthermore, it might be interesting to look at spectrum sensing using MIMO technology in the presence of CFO. In addition, the effects of other RF impairments such as IQ imbalance, sampling errors and jitter could be investigated on the performance of both the MF and the ED.

Second approach

This new approach is based on the investigation in chapter 3. Energy consumption can also be incorporated with the detection performance over NFS. The number of multitaps (L) may be estimated which can be exploited such that the number of received samples (N) is reduced and the target detection is satisfied subsequently reducing the energy consumption. In addition, the study may include cooperative spectrum sensing when both the sensing and the reporting channels are NFS.

Third approach

In chapter 4 both channel and the distance between the secondary users and the FC are assumed to be known. For a more realistic scenario, such parameters could be estimated leading to an investigation of estimation errors on the architecture of detection and the energy overhead problems. Furthermore, the problem would be more interesting if the primary user assumed mobility modeled by a Possion process. Moreover, the number of received samples can be incorporated into the evaluation of the energy overhead. In addition, both ξ and p_t have not yet been found in closed form expressions and that is something that could be investigated.

The work in chapter 4 was dependent on a centralized detection problem. However, an attack on, or a failure to the FC, may harm the detection solution. Thus another possibility is to use decentralized algorithms to tackle the problem of the FC failure, e.g., consensus algorithms.

Fourth approach

In chapter 5 the cognitive performance has been studied based on the outage detection probability. In this thesis the outage detection bound (θ) has been assumed to be known or determined by the primary user. In practice, the typical value of the θ could be analytically determined by relating it with the primary user's outage probability. In addition, the sensing time that maximises the throughput could be optimized in the presence of the NU and NFS.

In chapter 5 the sensing-throughput tradeoff problem has been studied only for the secondary link. This work can be extended for the case of the primary link by including the effect of the NU and the NFS on the primary user's receiver.

In the investigation of the sensing-throughput tradeoff problem, other detectors, for example cyclostationary and eigen detectors, might be included in the study in terms of secondary throughput, primary throughput and system complexity.

In this thesis, the performance evaluation of the cognitive radio has been conducted for a local secondary user. This could be extended to cooperative secondary users.

In the evaluation of sensing-throughput tradeoff the success probability has been used as a metric. Other metrics can also be used such as ergodic capacity, etc.

A

PROOFS OF CHAPTER 5

The joint p.d.f. for a bivariate Nakagami distribution is given by [104]

$$f_{xy} = \frac{4\bar{m}^2(xy)^{\bar{m}}\exp(-(\frac{x^2}{\Omega_x}+\frac{y^2}{\Omega_y})\times(\frac{\bar{m}}{1-\rho}))}{\Gamma(\bar{m})\Omega_x\Omega_y(1-\rho)(\sqrt{\Omega_x\Omega_y\rho})^{\bar{m}-2}} I_{\bar{m}-1}\left\{\frac{2\bar{m}\sqrt{\rho_1}xy}{\sqrt{\Omega_x\Omega_y(1-\rho_1)}}\right\} \quad \text{(A.1)}$$

where $x \geq 0,\ y \geq 0$. For our scenario, $x = |\mathbb{X}(k_1)|$, $y = |\mathbb{X}(k_2)|$, where $k_1 \neq k_2$, $\mathbb{X} = \{G, F\}$, and $k_{1,2} = 1 : J-1$. Also, $\bar{m} = \bar{m}_{|\mathbb{X}|}$, $\Omega_x = \mathbb{E}(x^2)$, $\Omega_y = \mathbb{E}(y^2)$, and $\rho_1 = \text{cov}(x,y)/\sqrt{var(x)var(y)}$ where $1 > \rho_1 > 0$.

Derivation of the mean and the variance of global SNR under $\mathcal{H}_1$ (see (5.56)) is derived in this Appendix. The global SNR under $\mathcal{H}_1$ is

$$\mathbb{T}_{GF} = \sum_{k=0}^{J-1} \frac{P_s|G(k)|^2}{\sigma_v^2 + P_p|F(k)|^2}. \quad \text{(A.2)}$$

By letting $x_k = |G(k)|^2$ and $y_k = |F(k)|^2$ then

$$\mathbb{T}_{GF} = \sum_{k=0}^{J-1} \frac{x_k}{a + by_k} \quad \text{(A.3)}$$

where $a = \frac{\sigma_v^2}{P_s}$ and $b = \frac{P_p}{P_s}$.

A.1 EXPECTED VALUE CALCULATION

Because x_k and y_k are independent thus

$$\mu_{\mathbb{T}_{GF}} = \mathbb{E}[\mathbb{T}_{GF}] = \sum_{k=0}^{J-1} \mathbb{E}\left[\frac{x_k}{a+by_k}\right] = J\mathbb{E}[x]\,\mathbb{E}\left[\frac{1}{a+by}\right]. \quad \text{(A.4)}$$

Because x_k and y_k are independent in k so we omit k in (A.4). Since both x and y follow Gamma distributions so

$$\begin{aligned}\mathbb{E}[x] &= \frac{1}{\Gamma(k_x)\left(\frac{\bar{\Omega}^2_{|G|}}{\bar{m}_{|G|}}\right)^{\bar{m}_{|G|}}} \int_0^\infty x \times x^{\bar{m}_{|G|}-1} e^{-\bar{m}_{|G|}x/\bar{\Omega}^2_{|G|}} \quad \mathrm{d}x \\ &= \frac{\Gamma(\bar{m}_{|G|}+1)}{\Gamma(\bar{m}_{|G|})}\end{aligned} \tag{A.5}$$

and

$$\mathbb{E}\left[\frac{1}{a+by}\right] = \frac{1}{\Gamma(\bar{m}_{|F|})\left(\frac{\bar{\Omega}^2_{|F|}}{\bar{m}_{|F|}}\right)^{\bar{m}_{|F|}}} \int_0^\infty \frac{y^{\bar{m}_{|F|}-1} e^{-\bar{m}_{|F|}y/\bar{\Omega}^2_{|F|}}}{a+by} \quad \mathrm{d}y. \tag{A.6}$$

By using [[50], eq. (3.353.5)], then (A.6) can be re-written as

$$\begin{aligned}\mathbb{E}\left[\frac{1}{a+by}\right] = &\frac{1}{b\Gamma(\bar{m}_{|G|})\left(\frac{\bar{\Omega}^2_{|G|}}{\bar{m}_{|G|}}\right)^{\bar{m}_{|G|}}} [(-1)^{\bar{m}_{|G|}-2}(a) e^{a\bar{m}_{|G|}/\bar{\Omega}^2_G} \mathrm{Ei}(-a\bar{m}_{|G|}/b\bar{\Omega}^2_{|G|}) \\ &+ b\sum_{k1=1}^{\bar{m}_G} (k1-1)!(-a/b)^{\bar{m}_G-k1}(\bar{m}_G/\bar{\Omega}^2_G)^{k_1}.\end{aligned} \tag{A.7}$$

where $\mathrm{Ei} = -\int_{-a_1}^{\infty} \frac{e^{-t}}{t}\, dt$. By substituting (A.7) and (A.6) into (A.6) we get the final result.

A.2 VARIANCE CALCULATION

The variance of A.2 can be written as

$$\sigma^2_{\mathbb{T}_{GF}} = \mathbb{E}\left[\mathbb{T}^2_{GF}\right] - \left[\mathbb{E}\left[\mathbb{T}_{GF}\right]\right]^2 \tag{A.8}$$

$$\begin{aligned}\mathbb{E}\left[\mathbb{T}^2_{GF}\right] &= \sum_{l=0}^{J-1}\sum_{k=0}^{J-1} \frac{x_l}{a+y_l}.\frac{x_k}{a+y_k} \\ &= \sum_{l=0}^{J-1} \mathbb{E}\left[\frac{x_l^2}{(a+y_l)^2}\right] + \sum_{\substack{l,k=0 \\ l\neq k}}^{J-1} \mathbb{E}\left[\frac{x_l}{a+y_l}.\frac{x_k}{a+y_k}\right].\end{aligned}$$

First we evaluate $\mathbb{E}\left[\frac{x_l^2}{(a+y_l)^2}\right]$. Because x_l and y_l are independent in l so we omit l

$$\begin{aligned}\mathbb{E}\left[\frac{x^2}{(a+y)^2}\right] &= \frac{1}{\Gamma(\bar{m}_{|G|})(\frac{\bar{\Omega}^2_{|G|}}{\bar{m}_{|G|}})^{\bar{m}_{|G|}}}\int_0^\infty x^{\bar{m}_{|G|}+1}e^{-\bar{m}_{|G|}x/\bar{\Omega}^2_{|G|}}\,\mathrm{d}x \\ &\times \frac{1}{\Gamma(\bar{m}_{|F|})(\frac{\bar{\Omega}^2_{|F|}}{\bar{m}_{|F|}})^{\bar{m}_{|F|}}}\int_0^\infty \frac{y^{\bar{m}_{|F|}-1}e^{-\bar{m}_{|F|}y/\bar{\Omega}^2_{|F|}}}{(a+by)^2}\,\mathrm{d}y \\ &= \frac{\Gamma(\bar{m}_{|G|}+2)(\frac{\bar{\Omega}^2_{|G|}}{\bar{m}_{|G|}})^2\int_0^\infty \frac{y^{\bar{m}_{|F|}-1}e^{-\bar{m}_{|F|}y/\bar{\Omega}^2_{|F|}}}{(a+by)^2}\,\mathrm{d}y}{\Gamma(\bar{m}_{|G|})\Gamma(\bar{m}_{|F|})(\frac{\bar{\Omega}^2_{|F|}}{\bar{m}_{|F|}})^{\bar{m}_{|F|}}}.\end{aligned} \tag{A.9}$$

By using (A.1) $\mathbb{E}\left[\frac{x_l}{a+y_l}.\frac{x_k}{a+y_k}\right]$ can be calculated as

$$\begin{aligned}\mathbb{E}\left[\frac{x_l}{a+by_l}.\frac{x_k}{a+by_k}\right] &= \int_0^\infty\int_0^\infty \frac{\exp(-(\frac{{x_l}^2}{\Omega_x}+\frac{{x_k}^2}{\Omega_y})\times(\frac{\bar{m}_{|G|}}{1-æ}))}{(1-\rho)(\sqrt{\Omega_{x_l}\Omega_{x_k}\rho})^{\bar{m_{|G|}}-2}} \\ &\times \frac{4\bar{m}^2_{|G|}(x_lx_k)^{\bar{m_{|G|}}+2}}{\Gamma(\bar{m})\Omega_{x_l}\Omega_{x_k}} \\ &\times I_{\bar{m_{|G|}}-1}\left\{\frac{2\bar{m}_{|G|}\sqrt{\rho}x_lx_k}{\sqrt{\Omega_{x_l}\Omega_{x_k}(1-\rho)}}\right\}\mathrm{d}x_l\mathrm{d}x_k \\ &\times \int_0^\infty\int_0^\infty .\frac{\exp(-(\frac{{y_l}^2}{\Omega_{y_l}}+\frac{{y_k}^2}{\Omega_{y_k}})\times(\frac{\bar{m}_{|F|}}{1-æ}))}{(\sqrt{\Omega_{y_l}\Omega_{y_k}\rho})^{\bar{m}_{|F|}-2}} \\ &\times \frac{4\bar{m}^2_{|F|}(y_ly_k)^{\bar{m}_{|F|}}}{a+by_l}\times\frac{1}{\Gamma(\bar{m}_{|F|})\Omega_{y_l}\Omega_{y_k}(1-\rho)} \\ &\times \frac{1}{a+by_k}\times I_{\bar{m_{|F|}}-1}\left\{\frac{2\bar{m}_{|F|}\sqrt{\rho}y_ly_k}{\sqrt{\Omega_{y_l}\Omega_{y_k}(1-\rho)}}\right\}\mathrm{d}y_l\mathrm{d}y_k.\end{aligned} \tag{A.10}$$

Finally by substituting (A.4), (A.9) and (A.10) into (A.8), then the variance in (A.8) is obtained.

BIBLIOGRAPHY

[1] "Table of frequency allocations used by the fcc and ntia," National Telecommunications and Information Administration Office of Spectrum Management, U. S. Department of Commerce,, Tech. Rep., August 2011. (Cited on pages xxiii and 2.)

[2] I. F. Akyildiz, W. Y. Lee, M. C. Vuran, and S. Mohanty, "Next generation/dynamic spectrum access/cognitive radio wireless networks: a survey," *The International Journal of Computer and Telecommunications Networking*. (Cited on pages xxiii and 3.)

[3] M. Buddhikot, "Understanding dynamic spectrum access: Models,taxonomy and challenges," in *IEEE International Symposium on New Frontiers in Dynamic Spectrum Access Networks*, 2007, pp. 649–663. (Cited on pages xxiii and 4.)

[4] D. B. Cabric, "Cognitive radios: System design perspective," Ph.D. dissertation, Electrical Engineering and Computer Sciences University of California at Berkeley, 2007. (Cited on page 1.)

[5] Fedral Communications Commission, "Spectrum policy task force," Rep. ET Docket no. 02-135, Nov. 2002. (Cited on page 1.)

[6] S. Haykin, "Cognitive radio: brain-empowered wireless communications," *IEEE Journal on Selected Areas in Communications*, vol. 23, no. 2, pp. 201–220, 2005. (Cited on pages 1 and 3.)

[7] M. E. Heikki Koivo, *Systems Engineering in Wireless Communications*. Wiley, 2009. (Cited on page 2.)

[8] J. Mitola *et al*, "Cognitive radio: making software radios more personal," *IEEE Pers. Commun.*, vol. 6, no. 4, pp. 13–18, 1999. (Cited on page 2.)

[9] S. M. Lars Berlemann, *Cognitive Radio and Dynamic Spectrum Access*. Wiley, 2009. (Cited on page 2.)

[10] E. Hossain and dusit nayato zhuhan, *Dynamic spectrum access and management In cognitive radio networks*. Combridge, 2009. (Cited on page 3.)

[11] Q. Zhao and B. Sadler, "A survey of dynamic spectrum access," *IEEE Signal Processing Magazine*, vol. 24, no. 3, pp. 79–89, 2007. (Cited on page 4.)

[12] Q. Zhao and A. Swami, "A survey of dynamic spectrum access: Signal processing and networking perspectives," in *IEEE International Conference on Acoustics, Speech and Signal Processing.*, vol. 4, 2007, pp. IV–1349–IV–1352. (Cited on page 4.)

[13] D. Hatfield and P. Weiser, "Property rights in spectrum: taking the next step," in *First IEEE International Symposium on New Frontiers in Dynamic Spectrum Access Networks*, 2005, pp. 43–55. (Cited on page 5.)

[14] L. Xu, R. To?njes, T. Paila, W. Hansmann, M. Frank, and M. Albrecht, "Drive-ing to the internet: Dynamic radio for ip services in vehicular environments," in *IEEE Conference on Local Computer Networks*, 2000, pp. 281–289. (Cited on page 5.)

[15] S. Srinivasa and S. Jafar, "The throughput potential of cognitive radio: A theoretical perspective," in *Conference on Signals, Systems and Computers*, 2006, pp. 221–225. (Cited on page 5.)

[16] S. M. Kay, *Fundamentals of Statistical Signal Processing Detection theory Volume II*. Englewood Cliffs, NJ: Prentice-Hall, 1998. (Cited on pages 6, 17, 21, 22, 29, 39, and 47.)

[17] Y.-C. Liang, Y. Zeng, E. Peh, and A. T. Hoang, "Sensing-throughput tradeoff for cognitive radio networks," *IEEE Transactions on Wireless Communica-*

tions, vol. 7, no. 4, pp. 1326 –1337, 2008. (Cited on pages 7, 110, 111, and 112.)

[18] C. Stevenson, G. Chouinard, Z. Lei, W. Hu, S. Shellhammer, and W. Caldwell, "Ieee 802.22: The first cognitive radio wireless regional area network standard," *IEEE Communications Magazine*, vol. 47, no. 1, pp. 130–138, 2009. (Cited on page 8.)

[19] D. Cabric, A. Tkachenko, and R. Brodersen, "Spectrum sensing measurements of pilot, energy, and collaborative detection," in *Proc. IEEE Military Communications Conference*, 2006, pp. 1–7. (Cited on pages 8, 19, 41, and 42.)

[20] E. Rebeiz and D. Cabric, "Blind modulation classification based on spectral correlation and its robustness to timing mismatch," in *Proc. IEEE Military Communications Conference*, 2011, pp. 277–282. (Cited on pages 8 and 19.)

[21] A. Zahedi-Ghasabeh, A. Tarighat, and B. Daneshrad, "Sampling clock frequency offset compensation for feature detection in spectrum sensing," in *IEEE International Conference on Communications*, 2010, pp. 1–6. (Cited on pages 8 and 19.)

[22] F. F. Digham, M.-S. Alouini, and M. K. Simon, "On the energy detection of unknown signals over fading channels," *IEEE Transactions on Communications*, vol. 55, no. 1, pp. 21–24, 2007. (Cited on pages 9, 40, 53, 59, 69, 86, and 88.)

[23] P. Sofotasios, E. Rebeiz, L. Zhang, T. Tsiftsis, D. Cabric, and S. Freear, "Energy detection based spectrum sensing over mu and extreme fading channels," *IEEE Transactions on Vehicular Technology*, vol. 62, no. 3, pp. 1031–1040, 2013. (Cited on pages 9 and 41.)

[24] S. Atapattu, C. Tellambura, and H. Jiang, "Performance of an energy detector over channels with both multipath fading and shadowing," *IEEE Trans-*

actions on Wireless Communications, vol. 9, no. 12, pp. 3662–3670, 2010. (Cited on page 9.)

[25] ——, "Energy detection of primary signals over gamma and mu fading channels," in *International Conference on Industrial and Information Systems*, 2009, pp. 118–122. (Cited on page 9.)

[26] W. Wang, W. Zou, Z. Zhou, H. Zhang, and Y. Ye, "Decision fusion of cooperative spectrum sensing for cognitive radio under bandwidth constraints," in . *Third International Conference on Convergence and Hybrid Information Technology*, vol. 1, 2008, pp. 733–736. (Cited on pages 9 and 70.)

[27] S. Maleki and G. Leus, "Censored truncated sequential spectrum sensing for cognitive radio networks," *Selected Areas in Communications, IEEE Journal on*, vol. 31, no. 3, pp. 364–378, 2013. (Cited on pages 9 and 71.)

[28] J. Lunden, V. Koivunen, A. Huttunen, and H. Poor, "Collaborative cyclostationary spectrum sensing for cognitive radio systems," *IEEE Transactions on Signal Processing*, vol. 57, no. 11, pp. 4182–4195, 2009. (Cited on pages 9 and 70.)

[29] S. Chaudhari, J. Lunden, and V. Koivunen, "Collaborative autocorrelation-based spectrum sensing of OFDM signals in cognitive radios," in *42nd Annual Conference on Information Sciences and Systems*, 2008, pp. 191–196. (Cited on pages 9 and 70.)

[30] J. Lunden, V. Koivunen, A. Huttunen, and H. Poor, "Censoring for collaborative spectrum sensing in cognitive radios," in *the Forty-First Asilomar Conference on Signals, Systems and Computers*, 2007, pp. 772–776. (Cited on page 9.)

[31] ——, "Collaborative cyclostationary spectrum sensing for cognitive radio systems," *IEEE Transactions on Signal Processing*, vol. 57, no. 11, pp. 4182–4195, 2009. (Cited on page 9.)

[32] Y. Chen, "Analytical performance of collaborative spectrum sensing using censored energy detection," *IEEE Transactions on Wireless Communications*, vol. 9, no. 12, pp. 3856–3865, 2010. (Cited on pages 9 and 70.)

[33] X. Kang, Y.-C. Liang, H. Garg, and L. Zhang, "Sensing-based spectrum sharing in cognitive radio networks," *IEEE Transactions on Vehicular Technology*, vol. 58, no. 8, pp. 4649–4654, 2009. (Cited on pages 9 and 113.)

[34] E. Peh, Y.-C. Liang, Y. L. Guan, and Y. Zeng, "Optimization of cooperative sensing in cognitive radio networks: A sensing-throughput tradeoff view," *IEEE Transactions on Vehicular Technology*, vol. 58, no. 9, pp. 5294–5299, 2009. (Cited on page 9.)

[35] Y. Pei, Y.-C. Liang, K. Teh, and K. H. Li, "How much time is needed for wideband spectrum sensing?" *IEEE Transactions on Wireless Communications*, vol. 8, no. 11, pp. 5466–5471, 2009. (Cited on pages 9 and 113.)

[36] J. Jafarian and K. A. Hamdi, "Non-cooperative double-threshold sensing scheme: A sensing-throughput tradeoff," in *IEEE Wireless Communications and Networking Conference*, 2013, pp. 3376–3381. (Cited on pages 9 and 113.)

[37] S. Stotas and A. Nallanathan, "On the outage capacity of sensing-enhanced spectrum sharing cognitive radio systems in fading channels," *IEEE Transactions on Communications*, vol. 59, no. 10, pp. 2871–2882, 2011. (Cited on pages 9 and 113.)

[38] W. Stoyan, D. Kendall and J. Mecke, *Stochastic Geometry And its Applications*. Wiley, 1995. (Cited on pages 11, 12, 75, 86, 87, 88, 89, 90, and 92.)

[39] H. Elsawy, E. Hossain, and M. Haenggi, "Stochastic geometry for modeling, analysis, and design of multi-tier and cognitive cellular wireless networks: A survey," *IEEE Communications Surveys Tutorials*, vol. 15, no. 3, pp. 996–1019, Third 2013. (Cited on page 11.)

[40] W. M. Pinto, P, "A unifying framework for local throughput in wireless networks," 2010. (Cited on page 11.)

[41] R. Tandra and A. Sahai, "SNR walls for signal detection," *IEEE Journal of Selected Topics in Signal Processing*, vol. 2, no. 1, pp. 4 –17, 2008. (Cited on pages 13, 112, and 120.)

[42] Y. Zeng and Y.-C. Liang, "Robustness of the cyclostationary detection to cyclic frequency mismatch," in *21st IEEE International Symposium on Personal Indoor and Mobile Radio Communications*, 2010, pp. 2704–2709. (Cited on page 18.)

[43] M. Oner, "On the effect of random sampling jitter on cyclostationarity based spectrum sensing algorithms for cognitive radio," in *69th IEEE Vehicular Technology Conference*, 2009, pp. 1–5. (Cited on page 18.)

[44] M. Oner and O. Dobre, "On the second-order cyclic statistics of signals in the presence of receiver impairments," *IEEE Transactions on Communications*, vol. 59, no. 12, pp. 3278–3284, 2011. (Cited on page 18.)

[45] J. Verlant-Chenet, J. Renard, J.-M. Dricot, P. De Doncker, and F. Horlin, "Sensitivity of spectrum sensing techniques to RF impairments," in *71st IEEE Vehicular Technology Conference*, 2010, pp. 1–5. (Cited on page 18.)

[46] A. Zahedi-Ghasabeh, A. Tarighat, and B. Daneshrad, "Spectrum sensing of OFDM waveforms using embedded pilots in the presence of impairments," *IEEE Transactions on Vehicular Technology*, vol. 61, no. 3, pp. 1208 –1221, 2012. (Cited on page 18.)

[47] A. Tkachenko, D. Cabric, and R. Brodersen, "Cyclostationary feature detector experiments using reconfigurable BEE2," in *IEEE International Symposium on New Frontiers in Dynamic Spectrum Access Networks*, 2007, pp. 216–219. (Cited on page 18.)

[48] E. Rebeiz, P. Urriza, and D. Cabric, "Optimizing wideband cyclostationary spectrum sensing under receiver impairments," *IEEE Transactions on Signal Processing*, vol. 61, no. 15, pp. 3931–3943, 2013. (Cited on page 19.)

[49] G. Colavolpe, A. Barbieri, and G. Caire, "Algorithms for iterative decoding in the presence of strong phase noise," *IEEE Journal on Selected Areas in Communications*, vol. 23, no. 9, pp. 1748–1757, 2005. (Cited on pages 21 and 31.)

[50] I. S. Gradshteyn and T. I. M. Ryzhik, *Table of Integrals, Series, and Products, 7th ed.*, N. Y. Academic, Ed., 2007. (Cited on pages 22, 50, 51, 52, 53, 134, and 156.)

[51] Z. Quan, S. Cui, H. Poor, and A. Sayed, "Collaborative wideband sensing for cognitive radios," *IEEE Signal Processing Magazine*, vol. 25, no. 6, pp. 60–73, 2008. (Cited on pages 28, 41, 45, and 69.)

[52] H. Urkowitz, "Energy detection of unknown deterministic signals," *IEEE Proceedings*, vol. 55, no. 4, pp. 523–531, 1967. (Cited on page 40.)

[53] A. H. Nuttall, "Some integrals involving the q -function," *Naval Underwater Syst. Center (NUSC)*, 1974. (Cited on page 40.)

[54] S. Atapattu, C. Tellambura, and H. Jiang, "Energy detection of primary signals over gamma and mu fading channels," in *Industrial and Information Systems*, 2009. (Cited on page 40.)

[55] S. Herath, N. Rajatheva, and C. Tellambura, "Energy detection of unknown signals in fading and diversity reception," *IEEE Transactions on Communications*, vol. 59, no. 9, pp. 2443–2453, 2011. (Cited on page 40.)

[56] S. Atapattu, C. Tellambura, and H. Jiang, "Performance of an energy detector over channels with both multipath fading and shadowing," *IEEE Transactions on IEEE Transactions on Wireless Communications*, vol. 9, no. 12, pp. 3662–3670, 2010. (Cited on page 41.)

[57] Y.-C. Liang, Y. Zeng, E. Peh, and A. T. Hoang, "Sensing-throughput tradeoff for cognitive radio networks," *IEEE Transactions on Wireless Communications*, vol. 7, no. 4, pp. 1326 –1337, 2008. (Cited on pages 41 and 42.)

[58] Y. Lim and Y. Sung, "Upper bound for the loss factor of energy detection of random signals in multipath fading cognitive radios," in *IEEE International Conference on Acoustics, Speech and Signal Processing*, 2009, pp. 2537–2540. (Cited on page 41.)

[59] Y. Huang and X. Huang, "Detection of temporally correlated signals over multipath fading channels," *IEEE Transactions on Wireless Communications*, vol. 12, no. 3, pp. 1290–1299, 2013. (Cited on page 42.)

[60] ——, "Optimal spectrum sensing over multipath channels," in *IEEE International Conference on Communications*, 2012, pp. 1522–1527. (Cited on page 42.)

[61] A. Cacciapuoti, M. Caleffi, D. Izzo, and L. Paura, "Cooperative spectrum sensing techniques with temporal dispersive reporting channels," *IEEE Transactions on Wireless Communications*, vol. 10, no. 10, pp. 3392–3402, 2011. (Cited on page 42.)

[62] R. Umar, A. Sheikh, and M. Deriche, "Unveiling the hidden assumptions of energy detector based spectrum sensing for cognitive radios," *IEEE Communications Surveys Tutorials*, vol. PP, no. 99, pp. 1–16, 2013. (Cited on page 43.)

[63] M. Nakagami, "The m-distribution, a general formula for intensity distribtion of rapid fading," *Statistical Methods in Radio Wave Propagation*, 1960. (Cited on pages 44, 129, and 130.)

[64] A. Goldsmith, *Wireless communications*. Cambridge University Press, 2005. (Cited on pages 44 and 76.)

[65] A. Costano-Martinez and F. Lopez-Blazquez, "Distribution of a sum of weighted noncentral chi-square variables," *Test: An official Journal of the*

Spanish Society of Statistical. and Operation Research, vol. 14, no. 2, pp. 397–415, 2005. (Cited on page 48.)

[66] M. D. Springer, *The Algebra of Random Variables.* John Wiley & Sons, 1979. (Cited on page 48.)

[67] M. Abramowitz and I. A. Stegun, *Handbook of Mathematical Functions with Formulas, Graphs, and Mathematical Tables*. Dover Publication, 1972. (Cited on pages 49 and 76.)

[68] Y. A. B. A.P Prudnikov and O. I. Marichev, *integral and series volume I.* Taylor and Francis, 1986. (Cited on page 53.)

[69] G. Ganesan and L. Ye, "Cooperative spectrum sensing in cognitive radio, part ii: Multiuser networks," *IEEE Trans. on Wireless Commun.*, vol. 6, no. 6, pp. 2214–2222, 2007. (Cited on page 69.)

[70] A. Ghasemi and E. Sousa, "Collaborative spectrum sensing for opportunistic access in fading environments," in *Proc. DySPAN*, 2005, pp. 131–136. (Cited on page 69.)

[71] R. Niu and P. K. Varshney, "Distributed decision and fusion in a large wireless sensor network of random size," *wireless communications and networking*, vol. 2, pp. 462–472, 2005. (Cited on page 69.)

[72] S. Herath, N. Rajatheva, and C. Tellambura, "Unified approach for energy detection of unknown deterministic signal in cognitive radio over fading channels," in *Communications Workshops*, 2009, pp. 1–5. (Cited on page 69.)

[73] A. Annamalai, O. Olabiyi, S. Alam, O. Odejide, and D. Vaman, "Unified analysis of energy detection of unknown signals over generalized fading channels," in *Wireless Communications and Mobile Computing Conference*, 2011, pp. 636–641. (Cited on page 69.)

[74] A. Rao and M. Alouini, "Performance of cooperative spectrum sensing over non-identical fading environments," *IEEE Transactions on Communications*, vol. 59, no. 12, pp. 3249 –3253, 2011. (Cited on page 69.)

[75] S. Appadwedula, V. Veeravalli, and D. Jones, "Robust and locally-optimum decentralized detection with censoring sensors," in *Proceedings of the Fifth International Conference on Information Fusion*, vol. 1, July,2002., pp. 56–63 vol.1. (Cited on page 70.)

[76] J.-W. Yao, K.-C. Leung, and V.-K. Li, "A random censoring scheme for cooperative spectrum sensing," in *IEEE Global Telecommunications Conference*, 2011, pp. 1–5. (Cited on page 70.)

[77] Q. Zou, S. Zheng, and A. Sayed, "Cooperative sensing via sequential detection," *IEEE Transactions on Signal Processing*, vol. 58, no. 12, pp. 6266–6283, 2010. (Cited on page 71.)

[78] R. Blum and B. Sadler, "Energy efficient signal detection in sensor networks using ordered transmissions," *IEEE Transactions on Signal Processing*, vol. 56, no. 7, pp. 3229–3235, 2008. (Cited on page 71.)

[79] Y. Xin, H. Zhang, and S. Rangarajan, "SSCT: A simple sequential spectrum sensing scheme for cognitive radio," in *IEEE Global Telecommunications Conference*, 2009, pp. 1–6. (Cited on page 71.)

[80] Y. Zeng, Y.-C. Liang, A. Hoang, and E. Peh, "Reliability of spectrum sensing under noise and interference uncertainty," in *IEEE International Conference on Communications Workshops*, 14-18 2009, pp. 1–5. (Cited on pages 112 and 121.)

[81] K. Hamdi and K. Ben Letaief, "Power, sensing time, and throughput tradeoffs in cognitive radio systems: A cross-layer approach," in *IEEE Wireless Communications and Networking Conference*, 2009, pp. 1–5. (Cited on page 113.)

[82] S. Stotas and A. Nallanathan, "Optimal sensing time and power allocation in multiband cognitive radio networks," *IEEE Transactions on Communications*, vol. 59, no. 1, pp. 226–235, 2011. (Cited on page 113.)

[83] M. Cardenas-Juarez and M. Ghogho, "Spectrum sensing and throughput trade-off in cognitive radio under outage constraints over nakagami fading," *IEEE Communications Letters*, vol. 15, no. 10, pp. 1110 –1113, 2011. (Cited on page 114.)

[84] T. E. Bogale and L. Vandendorpe, "Moment based spectrum sensing algorithm for cognitive radio networks with noise variance uncertainty," in *47th Annual Conference on Information Sciences and Systems*, 2013, pp. 1–5. (Cited on page 114.)

[85] S. S. Kalamkar and A. Banerjee, "On the performance of generalized energy detector under noise uncertainty in cognitive radio," in *National Conference on Communications*, 2013, pp. 1–5. (Cited on page 115.)

[86] Y. Zeng and Y.-C. Liang, "Spectrum-sensing algorithms for cognitive radio based on statistical covariances," *IEEE Transactions on Vehicular Technology*, vol. 58, no. 4, pp. 1804–1815, 2009. (Cited on pages 115, 117, and 121.)

[87] E. Axell and E. Larsson, "Optimal and sub-optimal spectrum sensing of OFDM signals in known and unknown noise variance," *IEEE Journal on Selected Areas in Communications*, vol. 29, no. 2, pp. 290 –304, 2011. (Cited on pages 115 and 117.)

[88] S. Chaudhari, V. Koivunen, and H. Poor, "Autocorrelation-based decentralized sequential detection of OFDM signals in cognitive radios," *IEEE Transactions on Signal Processing*, vol. 57, no. 7, pp. 2690–2700, 2009. (Cited on pages 115, 117, 120, 122, and 123.)

[89] S. Bokharaiee, H. Nguyen, and E. Shwedyk, "Blind spectrum sensing for OFDM-based cognitive radio systems," *IEEE Transactions on Vehicular Technology*, vol. 60, no. 3, pp. 858–871, 2011. (Cited on pages 115 and 117.)

[90] Y. Zeng and Y.-C. Liang, "Eigenvalue-based spectrum sensing algorithms for cognitive radio," *IEEE Transactions on Communications*, vol. 57, no. 6, pp. 1784–1793, 2009. (Cited on pages 115, 117, and 121.)

[91] S. Zhang and Z. Bao, "An adaptive spectrum sensing algorithm under noise uncertainty," in *IEEE International Conference on Communications*, 2011, pp. 1–5. (Cited on page 115.)

[92] A. Mariani, A. Giorgetti, and M. Chiani, "Effects of noise power estimation on energy detection for cognitive radio applications," *IEEE Transactions on Communications*, vol. 59, no. 12, pp. 3410–3420, 2011. (Cited on page 115.)

[93] M. Hassan and O. Nasr, "Adaptive spectrum sensing of wireless microphones with noise uncertainty," in *22nd IEEE International Symposium on Personal Indoor and Mobile Radio Communications*, 2011, pp. 445–450. (Cited on page 115.)

[94] N. Reisi, M. Ahmadian, V. Jamali, and S. Salari, "Cluster-based cooperative spectrum sensing over correlated log-normal channels with noise uncertainty in cognitive radio networks," *IET Communications*, vol. 6, no. 16, pp. 2725–2733, 2012. (Cited on page 115.)

[95] W. Lin and Q. Zhang, "A design of energy detector in cognitive radio under noise uncertainty," in *IEEE Singapore International Conference on Communication Systems*, 2008, pp. 213–217. (Cited on page 115.)

[96] G. Wei, L. Wang, D. Zhang, and S. Zhang, "The effect of noise uncertainty to the performance of energy detection in cooperative detection," in *3rd IEEE International Conference on Broadband Network and Multimedia Technology*, 2010, pp. 614–618. (Cited on page 115.)

[97] F. Li, Y. Liu, G. Jin, Y. Wu, and S. Ji, "Performance analysis of hard fusion rules under noise uncertainty at low snr," in *13th IEEE International Conference on Communication Technology*, 2011, pp. 192–196. (Cited on page 115.)

[98] Q. Liu, J. Gao, Y. Guo, and S. Liu, "Robustness improvement against noise uncertainty by cooperative spectrum sensing," in *International Conference*

on Wireless Communications and Signal Processing, 2010, pp. 1–6. (Cited on page 115.)

[99] K. Hamdi, X. N. Zeng, A. Ghrayeb, and K. Letaief, "Impact of noise power uncertainty on cooperative spectrum sensing in cognitive radio systems," in *Global Telecommunications Conference*, 2010, pp. 1–5. (Cited on pages 116 and 121.)

[100] D. Chen, J. Li, and J. Ma, "Cooperative spectrum sensing under noise uncertainty in cognitive radio," in *Wireless Communications, Networking and Mobile Computing*, 2008, pp. 1–4. (Cited on page 116.)

[101] A. Kortun, T. Ratnarajah, M. Sellathurai, Y.-C. Liang, and Y. Zeng, "On the eigenvalue based spectrum sensing and secondary user throughput," *IEEE Transactions on Vehicular Technology*, vol. PP, no. 99, pp. 1–1, 2013. (Cited on pages 116 and 121.)

[102] E. C. . 216076, *Sensor Network for Dynamic and cOgnitive Radio Access*, 2008. (Cited on page 117.)

[103] W. Gautschi, "The incomplete gamma functions since tricomi," *Tricomi's Ideas and Contemporary Applied Mathematics, Atti dei Convegni Lincei*, 1975. (Cited on page 125.)

[104] Z. Kang, K. Yao, and F. Lorenzelli, "Nakagami-m fading modeling in the frequency domain for OFDM system analysis," *IEEE Communications Letters*, vol. 7, no. 10, pp. 484–486, 2003. (Cited on pages 129, 130, 132, and 155.)

[105] M. Kaneko, K. Hayashi, P. Popovski, K. Ikeda, H. Sakai, and R. Prasad, "Amplify-and-forward cooperative diversity schemes for multi-carrier systems," vol. 7, no. 5, 2008, pp. 1845–1850. (Cited on pages 130 and 131.)

[106] B. G. L. Dai and L. Cimini., "Selective relaying in OFDM multihop cooperative networks," in *IEEE WCNC*, 2005, pp. 963–968. (Cited on pages 130 and 131.)

[107] W. Y. W. Yang and Y. Cai., "Outage performance of OFDM-based selective decode-and-forward coopera-tive networks over nakagami-m fading channels," in *Wireless Personal Commun.*, vol. 56, 2011, pp. 503–515. (Cited on page 131.)